University of Mohamed Boudiaf - M'sila

FACULTY OF SCIENCE

DEPARTMENT OF NATURAL AND LIFE SCIENCES

Serial Number:……

Registration Number: ……

THESIS

Presented for the graduation of

DOCTORATE 3rd Cycle (LMD)

Specialty: Ecology and environment
Option: *ecology of natural environments*

THEME

Assessing the quality of continental wetlands through the use of ecological indicators

Presented by

Miss**: Hadjer KERIA**

Defense on*:* 24- 07-2024

Before the jury composed of:

First Name & Last Name	Degree	Establishment	Quality
Yassine Nouidjem	Professor	Univ. of M'Sila	President
Ettayib BENSACI	Professor	Univ. of M'sila	Thesis Director
Asma ZOUBIRI	MCA	Univ. of M'sila	Thesis co-director
Djamel Khoudour	MCA	Univ. of M'sila	Examiner
Noureddine Slimani	Professor	Univ. of M'Sila	Examiner

Academic Year: 2023/2024

ACKNOWLEDGMENTS

At the end of this work, I thank above all God, almighty, for having given me the will, courage, and patience to complete this work.

I would like to express my sincere gratitude to my thesis supervisor, Pr. Ettayib Bensaci from M'Sila University, for his guidance, support, and expertise throughout this research project. His expert advice and commitment were essential to the success of this thesis.

I would also like to thank Asma Zoubiri, co-director of the thesis.

My thanks also go to all the members of the jury who agreed to evaluate this work despite their many occupations. I express my gratitude to the President of the jury, Pr. [..], for having presided over this modest thesis.

Many thanks to my colleagues at the CRAPC (Centre de Recherche Scientifique et Technique en Analyses Physico-Chimiques) laboratory in Bousmail, in particular to Mr. Belgacem Tadjer and Dr. Yasmine, as well as to my colleagues at the Agro Hydro group laboratory in Oran, for their support and contributions.

I warmly thank Prof. Yassine Nouidjema and BOUNAR Rabeh of the M'sila University for their wise advice and invaluable help.

My thanks also go to Mr. Guelil Abdelhamid for his assistance in the analysis of heavy metals.

I would also like to thank my colleague, who has never hesitated to offer valuable help and advice.

I am grateful to my colleague, Dr. Zineb BEN SI SAID who never hesitated to offer valuable help and advice.

Finally, I wish to express my deep gratitude to Pr. Ayhan Atesoglu of the University of Bartin, Turkey, for his help in the field of remote sensing, as well as to all those who contributed, directly or indirectly, to the realization of this thesis.

DEDICACES

My parents, Ahmad and Maleg Fatima No dedication can express the love, esteem, dedication, and respect I have always had for you. Nothing in the world is worth the effort I put in day and night for my education and well-being. This work is the fruit of the sacrifices that you have made for my education and training.

To my grandparents

To my sister Amina, and Halima Haroun who was my biggest supporter at every stage of my life.

To my brothers Mouhamed Amine, Saleh Eddin, Amir Abdelkader, and Fethi Saddam.

To my friends Imen Luiza Guebli, Asma Zerouki.

To all my teachers.

To all my friends.

Abbreviation's list

CHIRPS: Climate Hazards Groups

CFSR: Climate Forecast System Reanalysis

EMC: Environmental Modeling Center

EVI: Enhanced Vegetation Index

GEE: Google Earth Engine

GIS: Geographic Information Systems

LiDAR: Light Detection and Ranging

LST: Land Surface Temperature

NCEP: National Centers for Environmental Prediction.

NDMI: Normalized Difference Moisture Index

NDVI: Normalized Difference Vegetation Index

NDWI: Normalized Difference Water Index

SAR: Synthetic Aperture Radar

SPEI: Standardized Precipitation Evapotranspiration Index

SPI: Standardized Precipitation Index

PET: Potential Evapotranspiratio

Chapter I: Overview of Remote Sensing and Applied in Wetlands

Figure I.1. Semi-Supervised Techniques for Information Extraction in Remote Sensing Big Data (Wu et *al*., 2021). 8

Figure I.2. Semi-Supervised Information Extraction Workflow for Remote Sensing Big Data. 15

Chapter II: Material and Methods

Figure II.1 Geographical and Hydrological Situation of the Study Area. 21

Figure II.2. Topographic map of Algeria (Create by H. KERIA, 2024). 23

Figure II.3. Geologic map of Algeria 25

Figure II.4. Major watersheds, Hydrographic Network, and Main Hydrographic Sub-basins of Algeria (Create by H. KERIA, 2024). 26

Figure II.5. Annual average rainfall map of Algeria (1981-2022) (Create by H. KERIA, 2024)..... 28

Figure II.6. Average monthly rainfall of Algeria (1981-2022). 29

Figure II.7. Annual average Temperature map of Algeria (1981-2022) (Create by H. KERIA, 2024). 30

Figure II.8. Average monthly Temperature of Algeria (1981-2022). 31

Figure II.9. Average monthly Temperature of Algeria (1981-2022). 33

Figure II.10. A map of the study area's water systems, basin stations, sampling stations, and water supply..... 36

Figure II.11. Artificial neural network architecture. 38

Chapter III: Results and Discussion

Figure III.1. Patterns of NDVI change trends in 25 basins in Algeria from 1981 to 2021, with yearly average NDVI change. 48

Figure III.2. The factor of partial correlation of growth season between NDVI, rainfall, and temperature in the 25 watersheds during 1981–2021..... 57

Figure III.3. Standardized long-term fluctuations in NDVI and climatic variables (rainfall and temperature) across the 25 watersheds in Algeria during 1981–2021. 58

Figure III.4. Time-lag transfer matrix among NDVI and climate factors in 25 Algerian watersheds from 1981 to 2021. 64

Figure III.5. The Pearson correlation distribution pattern between both the multi-year average vegetation indices (NDVI) and the climatic factors temperature (a), and rainfall (b) in 25 basins from 1981 to 2021. 65

Figure III.6. The pattern of interannual changes in the annual average NDVI for 25 watersheds in Algeria over the period of 2000 to 2022. 69

Figure III.7. Interannual Fluctuations in Annual Average EVI Across 25 Algerian Watersheds (2000-2022). 71

Figure III.8. Interannual Fluctuations in Annual Average NDWI Across 25 Algerian Watersheds (2000-2022). 72

Figure III.9. Interannual Fluctuations in Annual Average LST Across 25 Algerian Watersheds (2000-2022). 72

Figure III.10. Annual averages of NDMI in 25 regions from 2000 to 2022..... 73

Figure III.11. Annual assessment on NDVI and LST indices relationship during 2000-2022. 74

Figure III.12. Mann-Kendall trend test for annual NDVI, EVI, NDWI, LST, 2020–2022. 80

Figure III.13. Spatial pattern of annual mean NDVI in Reghaia (a); Trend of interannual variation in annual mean NDVI (b) during 2000–2022. 81

Figure III.14. Partial association analysis between NDVI and extreme climates in the Reghaia Basin, 2000–2022. 82

Figure III.15. Spatial alteration of mean NDVI in various seasons. (a) Spring mean (b) Summer mean (c) Autumn mean. 83

Figure III.16. Annual temporal variation of the drought index in the Reghaia basin from 2000 to 2022. 86

Figure III.17**.** Seasonal temporal variation of the SPEI in the Reghaia basin from 2000 to 2022. (a Spring), (b Summer), (c Autumn). 87

Figure III.18. Correlation among the Drought Index and NDVI in the Reghaia basin from 2000 to 2022. 88

Figure III.19. Mean water pH values wetlands. 90

Figure III.20. Temporal average of water temperature in wetlands. 91

Figure III.21. Temporal average of water electrical conductivity wetlands. 91

Figure III.22. Average water total dissolved solids values in wetlands..... 92

Figure III.23. Average water Salinity values in wetlands..... 92

Figure III.24. Biplot Visualization of Principal Component Analysis of Heavy Metal Distribution Across Various Sampling Locations.....96

Figure III.25. Cluster Analysis of Sixteen Sampling Locations in Algeria Using Hierarchical Agglomerative Clustering (CAH). 97

Figure III.26. Network regression for a (Pb), b(Cd), c (Cu) and d (Zn). 99

Figure III.27. RMS for a (Pb), b(Cd), c (Cu) and d (Zn). 100

Chapter I: Overview of Remote Sensing and Applied in Wetlands

Table I-1 Remote sensing data attributes of primary medium- and high-resolution earth satellite images. 11

Chapter II: Material and Methods

Table II-1. Characteristics of the all-study areas 22
Table II-2. Aridity index values. 31
Table II-3. The climate types for 26 study zones in Algeria 32
Table II-4. Exploring Essential Datasets: An in-depth analysis in the research. 40
Table II-5. Five-grade category of the drought index. 41

Chapter III: Results and Discussion

Table III-1. Correlation coefficient between climate factors and the vegetation index. ... 61
Table III-2. Seasonal correlations between climatic conditions and NDVI (NDVI-P, NDVI-T) in the Basins. 62
Table III-3. Findings of the two-tailed test for seasonality in the NDVI time series using the Mann-Kendall method. 75
Table III-4. Findings of the two-tailed test for seasonality in the EVI time series using the Mann-Kendall method. 76
Table III-5. Findings of the two-tailed test for seasonality in the NDWI time series using the Mann-Kendall method. 77
Table III-6. Findings of the two-tailed test for seasonality in the LST time series using the Mann-Kendall method. 78
Table III-7. Seasonal relationships between extreme climatic factors and NDVI (NDVI-P, NDVI-T) in the Reghaia Basin from 2000 to 2022. 85
Table III-8. Evaluation of pollution indicators. 93
Table III-9. Correlation Analysis Among Heavy Metals and EC, TDS, pH, Salinity, and Temperature in the Water Body. 95
Table III-10. The Eigenvalues of the Principal component matrix. 96
Table III-11. Performance's multilayer of the artificial neural network models. 98

Table of Contents

Introduction 1

Chapter I: Overview of Remote Sensing and Applied in Wetlands

1. Remote sensing 6

.2 Advanced Sensors and Remote Monitoring Platforms 6

3. Preprocessing Techniques for Remote Sensing Data 7

3.1. Improving Image Quality 9

3.2. Change Detection Algorithms: 10

3.3. Algebraic Pattern Change Detection: 10

.3.4 Change Detection Based on Classification: 10

3.5. Change Detection Based on Advanced Models: 10

4. Obtain data from remote sensing sources. 12

5. Data processing 13

6. Neural Network and Fuzzy-Based Approach for Change Detection 13

6.1. Fuzzy Clustering Method: 13

6.2. Edge-Weighted Fuzzy Clustering: 13

6.3. Deep Learning: 13

6.4. Fuzzy Logic for Forest Fire Detection: 14

6.5. Tensor and Deep Learning: 14

6.6. Fuzzy Clustering and Markov Random Fields: 14

7. Geographic Information Systems (GIS) 14

8. Monitoring of wetlands by remote sensing: 15

8.1. Wetlands 15

8.2. The functions of wetlands 16

8.3. Descriptive typologies 16

8.4. Descriptive typologies and hierarchy 16

8.5. Description's typologies non-hierarchical 17

8.6. The wetlands in Algeria 17

8.7. Functional assessment of wetlands with remote sensing 18

8.8. Temporal surveillance of a wetland 18

Chapter II: Material and Methods

1. Geographical location of the study area 20

2. Topography 20

2.1. Mediterranean Coastal Chain 20

2.2. Atlas Tellien Mountains 20

2.3. Highlands 21

2.4. Sahara Desert 21

2.5. Chott and sebkha 21

2.6. The Saharan Massif 23

3. Geology 24

3.1. Precambrian and Lower Paleozoic: 24

3.2. Middle and Upper Paleozoi 24

3.3. Mesozoic 24

3.4. Tertiary 24

3.5. Quaternary 24

3.6. Tectonic 24

4. Hydrology 25

4.1. Chelif River Basin 26

4.2. Seybouse River Basin 26

4.3. Moulouya River Basin 26

4.4. Ouargla Basin 27

4.5. Tafna River Basin 27

4.6. In Salah Aquifer 27

4.7. Hauts Plateaux Basin 27
4.8. Hauts Plateaux Endorheic Basins 27
5. Climate 27
5.1. Rainfall 27
6. Temperatures 29
6.1. Climate synthesis 31
6.2. The Martonne index 31
6.3. The ombrothermic diagrams 33
7. Biodiversity in Algeria 33
7.1. Wildlife 34
8. Material and Method 36
8.1. Sample collection and analysis 36
8.2. Sampling equipment and preservation 36
8.3. Measuring Techniques and analyzing water 37
8.4. Artificial Neural Network 37
9. Data and processing: 38
9.1. Modis Dataset 38
9.2. Landsat dataset 39
9.3. Climate dataset 40
9.4. SPEI Drought Index 41
10. Methods 42
10.1. Analyzing the Dynamics: Regression Study on Long-Term Vegetation Index Trends 42
10.2. Normalization data 42
10.3. Investigating Correlations Between Vegetation Index and Climatic Variations 43
10.4. Exploring Various Remote Sensing Indices for Environmental Monitoring 43
10.5. Man-Kendall trend analysis 45
10.6. SPEI drought index 46

.10.7 Assessment of surface water quality in wetlands 46

10.8. Pearson correlation 47

10.9. Statistical Analysis.....47

Chapter III: Results and Discussion

1. Assessment of the long-term effects of climate on vegetation in 25 watersheds in dry and semi-dry areas, Algeria 47

1.1. The temporal-spatial distributions for NDVI during the past 40 years 47

.1.2 The association between the vegetation index and climatic changes 56

1.3. Long-time impact response for NDVI with rainfall/ temperature variations 61

1.4. Spatial distribution and influence of climatic factors on vegetation cover.....63

1.5. Unraveling Environmental Transformations: A Multifaceted Analysis of Climate, Vegetation Dynamics, and Human Influence in Algerian Watersheds (1981-2021) 66

2. Long-term disparity assessment of remote sensing indicators to monitor the dynamism of ecosystems in arid and semi-arid areas: contributions to sustainable resource management. 67

2.1. The evolving pattern of NDVI in the 25 areas over the course of the last 22 years.....67

2.2. Spatio-temporal of NDVI, EVI, NDWI, LST and NDMI: 69

2.3. The associations between NDVI and LST:.....73

2.4. Mann-Kendall analysis trends 74

3. Monitoring the effect of droughts and extreme climate variables for various time periods on vegetation density in the Reghaia catchment, Algeria 80

3.1. Variability of Vegetation Dynamics in the Reghaia Basin.....80

3.2. Relationships between NDVI dynamics and climatic variables with partial correlation82

3.3. Seasonal spatial changes in vegetation cover during the growing season in the Reghaia catchment over a 22-year period.....83

3.4. The impact of seasonal changes in long-term climate factors on the vegetarian index over the past 22 years.....84

3.5. Temporal characteristics: annual and seasonal evolution of SPEI in the Reghaia catchment 86

3.6. Association analysis 88

3.7. Characteristics of Vegetation: Dynamic and Climate Extremes 88

3.8. Analysis of the impact of drought on vegetation 89

4. Assess the quality of wetlands in Algeria 90

4.1. physico-chemical analyses 90

5. Assessing the presence of metals and potential health risks in surface waters; A case study conducted in Algeria using a combination of Artificial Neural Networks and multiple indices 93

5.1. Heavy metals Contamination Index (HPI, HEI) 93

5.2. Exploring the association between heavy metals, physical-chemical interactions, and HPI 94

5.3. Principal component analysis 95

5.4. Artificial Neural Network Modeling for Predicting Heavy Metal 98

Conclusion 102

References 106

APPENDIX

Abstract

Résumé

الملخص

Introduction

Introduction

Wetlands are highly valued ecosystems that are at risk. Over 33% of the world's wetlands are being converted due to man-made disruptions (Meng et *al*., 2017). Vegetation, which is a vital part of wetlands, has social, economic, and ecological benefits. These values include the ability to take in contaminants and the provision of ecosystems (Lin et *al*., 2022). To mitigate the downward trend of degradation and maintain the long-term viability of wetland areas, it is essential to conserve vegetation and make reasonable use of it (Peng et *al*., 2023). Nevertheless, climatic factors and human activities have lately caused significant harm to the growth and spread of wetland vegetation. Recently, this damage has been severe. As a consequence of this, the safety of the vegetation is in grave danger, which in turn increases the possibility of the deterioration of wetlands (Peng et *al*., 2022). Precisely, changes in rainfall and temperature contribute to changes in environmental conditions, which in turn impact the development and reproduction of plants (Ojdaniˇc et *al*., 2023). For this reason, it is intended to mimic vegetation trends with a high degree of accuracy to locate vulnerable regions. In the context of shifting settings, the findings are beneficial to the process of attaining sustainable growth by balancing the conservation of wetlands with the usage of resources (Liao et *al*., 2024).

A sustainable growth plan involves safeguarding biodiversity and the natural world, including the atmosphere, clean water, the sea, land, and forests, which are essential for humanity's survival (Xu et *al*., 2020). Where The United Nations Summit on Sustainable Development is responsible for the adoption and formulation of seventeen sustainable growth objectives for the next fifteen years. These objectives were approved and created in September 2015 (Wu et *al*., 2022). Included among them are the goals for ecology and combating climate change, which are strongly linked to the ecosystem changes in wetlands systems (Fuldauer et *al*., 2022). Relevant countries and organizations can develop laws to protect wetlands' resources, effectively reducing wetland degradation and change worldwide (Leal et *al*., 2022). Wetland’s deterioration and enhancement are significant topics in wetlands expansion studies (Mao et *al*., 2022). It is crucial to promptly and precisely track and assess the continued deterioration procedure for wetlands to safeguard the wetland ecology (Wang et *al*., 2022).

Utilizing data from remote sensing technologies enables extensive, extended, and precise studies on tracking and evaluating wetland ecosystem transformations (Pan et *al*., 2023). In contrast to the conventional way of conducting field surveys, which is lengthy, arduous, expensive, and has a limited monitoring spectrum, the new approach is more efficient (George & Ngole-Jeme, 2021). The assessment of wetland decline using earth images from satellites

offers a new approach to tracking wetland changes over a wide area. This approach includes a surroundings assessment, only one variable index, a comparison, a thorough assessment index, and ambiguous assessment techniques (Zhu et *al*., 2022). The approach to assessment in the environment involves identifying wetland environmental shifts by choosing indicators that include wetland landscape structure, wetland surroundings variety, and wetland dispersion of landscape. This analysis includes examining the area among various region types using surrounding data, like wetland location (Zhang et *al*., 2022). could not well describe the temporal and geographical variations of environmental parameters in identical kinds of wetlands (Sica et *al*., 2016). Some quantitative evaluation methods, such as index-based wetland decline categorization, health of ecosystems evaluation, and natural risk evaluation, can clearly show changes to environmental parameters in similar items on the ground (Zolfaghari et *al*., 2022). Yet, the single-factor indices technique can only provide a basic overview of the natural state of a specific factor like water, plants, or wetlands (Ablat et *al*., 2019). It is unable to conduct a thorough assessment of aquatic environmental transformations (Dybiec et *al*., 2020). Consequently, advanced academics are increasingly conducting thorough time series evaluations of wetlands' ecological alterations using a geographically large-scale data cloud computing platform with several indices. For instance, He et *al*. (2022) developed a model for detecting coastal wetland deterioration that integrates satellite imagery and a hydrological system. Zhu et *al*. (2022) used time-series data on earthly satellite imagery from Google Earth Engine spanning from 1985 to 2020 to create a WDI index for assessing the deterioration of water bodies. This index combined the LSI index, VDI index, and SDI index.

Ecology indexes such as the Normalized Difference Vegetation Index (NDVI), derived from various satellite imagery, offer crucial information for a wide range of ecosystem evaluations (Zhou et *al*., 2021). These include monitoring plants (Gao et *al*., 2016), predicting agricultural yields (Wang et *al*., 2012), and observing climatic change (Chang et *al*., 2011). Technical restrictions prohibit individual observatories from obtaining high-resolution pictures with both spatial and temporal detail at the same time. MODIS is popular among scientists because of its large scan coverage and regular return periods (Wang et *al*., 2022). However, its low spatial resolution limits its effectiveness for observing small-scale surface characteristics. Landsat offers extended data across time and high spatial resolution, which is advantageous for in-depth analysis in certain areas (Zeng et *al*., 2018). Yet, its inferior time resolution and data integrity may jeopardize chronological consistency and diminish its reach. Several spatiotemporal image fusion (STIF) approaches have been established to tackle these problems

(Meng et *al*., 2022). The approaches attempt to combine precise geographic datasets from advanced sensors with chronological information from high-frequency sensors to create datasets that have excellent spatiotemporal precision (Gao et *al*. 2017).

Google Earth Engine (GEE) is one of the most important applications, that allows users to access and process datasets using a Python and JavaScript API (application programming interface). The GEE Code Editor, an integrated development environment (IDE) using the JavaScript (JS) API, provides immediate access to all features of the GEE without requiring authorization or the installation of additional services. GEE utilizes Google's robust cloud computing infrastructure to store information and operate effectively. Employing parallel processing involves distributing tasks across several CPUs on servers. Investigators can carry out solar-scale GIS activities with thousands of images without access to powerful computers thanks to the GEE's computing capacity, which is greater than that of high-end computer workstations. The GEE is free to use and only requires a connection to the web. A single request has to be completed and is often granted within a few days to access the GEE (Schmid et *al*., 2017).

In the same vein, monitoring pollution to assess wetlands quality is important through monitoring the concentration of heavy metals, where water is essential for mining operations and often serves as the pathway for contaminants to enter the natural environment (Burritt & Christ, 2018). Cadmium, chromium, lead, and zinc are regarded as significant metals in aquatic settings because of their presence and their poisonous and persistent properties (Lazo et *al*., 2023). Mining activities, such as establishing mines, managing mining waste, and leaks from containment structures, are sources of these pollutants. It results in environmental problems that endanger both people and their habitats. The mining industry's biogeochemical processes may negatively affect both local groundwater and surface water (Baeten et *al*., 2018). Heavy metals have a significant impact on water supplies in arid and semi-desert regions. Mining poses a significant threat to water governance in these areas, where already detrimental effects can amplify the negative effects on the water supply, making a sustainable future in the area an uphill battle (Song et *al*., 2019). Many studies in the scientific community discuss metal contamination in wetlands. Many studies agreed that frequent monitoring of water quality was necessary in wetlands (Santana et *al*., 2020; Butler et *al*., 2018).

Algeria is confronted with considerable issues in terms of the preservation of wetland areas and the quality of these areas. A substantial amount of degradation has occurred in these areas

over the last several decades (Nedkov et *al*., 2018), and the enormous number of wet sites that have been damaged, which is around 5,404, is an indication of the rising stresses that are being placed on this essential habitat. On the other hand, research efforts on this phenomenon continue to be restricted since there are not enough thorough studies that concentrate on understanding the long-term development of land degradation and the factors that generate it. In addition, the fact that there is a substantial shortage of research that has been published on the levels of mineral concentrations in Algeria's surface waters demonstrates the need to do more studies to evaluate the consequences that these accumulations have on many aspects of public health and the environment (Bachouche et *al*., 2017). Because of this difficulty, it is necessary to increase the amount of research that is being conducted and to make investments in scientific studies to discover efficient methods of preserving Algeria's water resources and wetlands and guarantee that they will be sustainable for future generations.

From this point of view, this study aims to conduct a comprehensive analysis of 25 arid and semi-arid in Algeria over the long term by integrating remote sensing and artificial intelligence with the study of the contamination of heavy metals in 16 bodies of water. The specific objectives of this research are the following: (1) to extract spatial changes in the vegetation index over 40 years in 25 different climate regions of Algeria; (2) to examine the time-bound relationship between the national development index and climate parameters; (3) to use NDVI to study the effects of climatic change on vegetation growth and to identify the widespread independent and common effects of such changes; and (4) to identify the long-term effects of time delays on vegetation. (5) Analysis of the temporal patterns of EVI, NDVI, NDWI, NDMI, and LST indicators in a variety of water catchments in Algeria during the period from 2000 to 2022, to comprehend ecosystem alterations and the development of water resources over time. (6) To evaluate the influence of climate changes on Algeria's watersheds by analyzing data derived from GEE, to comprehend the association between climate variables and changes in spectral indicators and water resources in watersheds. (7) Identification of areas sensitive to environmental changes in Algeria's watersheds through analysis of data derived from GEE, with a view to identifying areas experiencing a clear degradation of vegetation and the factors affecting such changes. (8) Analysis of the severity of drought in seasonal and annual periods and its relationship to extreme climatic factors. (9) To enhance comprehension regarding the origins and impacts of pollution on the ecosystem of Algeria. This study focused on 16 water bodies in Algeria, located in several directions including north, west, and center regions, chosen specifically for their significant biological and environmental value. The research is primarily

concerned with determining the origins of pollution, particularly heavy metals, in these regions. The study aims to address many inquiries, such as determining the origins of probable contaminants and quantifying the levels of significant pollutants.

This work is divided into three main chapters:

Chapter I provides an overview of the methods of remote sensing and the use of artificial intelligence, their importance in recent studies, and how they are applied in wetlands.

Chapter II provides an overview of the overall framework of the field of study by presenting the study area, which included 26 wet areas, and emphasizing geology, hydrology, and climatology. The most important methods used in this study were then discussed in detail.

Chapter III: The most important findings were presented in all areas where the study was conducted and discussed in detail.

Finally, a general conclusion to draw key findings and perspectives from this work.

Chapter I: Overview of Remote Sensing and Applied in Wetlands

1. Remote sensing

Remote sensing encompasses the use of modern tools and techniques to study and understand Earth's events from a distance, without the need for direct physical contact. This is accomplished by employing specialized sensors that are installed on aircraft, handheld devices, or satellites. These sensors may consist of multispectral cameras, electronic scanners, traditional cameras, laser cameras, thermal devices, and radar equipment. Remote sensing technology is a highly prevalent and extensively employed method in the field of environmental science. The process entails acquiring photographs of the Earth's surface through the utilization of geographic information systems, contemporary sensors, and geospatial methodologies. The techniques encompass cartography of spatial distributions, examination of worldwide alterations, and construction of three-dimensional visualizations of natural habitats (Lechner et *al*., 2020).

In the last century, sensors for remote sensing have made substantial advancements, enhanced their abilities and improved their capacity to assess data and precise details that are challenging to observe without the aid of technology (Amani et *al*., 2019). These methods encompass a variety of methodologies, spanning from traditional aerial photographs that provide a perspective similar to that of humans to specialized images that can uncover structural and chemical barriers on the planet's surface (Liu et *al*., 2018). The use of current technology has resulted in many applications in several environmental and scientific domains. These applications share a common objective of enhancing our understanding, conservation, and evaluation of ecosystem health and dynamics (Chi et *al*., 2016).

2. Advanced Sensors and Remote Monitoring Platforms

The advancement of sensor technology has led to the integration of passive and active sensor systems into bigger platforms, such as satellites and drones. The connection has greatly improved the ability to collect and accurately analyze data across several applications. (Zhu et *al*., 2018; Feng et *al*., 2021). Platforms encompass many vehicles, such as Earth-observing satellites, manned planes, and fixed-wing drones (Wu et *al*., 2021). The most common types of sensors in remote sensing are standard digital cameras and optical sensors in their construction and application (Maes & Steppe, 2019), apart from their ability to collect data at hidden wavelengths, such as wavelengths of radiation such as infrared and thermal waves in the electromagnetic spectrum (Sagan et *al*., 2019). These materials reflect and absorb light at varying wavelengths. These differences in absorption and reflection can reveal and provide information on the Earth's features and resources. Using multi-spectrum sensors, optical

sensors can create images of different optical bands according to your needs (Kerekes & Baum, 2003).

Some multi-spectral sensors have only a limited number of bands, but ultra-spectral sensors have thousands of bands. This wide range of ranges allows sensors to distinguish between different materials and the earth's properties with great accuracy. Analyzing how these materials and properties absorb and reverse radiation across a wide range of wavelengths allows for this distinction (Lechner et *al*., 2020).

Remote sensing systems incorporate a blend of passive and active sensors, each with unique functionalities and possible applications. According to Fernandez-Vallejo & Lopez-Amo (2012), passive sensors include optical and thermal devices that make use of the heat energy and reflected radiation from various objects, including the Earth's surface. Active signals from radar systems are not required because they are used essentially by natural radiation or emitting. Conversely, active systems such as LiDAR (Light Detection and Ranging) do not require active signals sent from radar or laser systems (Wallace et *al*., 2012). For instance, LiDAR systems allow for a three-dimensional reconstruction through the issuance of Lidar pulses in the time it takes for the pulses to reverse back to the target (Lefsky et *al*., 2002). Synthetic Aperture Radar (SAR) relies on the transmission and reception of active radiation through sensors. Artificial aperture radar efficiently interacts with its surrounding environment and delivers precise data about the target (Kerekes & Baum, 2003). Utilized are active SAR systems capable of penetrating clouds and smoke and functioning during both day and night. The data can be analyzed to obtain information regarding surface features, three-dimensional structure, and even the amount of water available (Lefsky et *al*., 2002).

3. Preprocessing Techniques for Remote Sensing Data

Remote sensing images encompass a diverse array of Earth images captured in various hues, radiation intensities, and distinct wavelengths. The quality of the image is contingent upon the specific sensor employed and the altitude of the orbit. Daytime images predominantly rely on sunlight as their primary source. In contrast, infrared photographs provide a quantification of the Earth's surface temperature (Asokan & Anitha, 2019). Multispectral images encompass multiple wavelength ranges and find extensive utility in research fields such as agriculture and military applications. However, it is important to note that weather conditions can introduce artifacts into these images, presenting a significant challenge (Nink et *al*., 2019; Weiss et *al*., 2019).

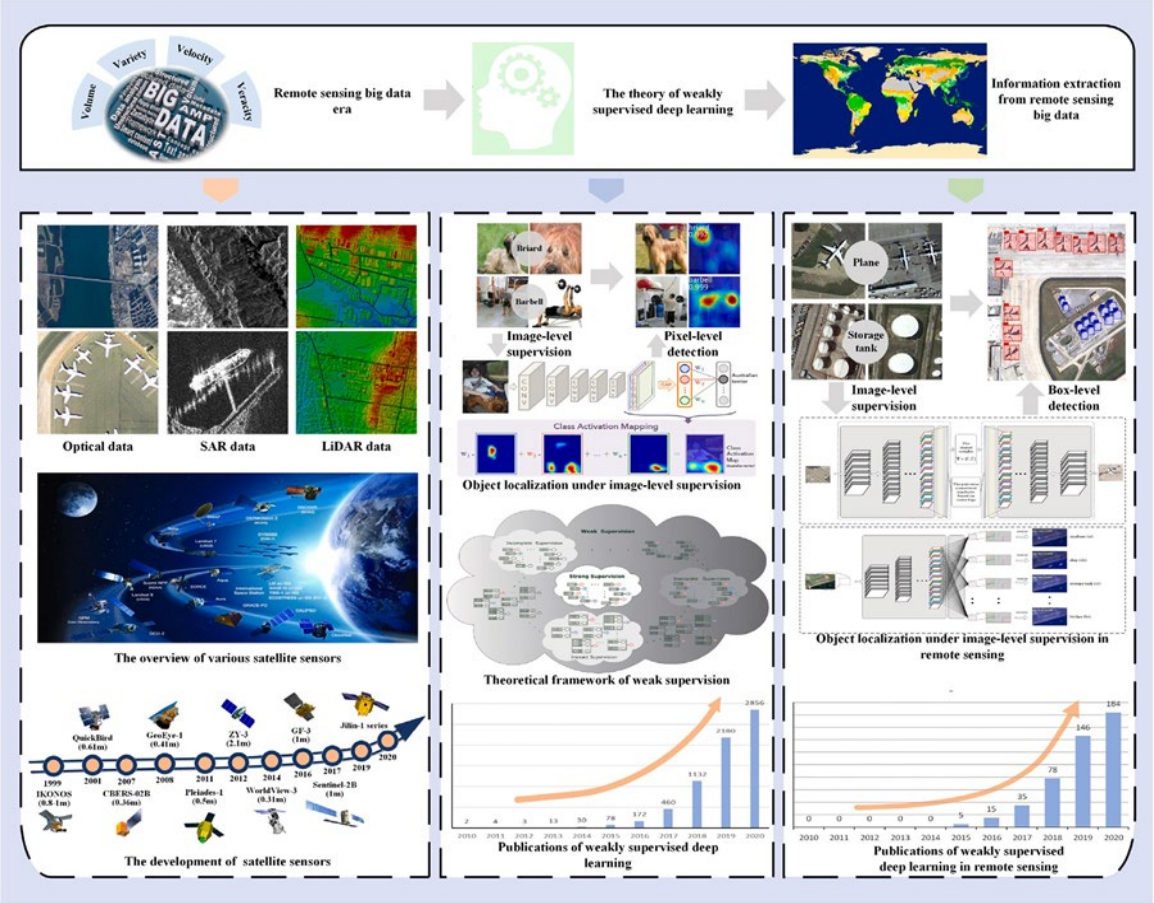

Figure I.1. Semi-Supervised Techniques for Information Extraction in Remote Sensing Big Data (Wu et *al*., 2021).

The utility of satellite imagery extends beyond mere variety, it hinges on the precision of data acquisition and subsequent processing. Visual images excel when captured under optimal daylight conditions, while infrared images provide crucial insights into surface temperatures. Multispectral imagery is instrumental in conducting comprehensive environmental and resource assessments, spanning applications in environmental monitoring, agriculture, and tracking environmental changes (Richards & Jia, 2006).

The accuracy of these images is intricately tied to the quality of the sensor equipment and the altitude of the orbit. Weather conditions pose a formidable challenge due to their impact on image quality, necessitating the development of specialized processing techniques to mitigate these effects. Given their regular data availability and moderate spatial coverage, Landsat and Modis images are frequently utilized for monitoring changes on the Earth's surface (Liggins et *al*, 2009). Due to the ongoing advancement of technology, a wide range of imaging analyses and scientific applications are readily accessible in numerous sectors. This tool aids in the

analysis of environmental studies, streamlines programming processes, and enhances decision-making accuracy across several industries(Chi et *al*., 2016; Liu, 2015).

3.1. Improving Image Quality

Preprocessing is a crucial and pivotal step in enhancing the accuracy of subsequent photo processing stages. Satellite images typically exhibit an average texture, which poses challenges in distinguishing ground elements clearly to the human eye. The emergence of undesirable effects in the image is often a consequence of atmospheric interference and noise. To aid in the identification and differentiation of ground elements, as well as to enhance the efficiency of change detection, advanced techniques such as false color formation have been employed as an innovative approach (Ma et *al*., 2018).

3.1.1. Image Processing in Engineering:

This process involves the correction and alignment of images obtained from various sources to ensure accurate conformity between them. It employs numerous logical boundary transactions, digital terrain models, and feature-matching techniques to achieve this goal. The accuracy of the recorded data heavily relies on the precision of the digital terrain model used (Fytsilis et *al*., 2016).

3.1.2. Radiation Correction:

This correction pertains to addressing differences in radiation intensity within an image caused by sensor angles and varying light intensity (Hao et *al*., 2016). Radiation correction techniques encompass intensity correction and radiometric terrain correction, which utilizes digital height models (Ajadi et *al*., 2016).

3.1.3. Stain Removal:

In the context of SAR images, stain removal is essential for handling speckle noise and enhancing image quality. Techniques for stain removal include temporal and spatial filtering (Wang et *al*., 2017), as well as the application of a Lee Sigma filter for accurate spot removal (Iino et *al*., 2018).

3.1.4. Noise Reduction:

This technique is employed to reduce noise in geographical images while preserving essential details. Noise often affects pixel intensity in images, and linear filtration techniques are commonly used to remove such noise (Liu et *al*., 2018).

3.2. Change Detection Algorithms:

These methods are used to identify changes in images by comparing images captured at different times. There are several approaches to change detection, which depend on preparation, remittance, and classification (Asokan & Anitha, 2019).

3.3. Algebraic Pattern Change Detection

This method involves applying conversions to pixels in the image to detect changes. It helps reduce information redundancy between different bands (Ke et *al*., 2018).

3.4. Change Detection Based on Classification

This approach utilizes post-classification, unsupervised methods, and neural networks to detect changes. It offers improved accuracy and enables precise change detection (Sadeghi et *al*., 2016).

3.5. Change Detection Based on Advanced Models

In remote sensing, advanced models aim to convert image reflection values into physical parameters, facilitating the extraction of relevant information (Asokan & Anitha, 2019). These models include:

3.5.1. Hopfield Neural Network (HNN)

HNN is utilized to extract information from spatially accurate land cover maps without spectral mixing. However, it may face challenges when accurately distinguishing between different Earth patterns (Wang et *al*., 2015).

3.5.2. Temporal Non-Mixing Analysis

This method employs spectral mixture models to detect changes in ground cover based on spectral differences. It primarily relies on spectral properties but may struggle with detailed Earth change detection (Xu et *al*., 2017).

3.5.3. Hybrid Spectral Differences

Hybrid models combine differences in spectral values and spectral shapes. While based on spectral features, they may encounter difficulties in precisely identifying the details of changes (Yuan et *al*., 2018).

3.5.4. Binary Spectral Change Vectors (SCVs)

SCVs are employed to detect change complexities using spectral change vectors. These SCVs are transformed into compact vectors through binary conversion techniques and organized into a tree structure, with tree leaves representing different change categories. This

method efficiently distinguishes between various categories but may have limitations, particularly when dealing with excessive aggregation in some categories (Marinelli et *al*, 2017).

Table I-1 Remote sensing data attributes of primary medium- and high-resolution earth satellite images.

Database	URL link	Resolution	Image
Landsat (5,7,8,9) (Singh & Singh, 2017; Zanchetta et al., 2016),	https://glovis.usgs.gov/	2634 × 3126	42,992
MODIS–VCF(MOD44B) (Amarnath et al., 2017)	https://ladsweb.modaps.eosdis.nasa.gov/missions-and-measurements/products/MOD44B	6406 × 5521	500
Moderate-resolution Imaging Spectroradiometer (MODIS) surface Reflectance products (MOD09A1) (Qiu et al., 2017)	https://ladsweb.modaps.eosdis.nasa.gov/missions-and-measurements/products/MOD09A1	600 × 483	Daily image
PALSAR mosaic Synthetic Aperture Radar (SAR), Sentinel C band SAR and optical data (Johnson et al., 2017)	https://www.eorc.jaxa.jp/ALOS/en/index_e.htm	4500 × 4500	108
Landsat databas (Haque & Basak, 2017)	https://landsat.gsfc.nasa	938 × 528	Daily image
Landsat surface reflectance images (Ye et al., 2018)	https://earth.google.com/web/	4096 × 4096	Daily image

Pleiades imagery (Suresh & Lal, 2017)	https://www.satpalda.com/	1464 × 1143	Daily image
IR imagery and HURDAT2 data (Pradhan et al., 2018)	https://www.nhc.noaa.gov/data/	625 × 625	200
Airborne Visible/Infrared Imaging Spectrometer (AVIRIS) sensor data (Hagag et al., 2017)	https://aviris.jpl.nasa.gov/	677 × 512	4000
World-View2 Multispectral and Panchromatic imagery(Luo et al., 2016)	https://www.digitalglobe.com/	1024 × 614	5000
Global land cover dataset (Wang et al., 2018)	https://glad.umd.edu/dataset/GLCLUC2020/	700 × 400	853
Landsat images (Pandey & Khare, 2017)	https://landsat.visibleearth.nasa.gov/	931 × 644	Daily image

4. Obtain data from remote sensing sources.

The selection of remote sensing data is a vital stage in obtaining the essential information needed to accomplish a certain purpose. Proficiency in comprehending many categories of sensor data is necessary for this task (Congalton, 2010). Furthermore, numerous factors exert an influence on the choice of remote sensing data. The objective of the study, the dimensions and unique characteristics of the study area, the accessibility of diverse data on images and their attributes, and proficiency in remote sensing (Lu & Weng, 2007).

5. Data processing

Data processing refers to the manipulation and transformation of raw data into meaningful information through various computational techniques and algorithms. Image processing relies on classification as its fundamental principle. The process often relies on categorizing and organizing pixels that depict the typical spectral reaction of each object (Ducrot, 2005). This is a selective metric that simplifies data retrieval for spectral pictures and temporal intervals. The choice of categorization method is contingent upon the study objectives. Selecting the categorization is a challenging decision that relies on various aspects that must be taken into account. The list comprises the classification software, data source, all training samples, and the geographic resolution of remote sensing data (Lu & Weng, 2007). The pixel algorithm class encompasses sophisticated techniques, such as synthetic neural networks and vector support machines, that have been devised to enhance classification accuracy (Mahmon & Ya'acob, 2014) The ultimate step in the analysis of remote sensing data Every method employed subsequent to classification is referred to as job classification processing. Although a post-classification pre-treatment may be carried out, such as the elimination of the majority due to the intricate nature of the biophysical environment or the application of technical adjustments (Lu & Weng, 2007).

6. Neural Network and Fuzzy-Based Approach for Change Detection

This category of change detection involves the assessment of change areas through the integration of remote sensing technology, neural networks, and fuzzy modeling. Here are some notable approaches:

6.1. Fuzzy Clustering Method:

Li et *al* (2016) introduced a fuzzy clustering method for SAR image change detection. This approach models change detection as an optimization problem, effectively addressing noise removal and preserving details images.

6.2. Edge-Weighted Fuzzy Clustering:

Tian & Gong (2018) proposed an edge-weighted fuzzy clustering method for change detection. This technique assigns weights to edges, enhancing the accuracy of change detection.

6.3. Deep Learning:

Su et *al* (2017) introduced a deep learning approach for change detection, capable of detecting multiple changes efficiently.

6.4. Fuzzy Logic for Forest Fire Detection:

Garcia-Jimenez et *al* (2017) developed a fuzzy logic system to detect forest fire-related changes, contributing to improved accuracy in this specific application.

6.5. Tensor and Deep Learning:

Huang et *al* (2018) presented a complex yet highly accurate change detection method based on tensor and deep learning techniques.

6.6. Fuzzy Clustering and Markov Random Fields:

Subudhi et *al* (2014) proposed a change detection method that combines fuzzy clustering with Markov random fields. This approach is effective in reducing misclassification errors during change detection processes.

7. Geographic Information Systems (GIS)

Geographic Information Systems (GIS) integrates diverse data sources to identify and analyze variations. One of the primary advantages of utilizing GIS is its ability to detect and offer a comprehensive view of changes in the research area, while also providing consistent and precise coverage. It is important to consider the impact of data accuracy and its diverse origins on the identification of changes in outcomes. (Mahmon, 2014b). The study conducted by Maurya & Yadav (2016) introduces a change identification algorithm that utilizes GIS and remote sensing methods to assess the distinctive alterations associated with natural disasters. The collection and mosaicking of photos are performed, followed by the computation of the water index. The utilization of Geographic Information Systems (GIS) in the identification of changes has facilitated the seamless incorporation of source data. Additionally, it has proven beneficial in facilitating successful visualization of the alterations. The integration of initial data with numerical data in GIS facilitates the collection and assessment of change detection data, hence streamlining the process. The paper by Gandhi et al (2015) introduces a method to detect changes, in plant cover using GIS) and remote sensing data. The authors employ the Normalized Difference Plant Index (NDVI) calculation to classify types of vegetation. In another study conducted by Rawat & Kumar (2015) they delve into the exploration of identifying changes, in land cover through the integration of sensing and Geographic

Information Systems (GIS). This technology enables a change detection process that improves accuracy and reduces overall complexity.

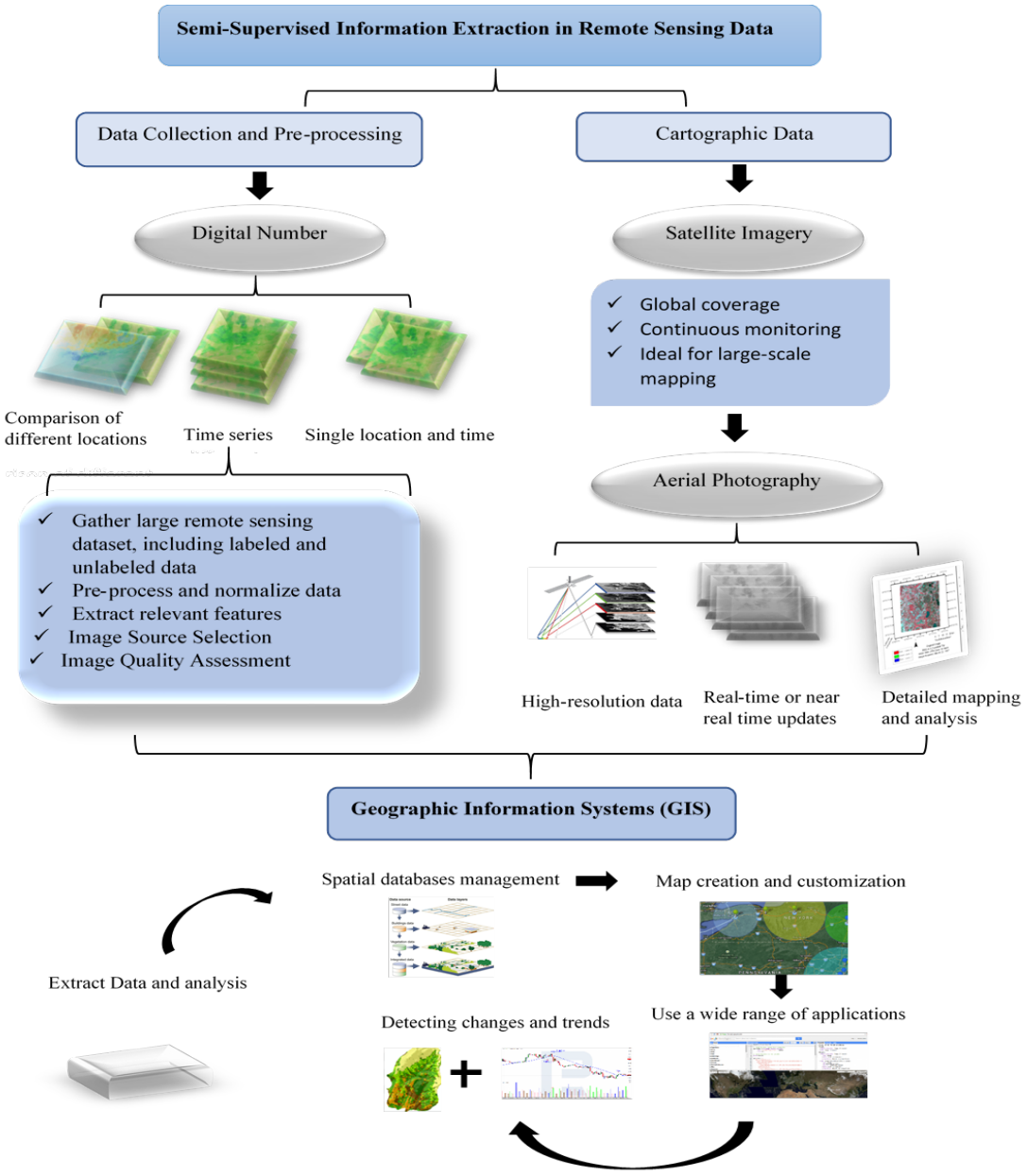

Figure I.2. Semi-Supervised Information Extraction Workflow for Remote Sensing Big Data.

8. Monitoring of wetlands by remote sensing:

8.1. Wetlands

According to (Rapinel, 2012), wetlands come in a range of forms and meanings. A wetland is defined by geological and geomorphological elements that are spatially extensive. Hydrological dynamics (flows and water levels) govern the wetland's operations and dynamics. Over 50 definitions of wetlands have been used globally since the 1970s.

8.2. The functions of wetlands

Wetlands have three primary purposes: hydrological, biogeochemical, and ecologic. Interactions between the stream, groundwater, and slope are crucial for hydrological processes. Wetlands exert influence on numerous hydrological processes. Quantifying the hydrological processes of wetlands necessitates meticulous data collection, rendering it highly intricate. Existing hydrological models designed for wetlands are limited in scope, focusing on a single function and lacking the flexibility to be applied to different places due to the spatial and temporal variability inherent in these ecosystems. Biogeochemical functions encompass various processes that occur in the environment, such as the cycling of nutrients, the transformation of energy, and the regulation of chemical elements. The water originating from the contributing zone and flowing through the wetland experiences physico-chemical alterations based on the prevailing conditions. The functions of the ecologies are as follows: The characteristics of wetland habitats are influenced by factors such as hydrology and hydrodynamics, substrate minerality, the availability of nitrogen and phosphorus, and vegetation utilization.

8.3. Descriptive typologies

Descriptive typologies were used in the initial functional assessments of wetlands, employing an intuitive methodology. Each wetland is summarily described by these typologies to evaluate its overall quality and condition (Rapinel, 2012).

8.4. Descriptive typologies and hierarchy

For wetland inventories, Cowardin et *al*. (1979) suggested an ordered typology. To identify plant forms and geomorphological standards, this categorization makes use of photo-interpretation of satellite pictures. The typology's hierarchical structure made it useful for a variety of uses, including local actors and the state. Several regional adjustments have been made. This method highlights the diversity and variances in the intensity of wetland functions, albeit being general and imprecise. By using broad geomorphological terminology, it is possible to determine global hydrological metrics and contextualize the environment. It appears that this description is too constrained to enable a thorough examination of the characteristics of wetland ecosystems. Currently, this typology is mostly applied in regulatory contexts (Cowardin et *al*, 1995).

8.5. Description's typologies non-hierarchical

Wetlands and adjacent regions' hydrological and geomorphological features provide the basis of a category founded on the Ramsar criteria. Within this typology, the "marine/coastal waters" class represents the majority of surveyed wetlands. It poses issues even if it is utilized to characterize Ramsar sites. Ramsar sites can have a variety of topographies and are frequently rather vast (Barnaud & Fustec, 2007). This typology can be used to characterize the overall makeup of Ramsar sites worldwide, but it is not tailored to regional leadership issues that would call for a more thorough characterization.

8.6. The wetlands in Algeria

Algeria boasts a diverse range of habitats, ecosystems, and landforms, with wetlands being of particular significance. These ecosystems serve several purposes and have major positive effects on the environment and the economy.

With 50 Ramsar sites spanning about 3 million hectares, Algeria is now the largest country in North Africa and the sixth most extensive country in the world (Abulhawa, 2017). The Garaats, Gueltas, Sebkhats the Oases, are among the new varieties of original wetland areas that the world community was able to identify and classify on the Ramsar list in 2001. The Oglats and Dayat took first place in 2004. These wetland habitats, except Oases, are being replaced by comparable ecosystems and are not yet included in the Ramsar typology (Saïfouni et al, 2020), Part of the total area of wetlands in the country.

(Saïfouni et *al*, 2020), a state that there are 5404 wetlands spread over the 58 Wilayas in the country. The Northern Area, which is divided into three biological zones (Northeast, North-Central, and North-West), has 3649 wetland sites, making up almost half of Algeria's total wetlands and 67.52% of its total area. The distribution of wetlands in the three biological zones of the North is as follows: With 1585 wetlands, the Northeast is the most significant biological region. The highest concentration of wetland sites in this region is found in the Wilayas of Skikda (342 sites), Jijel (266 sites), Annaba (249 sites), and Mila (246 sites). The Nord-Centre Ecological Zone, with 1479 wetland habitats, is ranked second. The majority of the wetland sites are located in four provinces: Béjaia (257 sites), Tipaza (181 sites), Boumerdès (165 sites), and Algiers (225 sites). The Northwest has the fewest wetlands, with 585 sites. The greatest concentration of wetlands in this region may be found in the Province of Oran (144 sites), Tlemcen (112 sites), and Ain-Temouchent (111 sites). The Highlands are composed of 1095 wetlands. In this region, the three provinces of Setif (95 sites), Laghouat (96 sites), Djelfa (132

sites), and Batna (147 sites) include the wettest sites. The South is home to 12.21% of the 660 wetlands in the country. There are 314 wetland habitats in the Adrar Province.

8.7. Functional assessment of wetlands with remote sensing

Functional evaluation and identification of wetlands are practical in situ in regions covering a few hectares (Janssen et *al*., 2005). However, the incomplete availability of data presents challenges for study sites spanning several hundred hectares (Rapinel et *al*., 2016). Remote sensing data, which may help us comprehend wetlands over huge areas, has shown interest in both temporal and spatial surveillance of various sorts of ecosystems. The current remote sensing data was too dispersed to evaluate the functions of wetlands up until this point (Hubert-Moy, 2003). There are intriguing opportunities in the space business due to recent technical advancements (Mahdavi, 2017). For instance, a detailed mapping of vegetation areas at a very fine spatial scale is made feasible by the acquisition of new satellite data at a very high spatial resolution (1–10 meters) using sensors like Quickbird, IKONOS, or SPOT-5 (Corbane et *al*. 2015). These sensors' spectral (visible and near-infrared) and radiometric (11-bit, 2048-color) capabilities allow them to detect subtle differences in the biomass and structure of vegetation. The hydrological system and micro-topography can be precisely recreated at the airport thanks to the deployment of LiDAR lasers (Rapinel et *al*., 2019).

8.8. Temporal surveillance of a wetland

The temporal aspect is crucial for the hydrological characterization of wetlands. Analyzing a particular date provides information on the wetland at that specific time, but it does not reveal its dynamics. Various techniques for monitoring wetlands are available, including the use of time series classification, which involves analyzing a sequence of photographs without considering the specific dates. The classification of stack pixels is performed using controlled classification, utilizing field data for training purposes (Betbeder et *al*., 2014). Temporal consistency has been demonstrated to be valuable in assessing changes in water levels, as evidenced by several studies (Kim et *al*., 2014); Hong & Wdowinski, 2014).

Chapter II: Material and Methods

1. Geographical location of the study area

Algeria is situated to the north of the African continent, bounded by the Mediterranean Sea on its northern edge. It shares its borders with several neighboring countries, including Tunisia and Libya to the east, Mali and Niger to the south, and Morocco, Western Sahara, and Mauritania to the west. Algeria is divided into 58 states, which are administrative units with in its organizational framework. The geographic landscape of Algeria exhibits diverse topography. The northern region features undulating formations stretching from the west to the east due to the presence of a dual mountain barrier composed of the Atlas Tellian Mountains and the Saharan mountain range. These ranges encompass numerous prominent peaks, such as Dahrah, Worsinis, and Hindna, alongside tribal chains like Djordjura, Babur, and Pepans, as well as the Auris region. The central regions are cloaked with extensive forest cover, while the eastern areas are characterized by expansive plains. The southern reaches are predominantly desert, accounting for 84% of the country's total land area. Algeria boasts an expanse of around 2.38 million square kilometers, solidifying its status as the largest country in Africa in terms of land area. The geographical composition of Algeria spans a wide spectrum, ranging from the Mediterranean's northern coasts to the expansive desert landscapes in the southern reaches. The study discussed in the context was conducted in Algeria's wetland complex, as described in Table 1. Additionally, the research focused on 25 selected watersheds, as shown in Fig.II.1.

2. Topography

Algeria is characterized by its diverse terrain due to its diverse geographical characteristics, including mountains, plateaus, deserts, and plains. Below is a general description of its topography (Fig. II.2).

2.1. Mediterranean Coastal Chain

The Mediterranean coast spans an estimated 1,200 km and features mountainous terrain that descends sharply into the waters in certain areas, with hills and cliffs stretching along the coast. This region stands out with a distinctive Mediterranean climate featuring hot and dry summers, moderate winter and rainy seasons.

2.2. Atlas Tellien Mountains

These mountains form a parallel range along the northern coast of Algeria. Among the prominent peaks are the Djurdjura massif, the Ouarsenis massif, and the Aurès massif. Lush forests envelop these mountains, providing habitat for numerous species of animals and plants.

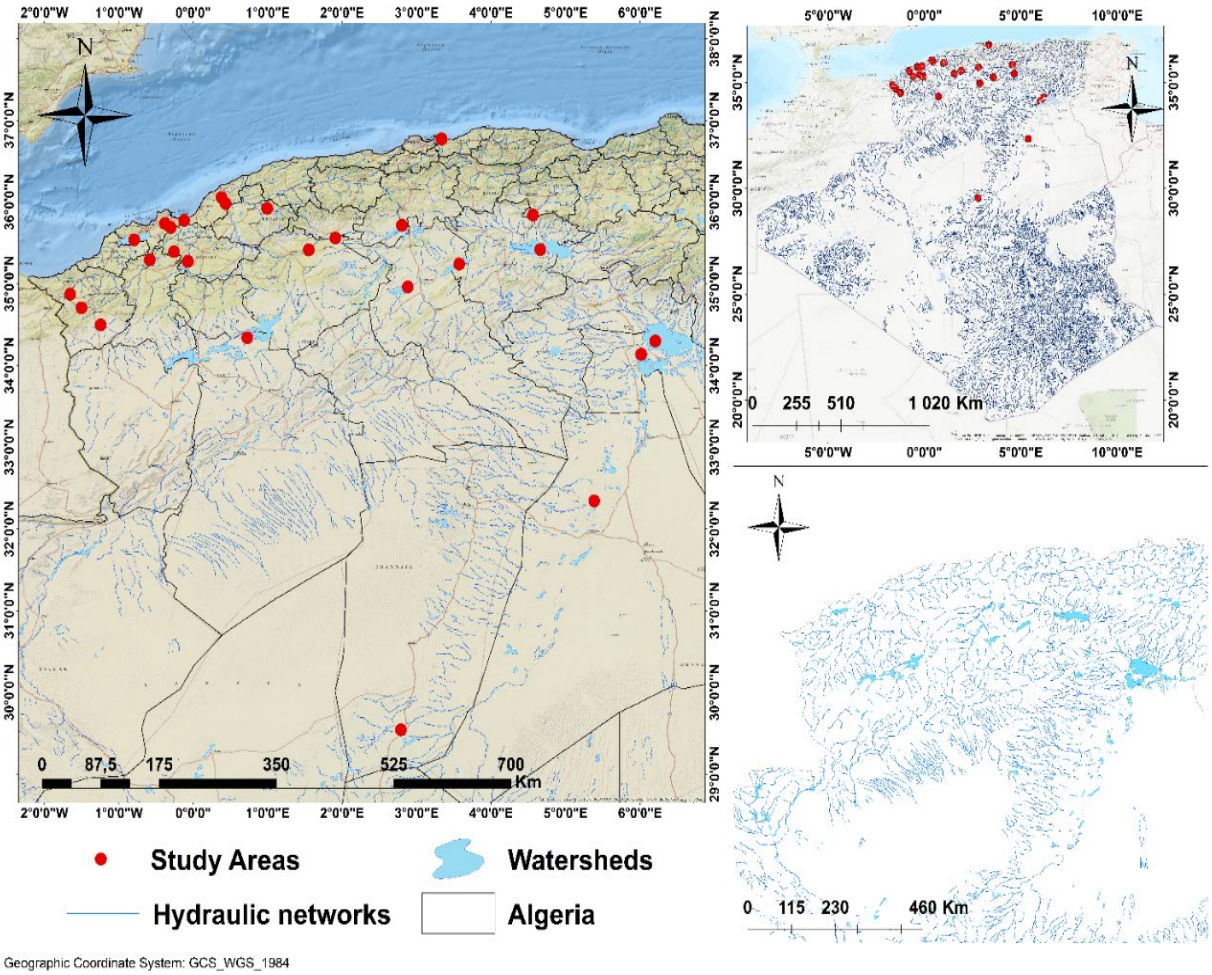

Figure II.1 Geographical and Hydrological Situation of the Study Area.

2.3. Highlands

Located south of the Atlas Thelin Mountains in the highlands, with altitudes generally ranging from 500 to 1200 meters, a vast area of plains and hills. It is an important agricultural area where cereals, legumes, and fruit trees are grown.

2.4. Sahara Desert

The Sahara is an important part of Algeria's reality, and is one of the largest and driest deserts in the world. Its landscapes include dunes, mountains such as stone plains and gravel plains, hummats, which are rocky plateaus, and separate mountains.

2.5. Chott and sebkha

In Algeria, there are saline and sandy regions, such as Chott Melrhir, which is a large Salt Lake, and Chott Ech Chergui, a sebkha (salt depression) located southeast.

Table II-1. Characteristics of the all-study areas

wetlands	Wetland's area (ha)	Hydrological cadency	Current status	Latitude (N)	Longitude (E), (W)	Climate
Macta Marsh	44,500	Permanent	Ramsar (2001)	35°38'52	00°06'16"W	Semi-arid
Great Sebkha	56,870	Permanent	Ramsar (2001)	35°31'29"	00°47'12"W	Semi-arid
Telamine Lake	2,399	Permanent	Ramsar (2004)	35°44'09"	00°22'57"W	Semi-arid
Arzew saline	5,778	Permanent	Ramsar (2004)	35°41'25"	00°19'22"W	Semi-arid
Boughezoul Dam	9,058	Permanent	Ramsar (2011)	35°41'55"	02°47'34"E	Semi-arid
Chott Zehrez Chergui	50,985	Permanent	Ramsar (2003)	35°12'59"	03°31'58"E	Arid
Chott Ech Chergui	855,500	Permanent	Ramsar (2001)	34°16'09"	00°33'25"E	Semi-arid
Dayet El Ferd	3,323	Permanent	Ramsar (2004)	34°29'55"	01°14'23"W	Semi-arid
Chott Zehrez Gharbi	52,200	Permanent	Ramsar (2003)	34°56"	02°48'06" E	Arid
Chott El Hodna	362,000	Permanent	Ramsar (2001)	35°26'04"	04°41'54" E	Arid
Chott Melghir	551,500	Irregular	Ramsar (2002)	34°10.631"	06°17.322"E	Arid
Beni Bahdel dam	54,630	Irregular	Not protected	34°42'42.70"	1° 30' 13.24" W	Semi-arid
Bougara dam	11,320	Irregular	Not protected	36° 32' 26"	3° 5' 7"E	Semi-arid
Boughrara dam	175,450	Irregular	Not protected	34°88'3854"	01°67'6169' W	Semi-arid
Bouhanifia dam	34,52	Irregular	Not protected	35°16'39"	0°3'36" W	Semi-arid
Chorfa dam	70,210	Irregular	Not protected	35° 25′ 55″	0° 14′ 43″W	Semi-arid
Cheliff Dam	50,000	Irregular	Not protected	35° 59′ 00″	0° 24′ 47″ W	Semi-arid
Chott Marouane	337,700	Irregular	IBA-Ramsar (2001)	34°02′433"	5°58′748"E	Hyper-arid
Dahmoni dam	39,520	Irregular	Not protected	35°41′67"	14°76′29"E	Semi-arid
Gargar dam	358,280	Irregular	Not protected	35°55′ 52″	0° 59′ 15″E	Semi-arid
Karrada dam	65,000	Irregular	Not protected	36°05′1162"	00°38′ 5519" E	Semi-arid
Ksob dam	22,72	Irregular	Not protected	35°58'05"	04°42'33"	Semi-arid
Sarno dam	21,250	Irregular	Not protected	35°29'94'99"	00°59'0768"W	Semi-arid
El Golea	18,947	Permanent	Ramsar (2004)	20°25'00'	02°95'	Hyper-arid
Chott Ain El Beida	6,853	Irregular	Ramsar (2004)	31°57'30'	31°59'2'	Hyper-arid

2.6. The Saharan Massif

The mountainous massif of Hoggar in the Sahara Desert represents one of the prominent symbolic elements in the Algerian desert landscape. The Hoggar Mountains hold a distinct position, with Mount Tahat standing as the highest peak in Algeria, soaring to an elevation of 2918 meters above sea level. Tassili n'Ajjer also stands as a unique landmark, distinguished by its remarkable rock formations and rock paintings that bear a history dating back thousands of years.

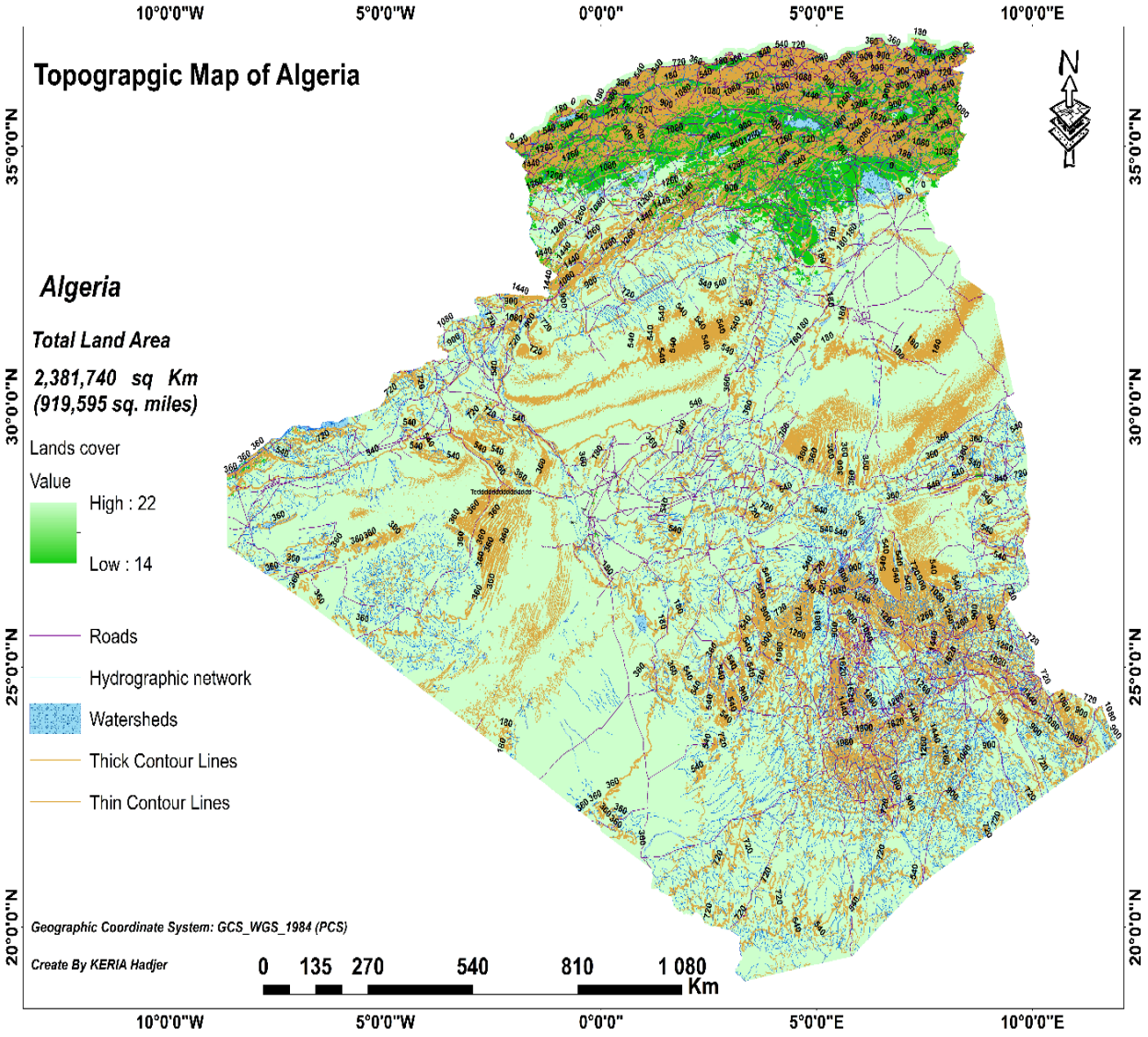

Figure II.2. Topographic map of Algeria (Create by H. KERIA, 2024).

3. Geology

Algeria's geology is distinguished by its remarkable diversity in geological formations, stemming from its intricate and diverse geological history, here is an overview of Algeria's main geological features (Fig. II.3).

3.1. Precambrian and Lower Paleozoic:

A significant portion of the Algerian desert consists of pre-Cambrian rock formations, including gneiss, schist, and granite. These formations are frequently interwoven with low-grade sedimentary sequences from ancient times, such as sandstone and carbonate deposits.

3.2. Middle and Upper Paleozoi

Ancient sedimentary deposits may be discovered in the Hogar and Ahagar mountains throughout the middle and higher stages of geological history. These formations are made up of a variety of materials, including solid rock, sand, and carbonate. These rocks document changes in environmental circumstances over that time period.

3.3. Mesozoic

The presence of marine sedimentary strata developed with the fracture of the continent "Pangea" characterizes the Mesozoic epoch in Algeria. Jurassic and Cretaceous geological formations may be found in numerous areas of the nation, including coastal mountain ranges and the south.

3.4. Tertiary

The third sedimentary strata, which are mostly composed of limestone and sandstone, are found across Algeria. The existence of the third sedimentary formation in the country's northern area, which overlooks the Mediterranean Sea, attests to its prior nautical history.

3.5. Quaternary

The quadripartite region is distinguished by contemporary deposits such as silphium, wind sand, and sand dunes in arid locations. This area is also known for its dry lakes and historic river cottages.

3.6. Tectonic

Algeria is distinguished by its location at the meeting point of the African and Eurasian plates, which has had a considerable impact on tectonic processes. As a result of the overlaying of these two plates, the Atlas Mountain range runs from the northeast to the southwest of the

nation. This intricate tectonic process resulted in the production of folds, fissures, and stress-exposed places.

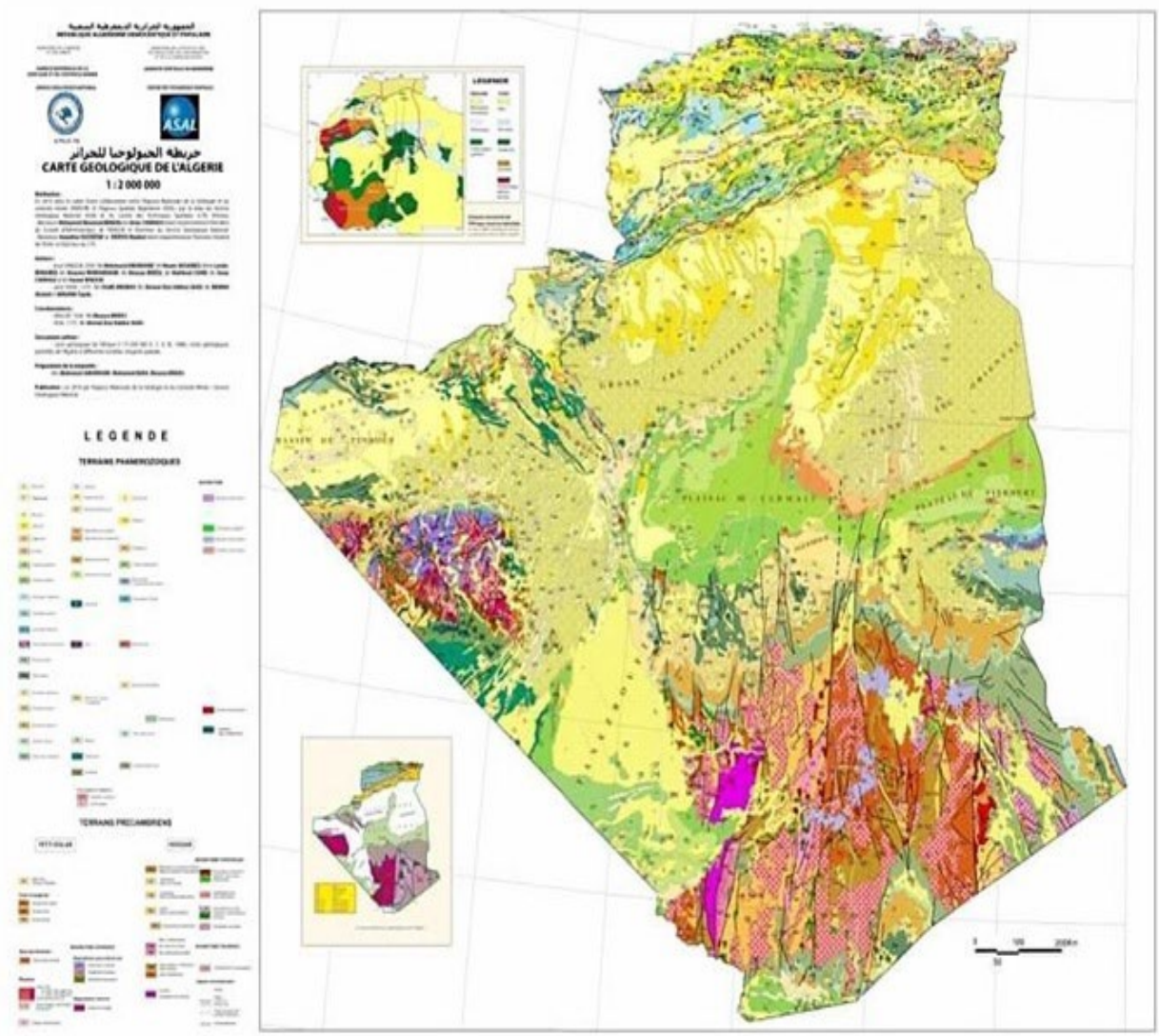

Figure II.3. Geologic map of Algeria.

4. Hydrology

Algeria is characterized by the existence of large water basins that play an important role in providing water and supporting ecosystems and the economy, according to the National Agency for Water Resources (NAWR), Algeria has 17 large watersheds. Here are some of the major watersheds in Algeria (Fig. II.3.):

Figure II.4. Major watersheds, Hydrographic Network, and Main Hydrographic Sub-basins of Algeria (Create by H. KERIA, 2024).

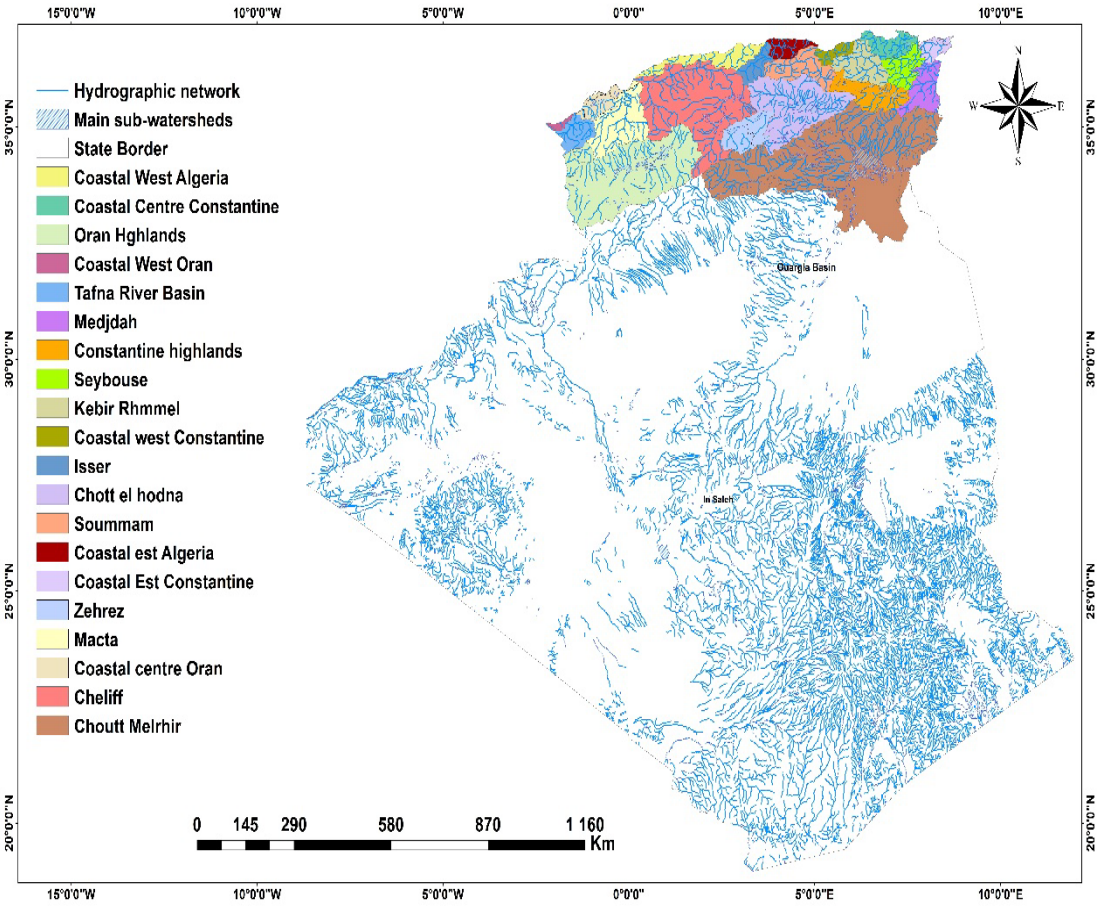

4.1. Chelif River Basin

The Chelif is the most important river in Algeria, as well as its longest and most significant. This river originates in the Atlas Mountains and flows across diverse terrain before emptying into the Mediterranean Sea. It is interwoven with a slew of tributaries that meet him over its course**.**

4.2. Seybouse River Basin

The Seybouse River flows from the Tell Atlas Mountains to the Mediterranean Sea in Annaba. It is a vital supply of water for the agricultural areas that surround it.

4.3. Moulouya River Basin

The Moulouya River is an important river in northern Algeria. This river rises in the Atlas Mountains and flows northeast through Algeria and Morocco. It continues to flow till it reaches the Mediterranean Sea.

4.4. Ouargla Basin

Which contains the Ouargla basin, is located in southern Algeria. This basin is critical for supplying water for irrigation and agricultural assistance in semi-arid and dry regions.

4.5. Tafna River Basin

Situated in northwest Algeria, the Tafna River flows through this basin, supplying water to the area. The riverbed runs all the way down to the Mediterranean Sea.

4.6. In Salah Aquifer

Despite not being a traditional river basin, the Salah aquifer is an important groundwater supply in the desert. This class provides people with essential and dependable water sources.

4.7. Hauts Plateaux Basin

The basin encompasses a considerable chunk of Algeria's plateau. This basin has seasonal rivers and valleys with erratic water flows. where they occur sporadically and rarely.

4.8. Hauts Plateaux Endorheic Basins

The basins are found in central Algeria and are distinguished by inland drainage networks. Water is captured in salty regions or shallow lakes rather than being released into the sea in these basins.

5. Climate

Climate is a pivotal factor in determining significant changes in the natural environment and biodiversity (Ramade, 2009). This includes the study of climatic variables in a specific location over extended periods of up to 30 years or more. These variables encompass temperatures, amounts of rainfall, wind speed, atmospheric pressure, humidity, and other weather conditions.

5.1. Rainfall

Precipitation is an environmental factor with far-reaching impacts. It plays a vital role in shaping ecosystems, influencing aquatic systems, and affecting the distribution and behavior of various organisms. The amount, frequency, intensity, and timing of precipitation events can influence everything from plant growth and animal behavior to water availability and the overall functioning of ecosystems (Medjerab & Henia, 2005).

Algeria displays significant temporal and spatial variations in rainfall across its diverse physiological regions. Analyzing the annual average rainfall map spanning from 1981 to 2022 (Figure II.5), it's evident that the distribution of rainfall across Algeria is notably

heterogeneous. In the northern regions of Algeria, the annual rainfall surpasses 600 mm on average. This substantial precipitation can be attributed, in part, to the geographical proximity to the Mediterranean coast. The coastal areas are influenced by maritime air masses that retain moisture, leading to increased precipitation in these regions. Conversely, the southern and desert regions of Algeria experience considerably lower levels of rainfall, often ranging from 150 mm to even less. This scarcity of rainfall can be attributed to the prevailing dry and desert climatic conditions that dominate these areas. These arid conditions significantly limit the occurrence of precipitation. Furthermore, discernible differences in rainfall exist between the upper and lower tributaries. The upper tributaries generally receive between 300-400 mm of annual rainfall. Conversely, the lower tributaries experience drier conditions with less than 300 mm of annual rainfall. The disparities in rainfall distribution play a pivotal role in shaping the quality of environments and ecosystems throughout various regions of Algeria. These variations notably impact the distribution of plant and animal species, as well as the availability of water resources. These factors collectively contribute to the intricate ecological makeup of Algeria's diverse landscapes.

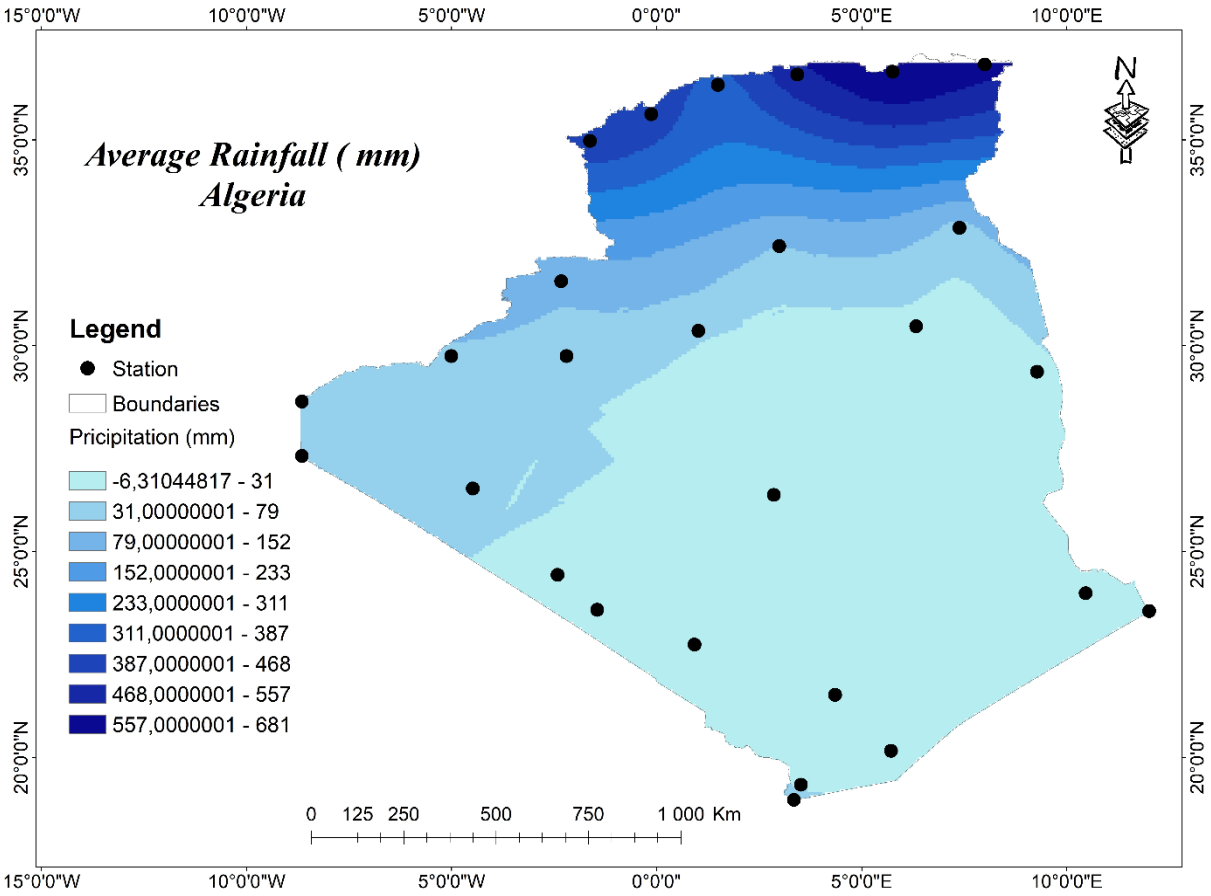

Figure II.5. Annual average rainfall map of Algeria (1981-2022) (Create by H. KERIA, 2024).

The evolution of average monthly rainfall in Algeria between 1981 and 2022 reveals that the highest amount of precipitation was recorded in December (28 mm), whereas the driest month was July (5 mm) (Figure II.6).

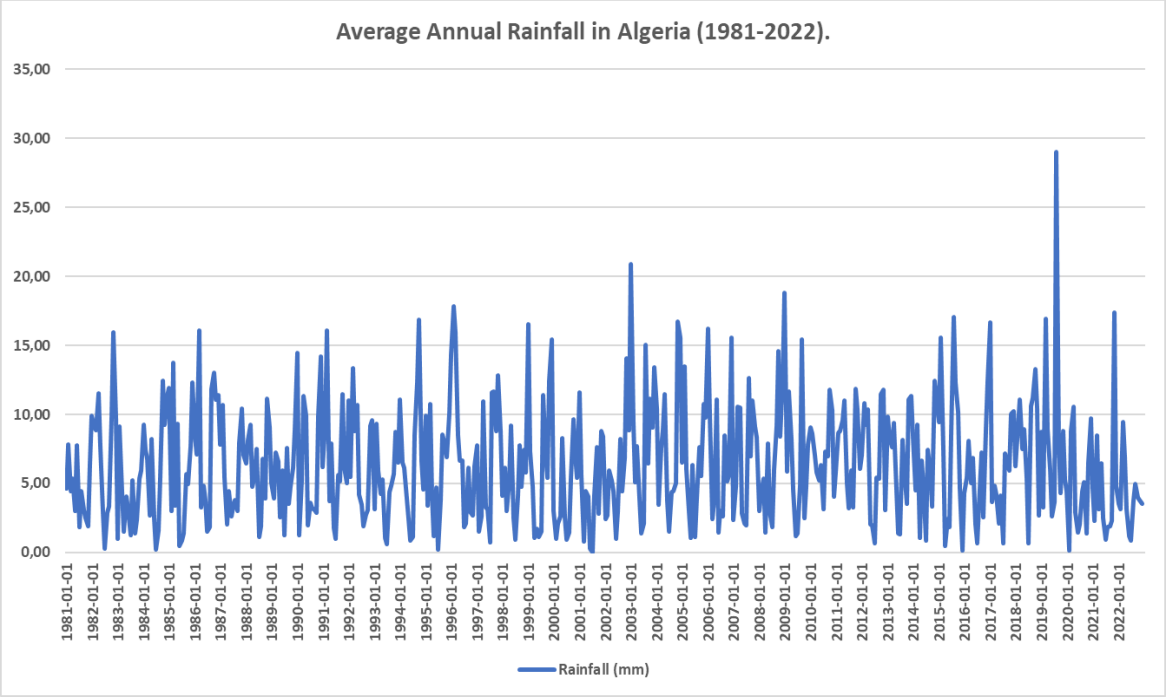

Figure II.6. Average monthly rainfall of Algeria (1981-2022).

6. Temperatures

Temperature is a vital element in determining the distribution and composition of plants and organisms in general. They are an essential environmental factor that significantly affects the biological growth and development of organisms (Babali, 2014). Plants and animals are directly affected by temperature changes, and their ability to adapt and survive is linked to the extent of such changes.

Temperatures play a crucial role in shaping the distinct environments of the Algiers region. Annual temperature variations exhibit a significant contrast between Algeria's northern and southern regions (Figure II.7). This divergence can be primarily attributed to the interplay of topography and geographical elevations. Elevated temperatures dominate the desert and southern areas, where average annual temperatures exceed 30°C. Conversely, the northern regions experience milder conditions, with average temperatures staying below 17 degrees Celsius. These temperature disparities between Algeria's desert and northern areas stem from the distinct climatic conditions each area embodies. The desert regions endure higher temperatures due to the arid and hot desert climate they possess. In contrast, the northern

regions enjoy a Mediterranean influence, leading to more temperate conditions. Across the various elevations, temperature differentials decrease as altitude rises. This phenomenon mirrors the broader global heat distribution trend, where mountainous terrains tend to be cooler than low-lying plains. This gradient in temperatures across different altitudes contributes to the diverse range of environments and ecosystems throughout Algeria. This diversity underscores the intricate environmental tapestry of the region, showcasing its richness and complexity.

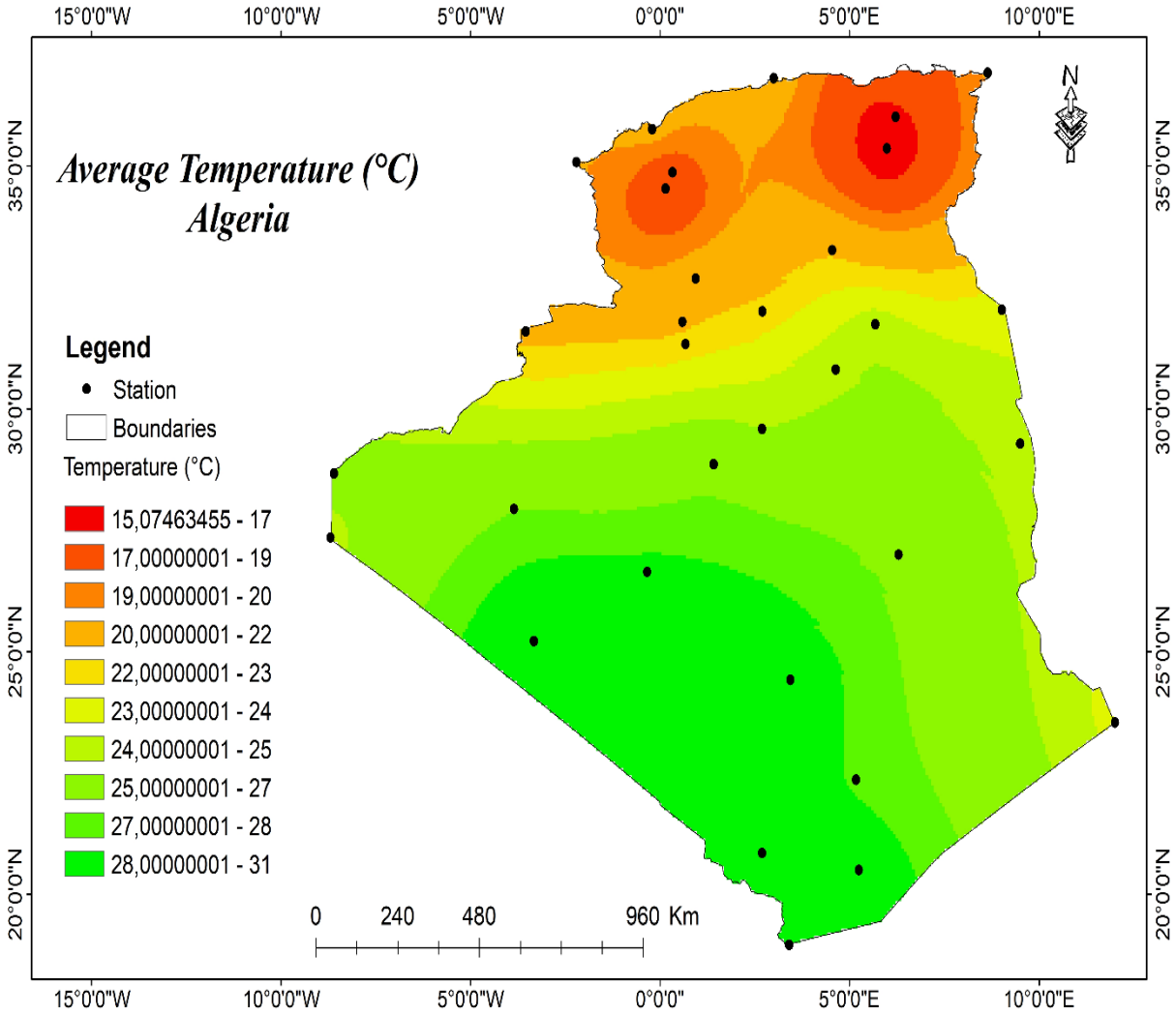

Figure II.7. Annual average Temperature map of Algeria (1981-2022) (Create by H. KERIA, 2024).

The average monthly temperatures in Algeria exhibit distinct seasonal variations. During the summer months of June to August, the highest temperatures can soar to around 41 °C. Conversely, the winter months of December and January experience the lowest temperatures, averaging around 19 °C (Figure. II.8).

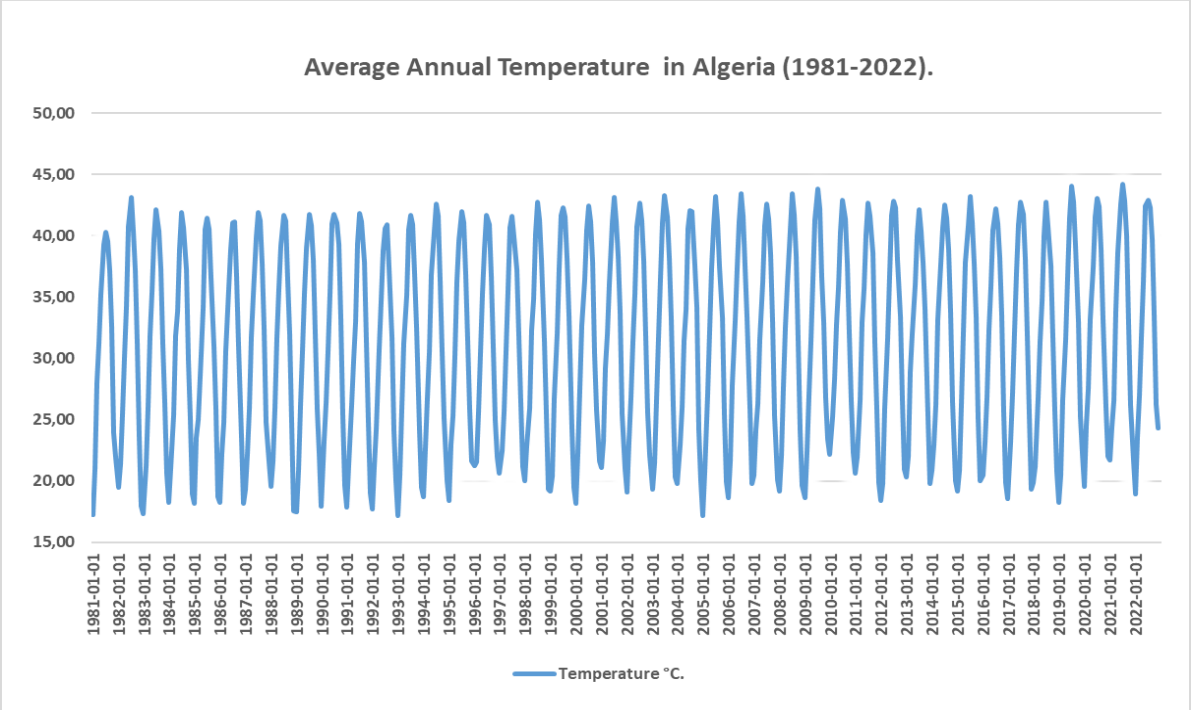

Figure II.8. Average monthly Temperature of Algeria (1981-2022).

6.1. Climate synthesis

Climate indicators are often categorized. In this study, we will calculate and discuss the most frequently utilized indicators. This categorization aims to offer a comprehensive perspective on the climate's condition.

6.2. The De Martonne index

The De Martonne (1926) drought index is employed to assess the severity of drought using the following relationship:

$$I = P/T + 10$$

Where: P, average annual rainfall (mm); T, Annual temperature (°C).

This aspect enables the specific examination of the correlation between climate and vegetation coverage, and facilitates the appropriate selection of the study station's location accordingly.

Table II-2. Aridity index values.

Index value	The type of climate
I <5	Hyper-arid

5<I <10	Arid
10<I <20	Semi-arid
20<I <30	Semi-wet
30< I <50	Wet

Algeria boasts a remarkable diversity of climates due to its expansive territorial expanse and varied topography. A multitude of climatic conditions can be discerned across the watershed analyzed in Table II.3.

Table II-3. The climate types for 26 study zones in Algeria

Wetland's	**T (°C)**	**P (mm)**	**I (mm/°C)**	**Climate type**
Macta Marsh	22,4	380	11,7284	Semi-arid
Great Sebkha	22,7	370	11,31498	Semi-arid
Telamine Lake	22,4	330	10,18519	Semi-arid
Reghaia Lake	21	600	19,35484	Semi-arid
Arzew saline	22,3	340	10,52632	Semi-arid
Boughezoul Dam	22,8	440	13,41463	Semi-arid
Chott Zehrez Chergui	23,74	260	7,705987	Arid
Chott Ech Chergui	23,53	344	10,25947	Semi-arid
Dayet El Ferd	22,7	440	13,45566	Semi-arid
Chott Zehrez Gharbi	23,5	289	8,626866	Arid
Chott El Hodna	25,74	280	7,83	Arid
Chott Melghir	30,6	160	3,940887	Arid
Beni Bahdel dam	22,4	440	13,58025	Semi-arid
Bougara dam	22,5	430	13,23077	Semi-arid
Boughrara dam	23,33	506	15,18152	Semi-arid
Bouhanifia dam	23,19	420	12,65441	Semi-arid
Chorfa dam	23,4	400	11,97605	Semi-arid
Cheliff Dam	22,5	427	13,13846	Semi-arid
Chott Marouane	30,72	127	3,118861	Hyper-arid
Dahmoni dam	22,31	447	13,83473	Semi-arid
Gargar dam	23,69	420	12,46661	Semi-arid

Karrada dam	23,32	427	12,81513	Semi-arid
Ksob dam	25,3	360	10,1983	Semi-arid
Sarno dam	22,86	406	12,35545	Semi-arid
El Golea	32,74	154	3,603182	Hyper-arid
Chott Ain El Beida	32,3	167	3,947991	Hyper-arid

Note: P: The average annual rainfall; T: The average annual temperature; I; aridity index.

6.3. The ombrothermic diagrams

Ombrothermic diagrams, developed by scientists Bagnouls and Gaussen, are utilized to depict temperature and precipitation data across the span of a year. This methodology is primarily employed to analyze and visualize climate fluctuations within specific regions. These diagrams serve the purpose of elucidating the correlation between temperature and rainfall over an extended period, thereby aiding in the identification of prolonged dry spells and periods of limited rainfall (Gaussen, 1954). Algeria experiences a distinct dry period from April to October (Figure II.9).

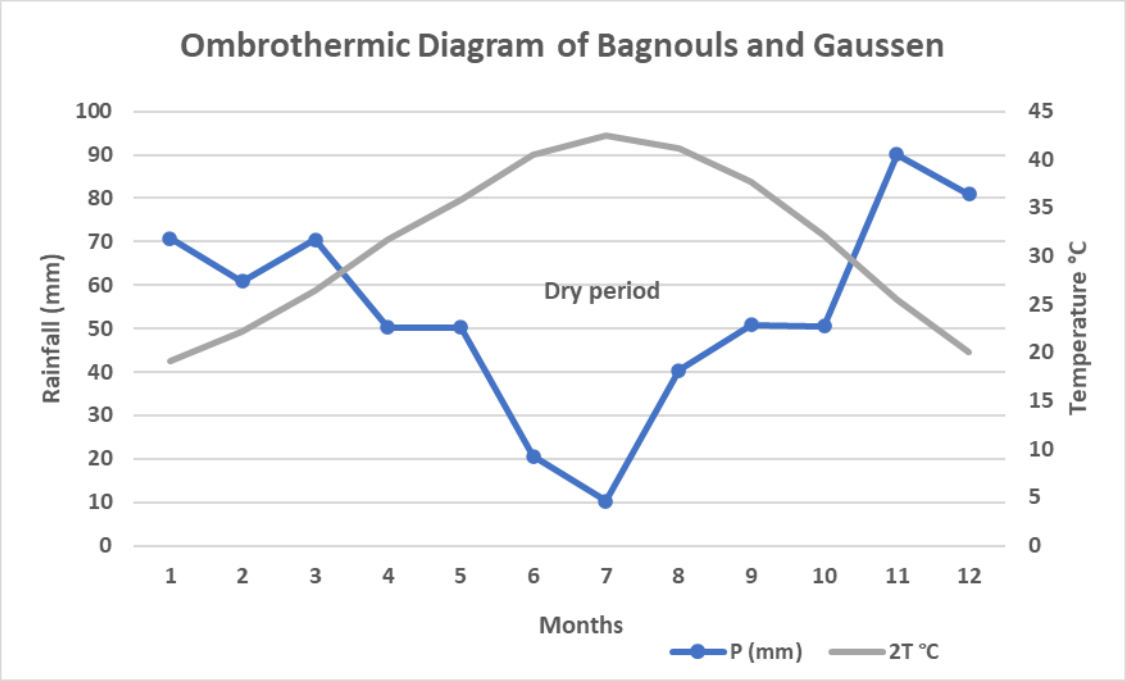

Figure II.9. Average monthly Temperature of Algeria (1981-2022).

7. Biodiversity in Algeria

Algeria boasts a country abundant in rich and diverse biodiversity, which has flourished due to the interplay of nature's variety, climate, and terrain.

7.1. Wildlife

7.1.1. Algerian freshwater fish

Algeria has a diverse range of freshwater fish, with 48 different species belonging to 15, these species were exchanged as part of the introduction of alien species into the aquatic ecosystem, posing a threat to native species. This process has the potential to disrupt the environmental balance of the water system, making native species vulnerable and endangered (Kara, 2012).

7.1.2. Reptiles

Algeria's reptilian population is characterized by a rich diversity, encompassing 80 species across various taxonomic groups. These include mock vipers (50 species of lizards), Avidians (25 species of snakes), and Chilonians (4 species of turtles), alongside the presence of amphibians known as amphisbaenians. Of these reptilian inhabitants, approximately 13 are endemic to the region, contributing to about 16% of the overall reptile species present in the Arab region of Morocco (MEER, 2016).

7.1.3. Aamphibian

Algeria harbors a diverse array of 14 distinct amphibian species. While these species are distributed throughout the country, the northern region stands out, particularly in its humid habitats like lakes, marshes, and rivers, where the richness of amphibian species is notably higher (Mateo et al, 2013).

7.1.4. Avian

Algeria boasts a rich and varied avian population, encompassing 281 species distributed among 55 distinct groups. Beyond these prevalent bird species, the country has also recorded 97 migratory bird species along with 6 rare occurrences. Notably, among these avian inhabitants, the kabeel (S. ledantii) hazelnut bird stands as Algeria's exclusive resident bird species. Additionally, there is a focused effort on monitoring predators and species associated with humid environments, reflecting the special attention devoted to their conservation (MEER, 2016).

7.1.5. Mammals

Algeria has been documented to have 111 mammal species. However, the International Union for Conservation of Nature (IUCN) lists 106 mammal species as well as two endemic mammals in its list. The disparity between the two figures can be attributed to differences in the classification and definition of these species (Ahmim, 2019).

7.1.6. Flora

Over time, we have noted an increase in the diversity of plants in Algeria, where the number of registered species increased from 3,741 in 2000 to 4,185 in 2014. These enrichments are attributed to multiple factors, such as improved data collection methods, heightened interest in biodiversity, and the discovery of new plant species. A classification analysis was carried out on the data, which revealed some 4,000 native plant species in Algeria. With the inclusion of the added species, the number reaches about 4,500. The present addendum highlights the importance of assessing biodiversity, focusing on both indigenous and additive species (Dobignard & Chatelain, 2010-2013).

Research indicates that Algeria boasts a remarkable count of approximately 290 species of endemic plants. Among the marine species, a categorization has been established, revealing distinct groups. Notably, the Benthos category stands out with a substantial species count of around 3,360, showcasing the diverse array of organisms residing in the seabed and shallow waters. In contrast, the planktonic category exhibits comparatively fewer species, totaling 457, highlighting the unique composition and ecological importance of these microscopic organisms in the marine ecosystem (Bakalem et al, 2014).

A comprehensive inventory of marine algae along the Algerian coast has revealed the presence of 468 identified species. Recent studies have contributed to this knowledge by discovering an additional 27 new species. Notably, among the identified species, 303 belong to the category of single-cell algae. These findings underscore the remarkable marine biodiversity in the region (MEER, 2016).

Furthermore, the list of benthic invertebrates has been expanded significantly, incorporating 597 distinct types of solid substrates that had not been previously documented. Of particular concern is the discovery of 13 endangered species within the Mediterranean region, specifically inhabiting the hard pillars along Algeria's coast. Moreover, numerous species that have symbiotic relationships with seaweed have been meticulously cataloged. These species are found either within the list of benthic invertebrates or among the stock of soft substrates. This comprehensive assessment highlights the intricate interplay of marine life within the Algerian coastal ecosystem (Grimes, 2003).

8. Material and Method

8.1. Sample collection and analysis

Sampling is the first phase in the analysis process; it affects the findings of the analysis and their subsequent interpretations, which in turn determine all the results obtained downstream. The sample needs to be representative, homogenous, and acquired without changing the water's physicochemical properties (Rodier et *al*., 2009). A summary of the sampling locations for 16 wetlands in Algeria was given by field surveys (Figure II.10).

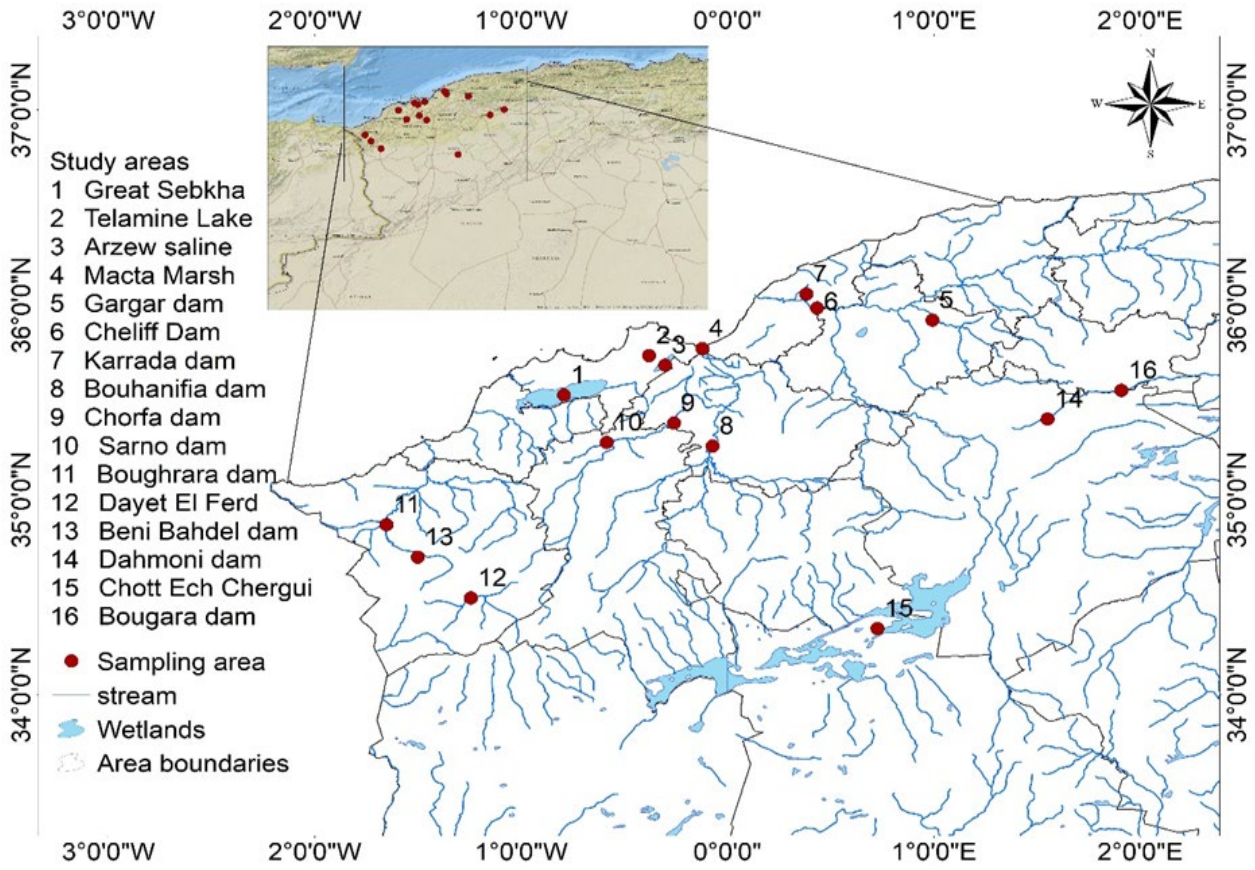

Figure II.10. A map of the study area's water systems, basin stations, sampling stations, and water supply.

8.2. Sampling equipment and preservation

For this study, we employed the following materials: plastic bottles; double-distilled water; cooling and ice box; an extendable filling stick (4-5 m); nitric acid (HNO3); and multifunctional HI 9811-5.

To inspect water quality, samples of surface water in wetlands were collected in February and March of 2022. 1.5 liters of water were filled in plastic bottles in each area. A thorough cleaning was carried out with double-distilled water to avoid any possible contamination. The

samples were stored at 4 ° C in the icebox to preserve the samples, and each sample was named to facilitate heavy metal detection, the water samples were acidified to maintain a pH below 2.0 using 0.5% nitric acid (HNO3). According to Sharma & Tyagi (2013) this procedure was implemented to prevent sediment accumulation, absorb minerals on the outer surface of the container, and reduce the biological activity of microorganisms.

8.3. Measuring Techniques and analyzing water

8.3.1. Physical-chemical analysis

8.3.1.1. Field measurements

Temperature (° C), pH, electrical conductivity (µ S/cm), Temperature (°C), pH, electrical conductivity (µ S/cm), salinity, and total dissolved substances (TDS) were measured directly on-site using HI 9811-5.

8.3.1.2. laboratory analysis

The samples were transferred to the laboratory of the Scientific and Technical Center for Physical and Chemical (CRAPC), in Algeria. For the analysis of heavy elements in water. To determine the exact quantities of these elements, Atomic Spectrum Absorption (AAS) was used.

8.4. Artificial Neural Network

ANN (Artificial Neural Network) is a method of analyzing nerves that rely on input data. Artificial Neural Networks (ANN) are widely employed in scientific research due to their capacity to effectively carry out classification and regression tasks on intricate non-linear datasets (Cho et *al*., 2011). This configuration comprises three crucial components: the input layer, the concealed layer, and the output layer. Hidden layers in neural networks often contain nodes with adjustable preferences and weights. Hidden layers are utilized to capture and extract the information included within anomalies. The activation function facilitates the transmission of data from one node to the subsequent layer, hence improving the linearity of the factor. Throughout this process, the weights and biases are adjusted to minimize discrepancies between anticipated outcomes, actual measurements, and probable forecasts. This approach is applicable in the field of environmental research as it offers forecasts for intricate datasets (Pyo et *al*., 2020).

Using ANN methodologies, this study analyzed the data for water samples. The complete dataset used for training and testing was divided into two parts: 70% for training the neural network and 30% for validation and testing. The training involved presenting full pattern pairs and adjusting connection weights using an iteration-based method in MATLAB Neural Network Toolbox. After training, the network was tested with data to verify the training efficiency. In ANN, this step is called "testing" because it ensures that the system has learned from specific patterns of application instead of memorizing a particular dataset. It is also known as a generalization set, which is used to validate the trained network's performance on unseen data. If we can generalize outputs from test datasets, then we can predict new data correctly. To avoid an overly complex model, the number of hidden layers was reduced to one, and the number of hidden neurons was set between 1 and 30. An early stopping approach was also used to prevent overfitting, where training is halted at the point of minimal error as shown in Figure II.11.

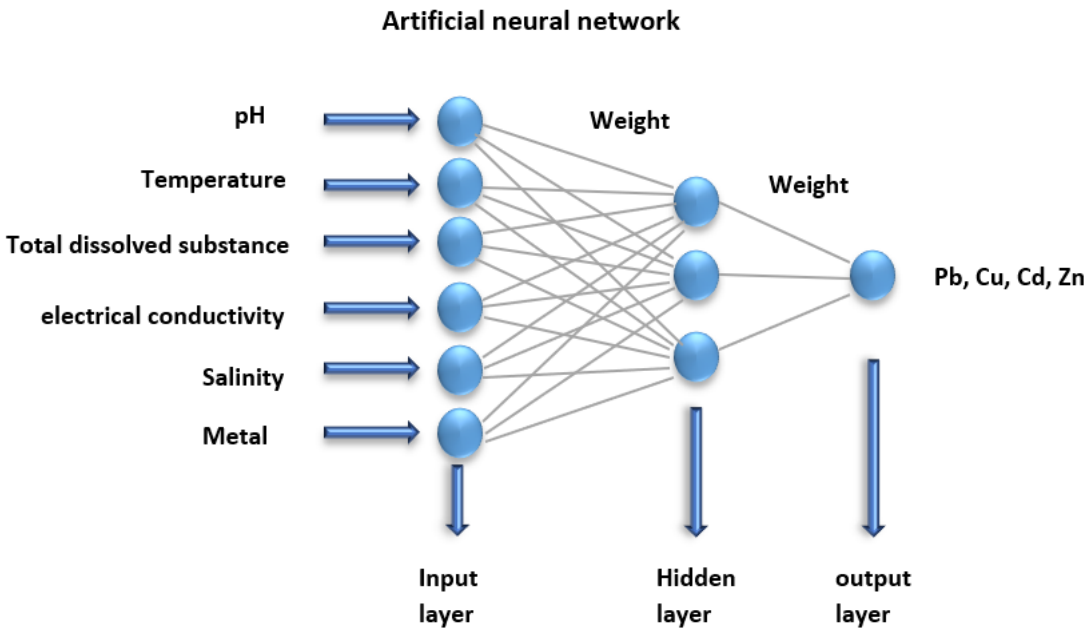

Figure II.11. Artificial neural network architecture.

9. Data and processing

9.1. Modis Dataset

The GEE platform (https://developers.google.com/earthengine/datasets/) was the source of the data that was analyzed for this research project (Gorelick et *al*, 2017). They state that the platform is equipped with powerful data processing capabilities and has a large variety of datasets about remote sensing. Data from MODIS and Landsat were included in the dataset

that was used for this investigation. Early in the year 2000, the Modis Group was utilized for the first time after it was initially introduced on the Terra platform on December 18th, 1999. As a result of its practical features, its photos have found widespread application across a wide variety of industries and products all around the world (Justice et *al*., 2002). According to Didan et *al*. (2015), the algorithms that Modis employs are responsible for determining the best pixel values at regular intervals of sixteen days. During our inquiry, we made use of Model 11A1, Model 09GA, and Model 13Q1 items. These datasets include essential information on a variety of factors, including the normalized difference vegetation index (NDVI), the enhanced vegetation index (EVI), the normalized difference water index (NDWI), and the land surface temperature (LST). Table II.4 contains data that details the sources and characteristics of the various datasets that were utilized in this investigation. Research conducted by Dubovy et al. (2015), Eckert et al. (2015), and Zhang and Ye (2020) has all demonstrated that the MODIS vegetation index is widely acknowledged throughout the scientific community. For this investigation, a total of 503 images of the NDVI were taken over the course of sixteen days, specifically during the growth season that lasted from 2000 to 2022. After that, the average value of all images taken with NDVI over the period of plant growth was computed in order to investigate the annual trends.

9.2. Landsat dataset

Since 1972, the Landsat satellite network has been collecting time-series photographs from all around the world. Both the United States Geological Survey (USGS) and the National Aeronautics and Space Administration (NASA) are in charge of supervising the project, and the photos have been freely available to the public since 2008 (Woodcock et *al*., 2008). Landsat missions provide coverage of the whole planet with a high degree of spatial precision, and they return to the area every 16 days. GEE is responsible for providing corrected Landsat surface reflectance for the Landsat Thematic Mapper (TM) and the Enhanced Thematic Mapper Plus (ETM+), in addition to cloud, cloud shadow, surrounding cloud, land, and water masks. With a resolution of thirty meters and a repetition cycle of sixteen days, the Landsat archives provide accuracy that is uniform throughout the globe in terms of both geography and time (Irons et al., 2012; Claverie et *al*., 2015). According to the description provided by Gorelick et al. (2017), all of the Landsat data were collected and analyzed by utilizing the cloud-based platform known as GEE (Google Earth Engine). We have produced a historical series of cloudless photographs, beginning in January and ending in December, beginning in 1981 and continuing until 2021. Validation and adjustments have been made to Landsat data sets 5, 7, and 8 to take

into account surface reflection. This was accomplished by the use of the "USGS Landsat Surface Reflectance Tier 1" technique. According to Zhu et *al*. (2015) and Kennedy et al. (2018), the datasets that have been supplied include modified atmospheric data, cloud masks, water, shadows, and snow. These datasets were developed with the help of CFMASK. LandTrendr is a temporal classification approach that was developed in the GEE. We used it to identify and analyze changes in the vegetation. Following Kennedy et *al*. (2010), LandTrendr is a tool that is capable of recognizing short-term occurrences and assisting in the recognition of long-term patterns. It does this by separating the various components of the spectrum by using certain satellite ranges or a spectrum indicator. The Normalized Difference Vegetation Index (NDVI) value that was derived from Landsat data was employed continuously throughout the year, and throughout forty years, changes were noticed at a low resolution of thirty meters.

Table II-4. Exploring Essential Datasets: An in-depth analysis in the research.

Data Products	Data Types	Spatial Resolution	Temporal resolution	Spatial coverage	Duration
Landsat 5/7/8 ETM+	NDVI/NDMI	30m	16 day	Globale	1981-2021
MOD09GA	NDWI	250m	16 day	Global	2000-2022
MOD13Q1	NDVI/EVI	250m	16 day	Global	2000-2022
MOD11A1	LST	1000m	8 day	Global	2000-2022

9.3. Climate dataset

Each of the temperature data and precipitation data that we utilize comes from CFRS and CHIRPS, respectively. Both sets of data are gathered daily and have an accuracy of 0.05 degrees. When it comes to data, both of these are regarded as occurring every day. All of these datasets have been included in the Climate Engine's (http://climateengine.org) databases, which have been updated to reflect the new information. The use of CHIRPS data proved to be beneficial when it came to the computation of long-term average rainfall that included several years and growth seasons. In addition to enabling the monitoring of drought conditions, this made it possible to investigate patterns that had developed over time. The multi-annual and seasonal average temperatures (1/5 and 3/10 degrees) from the Climate Forecast System Reanalysis (CFSR) datasets were gathered and reanalyzed with the use of NDVI data extending from 1981 to 2021. This was done to better understand the climate. These datasets were provided by the National Center for Environmental Prediction (NCEP).

It has been discovered via the examination of rainfall, temperature, and drought data obtained at Reghaia Lake between the years 2000 and 2022 that the study region is characterized by considerable climatic differences. In previous studies, the analysis of temporal and geographical changes in climate was dependent on data acquired at particular places. This limited the precision of the analysis when it came to capturing spatial fluctuations. Several examinations have shown that this dataset has a high degree of accuracy.

9.4. SPEI Drought Index

The Standardized Precipitation Evapotranspiration Index (SPEI) is a helpful instrument that may be used in dry and semi-arid areas to recognize drought and track the consequences of climate change. Vicente-Serrano was the one who came up with the idea of including potential evaporation in the Standardized Precipitation Index (SPI) (Zhao et *al*., 2018; Vicente-Serrano et *al*., 2013). As a result of the inconsistency that exists in the geographical distribution of relative humidity, wind speed, and solar radiation, the Thornthwaite method was used to predict the possibility of evaporation. Thornthwaite et al. (1948) and Xu et *al*. (2018) state that this approach requires just monthly average temperature data to function properly. The Standardized Precipitation-Evapotranspiration Index (SPEI) has been shown to have a significant relationship with changes in the development patterns of vegetation over the past three months, according to research carried out by Vicente-Serrano and colleagues (2013). In the same way that earlier research (Zhao et *al*., 2018; Wang et *al*., 2022) has investigated droughts, this study employed the Standardized Precipitation Evapotranspiration Index (SPEI) to explore droughts. Five different categories of the SPEI drought index are shown in this location's Table II.5.

Table II-5. Five-grade category of the drought index.

Drought Class	SPEI Value
Normal	$-1 < \text{SPEI}$
Moderate drought	$-1.5 < \text{SPEI} \leq -1$
Severe drought	$-2 < \text{SPEI} \leq -1.5$
Extreme drought	$-2.5 < \text{SPEI} \leq -2$
Exceptional drought	$\text{SPEI} \leq 3$

10. Methods

10.1. Analyzing the Dynamics: Regression Study on Long-Term Vegetation Index Trends

NDVI is an important statistic that is used to evaluate the differences in both visible and near-infrared light that are present inside greenery. It is possible to do this by computing the disparity among these spectral ranges within the range of frequency periods that have been defined and then normalizing that difference throughout the whole spectrum. After deducting the spectrum reflectance in the visible spectrum (VIS) from the spectra reflectance in the near-infrared band (NIR), the NDVI is determined by multiplying the result by the total of the spectral reflectances in the transparent band and the near-infrared band taken together. NDVI trends for every pixel were subjected to regression analysis for the periods 1981–2021 and 2000–2022. These patterns have been widely used to assess alterations and the development of vegetation (Tucker et *al*., 1986; Myneni et *al*., 1997; Nemani et *al*., 2003; Piao et *al*., 2011; Donohue et *al*., 2012). Based on the findings of Hu et al. (2019), the formula that was applied for linear analysis is as follows:

$$slope = \frac{n \times \sum_{i=1}^{n} i \times NDVI_I - \sum_{i=1}^{n} i \sum_{i=1}^{n} NDVI_i}{n \times \sum_{i=1}^{n} i^2 - (\sum_{i=1}^{n} i)^2} \quad (1)$$

'Slope' is a word that represents the rate of change of NDVI concerning time. In the equation that has been presented, the variable $NDVI_i$is used to indicate the calculated NDVI level for the *i*-th year using the formula that has been provided. Throughout the evaluation period, the total number of years that were taken into consideration is denoted by the value of 'n'. The 'Slope' is a statistic that is used to evaluate the pace at which the development of vegetation varies over longer periods. When the Slope > 0, it indicates that there is a link between the growth of vegetation and the reduction of plant coverage. The presence of a slope of 0 indicates that the development of vegetation in the area is both consistent and unbroken. In contrast, when the slope > 0, it signifies a decrease in the activity of plant growth occurring in conjunction with an increase in the covering of vegetation (Zhe & Zhang, 2021).

10.2. Normalization data

Min-max normalization was used to scale the data between 0 and 1 to evaluate the temporal fluctuations of NDVI, rainfall, and temperature over a variety of sites. Luo et *al*. (2020) have indicated that the following formulas are the ones that should be used for this normalization:

$$x' = \frac{x - x_{min}}{x_{max} - x_{min}} \quad (2)$$

where the number x indicates the real value, whereas the terms x_{min} and x_{max} refer to the values that are the lowest and highest in the collection, respectively. At the same time, the value x' indicates the normalized value.

10.3. Investigating Correlations Between Vegetation Index and Climatic Variations

The following is a description of how we estimated the connection between temperature, rainfall, and NDVI in order to evaluate the reactions of vegetation to the various climatic factors (Bhuyan et *al*., 2017):

$$r_k(x,y) = \frac{\sum_{i=1}^{n-k}[(x_i-\bar{x})\times(y_i-\overline{y})]}{\sqrt{\sum_{i=1}^{n-k}(x_i-\bar{x}\times\sum_{i=1}^{n-k}(y_i-\bar{y}}} \quad (3)$$

There is a series of relationship analyses that are carried out among the NDVI with the weather conditions, which are represented by the symbol $r_k\ (x,y)$. In this context, the variable n denotes the length of the chain, x_i stands for the NDVI time series, k is the amount of time that has passed, and y_{i+1}denotes the temperature or rainfall data series with a period of lag of k.

Prior research indicates that climatic and plant changes often occur over months. Seasonal variations in climate and vegetation may be used to determine time discrepancies or delays. Climate elements like temperatures and precipitation directly affect vegetation, which then impacts the timing of plant growth and seasonal variations (Peng et *al*., 2019; Zhe & Zhang, 2021). Therefore, the delays or changes in the timing of certain seasons may be analyzed for patterns that are deemed typical. Significant deviations in the typical weather patterns might result in a three-month delay in the growing season, significantly impacting the environment's operations. Researchers may assess the connection between climate change and vegetation and determine how climate change affects plant environments throughout time (Chen et *al*., 2014; Wu et *al*., 2015). Using the available information on vegetation and climate change may help achieve this.

10.4. Exploring Various Remote Sensing Indices for Environmental Monitoring

The NDWI was used to evaluate the hydrological condition of the wetland areas. For the objective of enhancing the detectability and distinctiveness of open water features in remotely acquired photos, this index was developed with a particular goal in mind. The values of the NDWI vary from -1 to 1. The presence of water bodies is indicated by NDWI values that are

more than zero, while the absence of water is indicated by values that are less than zero. To calculate NDWI, the following procedure is used (McFeeters, 1996):

$$NDWI = \frac{NIR-RED}{NIR+RED} \quad (4)$$

This research recognizes the limits in the geographic resolution of MODIS LST data, which inhibits their accuracy for ecological evaluation and tracking of dynamic land use changes (Chen et *al*., 2006). Despite this restriction, it is possible that spatial resolution limits will not have a substantial influence on the links between land consumption and changes over time. As a result, these products may still be applied successfully to monitor precise fluctuations in land usage over time. There is a technology that has been created to improve the spatial resolution of quick measurements to solve the problem of restricted spatial resolution. A high-accuracy spatial spectrometer is included in the system to accomplish this goal. The fundamental idea is that the quantitative spectral index is stable regardless of the circumstances that are being considered. This consistency makes it possible to use the correlation that is determined from sensors with limited spatial detail to LST outputs that have a high spatial resolution. The formula for the particular computation is as follows: (Wang et *al*., 2014; Hua et *al*., 2018).

$$T_{h=}f(SI_h) + \Delta T_C \quad (5)$$

$$\Delta T_C = T_c - f(SI_C) \quad (6)$$

Here, the spectral indexes SI_C and SI_h represent low- and great-resolution spectrum indices, respectively. At the same time, T_c and T_h represents the LST at low and high resolutions, respectively (Xu et *al*, 2021).

The EVI index takes into consideration specific temperature changes and background noise that are connected with plant canopies. It also demonstrates a higher degree of responsiveness in places that are defined by an abundance of greenery. The calculation of the indicator takes into account the "L" value, which is used to compensate for the backdrop of the covering, the "C" values, which are used as variables to calculate the resistance to air, and values from the blue spectra. Generally speaking, this upgrade makes it possible to compute the indicator by contrasting the R and NIR readings while simultaneously lowering the saturation, background noise, and noise from the environment levels. The components C1 and C2 are resistant to the dispersion of tiny solids or liquids in the air. They can withstand this dispersion. They make use of the blue section of the electromagnetic spectrum to mitigate the negative effects that are caused by aerosols that are located in the red part of the spectrum. Additionally, the symbol ρ

represents the reflection of the air- or partly atmospheric-adjusted surface, while the symbol L represents the background change of the canopy. This change encompasses the movement of nonlinear light as well as changes in spectral ranges between near-infrared and near-infrared throughout the canopy. Several algorithmic transactions are employed in EVI. These transactions include L = 1, C1 = 6, C2 = 7.5, and G (profit factor) = 2.5 (Huete et *al*., 1994, 1997). The formula is as follows:

$$EVI = G\frac{\rho_{NIR}-\rho_{RED}}{\rho_{NIR}+C_1\times\rho_{RED}-C_2\times\rho_{BLUE}+L} \quad (7)$$

A measure that was developed explicitly for the amount of moisture that is present in vegetation is known as NDMI. It is typically determined by dividing the total number of observations taken in the near-infrared (NIR) and short-wave infrared (SWIR) wavelength ranges. SWIR is an abbreviation for the short-wave infrared section of the electromagnetic field. This index offers useful insights into the moisture state of plants, with greater NDMI values often suggesting higher moisture levels that are present. Because the NIR and SWIR bands are sensitive to changes in the volume of water of plants, the NDMI is a helpful instrument for tracking and evaluating moisture levels in a variety of natural contexts (Vermote et *al*., 2016).

$$NDMI = \frac{NIR-SWIR1}{NIR+SWIR1} \quad (8)$$

10.5. Man-Kendall trend analysis

MK is an important statistical analysis used to estimate the direction of the variable, both increasing and decreasing over time (Man, 1945; Kendall, 1975). MK analysis is based on the calculation of rated regression Sen's slope (Sen, 1968). This tendency assesses the direction of time chains without a specific distribution assumption, making it important in the presence of extreme and abnormal values (Tiberi et *al*., 2011; Suryavanshi et *al*., 2014; Pingale et *al*., 2016; Gajbhiye et *al*., 2016; Kumar et *al*., 2017). Calculates the MK analysis as follows:

$$S = \sum_{i=1}^{n-1}\sum_{j=i+1}^{n}\mathrm{sgn}(y_j - y_i) \quad (9)$$

Where n represents the value of the variable, y_j and y_i are variables in the time series at the values at time j and i, respectively. S represents the type of trend (increasing or decreasing). Calculating the value of S is necessary to evaluate the value of MK, which is as follows:

$$t = S/(n(n-1)/2) \quad (10)$$

10.6. SPEI drought index

To determine the SPEI, the Thornthwaite technique was used. This approach makes use of the monthly difference between PET and precipitation (Thornthwaite, 1948). After being computed in the following manner:

$$D_i = P_i - PET_i \quad (11)$$

where D values are compiled over a variety of time scales:

$$D_n^K = \sum_{i=1}^{K-1}(P_{n-1} - PET_{n-1}), n \geq k \quad (12)$$

Listed below are the factors that are included in the equation: In this equation, P stands for precipitation, PET stands for potential evapotranspiration that is calculated using the Thorthwaite technique, k stands for the number of months, and n stands for the aggregate time and the calculation number, respectively. When calculating D_n^k, it is necessary to take into account the climatic equilibrium for the nth month, in addition to the water content for the k-1 months that came before it, The three-month SPEI (McKee et *al*.,1993; Potopová et *al*.,2015).

10.7. Assessment of surface water quality in wetlands

10.7.1. Metal Assessment Index

Heavy Metal Evaluation Index (HEI) is commonly used to investigate the extent to which water systems are contaminated by heavy metals. This indicator is calculated according to Sahoo & Swain as follows:

$$HEI = \sum_{i=1}^{n} \frac{H_c}{H_{Mac}} \quad (13)$$

Where the criteria for H_{Mac} and H_c are set for the i-th variable and the greater limit of the dependable concentration, respectively.

10.7.2. Heavy Metal Pollution Index (HPI)

A variety of statistics were used to illustrate the data to facilitate better comprehension The heavy metal pollution index (HPI), is a grading system that illustrates the cumulative impact of several metals on the health of water resources (Zhang et *al*., 2021). HPI is calculated by the following equation:

$$HPI = \frac{\sum_{i=1}^{n} W_i Q_i}{W_i} \quad (14)$$

where Wi is the unit weight of the ith parameter, Qi is the subindex of the ith parameter and n is the number of parameters considered. Value Qi is determined by the equation that follows:

$$Q_i = \sum_{i=1}^{n} \frac{(M_i - I_i)}{(S_i - I_i)} \times 100 \qquad (15)$$

where Mi is the monitored value of the heavy metal of the ith parameter, Ii is the ideal value of the ith parameter, and Si is the standard value of the ith parameter.

10.8. Pearson correlation

The Pearson correlation assesses the linear association among multiple combinations of parameters. This indicates a strong correlation between the factors (Joshi et al., 2009). A linear connection indicates that if one variable increases, the other variable increases or declines in a straight-line manner. The Pearson correlation coefficient quantifies the extent of a linear association between two sets of data, with possible values ranging from -1 to +1. A correlation coefficient value approaching +1 (positive correlation) suggests that one variable exhibits a nearly linear increase when the other variable grows. Conversely, a correlation value near -1 indicates that one variable exhibits a nearly linear decrease while the other variable shows a nearly linear increase. Values approaching zero imply the absence of both linear and non-linear correlations between variables (Mudgal et *al*., 2009).

10.9. Statistical Analysis

Principal Component Analysis (PCA) is a statistical technique that utilizes comparisons of persons or data (in rows) and quantitative parameters (in columns) to create graphical illustrations of these individuals and factors. The CPA is utilized to enhance the visualization of intricate connections among measured variables due to its robust capacity for compressing and synthesizing information (Sharma et al., 2020).

This study utilized XLSTAT 2024, for statistical analysis. The relationship between different elements was assessed through Pearson Correlation Analysis. Additionally, Hierarchical Clustering Analysis (HCA) was employed to group sample points based on their metal concentrations. Variables were divided into clusters using variable distances, employing the intergroup linkage method and the square Euclidean distance, known for its stability in systematic clustering analysis. Principal Component Analysis (PCA) was also conducted to determine how much variance each variable explains after dimension reduction. PCA explored the relationship between elements by extracting potential factors and simulating similarity in the distribution of heavy metal sources [15].

Chapter III: Results and Discussion

1. Assessment of the long-term effects of climate on vegetation in 25 watersheds in dry and semi-dry areas, Algeria

1.1. The temporal-spatial distributions for NDVI during the past 40 years

The NDVI results, spanning the extensive period from 1981 to 2021 and depicted in Fig. III.1, unveil marked spatial variations that provide crucial insights into the changing vegetation dynamics across the study regions. Approximately 59.6% of the overall greenery area exhibited an NDVI level below 0.45, indicative of relatively lower vegetation density. Notable areas with consistently low NDVI values include Chott Ech Chergui, Arzew Saline, Chott Melghir, and Chott Merouane. In contrast, regions with distributed NDVI values greater than 0.45 accounted for 40.4% of the total, showcasing a relatively modest increase. Particularly noteworthy are areas such as Macta Swamp, Chott Sebkha, Sarno Dam, Chott Zehrez Chergui, and Karrada Dam, which exhibited the highest NDVI values.

However, a concerning trend emerges as negative NDVI values dominate the watersheds, as depicted in Fig. III.1, indicating areas with limited or no vegetation cover. Moreover, a noticeable reduction in the airspace of water sources, with some disappearing over time, raises concerns about the depletion of crucial water bodies. Remarkably, the volume of surface water bodies has consistently decreased across all regions over the years. This decrease can be linked to human-induced factors such as land use, factories near these basins, chemical leakage, and infrastructure projects, coupled with the expanding footprint of urbanization. These human-induced changes have significantly contributed to a decline in vegetation, leading to a notable shift in the NDVI ratio over the past four decades.

The observed distribution pattern of NDVI trends in each location underscores a robust correlation among vegetation indices, elevation, and water supply. Spatial differences in NDVI across all study regions remained relatively tight, with slope values ranging from 0.0005 to 0.04 during the study period (1981–2022). This tight correlation emphasizes the interconnected nature of vegetation patterns, elevation variations, and water availability, portraying a comprehensive picture of the complex environmental dynamics shaping these regions. As the spatial patterns of NDVI continue to evolve, understanding these intricate relationships becomes imperative for informed conservation and land management strategies in the face of ongoing environmental changes.

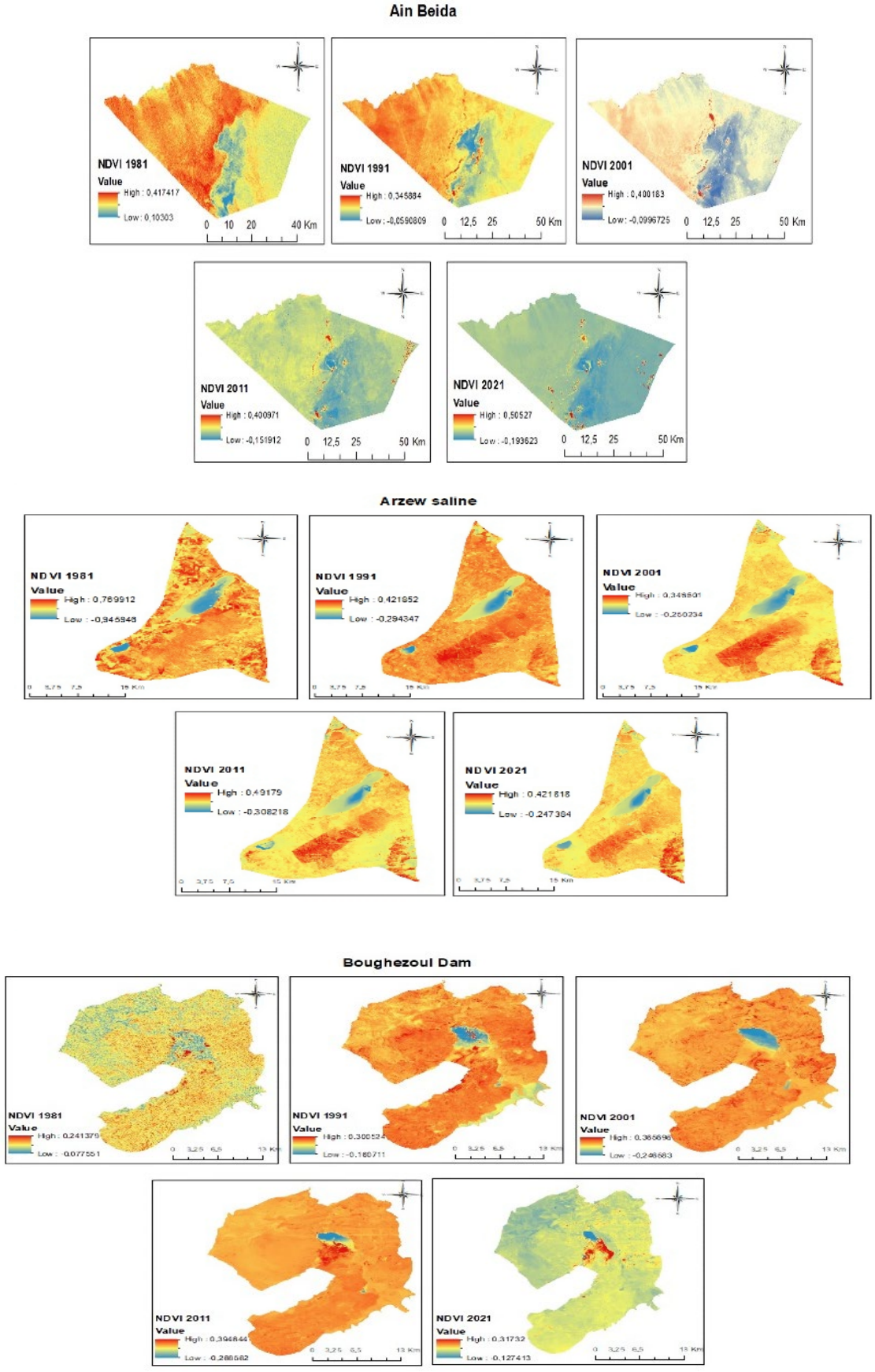

Figure III.1. Patterns of NDVI change trends in 25 basins in Algeria from 1981 to 2021, with yearly average NDVI change.

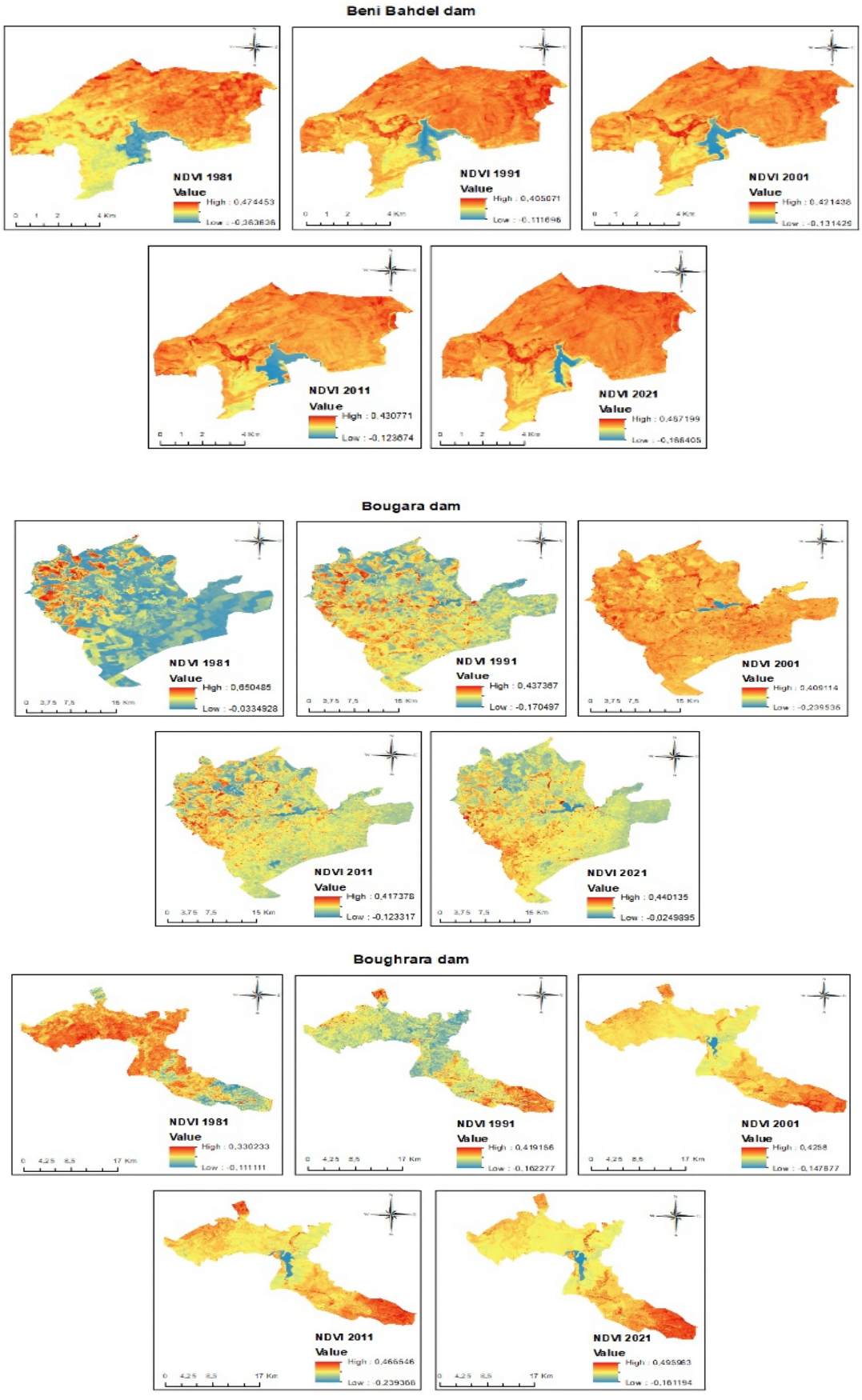

Figure III.1. (continued)

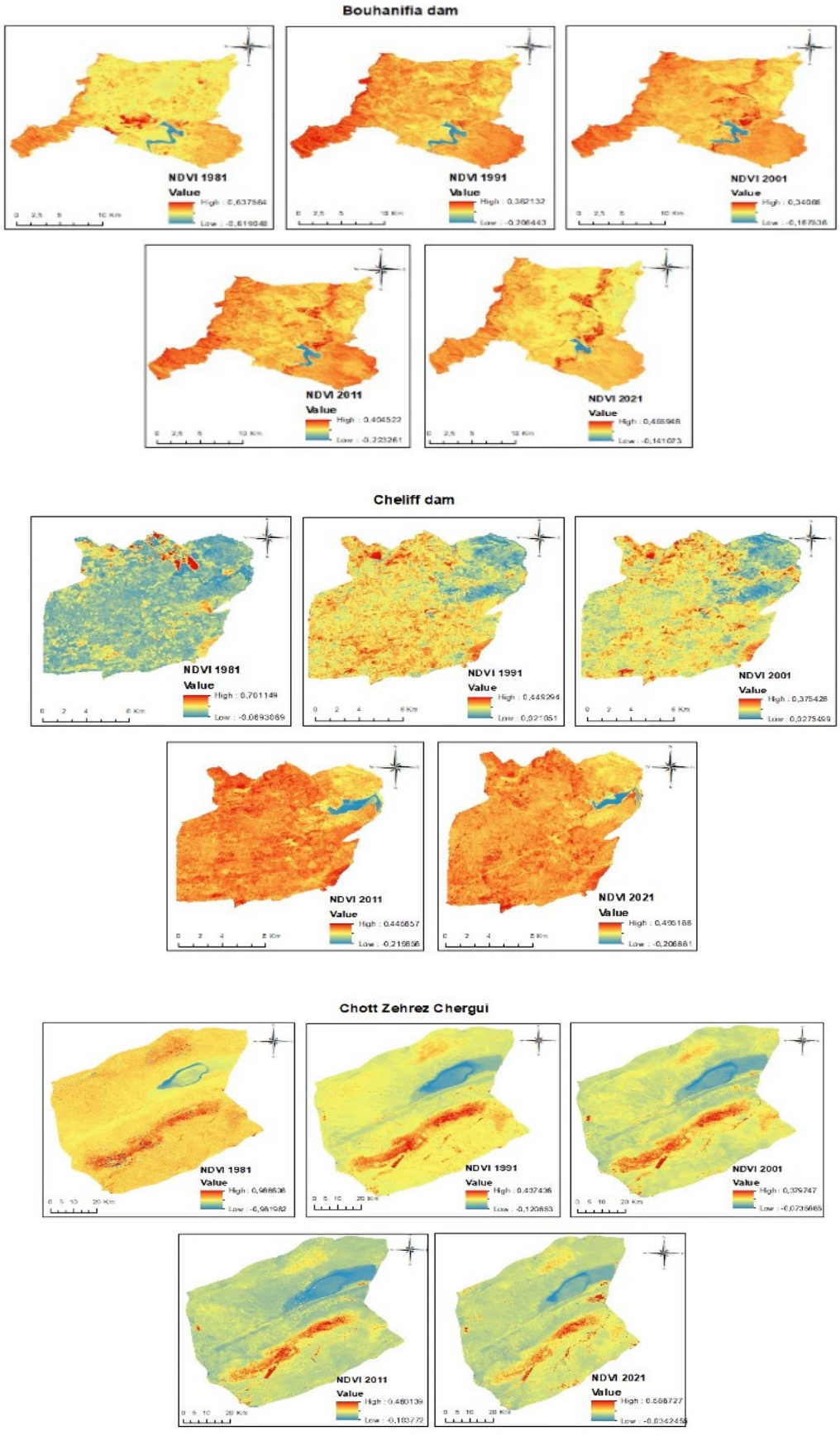

Figure III.1. (continued).

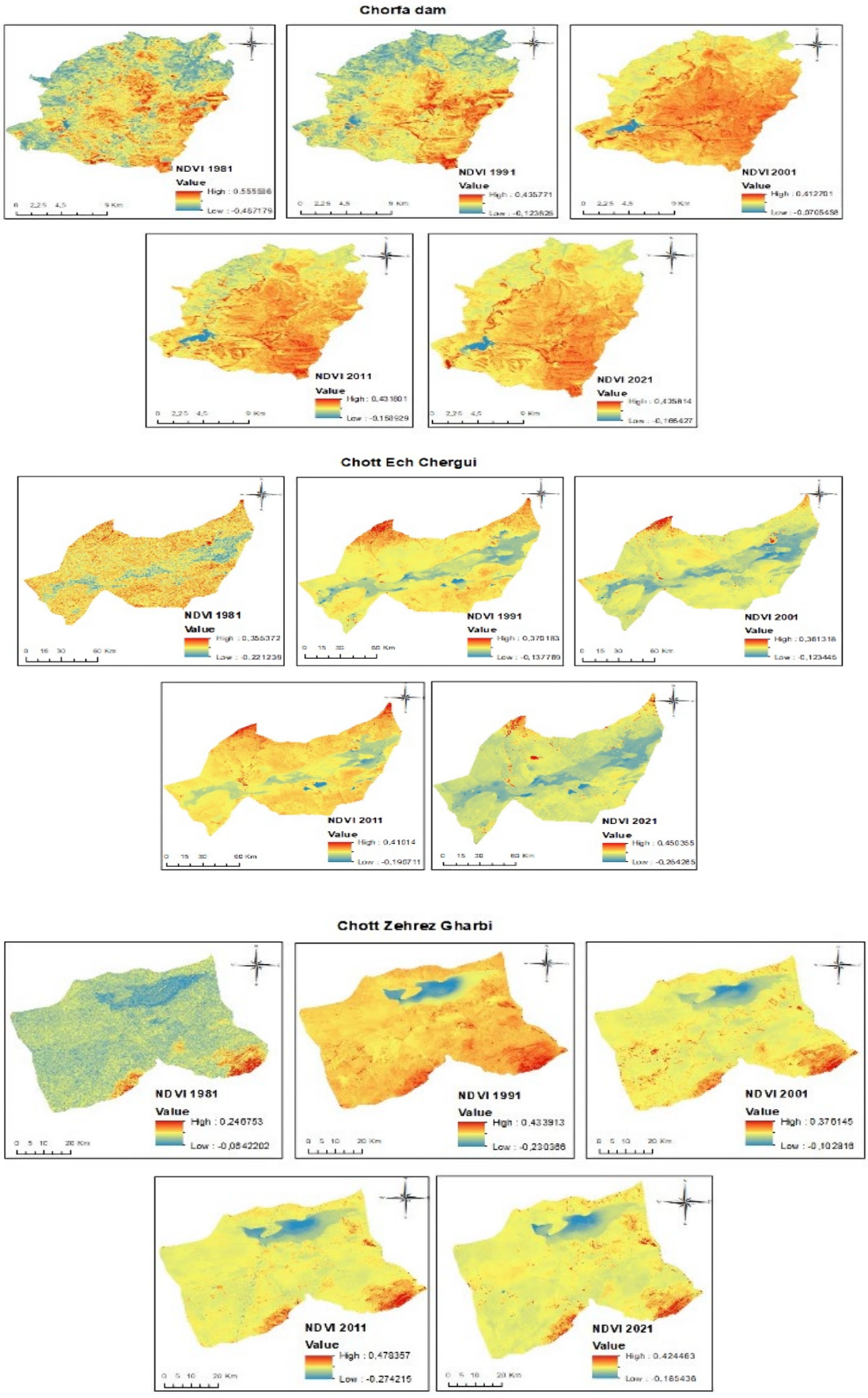

Figure III.1. (continued).

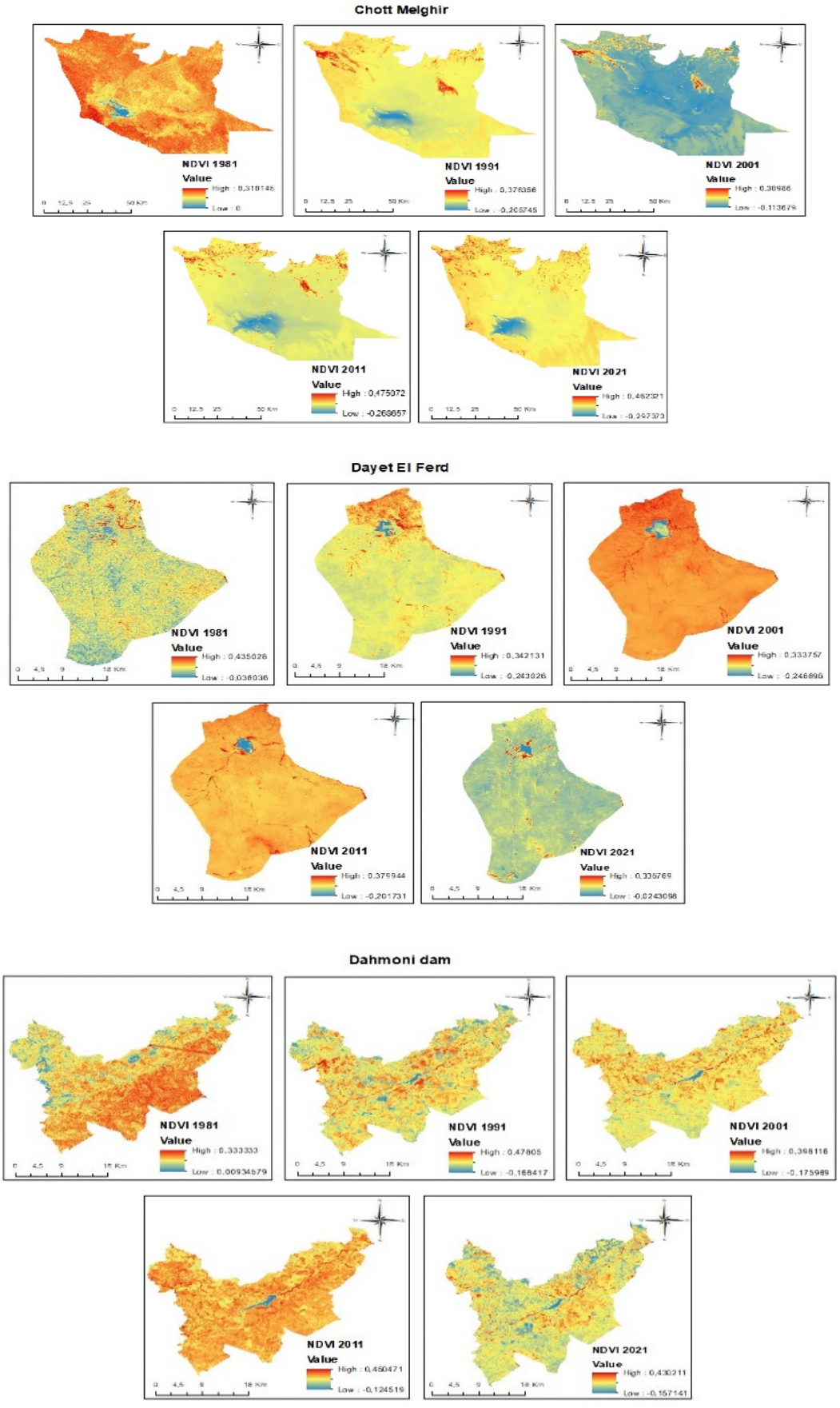

Figure III.1. (continued).

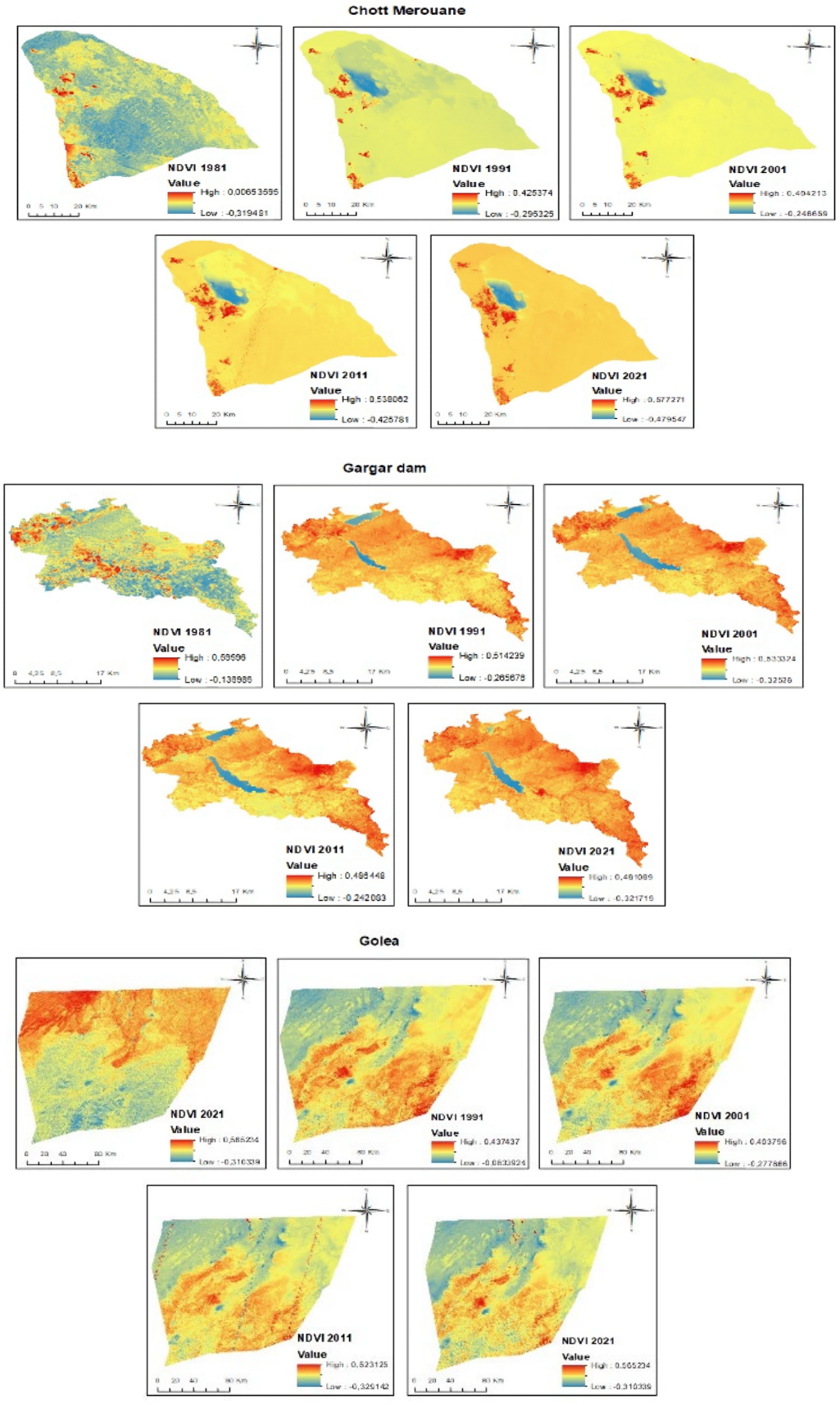

Figure III.1. (continued).

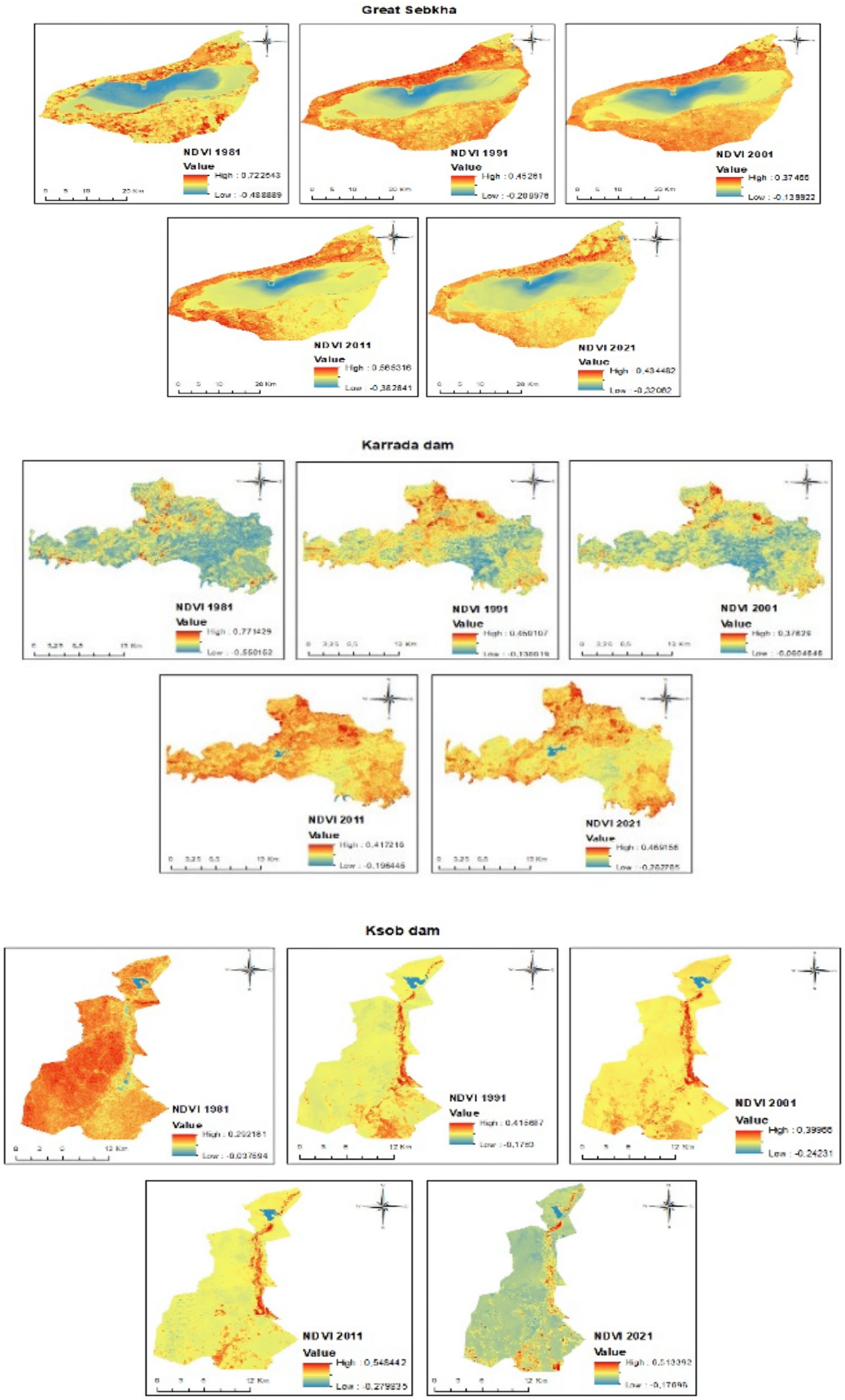

Figure III.1. (continued).

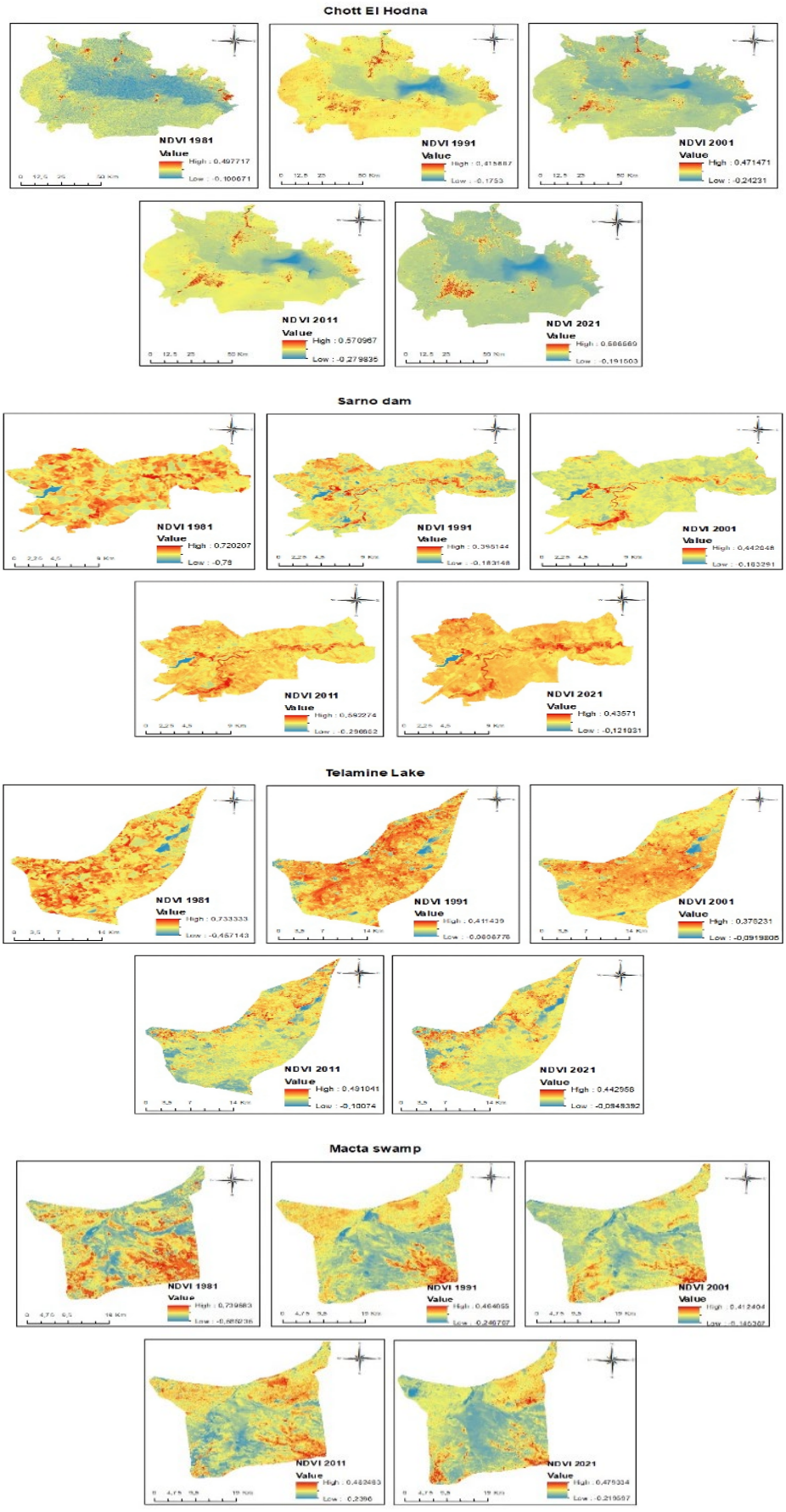

Figure III.1. (continued).

1.2. The association between the vegetation index and climatic changes

In arid and semiarid landscapes, the intricate relationship between alterations in vegetation and climatic variables unfolds a complex interdependence. As illustrated in Fig. III.2, the partial correlation analysis between NDVI values and rainfall (NDVI-P) consistently showed a negative association across all watersheds. On the other hand, the relationship for temperature (NDVI-T) was not always positive. Positive correlations were seen in Chott Zehrez Chergui, Chott Ech Chergui, Dayet El Ferd, Chott Zehrez Gharbi, Chott El Hodna, Beni Bahdel dam, Chott Merouane, Dahmoni dam, Golea, Gargar dam, and Ksob dam from 1981 to 2021. Notably, NDVI-T exhibited a decline during this timeframe, challenging the conventional notion that higher temperatures inherently promote plant development. This decline suggests that the positive impacts of climate change on natural vegetation may diminish over time, aligning with the findings of previous studies (Wu et *al*., 2012; Chen et *al*., 2015).

In general, the analysis highlights that NDVI is more closely linked to temperature (T) than to precipitation (P). This could be attributed to the prevalent dry and semi-dry climatic conditions, where the influence of temperature on greenery surpasses that of rainfall on vegetative cover. Furthermore, a closer examination of seasonal relationships reveals that NDVI in spring demonstrated the highest positive association with both temperature and rainfall. However, the recent decline in NDVI with increased rainfall and temperature in spring suggests a shifting dynamic, possibly influenced by changing climate patterns.

This decline in NDVI with elevated rainfall and temperature in spring contrasts with the substantial positive connection observed in autumn across all wetlands, except for specific areas such as Chott Melghir, Chott Merouan, Golea, Chott Houdna, Chott Zehrez Chergui, and Chott Zehrez Gharbi. Conversely, summer NDVI exhibited a weak link, particularly with temperature. By considering the equivalent grades of the greatest coefficient as a time delay, the study suggests that climate change induces changes in climatic indicators (temperature, rainfall), which are critical for the growth of greenery (Wang et al., 2022). This intricate interplay underscores the dynamic and complex nature of the relationship between vegetation and climate in these dry and semiarid regions.

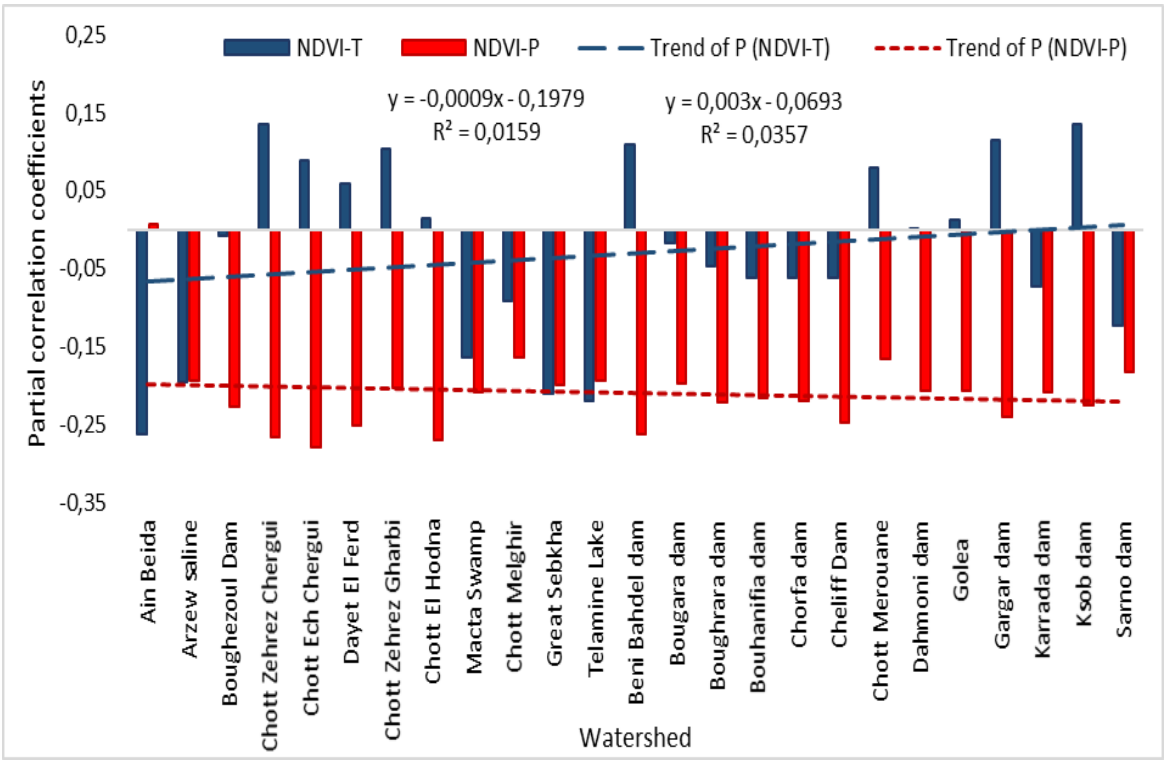

Figure III.2. The factor of partial correlation of growth season between NDVI, rainfall, and temperature in the 25 watersheds during 1981–2021.

The intricate interplay between NDVI and climatic variability was meticulously examined at the month-level, utilizing NDVI data and the normalization of rainfall and temperatures across 25 water bodies from 1981 to 2021, as illustrated in Fig. III.3. Across these basins, temperature changes exhibited a smooth cyclical pattern, indicating a consistent and predictable seasonal variation. In contrast, cyclical precipitation changes were observed to be widely dispersed, reflecting the inherent variability and unpredictability of rainfall patterns in these regions.

An intriguing observation emerged as maximum NDVI readings did not consistently align with the trends observed in climate data. Instead, there were considerable delays evident over the entire research period. This temporal disjunction implies that the influences of rainfall and temperature on NDVI in these basins are characterized by complex temporal dynamics. The delays in NDVI responses to climatic changes underscore the intricate and nuanced relationships between vegetation and climate, suggesting that the impact of climatic factors on vegetation takes time to manifest.

These delays could be attributed to the intricate mechanisms governing vegetation responses to climatic variations, including factors such as soil moisture retention, plant

acclimatization, and the cumulative effects of climate over time. The temporal delays underscore the importance of considering long-term perspectives in assessing the impact of climatic changes on vegetation dynamics in these water bodies.

the findings from this month-level analysis emphasize the need for a nuanced understanding of the temporal dynamics governing the relationship between NDVI and climatic variability in these basins. This insight is crucial for devising effective strategies for managing and adapting to the evolving impacts of climate change on vegetation in these complex ecosystems.

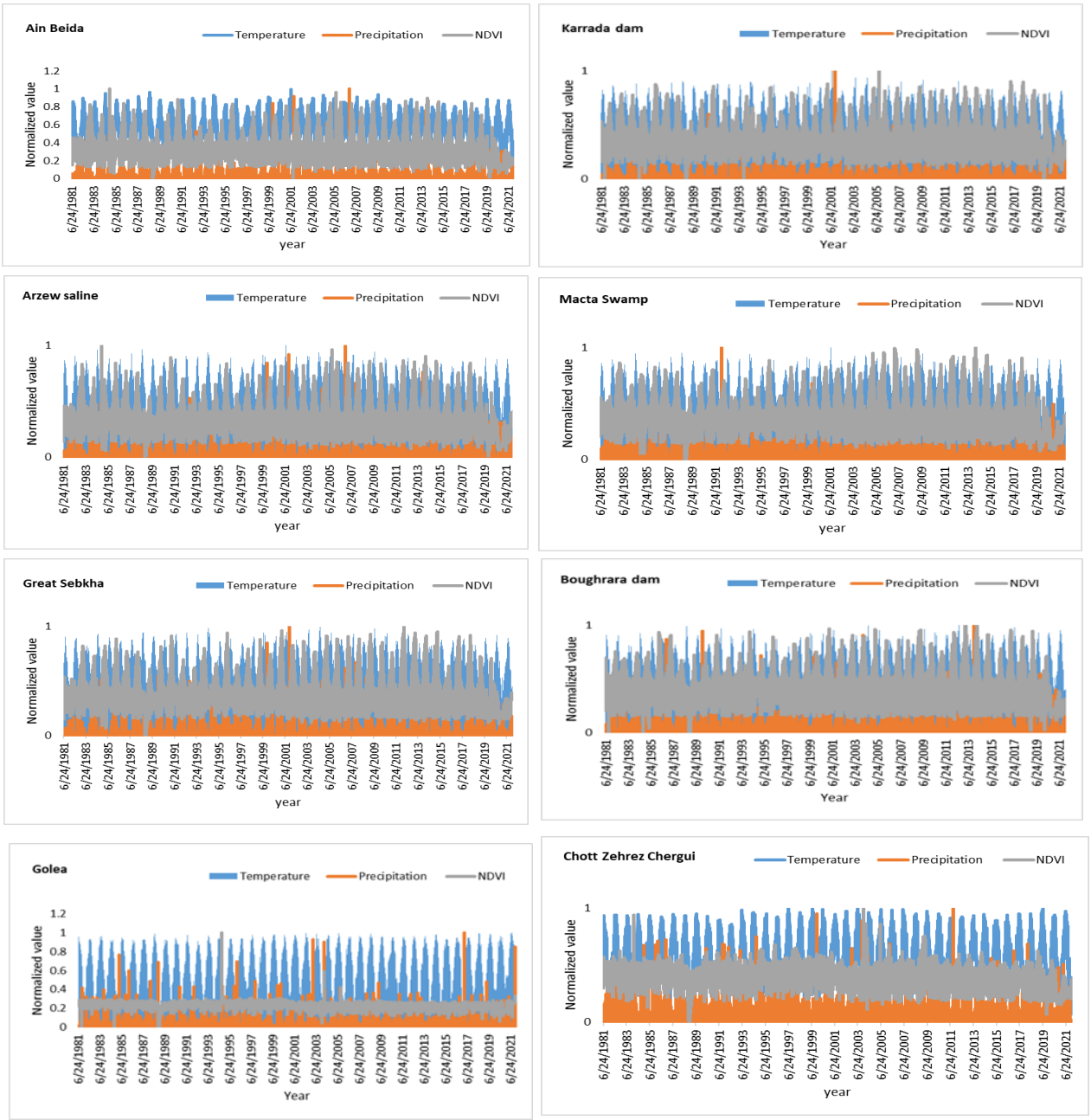

Figure III.3. Standardized long-term fluctuations in NDVI and climatic variables (rainfall and temperature) across the 25 watersheds in Algeria during 1981–2021.

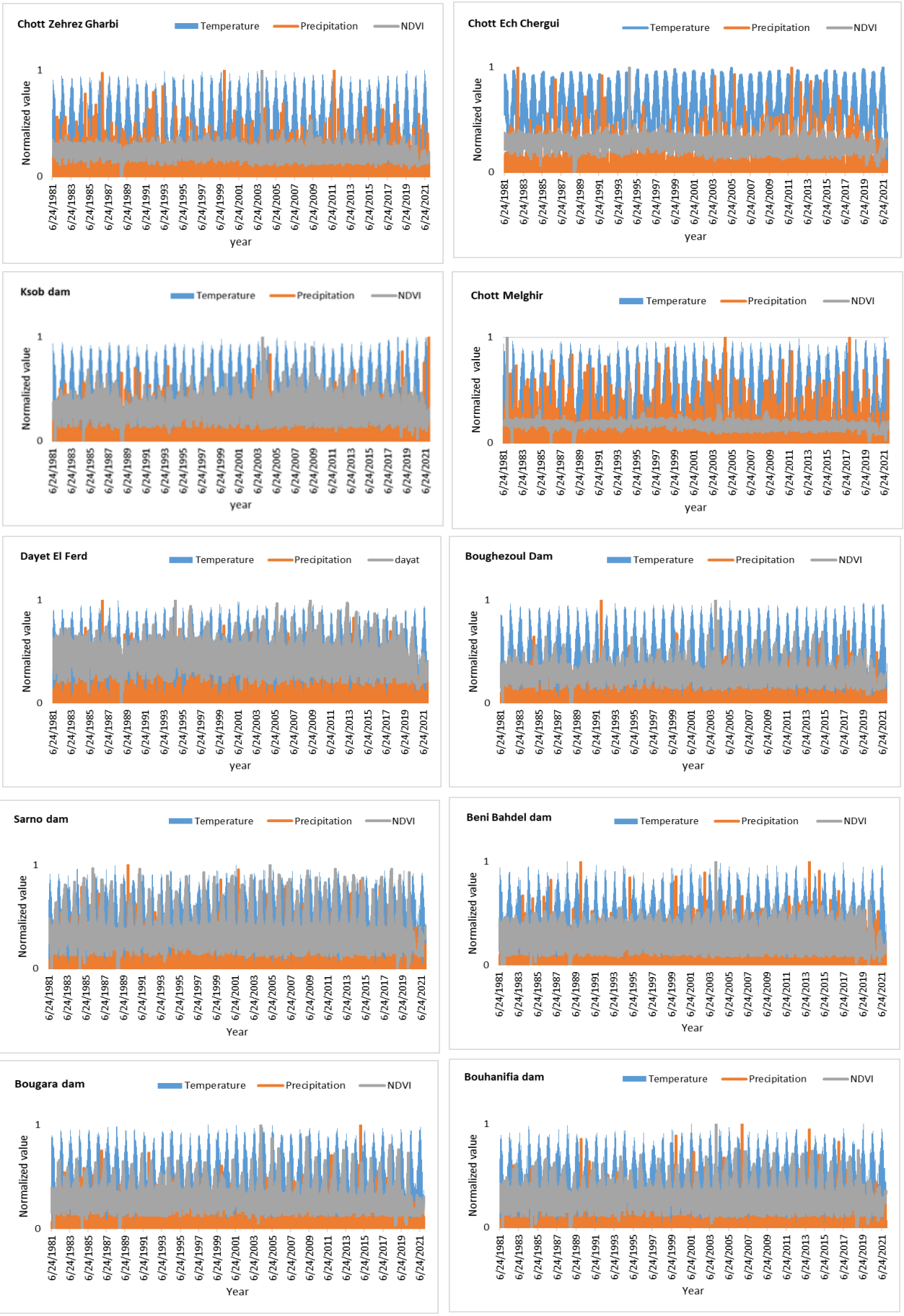

Figure III.3. (continued).

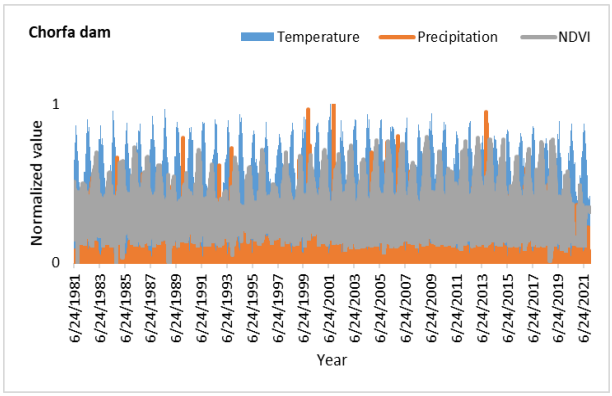

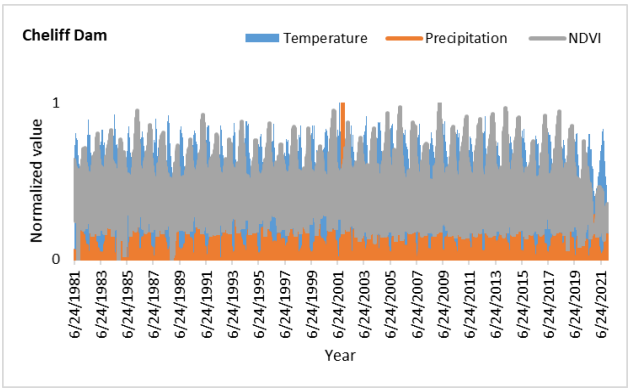

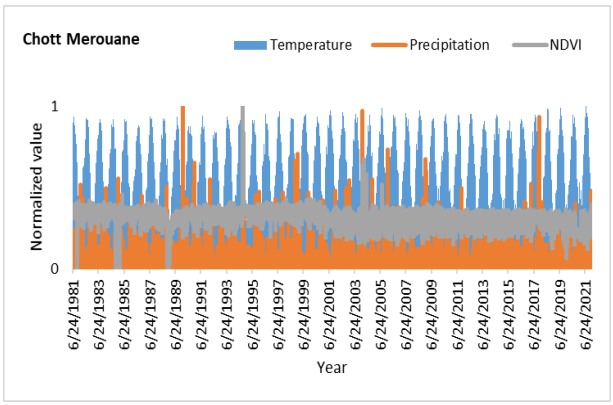

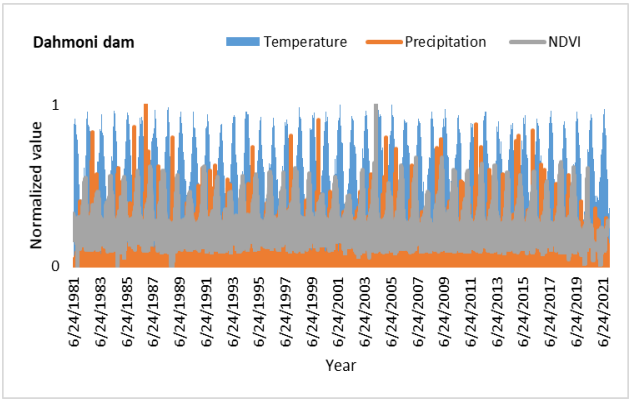

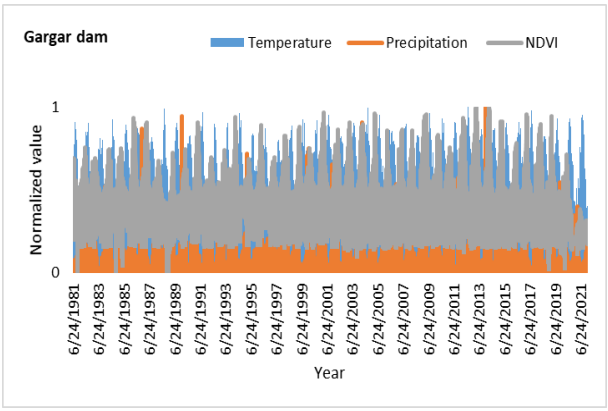

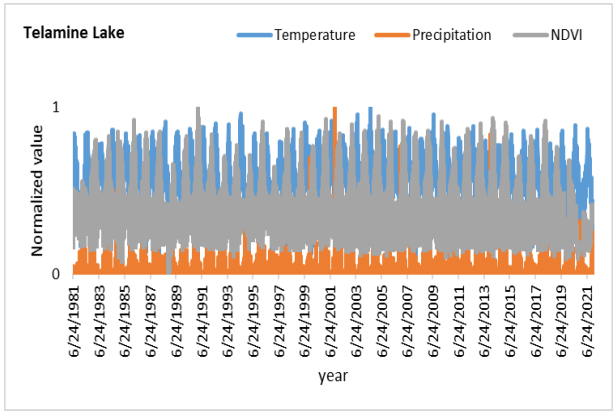

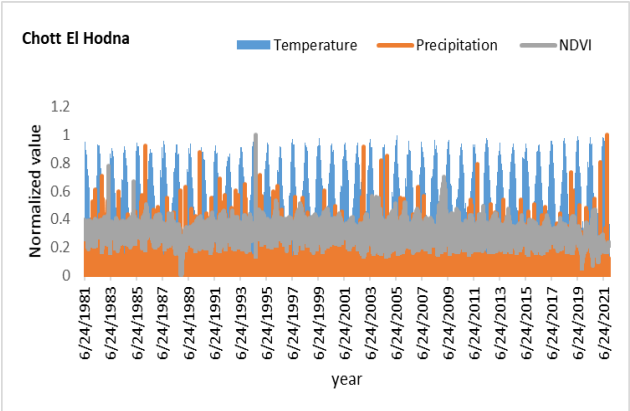

Figure III.3. (continued).

1.3. Long-time impact response for NDVI with rainfall/ temperature variations

The effects of the delay period are being examined by considering annual and seasonal coherence factors between NDVI and climate indicators in basins, as depicted in Tables III.1 and 2. Annual correlations between NDVI and rainfall across all basins showed negative associations, with similar negative correlations observed across all seasons. There appears to be an uneven distribution, with this correlation's impact being more pronounced in autumn. From September to December, rainfall appears to correlate somewhat with the climatic drought experienced in spring, attributed to a lack of rainfall from mid-March to June. Conversely, temperature exhibited positive correlations in many basins throughout the seasons; however, plant density decreased due to higher temperatures and reduced rainfall in spring and autumn.

Furthermore, these analyses revealed significant seasonal variations in plant growth within the basins, with delays in plant growth attributed to delayed rainfall. At times, this delay resulted in a 1–3-month lag in recording due to the delayed NDVI response to climate changes. Vegetation also displays periodic fluctuations, corresponding to variations in temperature and precipitation. While the overall functions of these two components, along with temperature and precipitation, govern periodic vegetation adjustments, the maximum value of NDVI during a given period does not precisely align with precipitation and temperature, indicating a slight delay (Fig. III.4). Additionally, periods of abundant rainfall were not necessarily linked to low NDVI values.

Moreover, significant annual changes were observed, with the National Development Index declining in 1989–1988 across all regions and rising in 1994–1996 compared to the preceding period. These changes highlight the impact of delays in vegetation response to changes in temperature and precipitation.

Table III-1. Correlation coefficient between climate factors and the vegetation index.

Basins	**Correlation coefficient**		
	NDVI-T	**NDVI-P**	**R^2**
Ain Beida	-0.26187	0.007151	0.0106
Arzew Saline	-0.19597	-0.1938	0.0096
Boughezoul Dam	-0.00785	-0.22668	0.0237
Chott Zehrez Chergui	0.135913	-0.26638	0.0518

Chott Ech Chergui	0.088362	-0.27977	0.0439
Dayet El Ferd	0.058209	-0.25218	0.0191
Chott Zehrez Gharbi	0.104216	-0.20293	0.0339
Chott El Hodna	0.014254	-0.26994	0.04
Macta Swamp	-0.16343	-0.20898	0.0073
Chott Melghir	-0.09173	-0.16453	0.0005
Great Sebkha	-0.21125	-0.19904	0.0047
Telamine Lake	-0.21915	-0.19317	0.0155
Beni Bahdel Dam	0.109324	-0.2635	0.0013
Bougara Dam	-0.01723	-0.19687	0.0175
Boughrara Dam	-0.04696	-0.22146	0.0034
Bouhanifia Dam	-0.061	-0.21703	0.0016
Chorfa Dam	-0.06196	-0.22078	0.005
Cheliff dam	-0.06187	-0.24869	0.0098
Chott Merouane	0.079735	-0.16671	0.0917
Dahmoni Dam	0.000705	-0.20711	0.0072
Golea	0.011864	-0.20599	0.0442
Gargar Dam	0.114363	-0.23949	0.0034
Karrada Dam	-0.07234	-0.20797	0.002
Ksob Dam	0.135599	-0.2246	0.0049
Sarno Dam	-0.12339	-0.18363	0.0047

Table III-2. Seasonal correlations between climatic conditions and NDVI (NDVI-P, NDVI-T) in the Basins.

Basins	**NDVI- T**			**NDVI-P**		
	Autumn	Spring	Summer	Autumn	Spring	Summer
Ain Beida	-0,01	0,11	0,15	0,03	-0,012	-0,010
Arzew Saline	-0,01	0,001	-0,23	-0,20	-0,023	-0,023
Boughezoul Dam	0,03	0,001	0,13	-0,20	-0,027	-0,022
Chott Zehrez Chergui	0,10	0,04	0,10	-0,22	-0,033	-0,02
Chott Ech Chergui	0,13	0,04	0,07	-0,21	-0,029	-0,029

Dayet El Ferd	0,04	0,10	0,20	-0,23	-0,029	-0,022
Chott Zehrez Gharbi	0,11	0,02	0,05	-0,017	-0,023	-0,022
Chott El Hodna	0,05	0,07	0,03	-0,022	-0,031	-0,024
Macta Swamp	0,03	0,15	0,08	-0,021	-0,025	-0,023
Chott Melghir	-0,08	0,08	0,08	-0,013	-0,029	-0,014
Great Sebkha	0,06	0,19	0,07	-0,021	-0,026	-0,021
Telamine Lake	0,001	-0,21	0,03	-0,020	-0,026	-0,020
Beni Bahdel Dam	0,10	0,13	0,19	-0,025	-0,029	-0,022
Bougara Dam	0,06	-0,12	0,06	-0,025	-0,025	-0,019
Boughrara Dam	0,12	0,03	0,17	-0,022	-0,026	-0,019
Bouhanifia Dam	0,05	-0,07	0,12	-0,022	-0,025	-0,024
Chorfa Dam	0,04	-0,07	0,08	-0,020	-0,027	-0,023
Cheliff dam	0,04	-0,09	0,10	-0,023	-0,027	-0,024
Chott Merouane	0,01	0,09	0,001	-0,013	-0,026	-0,019
Dahmoni Dam	0,11	0,12	0,26	-0,022	-0,027	-0,023
Golea	-0,03	0,02	-0,06	-0,018	-0,026	-0,023
Gargar Dam	0,26	0,17	-0,09	-0,023	-0,029	-0,023
Karrada Dam	0,12	-0,05	-0,22	-0,020	-0,025	-0,018
Ksob Dam	0,08	0,16	-0,05	-0,018	-0,025	-0,020
Sarno Dam	0,06	-0,18	-0,09	-0,021	-0,024	-0,20

1.4. Spatial distribution and influence of climatic factors on vegetation cover

The results of our extensive analysis, encapsulated in Fig. III.5, illuminate a nuanced understanding of the intricate interplay between vegetation dynamics and climatic factors over a substantial 40-year timeframe. The compelling revelation that NDVI values exhibit a robust correlation with temperature and rainfall in over 95% of vegetated areas ($p < 0.05$) unveils the pivotal role climatic elements play in shaping ecological landscapes. The observed correlation coefficient of less than 0.4 between NDVI and temperature across approximately 85% of the

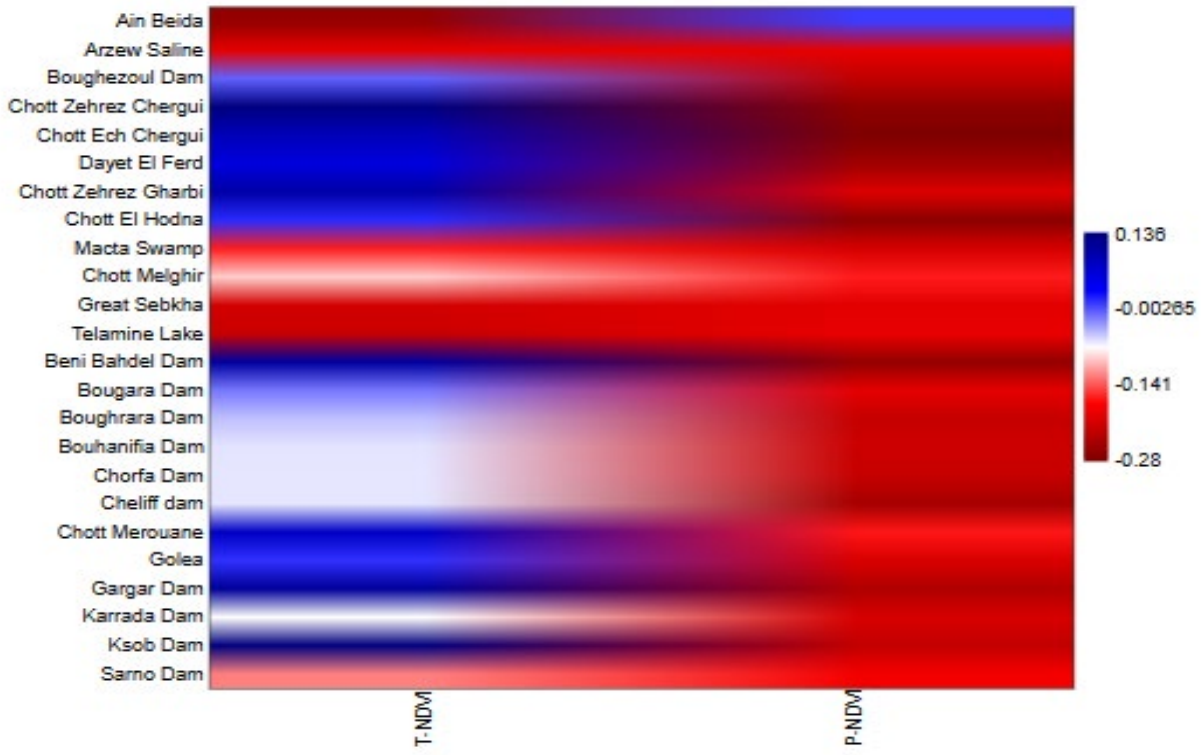

Figure III.4. Time-lag transfer matrix among NDVI and climate factors in 25 Algerian watersheds from 1981 to 2021.

vegetation area underscores the complex sensitivity of vegetation growth to temperature variations. Delving deeper into the temporal dynamics, Fig. III.5 a portrays a uniform negative impact on vegetation across all regions during specific time periods, signaling a widespread vulnerability of greenery to adverse climatic conditions. This temporal pattern is echoed in the corresponding NDVI-P representation (Fig. III.5b), where a pronounced negative response to changes in vegetation cover is accentuated, emphasizing the salient positive influence of rainfall.

The intricate examination of NDVI-P further reveals a substantial shift, with over 70% of observed changes showcasing a negative trajectory or a continuous shift from positive to negative values, particularly evident in recent years. This amplifies the significance of precipitation as the primary driver of vegetation density in these regions. An intriguing observation is the notable transition in 45% of NDVI-T from better to worse, indicative of a marked alteration in vegetation productivity attributable to the overarching impact of climate warming in these specific areas. In essence, these results not only validate the substantial influence of temperature and rainfall on vegetation growth but also underscore the preeminent role of precipitation in shaping vegetative landscapes. The temporal nuances further emphasize

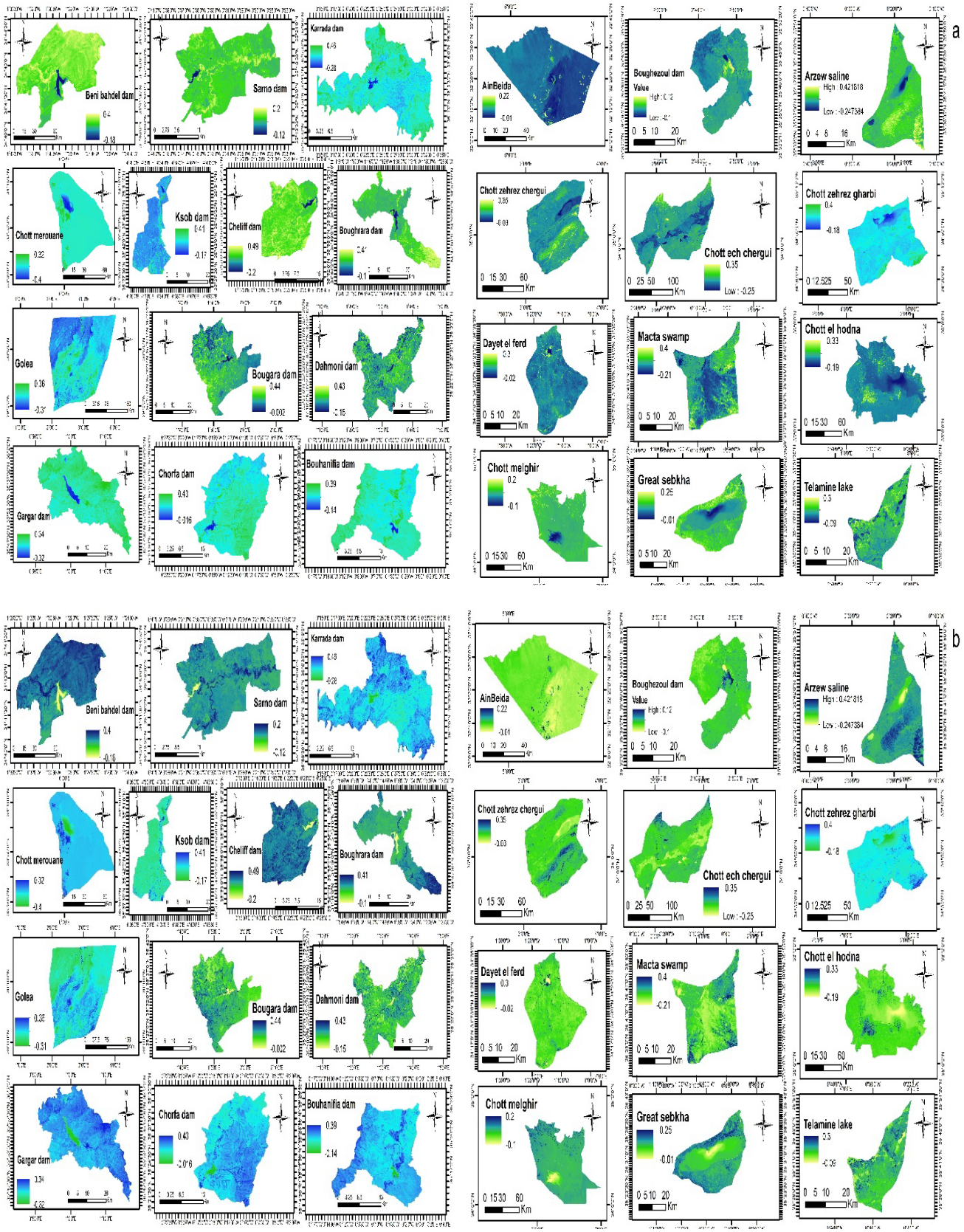

Figure III.5. The Pearson correlation distribution pattern between both the multi-year average vegetation indices (NDVI) and the climatic factors temperature (a), and rainfall (b) in 25 basins from 1981 to 2021.

the vulnerability of vegetation to climatic shifts, with climate warming emerging as a transformative force impacting the productivity of these ecosystems. This in-depth exploration of results urges continued vigilance and comprehensive monitoring, providing invaluable insights for adaptive strategies to navigate the evolving environmental dynamics.

Moreover, the results not only spotlight the immediate consequences of climatic fluctuations on vegetation but also unravel a complex narrative of resilience and vulnerability within these ecosystems. The nuanced negative effects on vegetation, as depicted in Fig. 6a, signify a collective response to climatic stressors across diverse regions, echoing the broader implications of climate change on global ecosystems. The parallel patterns observed in NDVI-P (Fig. 6b) intricately weave a tale of vegetation's adaptive strategies, with an apparent reliance on precipitation as a lifeline during adverse periods. The temporal evolution of NDVI-P, with its substantial proportion of negative changes, underscores the sensitivity of vegetation cover to variations in precipitation, especially in recent years. This temporal specificity invites contemplation on the immediacy of these shifts and their potential long-term ramifications on ecological balance.

The intricate association between NDVI-T and climate warming, evidenced by the transition in 45% of vegetation productivity from better to worse, poses compelling questions about the adaptability of ecosystems to sustained temperature increases. This observation prompts a deeper exploration into the mechanisms by which climate warming exerts its influence on vegetation, necessitating a comprehensive understanding of the underlying ecological processes. The results, thus, not only serve as a snapshot of the present state of vegetation-climate dynamics but also beckon further research avenues to unravel the intricacies of these relationships.

1.5. Unraveling Environmental Transformations: A Multifaceted Analysis of Climate, Vegetation Dynamics, and Human Influence in Algerian Watersheds (1981-2021)

The NDVI in all areas where the study was conducted fell markedly from 1981 to 2021. The relationship and effects of the time difference between climate variables and vegetation coverage have been studied in 25 areas of Algerian water bodies, which possess significant importance in detail and are crucial for comprehending environmental processes in these areas (Zhou et *al*., 2018; Bai et *al*., 2020), where vegetation is strongly linked to climatic change (Roerink et *al*., 2003; Piao et *al*., 2006; Chu et *al*., 2019).

According to the outcome in this research, the positive relationship among temperature and NDVI turned negative during the study period, pointing out that the positive effect of rising temperatures on greenery cover has waned over time. This negative impact is likely to be the main cause of the watershed's drought that has been experienced during the last few decades. This may be an indirect effect of temperature on vegetation water, but it is an important cause of poor vegetation growth. The negative correlation of NDVI-P represented 70% of the study area, its negative effect appeared in all regions, and this was consistent with NDVI-T. This negative effect was persistent and increasing, especially in recent years, which showed the drought that affected these basins. This shows that precipitation is of great importance, especially in the growth of vegetation, so it is an important driver. Accordingly, it can be highlighted that rainfall and temperature can determine the dynamics of vegetation and interpret them effectively, especially in dry and semi-dry areas (Gao et *al*., 2022). were the sensitivity levels in all areas. It should also be noted that these basins have seen a decrease in the amount of water. These changes will lead to the disappearance of many of them, and this has emerged in the Dayet El Ferd and Great Sebkha basins, which are currently experiencing an unprecedented drought. These results have also indicated that the warming climate has decreased its positive effect on the growth of vegetation over time.

Vegetation response to climate change varies greatly, especially due to variations in environmental patterns and climate conditions (Filippa et *al*., 2019). It should be noted that these climatic factors alone do not suffice in the presence of the human factor, such as the expansion of agricultural and urban land and the practice of overgrazing, as they play a role in their impact on vegetation growth (Xu et *al*., 2016; et *al*., Luo et *al*., 2018; Ma et *al*., 2019). This is what we will focus on in our future studies, as well as paying attention to the overall relationship between vegetation and other impacts (such as relative humidity and evaporation), as well as topographic and demographic factors.

2. Long-term disparity assessment of remote sensing indicators to monitor the dynamism of ecosystems in arid and semi-arid areas: contributions to sustainable resource management.

2.1. The evolving pattern of NDVI in the 25 areas over the course of the last 22 years

The extensive analysis of NDVI trends in Algeria spanning from 2000 to 2022 offers a comprehensive insight into the spatial and temporal dynamics of vegetation across diverse

regions. The average yearly NDVI values, ranging from 0 to 0.7 with an average between 0.098 and 0.34% (Fig. III.6), form the basis for discerning patterns that reflect the environmental conditions prevailing in different parts of the country. Notably, the observed gradual decrease in NDVI values from the northwest coast to the eastern and western interior and further south highlights a distinct disparity in environmental quality. The northwest regions emerge as having superior environmental conditions, evident from elevated NDVI values ranging between 0.4 to 0.6, while the interior and southern regions predominantly exhibit lower values, mainly ranging from 0 to 0.2.

The watershed-specific examination adds granularity to the analysis, revealing extremes in vegetation health. The Sarno watershed's remarkable peak in 2001, surpassing 0.6, signifies robust vegetation cover, whereas the Chott Marouane watershed's plunge to 0.07 in 2006 indicates environmental challenges demanding attention. This watershed-level scrutiny provides valuable information for localized conservation efforts.

Zooming into the upper reaches of the region, the 22-year average NDVI of 0.4 indicates a moderate overall vegetation level, with a noteworthy upward trend from inland areas towards the northwest. The identification of specific areas with the lowest vegetation proportions, such as the Chott Merouane area in the northeast of the North Sahara, followed by the Golea Basin, Chott Melehir, Ain Beida, Chott El Hodna, and Ksob Dam, contrasts sharply with regions showcasing the highest vegetation ratios. The northwest regions, including Sarno Dam, Telamine Lake, Arzew saline, Macta Marshes, Great Sebkha, Boughrara Dam, Cheliff Dam, Chorfa Dam, Beni Bahdel Dam, Karrada Dam, and Bouhanifia Dam, present annual average NDVI values of 0.6, indicating medium to high vegetation levels. Similarly, Bougara Dam, Dahmoni Dam, and Gargar Dam, located in the central and upper reaches, exhibit relatively high vegetation cover.

Conversely, the areas around Ksob Dam, situated off the southern salt of Golea, depict the lowest average NDVI at 0.05, classifying them as regions with sparse vegetation cover and unfavorable environmental conditions. This prompts a call for the implementation of targeted measures to augment green spaces in these areas. Moreover, the average NDVI index for Boughezoul Dam, Chott Zehrez Chergui, Chott Ech Chergui, Chott Zehrez Gharbi, and Dayet El Ferd, ranging from 0.2 to 0.4, designates them as medium/low vegetation areas with a notably poor vegetation condition, emphasizing the urgency of conservation strategies.

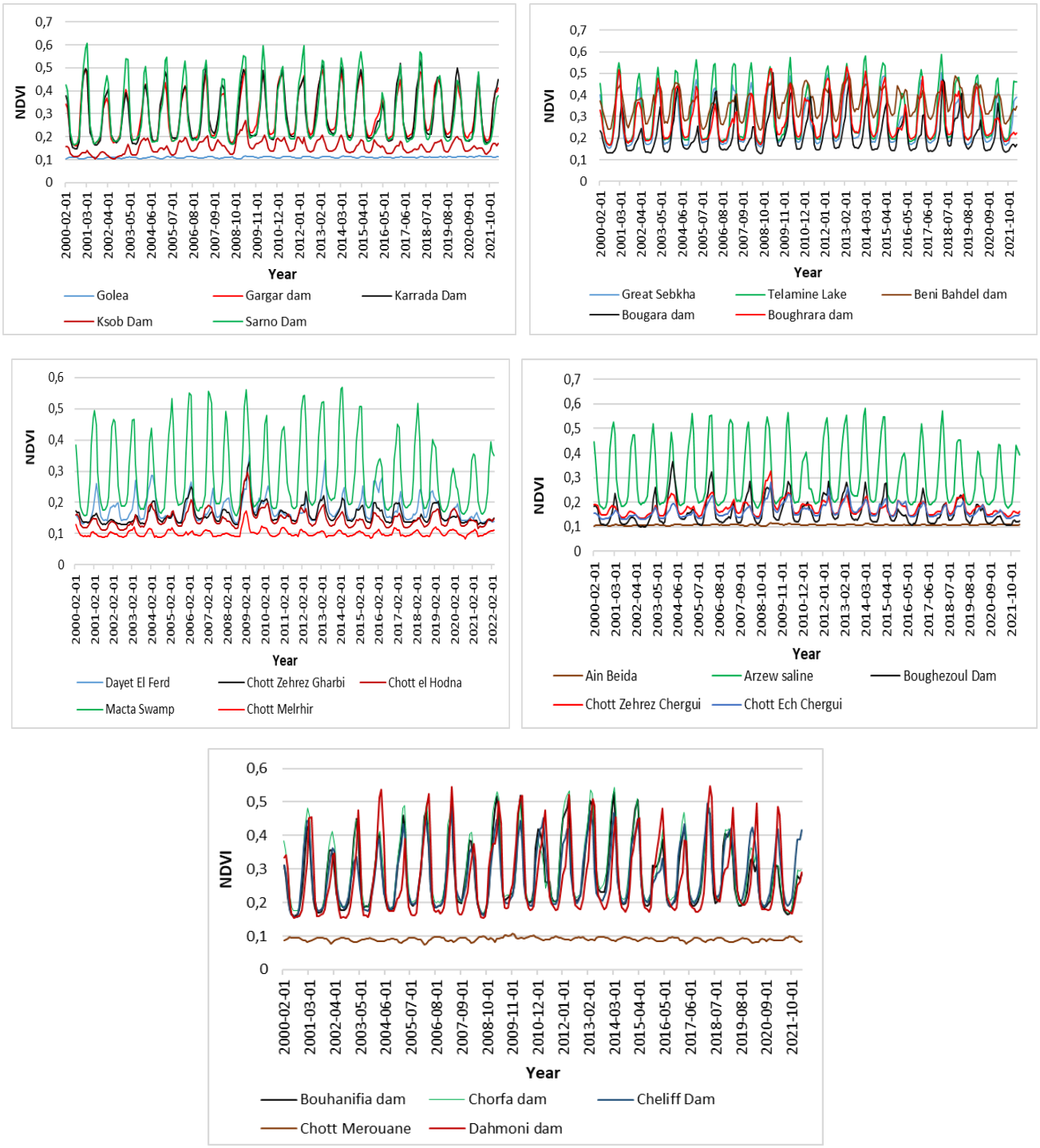

Figure III.6. The pattern of interannual changes in the annual average NDVI for 25 watersheds in Algeria over the period of 2000 to 2022.

2.2. Spatio-temporal of NDVI, EVI, NDWI, LST and NDMI

The integration of four remote sensing indicators (NDVI, NDWI, EVI, and LST) using average values from the NIR and SWIR bands of Modis datasets enabled a thorough examination of environmental changes in the study regions from 2000 to 2022 (Fig. III. 7, 8, 9). The average yearly values of these variables provide insights into different elements of the

research areas. Initially, the water content indicated by NDWI values remained consistently low during the whole time analyzed, ranging between 0.07 and -0.2 across all locations. It indicates a consistent presence or lack of water in certain areas, serving as a foundation for comprehending hydrological conditions.

The average NDVI index ranged from 0 to 0.7, displaying various patterns depending on the location. This location has unique features with higher NDVI values compared to other areas in the Northwest and the sites being reviewed. This aligns with previous study findings that identified suitable ecological conditions for them in the northwest regions. This demonstrates regional variations in vegetation health levels across different places on the research site.

The EVI index range, which indicates vegetation health and cover status, was between 0.06 and 0.41. The Sarno Dam and Ksob Dam in 2012 and the Macta Marsh in 2014 saw the greatest peak value of EVI at 0.41 per unit area, suggesting times of more intense plant development. Simply put, an EVI score of 0.066 indicated that Chott Merouane had fewer healthy plants in 2006. Therefore, these modifications aid in comprehending the variations in plant coverage across various areas throughout time. This is because EVI is more sensitive to the spectral effects of soil composition and moisture in places with little vegetation (Lu et *al*., 2015).

The mean LST varied from 13°C to 18°C, indicating a little temperature discrepancy across the research sites, despite differences in geographical location and land characteristics. The southern areas consistently had the highest surface temperatures, suggesting a temperature gradient with fluctuation throughout the research zones. Consistent surface temperatures across different landscapes may indicate broader climatic influences on temperature trends.

Figure III.10 displays the fluctuation in NDMI values from 2000 to 2022, showing a higher level of variability compared to other spectral indicators. There is a consistent downward trend seen from 2000 to 2007, 2008 to 2013, and 2014 to 2022. Values fluctuated between -0.5 and 0.2 over these times. NDMI readings exhibited a consistent decline over that period, indicating significant water stress in the studied locations during those years. Our data indicates distinct phases with reduced NDMI values, particularly during the early years of our research. During that period, NDMI values often dropped below -0.1. This indicates that the plants had reduced water and humidity levels. We believe this period saw less precipitation or drier conditions. It demonstrates how rapid water fluctuations may significantly damage the wetlands. Fluctuations in NDMI values demonstrate the dynamics of water stress in the research areas

throughout time. This may indicate various weather patterns, human actions, or changes in land use that impact water availability. The trends in NDMI values indicate the need for careful monitoring and judicious management of water in these regions. However, the study highlights the effectiveness of the NDMI as a powerful indicator, capturing the temporal dynamics of water scarcity in the ecosystems under investigation. NDMI demonstrated significant decreasing trends, indicating a profound correlation between vegetation dynamics and land surface moisture. The fact that NDMI is sensitive to water absorption shows that it can accurately show changes in vegetation. This shows how closely vegetation dynamics and the availability of water are connected across the studied areas.

Figure III.7. Interannual Fluctuations in Annual Average EVI Across 25 Algerian Watersheds (2000-2022).

Figure III.8. Interannual Fluctuations in Annual Average NDWI Across 25 Algerian Watersheds (2000-2022).

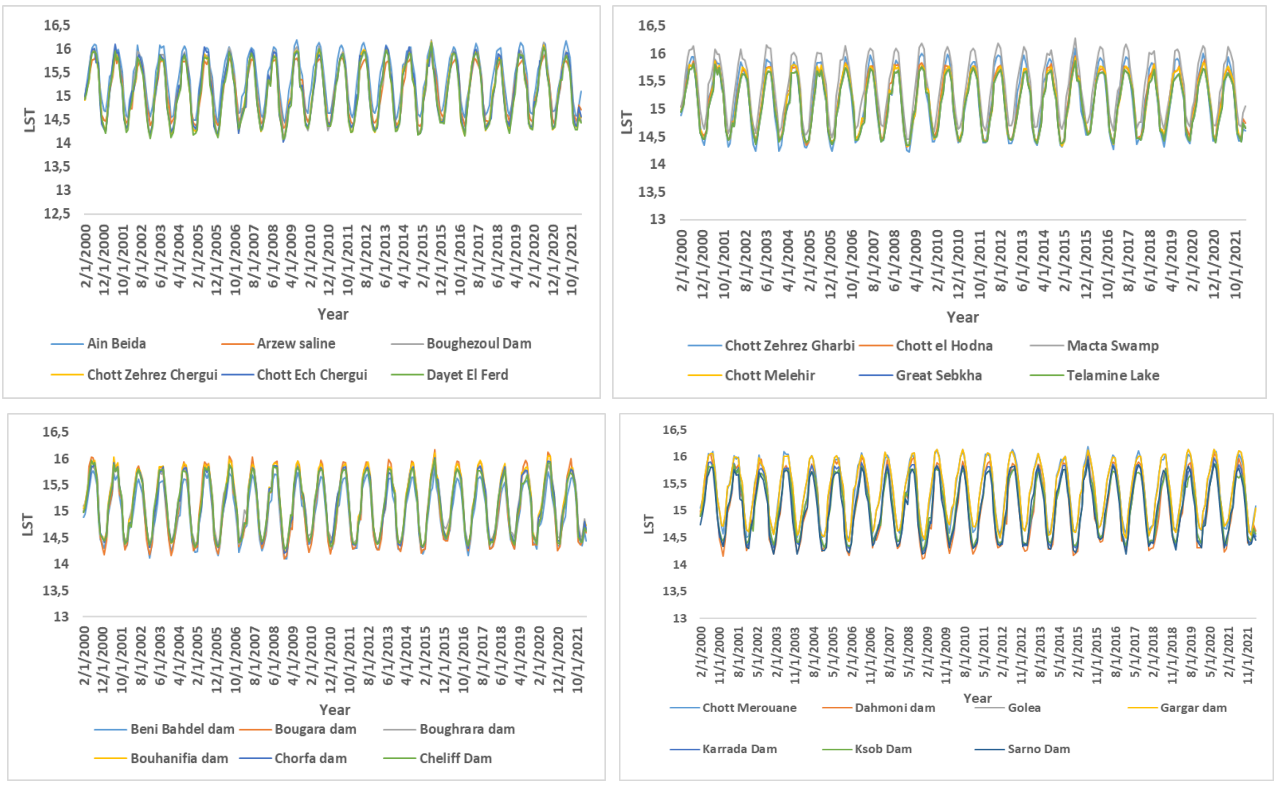

Figure III.9. Interannual Fluctuations in Annual Average LST Across 25 Algerian Watersheds (2000-2022).

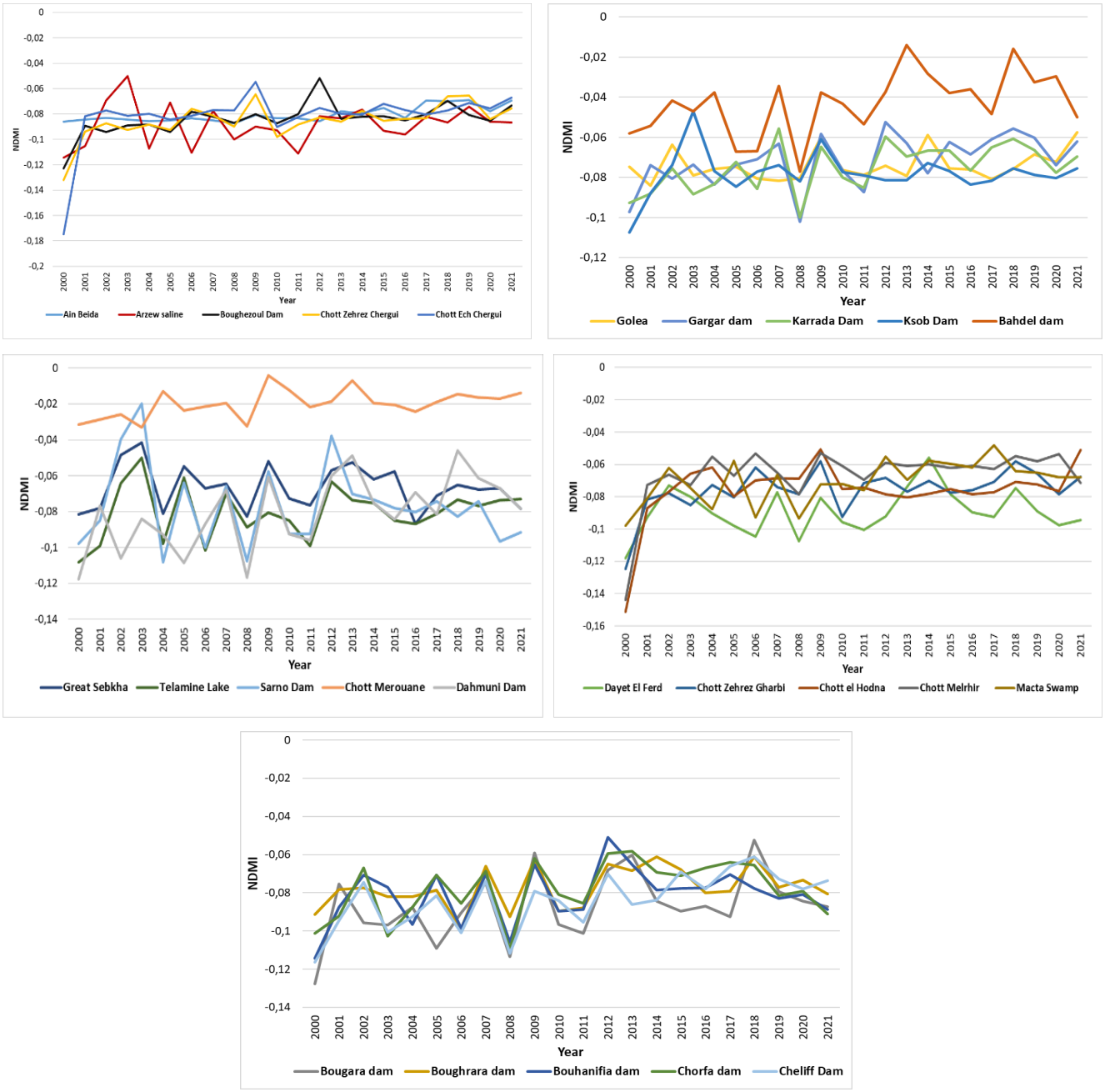

Figure III.10. Annual averages of NDMI in 25 regions from 2000 to 2022.

2.3. The associations between NDVI and LST

Fig. III. 11 illustrates a frequent negative association between NDVI and LST. This negative correlation defines the whole study area. There is a moderate negative correlation between NDVI and LST in some sites, including Macta Marsh, Arzew Saline, Great Sebkha, Chott Melehir, Beni Bahdel Dam, Cheliff Dam, Chorfa Dam, Bouhanfia Dam, Karrada Dam, Gargar Dam, and Telamine Lake. These locations have a value of R = 0.4811. A small correlation exists between variations in LST and vegetation, as the NDVI tends to decrease with rising LST in certain regions. The formerly robust negative link between NDVI and LST

is diminishing in different regions. The R^2 values in these locations range from 0.109 to 0.3793. This indicates that when LST levels rise, vegetation diminishes. The negative correlation between NDVI and LST demonstrates that higher temperatures are associated with less vegetative activity in these areas. The correlation between NDVI and LST differs for aquatic bodies. When NDVI is negative, it indicates the presence of water in wetlands. Overall, we get valuable insights into the site's plant life and land surface temperature changes via the correlations between NDVI and LST. Understanding the impact of temperature on plant health and monitoring long-term environmental changes is crucial.

Figure III.11. Annual assessment on NDVI and LST indices relationship during 2000-2022.

2.4. Mann-Kendall analysis trends

The Mann-Kendall analysis was performed on the NDVI, EVI, NDVI, and LST datasets at a 95 % confidence level with serial correlation applied. The results of the MK test for the NDVI data are summarized in Table III.3 Among the 25 regions examined, 15 displayed negative Mann-Kendall statistics, indicating an overall decreasing trend in NDVI over the study period.

The associated p values for these regions exceeded the specified significance level alpha, indicating significant evidence of a monotonic decline in vegetation activity within these areas.

On the contrary, the MK analysis revealed a positive slope for the remaining 10 regions, indicating a generally increasing trend in NDVI. The positive values of the statistic were relatively high, providing additional support for the presence of a significant upward pattern. The p values associated with these regions were lower than the specified significance level alpha, indicating strong evidence of a monotonically increasing trend in vegetation activity within these areas. In Fig. III. 12, it is noteworthy that each region's p-value was either greater than or less than 0.05, serving as the threshold for statistical significance (Guo et al., 2018). These results provide insights into the direction and significance of trends in vegetation indices across the study regions.

Table III-3. Findings of the two-tailed test for seasonality in the NDVI time series using the Mann-Kendall method.

Study area	Tau	P-value	Sen slope
Ain beida	0.167	0.00013	0.0004
Arzew saline	0.016	0.700	0.006
Boughezoul dam	-0.007	0.871	0.005
Chott zehrez chergui	0.014	0.732	0.000
Chott ech chergui	0.136	0.001	0.006
Dayet el ferd	-0.029	0.480	-0.001
Chott zehrez gharbi	0.021	0.621	0.002
Chott el hodna	0.009	0.829	-0.001
Macta marsh	-0.028	0.490	0.004
Chott melrhir	0.088	0.036	0.000
Great sebkha	0.049	0.234	0.004
Telamine lake	0.053	0.203	0.004
Beni bahdel dam	0.127	0.002	0.017
Bougara dam	0.070	0.091	0.007
Boughrara dam	0.049	0.239	0.014
Bouhanifia dam	0.052	0.208	0.014
Chorfa dam	0.024	0.560	0.009
Cheliff dam	0.138	0.001	0.012

Chott merouane	-0.047	0.262	0.000
Dahmoni dam	0.092	0.026	0.007
Golea	0.344	<0.0001	0.001
Gargar dam	0.114	0.006	0.012
Karrada dam	0.089	0.031	0.002
Ksob dam	0.162	<0.0001	0.005
Sarno dam	-0.002	0.960	-0.001

The MK test outcomes for EVI outlined in Table III.4 mirrored the NDVI results in the majority of regions, suggesting a similar trend. However, an exception was noted in the Ksob dam, where the EVI trend displayed a distinct positive direction, signifying an overall increase in vegetation activity. The p-value associated with this region was lower than the specified significance level alpha, providing strong evidence of a significant monotonic upward trend in vegetation activity in the Ksob dam (Fig. III. 12).

Table III-4. Findings of the two-tailed test for seasonality in the EVI time series using the Mann-Kendall method.

Study areas	**Tau**	**P-value**	**Sen slope**
Ain beida	0.142	0.001	0.0002
Arzew saline	-0.003	0.951	0.002
Boughezoul dam	-0.003	0.942	0.002
Chott zehrez chergui	0.080	0.055	0.002
Chott ech chergui	0.199	<0.0001	0.002
Dayet el ferd	0.000	0.993	-0.001
Chott zehrez gharbi	0.051	0.220	0.001
Chott el hodna	0.068	0.103	0.001
Macta marsh	-0.046	0.262	0.000
Chott melrhir	0.121	0.004	0.001
Great sebkha	0.025	0.548	-0.002
Telamine lake	0.024	0.558	-0.002
Beni bahdel dam	0.109	0.008	0.005
Bougara dam	0.079	0.058	0.002

Boughrara dam	0.036	0.387	0.007
Bouhanifia dam	0.059	0.153	0.004
Chorfa dam	0.003	0.947	0.000
Cheliff dam	0.107	0.010	0.000
Chott merouane	0.069	0.105	0.006
Dahmoni dam	0.089	0.031	0.001
Golea	0.301	<0.0001	0.005
Gargar dam	0.109	0.008	0.002
Karrada dam	0.086	0.036	0.005
Ksob dam	0.010	0.803	0.005
Sarno dam	0.010	0.803	0.000

In NDWI, positive values observed in 18 regions suggest an increasing trend in water content; the corresponding p values ($P > 0.05$) for these regions indicate a monotonically positive trend (Table III.5**).** conversely, other regions with p values below 0.05 show a significant negative trend in water content. Mann-Kendall test results provide evidence of monotonic trends either increasing or decreasing in NDWI values across the study regions (Fig. III. 12).

Table III-5. Findings of the two-tailed test for seasonality in the NDWI time series using the Mann-Kendall method.

Study area	**Tau**	**P-value**	**Sen slope**
Ain Beida	0.028	0.0521	-0.0001
Arzew saline	0.050	0.227	-0.002
Boughezoul Dam	0.080	0.055	0.001
Chott Zehrez Chergui	0.069	0.098	0.0001
Chott Ech Chergui	-0.044	0.292	-0.001
Dayet El Ferd	0.036	0.384	0.0002
Chott Zehrez Gharbi	0.048	0.251	0.001
Chott El Hodna	-0.026	0.527	0.000
Macta Swamp	0.083	0.044	0.003
Chott Melrhir	0.019	0.657	0.0003
Great Sebkha	0.075	0.069	0.006

Telamine Lake	0.106	0.010	-0.0004
Beni Bahdel dam	0.086	0.038	0.005
Bougara dam	0.078	0.062	0.001
Boughrara dam	0.035	0.401	0.001
Bouhanifia dam	0.034	0.412	0.001
Chorfa dam	0.015	0.712	0.002
Cheliff Dam	0.134	0.001	0.001
Chott Merouane	0.014	0.738	-0.001
Dahmoni dam	0.088	0.034	0.006
Golea	-0.132	0.002	-0.001
Gargar dam	0.079	0.058	-0.0006
Karrada dam	0.057	0.171	-0.0001
Ksob dam	0.153	0.0001	0.002
Sarno dam	-0.020	0.621	-0.001

The application of long-term sequence analysis (LST) with the MK test provides results from the statistical trend analysis of annual temperature degrees as outlined in Table III.6. These findings reveal a statistically significant positive trend in all wetlands, indicating a gradual increase over time. The analysis suggests a substantial alteration in annual temperature magnitudes, particularly between the years 2020 and 2022. The confirmed results based on the MK statistics and accompanying p values at significance levels of 5% and 1% demonstrate statistical significance in Fig. III. 12. As anticipated, both variables representing the maximum temperature show a consistent upward trend. In summary, the findings of the trend test demonstrate a statistically significant pattern of temperature rise in all regions.

Table III-6. Findings of the two-tailed test for seasonality in the LST time series using the Mann-Kendall method.

Study area	**Tau**	**P-value**	**Sen slope**
Ain Beida	0.056	0.120	0.023
Arzew saline	0.068	0.074	0.010
Boughezoul Dam	0.068	0.077	0.040
Chott Zehrez Chergui	0.068	0.077	0.063
Chott Ech Chergui	0.072	0.067	0.044

Dayet El Ferd	0.072	0.066	0.053
Chott Zehrez Gharbi	0.056	0.117	0.045
Chott El Hodna	0.056	0.117	0.017
Macta Swamp	0.036	0.221	0.028
Chott Melrhir	0.064	0.083	0.013
Great Sebkha	0.060	0.110	0.003
Telamine Lake	0.060	0.110	0.003
Beni Bahdel dam	0.072	0.067	0.002
Bougara dam	0.072	0.060	0.006
Boughrara dam	0.084	0.044	0.005
Bouhanifia dam	0.072	0.061	0.009
Chorfa dam	0.072	0.067	0.014
Cheliff Dam	0.024	0.309	0.007
Chott Merouane	0.032	0.249	0.038
Dahmoni dam	0.056	0.109	0.000
Golea	0.048	0.151	0.021
Gargar dam	0.048	0.151	0.021
Karrada dam	0.040	0.189	0.006
Ksob dam	0.044	0.183	0.022
Sarno dam	0.076	0.062	0.040

The Sen's slope was utilized to analyses time series data of natural indicators from 2020 to 2022 Table III 3,4,5, and 6. In all scenarios, the indicators exhibited a noticeable and continuous upward trend. There was an increase in vegetation density based on NDVI and EVI values in Beni Bahdel Dam, Bouhanifia Dam, Boughrara Dam, and Gargar Dam. Additionally, NDWI analysis indicated an increase in water content in Ksob Dam, Boughezoul Dam, and Chott Zehrez Gharbi. The rise in surface temperature over time suggests environmental conditions characterized by excessive heat, which may negatively impact vegetation density.

The results of the Sen's slope analysis revealed that the most affected areas in terms of vegetation cover are Dayet El Ferd, Sarno Dam, Chott El Hodna, Ain Beida, Arzew Saline, Chott Ech Chergui, Telamine Lake, Chott Merouane, Golea, Gargar Dam, Karrada Dam, and Sarno Dam. The trend test results, with a significance level of 1%, showed statistically

significant trends for the indicators, with the results remaining statistically significant at a 95% confidence level from 2020 to 2022.

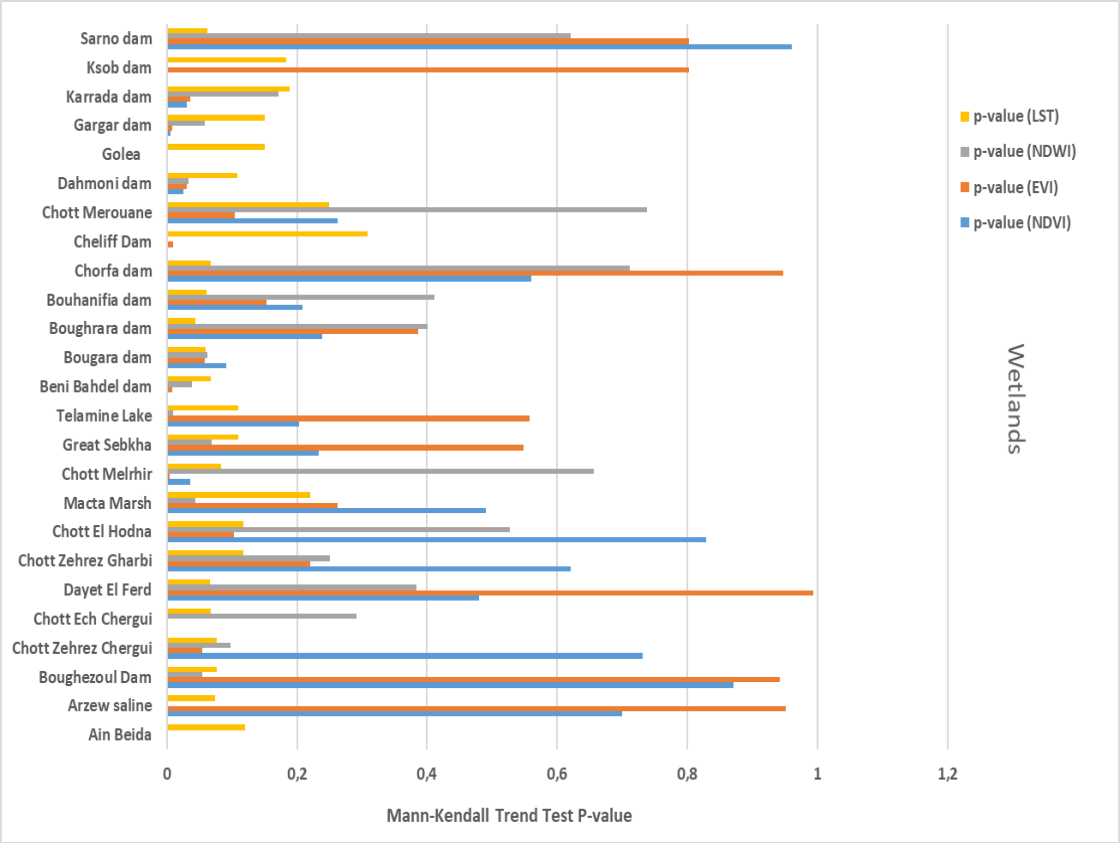

Figure III.12. Mann-Kendall trend test for annual NDVI, EVI, NDWI, LST, 2020–2022.

3. Monitoring the effect of droughts and extreme climate variables for various time periods on vegetation density in the Reghaia catchment, Algeria

3.1. Variability of Vegetation Dynamics in the Reghaia Basin

The metrics gleaned from the Modis NDVI dataset, captured from 2000 to 2022, provide an important understanding of the variations in vegetation index both over time and across areas within the Reghaia basin. A scrutiny of these fluctuations, visually represented by fig III.13 a, unearths noticeable diversities along with distinct geographical trends during the said time. Almost 60 % of vegetation cover in the baseline showed NDVI readings beneath 0.35, indicative of areas embodying reduced greening. Conversely, regions placed on the eastern edge and in proximity to the basin sported NDVI readings above 0.35, connoting denser green spaces. Regularly, the lowest values of NDVI were reported in the basins, west, and towards the south, which allude to the dissimilarities in the liveliness and growth behavior of vegetation in divergent territorial zones.

The variation in NDVI spatial values fell between -0.21 and 0.53, indicating a noticeable vegetation transition from the eastern to the western side of the basin. An annual average NDVI value of 0.349 was determined for the Reghaia basin, signifying the general status of plant health within that territory. Importantly, a rising NDVI value of 0.63 was observed in 2005, displaying heightened plant density during that time. On the contrary, 2003 experienced a low of -0.08, hinting at weakening dynamics in plant life and a subsequent negative impact on overall plant health (Fig. III.13 b).

Additionally, when observing the NDVI index annually, an uptrend is detected, recording at 0.008 year-1. This turning point, although fluctuating, signals a cautious enhancement in plant density as the years progress. However, a significant downward movement stands out in the period from 2018 to 2022, where the NDVI proportion noticeably reduces. This type of decrease can be connected to the most recent changes in land utility and urban spread, emphasizing their influence on how plant dynamics behave, particularly in the Reghaia basin. The fusion of time-specific and geospatial evaluations in this investigation offers a comprehensive insight into the complicated interplays molding plant dispersion a crucial contribution that aids environmental observation and supports sustainable management plans focused on land in the reviewed zone.

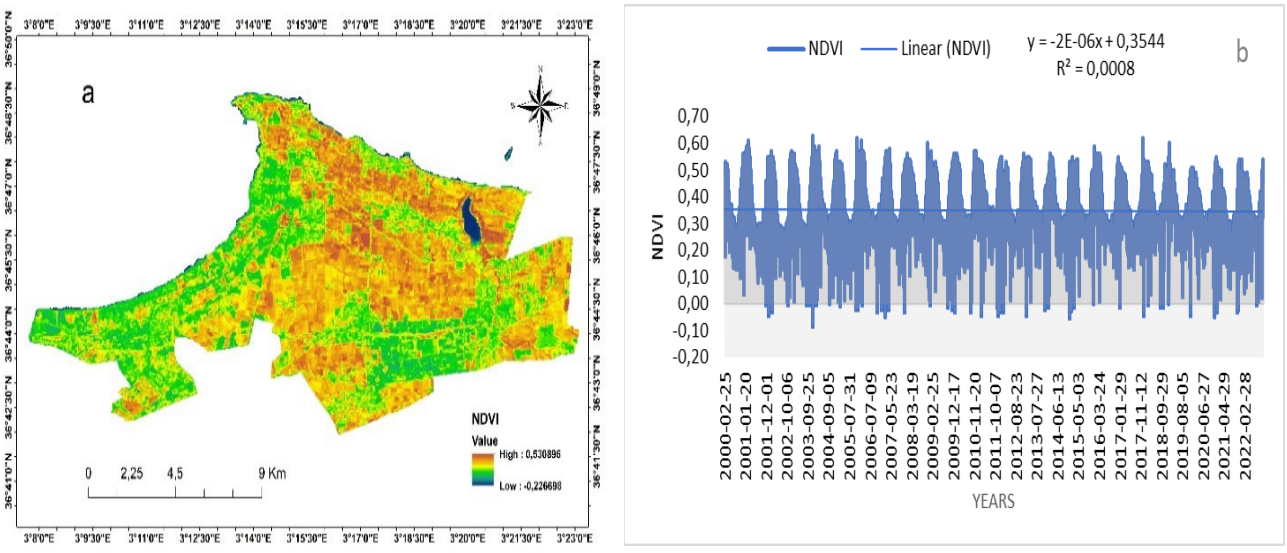

Figure III.13. Spatial pattern of annual mean NDVI in Reghaia (a); Trend of interannual variation in annual mean NDVI (b) during 2000–2022.

3.2. Relationships between NDVI dynamics and climatic variables with partial correlation

The examination of relationships between NDVI dynamics and climatic variables, with a focus on the Reghaia Basin during the period 2000–2022 (Fig. III.14), provides crucial insights into the intricate interplay between vegetation patterns and climatic conditions. The correlation analysis revealed compelling patterns, particularly in sporadic years where the correlation between NDVI and precipitation surpassed 0.6. This positive correlation signifies a direct influence of precipitation on vegetation health, underscoring the sensitivity of the region's flora to changes in rainfall patterns. These findings align with the broader understanding that adequate precipitation fosters favorable conditions for vegetation growth, emphasizing the importance of water availability in sustaining a healthy vegetative cover.

Conversely, the relationship between NDVI and temperature exhibited a predominantly negative trend over the years. The negative correlations observed can be attributed to the impact of warming temperatures on vegetation growth. The study suggests that the warming climate has led to a decline in vegetation growth, particularly evident in recent years. This negative correlation emphasizes the adverse effects of temperature increases on the health and dynamics of vegetation within the Reghaia Basin. Such changes are indicative of the complex and multifaceted impacts of climate change on ecosystems, with temperature fluctuations playing a pivotal role in shaping vegetation patterns.

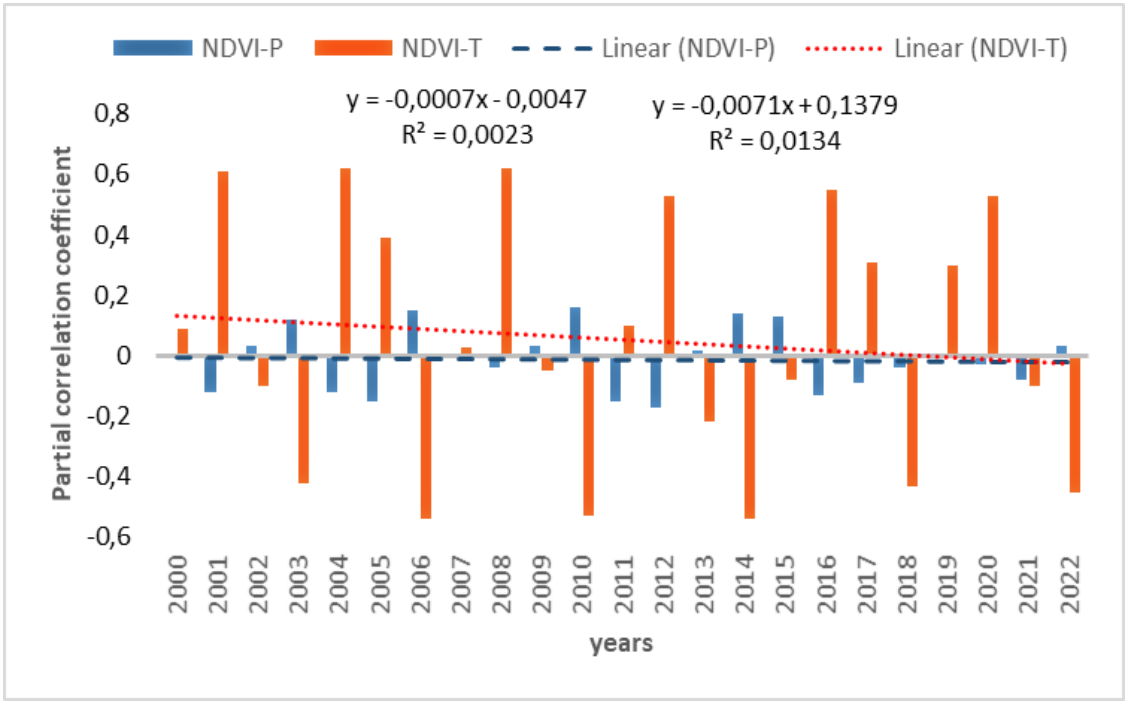

Figure III.14. Partial association analysis between NDVI and extreme climates in the Reghaia Basin, 2000–2022.

The study further underscores the relevance of these two climatic factors in gauging the current impact of climate change, especially in the aftermath of drought in the Reghaia area. The decline in rainfall during the growing season, coupled with a decrease in the aquifer level in the basin.

3.3. Seasonal spatial changes in vegetation cover during the growing season in the Reghaia catchment over a 22-year period

Looking into the changes in NDVI during different times of the year in the Reghaia area, as shown in Figure III.15, gives us a more complete picture of how plant patterns change over time. The variability trends of NDVI exhibit both similarities and distinct differences across various seasonal spatial distributions. Notably, vegetation deterioration is particularly pronounced in the summer season, as highlighted in Fig. III.15 b. This observation underscores the vulnerability of the region's flora during the hotter months, possibly exacerbated by factors such as increased temperatures and reduced water availability.

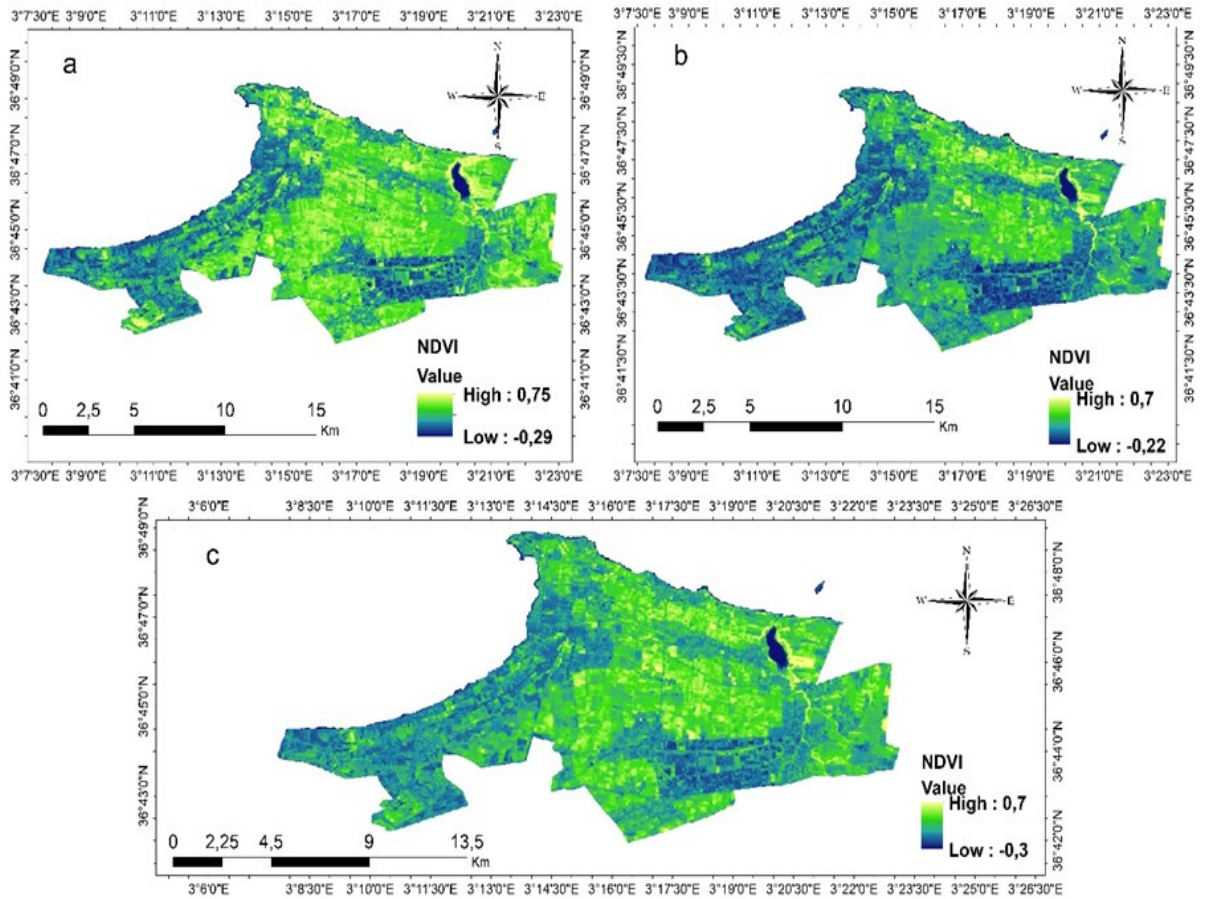

Figure III.15. Spatial alteration of mean NDVI in various seasons. (a) Spring mean (b) Summer mean (c) Autumn mean.

Conversely, the remaining seasons portray important green patterns, with the most significant homogenization of vegetation observed in spring at 65% (Fig. III.15 a). This suggests that spring is a critical period for robust vegetation growth and health in the Reghaia area. The NDVI index values reinforce this observation, with the highest value recorded in spring at 0.75 and the lowest in summer at -0.3. The spatial distribution of NDVI values indicates a concentration of high vegetation density in areas near the basin, gradually declining towards the western regions. The consistent ratio in autumn, though relatively lower compared to spring, reflects a season that still contributes significantly to maintaining vegetation health (Fig. III.15 c).

However, the overarching trend across the seasons signals a broader concern for vegetation degradation and reduced productivity within the study area. This decline is attributed to factors such as irrational exploitation, leading to erosion and the depletion of plant species. The escalation of the erosion process further compounds the challenges faced by the local ecosystem.

3.4. The impact of seasonal changes in long-term climate factors on the vegetarian index over the past 22 years

The comprehensive assessment of growth differentials and the impact of climate factors on vegetation in the Reghaia area, as presented in Table III.7, sheds light on the intricate relationships between climate variables and NDVI throughout the year. The analysis unveils intriguing patterns, emphasizing the significant influence of climatic conditions on vegetation dynamics. The relationship between NDVI and rainfall consistently shows opposing trends in all seasons, with the effect especially noticeable during the fall. This inverse correlation indicates that as rainfall amounts decrease, vegetation density correspondingly reduces as well, emphasizing how vital rain is for maintaining flora in the Reghaia basin. The association of temperature represented with this trend is positive frequently over the years, specifically noted most potently during the summers of 2004 and 2016 (R stands at 0.65 and R is 0.64, respectively). This positive correlation implies that higher temperatures are associated with increased vegetation density during the summer months.

However, the study also highlights the adverse effects of high temperatures and a lack of rain on plant density, particularly evident in spring and autumn. The decline in plant density is attributed to delayed rains and, at times, a delayed registration of 1-2 months due to the delayed response of NDVI to climate changes. These findings underscore the sensitivity of vegetation

growth to the timing and amount of rainfall, with delays impacting the overall plant density in the Reghaia area.

Furthermore, the results emphasize that the impact of rainfall outweighs the effect of temperature on the vegetation index, especially evident in the spring. Changes in rainfall patterns significantly influence vegetation dynamics, with lower water levels in the basin attributed to global climate impacts, particularly rising temperatures in the Reghaia basin and reduced regional rainfall. The findings underscore the complex interplay between climate variables and vegetation dynamics, highlighting the vulnerability of the Reghaia area's ecosystem to variations in precipitation and temperature.

Table III-7. Seasonal relationships between extreme climatic factors and NDVI (NDVI-P, NDVI-T) in the Reghaia Basin from 2000 to 2022.

Years		**NDVI-P**			**NDVI-T**	
	Autumn	Spring	Summer	Autumn	Spring	Summer
2000	-0,03	-0,15	-0,05	-0,5**	0,52**	0,53**
2001	-0,03	-0,2	-0,06	0,17	0,32*	0,56**
2002	0,03	0,09	0,02	0,44*	-0,35	-0,53**
2003	-0,001	0,18	-0,02	-0,25	-0,22	0,07
2004	-0,02	-0,13	-0,08	-0,12	0,40*	0,64**
2005	-0,16	-0,05	0,09	0,28*	-0,05	-0,05
2006	-0,017	0,26	0,15	0,02	-0,32	-0,46*
2007	-0,10	-0,21	0,03	-0,27	0,52**	0,28*
2008	0,04	0,01	-0,12	-0,04	0,12	0,43*
2009	0,03	0,01	0,11	0,32*	-0,23	-0,27
2010	-0,008	0,14	0,18	-0,03	-0,47	-0,49*
2011	-0,06	-0,13	-0,29	-0,38	0,38*	0,41*
2012	-0,07	-0,011	-0,11	0,50**	-0,05	0,28*
2013	-0,18	0,19	0,10	0,39*	-0,73	-0,44*
2014	-0,008	0,14	0,18	-0,03	-0,47	-0,49*
2015	0,17	0,012	0,17	-0,61**	0,37*	0,41*
2016	-0,07	-0,01	-0,10	0,17	0,15	0,65*
2017	-0,16	0,07	-0,02	0,46*	-0,23	0,07
2018	-0,32	-0,01	-0,12	-0,14	-0,23	0,038

2019	0,04	-0,14	0,05	-0,58	0,43*	0,43*
2020	0,21	0,11	-0,03	0,28*	-0,05	0,51**
2021	-0,16	0,01	-0,01	0,23*	-0,37	-0,09
2022	-0,13	0,13	0,10	-0,19	-0,07	-0,42

**significant association ($p < 0.01$)
*significant association ($p < 0.05$)

3.5. Temporal characteristics: annual and seasonal evolution of SPEI in the Reghaia catchment

To estimate the rate of drought in the catchment in Reghaia over 22 years, the SPEI index was used (Fig. III.16). Data showed disparities in droughts. There were recorded mild droughts in each of the years 2002, 2004, 2006, 2007, 2010, 2011, 2012, 2013, and 2018, and the drought rate was heavier during the years 2003, 2015, 2017, 2020, 2021, and 2022 as the frequency of droughts increased and the cumulative rate of SPEI increased. In addition to that, there were various droughts over these years. This suggests that wet conditions have become rare in the region. The high rate of drought has had an impact on water resources, and this is likely to continue with climate change, especially with the scarcity of rain that was evident from 2019 to 2022.

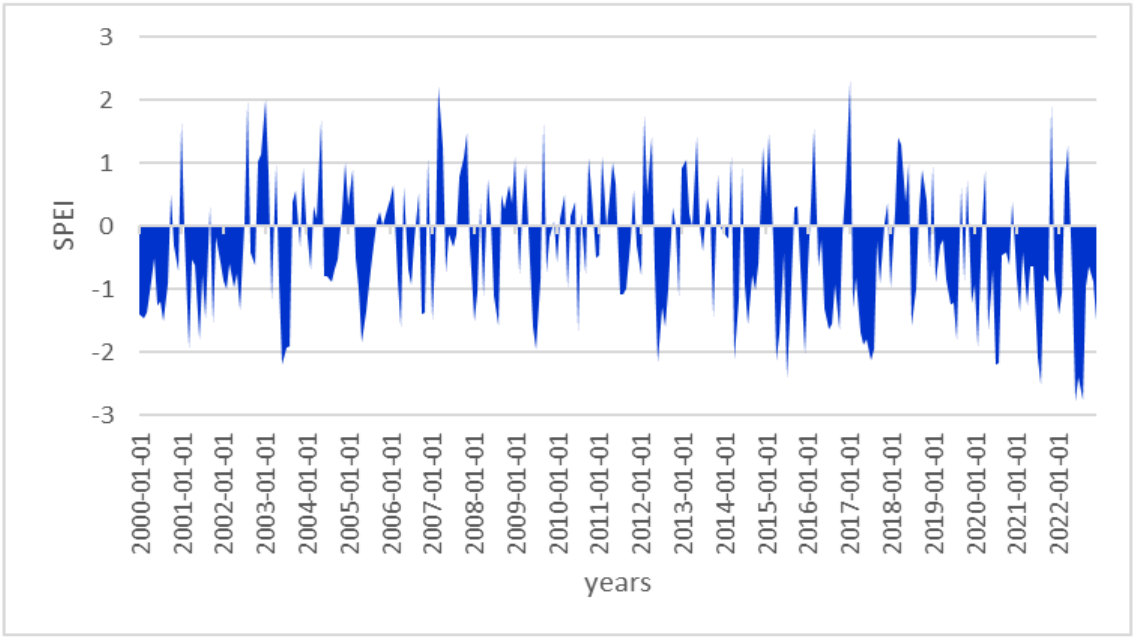

Figure III.16. Annual temporal variation of the drought index in the Reghaia basin from 2000 to 2022**.**

In the seasonal ranges, the drought index showed significant fluctuations as it recorded an increasing trend in the spring (0.0011/a, $R^2 = 0.0001$); the fluctuation range between 2004 to 2017 was large and decreased between 2018 to 2022, indicating that the range in the Reghaia basin fluctuations took a trend towards drought in the spring (Fig III.17 a). SPEI took a decreasing trend in summer and autumn, with a downward rate of (-0,0539/a, $R^2 = 0.3401$) and (-0,0231/a, $R^2 = 0.1217$), respectively (Fig III.17 b, c). However, summer showed large and irregular fluctuations, and SPEI reached its lowest levels in 2022. In addition, these results have shown an increase and recurrence of drought intensity in recent years in all seasons.

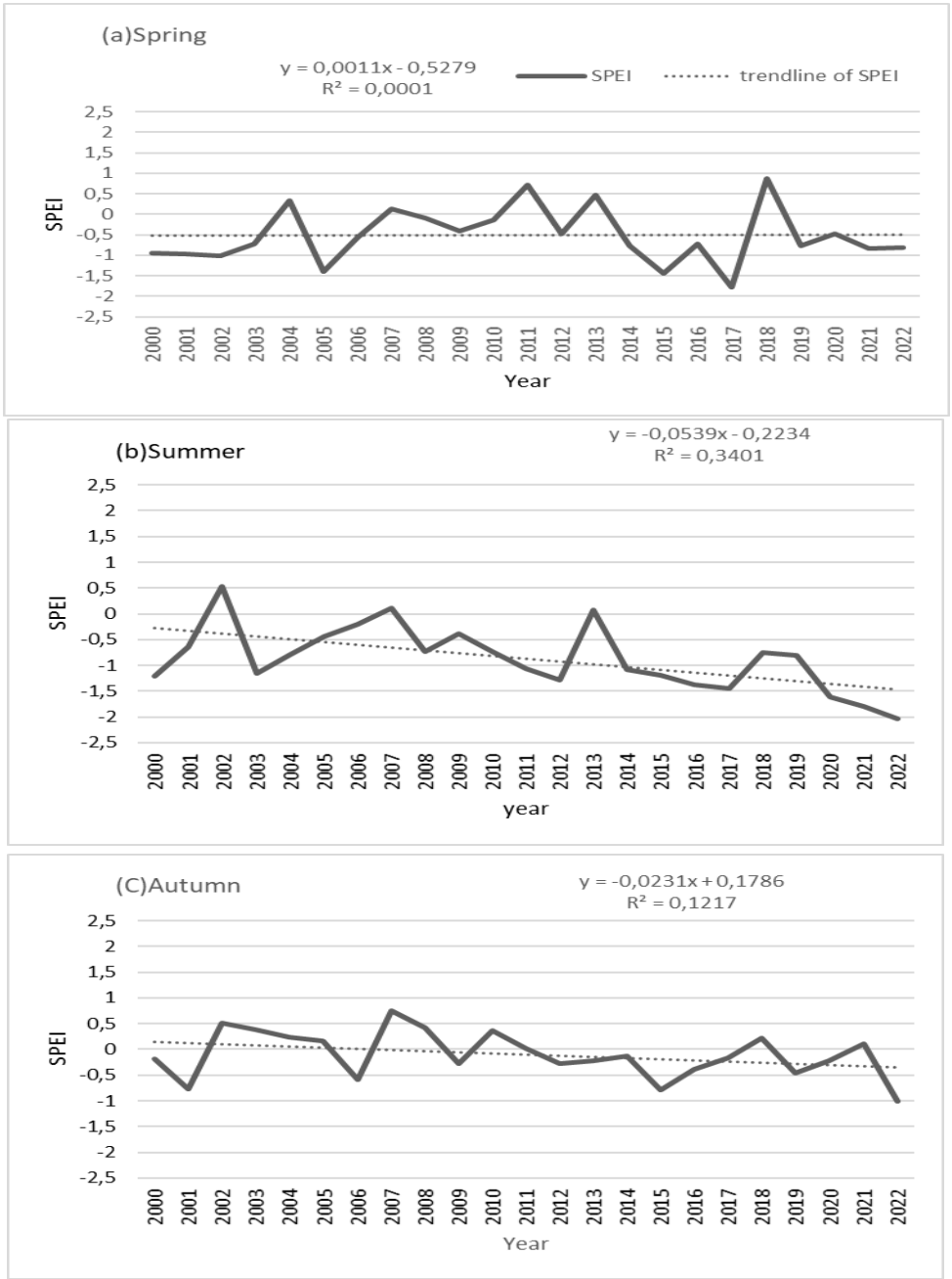

Figure III.17. Seasonal temporal variation of the SPEI in the Reghaia basin from 2000 to 2022. (a Spring), (b Summer), (c Autumn).

3.6. Association analysis

To further understand the effect of drought on vegetation, the association between the two indicators, NDVI and SPEI, was analyzed **(**Fig. III.18**)**. The NDVI had the highest correlation with SPEI in 2021, as the relationship was positive (R = 0.5) and the region's drought rate has eased, while negative correlations have been recorded from 2000 to 2007, 2010 to 2012, 2014, and 2017 to 2021. The drought rate has been the highest in these years. These results indicate the extent to which droughts affect vegetation. Moreover, the NDVI peak has decreased with a negative SPEI, as 2002 was most affected by the high drought rate. (R = -0,6), as evidenced by the presence of large oscillations in the index, especially in recent years.

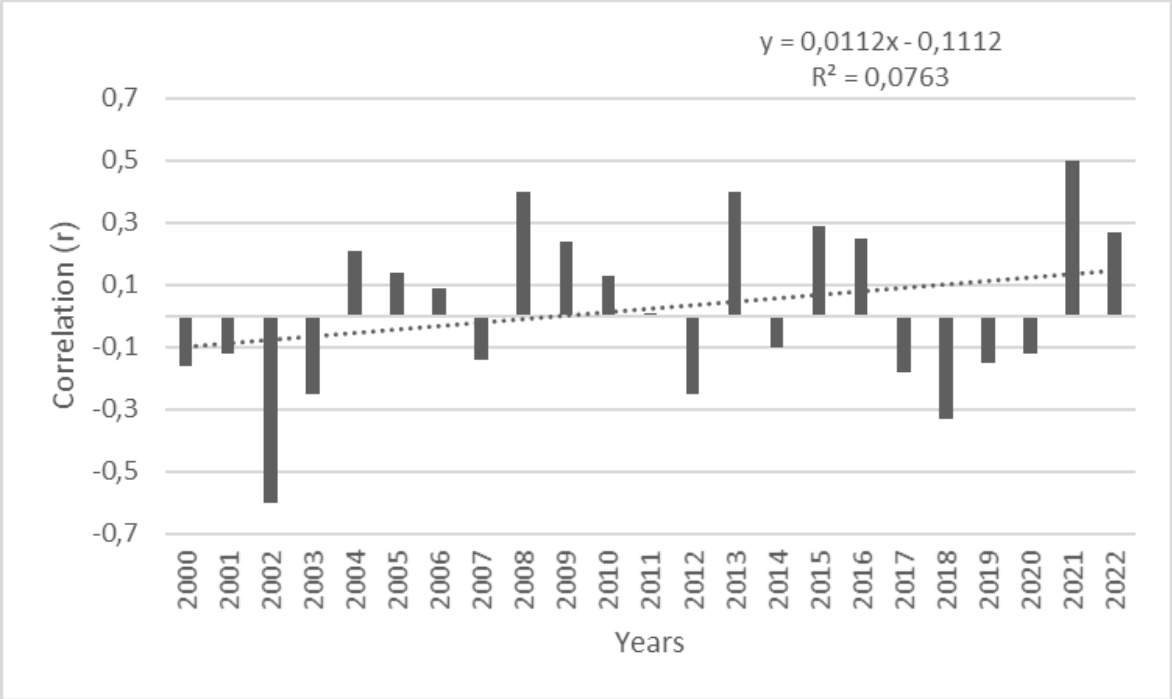

Figure III.18. Correlation among the Drought Index and NDVI in the Reghaia basin from 2000 to 2022.

3.7. Characteristics of Vegetation: Dynamic and Climate Extremes

During 2000–2022, a decrease in vegetation was detected in the Reghaia basin, not only at the annual level but also at the seasonal level. Spatial changes also showed distinct variations, and greenery was gradually leaning from east to west in the region, where it recorded the highest value for plant density in 2005 and was concentrated in forest areas and agricultural land. Comparing the annual temporal and spatial distributions of the NDVI, our study revealed an increasing trend of 0.008 year-1 from 2000 to 2022. In addition, the vegetation balance underwent several seasonal fluctuations, with NDVI showing in the spring a decrease in greenery in the growing season, and in the autumn, the consistency ratio was relatively lower.

Climate indicators on vegetation showed strong trends but were somewhat heterogeneous. Annual associations between NDVI and extreme climate showed negative trends as the proportion of temperatures that negatively affected vegetation dynamics increased. It has also recorded positive correlations between NDVI and rainfall in some years, which have enhanced plant activity during these years, but the positivity of this correlation has not been strong due to the effect of rising temperatures. The timing of the rain was also sporadic. Seasonal associations between the vegetation index and climatic factors in the Reghaia basin also indicated a negative relationship that significantly affected growth, prevalence, and plant diversity in all regions.

During the past 22 years, the Reghaia region has experienced excessive weather fluctuations, particularly in recent years. Climate changes in this area have been characterized by high heat and evaporation (Peng et *al*., 2013; Tan et *al*., 2015), affecting the basin's water ratio, reducing vegetation productivity in the region, and increasing hazardous natural phenomena such as desertification. In addition, the percentage of rainfall is decreasing, especially in the autumn and spring, which has increased the rate of decline in the green areas covered and decreased the water level in the basin.

3.8. Analysis of the impact of drought on vegetation

The vegetation response to the seasonal ranges of the drought index in the Reghaia catchment varies over time, as drought resistance varies depending on ecosystems (Xu et *al*., 2018). In this work, a strong relationship was recorded between the vegetation index and SPEI due to the distribution of green cover in the region. The association between NDVI and SPEI has been negative, and the region's drought rate has increased, reducing the proportion of available water that affects plant growth. According to the correlation characteristics between the two NDVIs and SPEIs in the annual ranges, 2021 recorded the strongest R = 0.5 correlation. At the level of seasonal ranges, droughts affected the summer, followed by spring and then autumn. In the summer, the drought rate increased. The green cover is going through a critical period because of the lack of water available to plants, which reduces their growth and leads to a change in the plant index (Huang et *al*., 2009). The cover level in autumn decreased significantly, showing a negative relationship between NDVI and SPEI.

In general, drought changes the plant environment, especially with severe climatic changes and changing rainfall patterns in the region, rising temperatures in spring and autumn, repeated

cases, and increased drought intensity. In the future, it is important to broaden the focus on the causes of increased drought, which is what we will focus on in our next study.

4. Assess the quality of wetlands in Algeria

4.1. physico-chemical analyses

4.1.1. Water potential (pH)

The pH values record significant differences in stations, with values varying between acidity, neutrality, and alkalinity. The maximum average value (pH = 10.8) was recorded in Dayet El Ferd and the minimum (pH = 2) in Karrada Dam (Fig. III.19). The pH of wetlands water depends on water sources, geochemical effects, and natural and human environmental changes affecting these ecosystems.

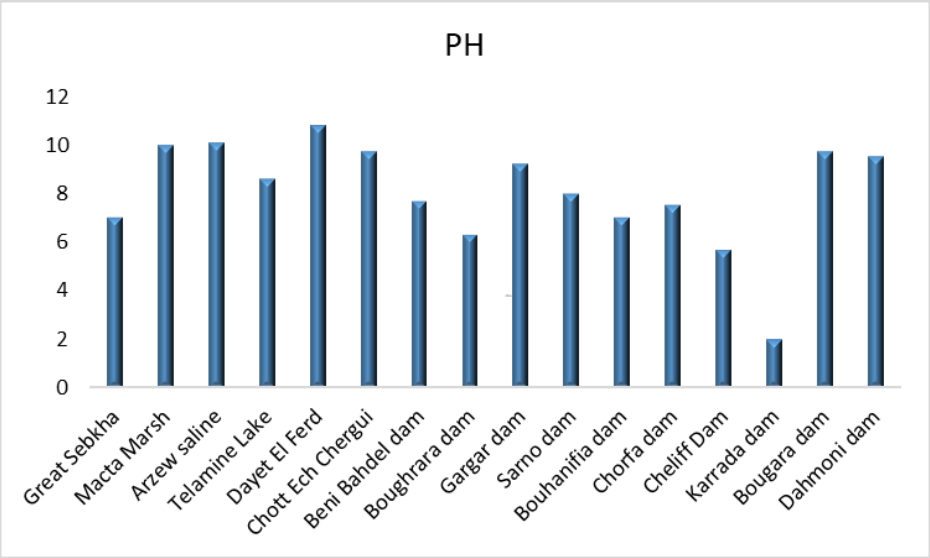

Figure III.19. Mean water pH values wetlands.

4.1.2. Water temperature

During the study period, mean temperature values show slight temporal differences, and these differences are mainly due to factors such as time differences between measurements taken at different stations and geographical features that can affect surface water temperature in different ways (Fig III.20).

4.1.3. Electrical Conductivity (CE)

Electrical conductivity is measured to assess water mineralization in general. In general, we have not noticed significant differences in the CE. The maximum average at Cheliff Dam (CE = 2000 µ s/cm), which means strong salting of this station, The minimum value is recorded in Beni Bahdel dam (CE = 770 µ s/cm). The variations in water temperature and dissolved

substance concentration at each site can partially explain these differences in conductivity levels between different stations (Fig. III.21).

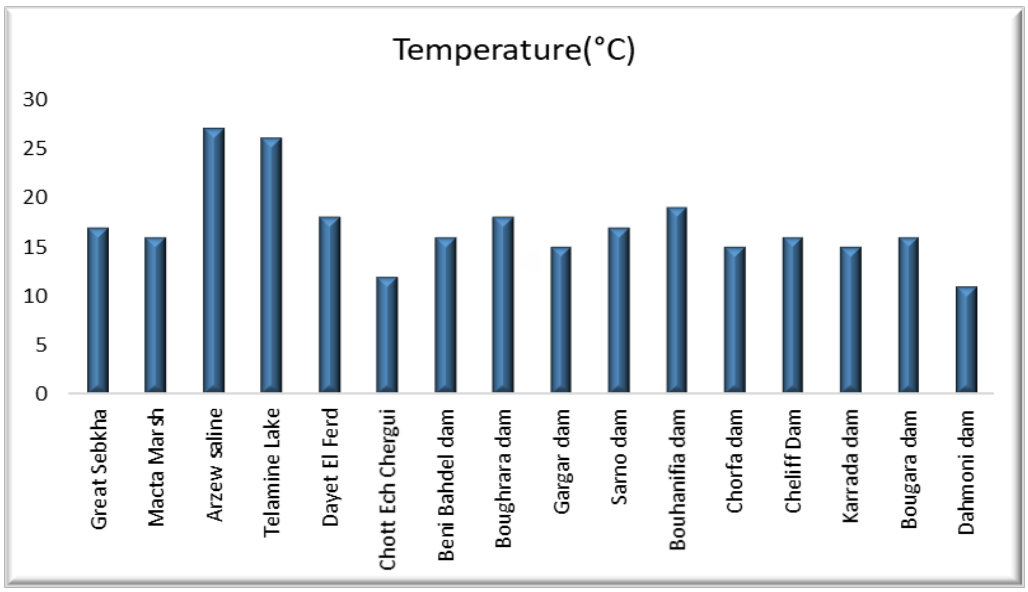

Figure III.20. Temporal average of water temperature in wetlands.

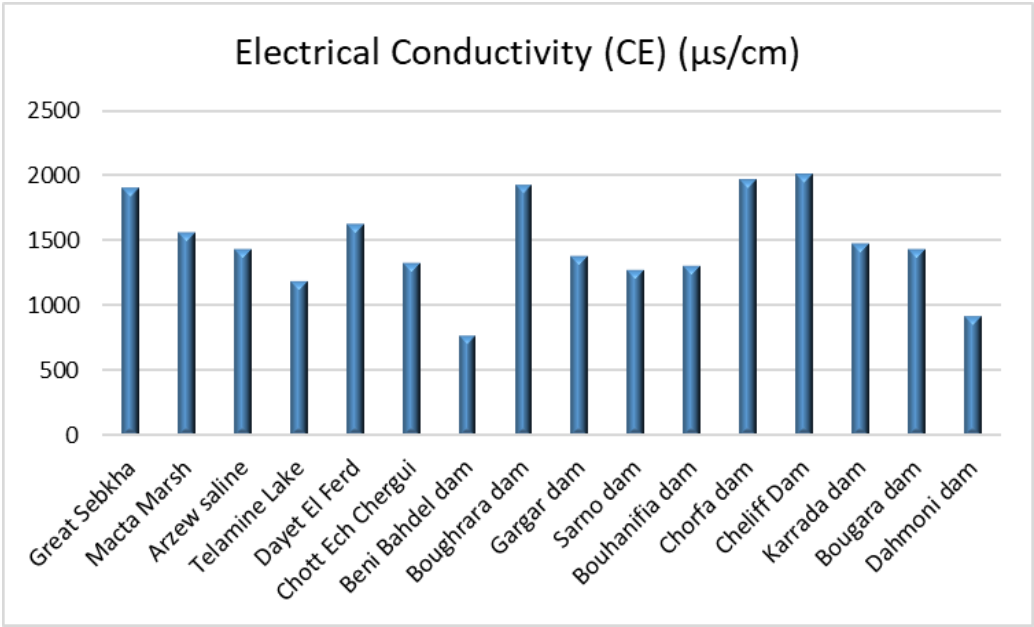

Figure III.21. Temporal average of water electrical conductivity wetlands.

4.1.4. Total dissolved solids and salinity

There was a noticeable difference in TDS and salinity concentrations among the sites, with the Bougara Dam and Great Sebkha having the highest values, respectively. This might have something to do with the different industrial discharges in these stations, which speed up the breakdown of microbiologically complex organic matter into simple metal compounds. This makes more salts and dissolved materials float in the water. This also demonstrates how both

natural and human factors affect the water quality in various water areas. The Beni Bahdel dam has the lowest salinity and TDS concentrations ever measured. The decline in rainfall inputs may be attributed to the impact of water dilution. Runoff, changes in liquid flows, and breaks in vegetation all have a significant impact on water erosion by increasing the solid load in a water body (Fig III.22,23).

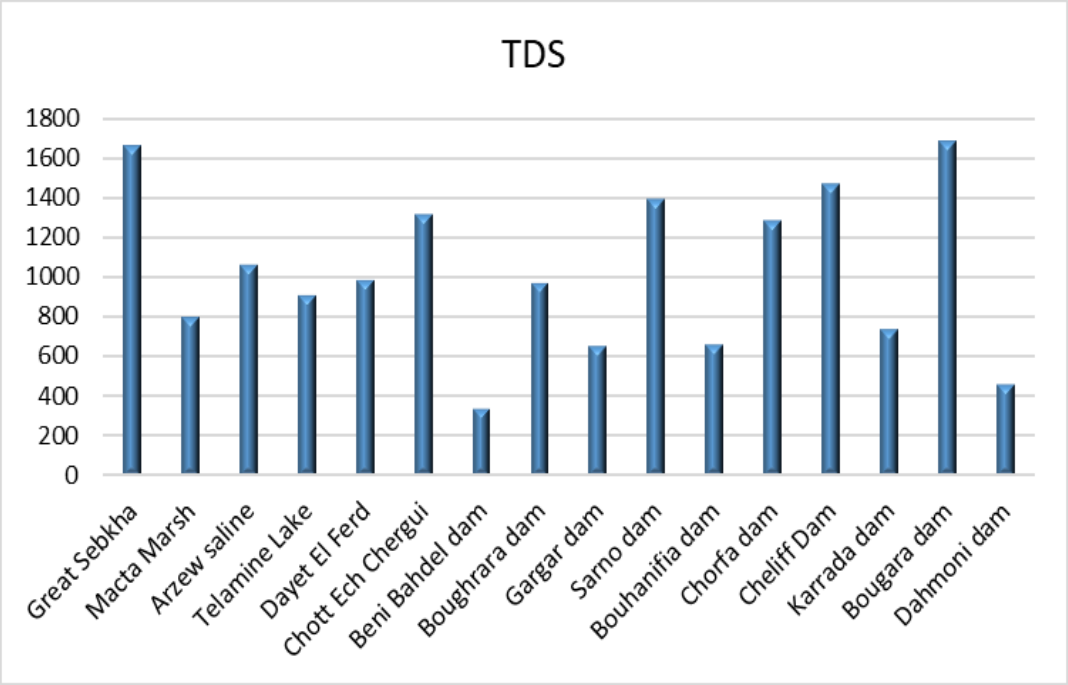

Figure III.22. Average water total dissolved solids values in wetlands.

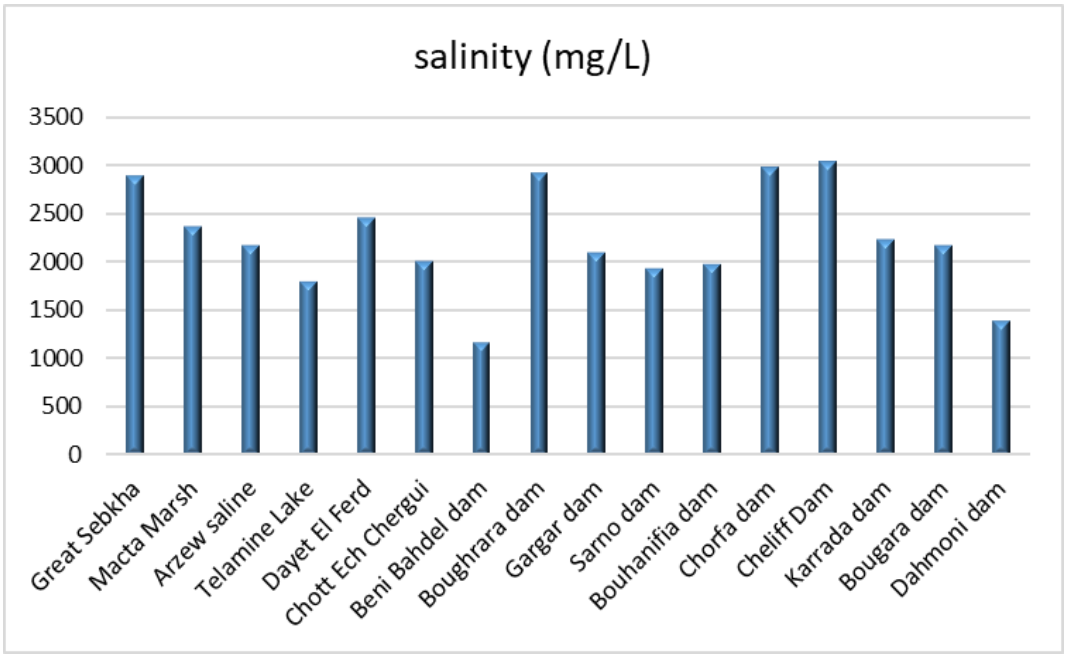

Figure III.23. Average water Salinity values in wetlands.

5. Assessing the presence of metals and potential health risks in surface waters; A case study conducted in Algeria using a combination of Artificial Neural Networks and multiple indices.

5.1. Heavy metals Contamination Index (HPI, HEI)

The pollution study evaluates the levels of heavy metals in samples of surface water from wetlands, utilizing two primary indicators HEI and HPI. Prasanna et *al*. (2012); Tokatli et *al*. (2021) categorizes HEI results into three pollution levels: HEI < 10 represents low pollution, HEI = 10–20 represents medium pollution, and HEI > 20 represents high pollution. Bhuiyan et *al*. (2010); Siegel, (2002) classified HPI results into three pollutant categories: minimal HPI (< 50), moderate HPI (50–100), and elevated HPI (> 100). HPI is estimated using heavy metal values in surface water (lead, mercury, cadmium, nickel, chromium, and zinc). HEI reflects the biological response to heavy metal contamination.

The results indicate a notable disparity in HPI and HEI levels among various monitoring locations. The majority of stations exhibit increased HEI values, which indicate moderate to high levels of heavy metal contamination. Stations like Gargar Dam, Bouhanifia Dam, and Chott Ech Chergui exhibit notably elevated HEI values, signifying significant heavy metal contamination. Although there is considerable variety in HPI readings, it is evident that the majority of stations exhibit high to medium HPI values, indicating large amounts of heavy metal contamination. The study shows that there is widespread heavy metal contamination in the areas examined, which can hurt both the environment and public health. The contamination can be attributed to elements such as industrial and agricultural activity, as well as industrial and home leftovers (Table III.8).

Table III-8. Evaluation of pollution indicators.

Watersheds	Mean HPI	HEI
Great Sebkha	109,6506	1.937
Telamine Lake	101,8695	9.447
Macta Marsh	106,7901	4.081
Arzew saline	100,9385	40.479
Sarno dam	126,7755	5.812
Beni Bahdel dam	197,3031	5.529
Boughrara dam	266,2346	50.141
Bougara dam	132,4949	9.314

Chorfa dam	149,3703	15.198
Karrada dam	150,5508	30.131
Gargar dam	415,6029	957.942
Dahmoni dam	126,842	8.512
Chott Ech Chergui	120,5877	197.478
Bouhanifia dam	197,2699	297.818
Cheliff Dam	135,0886	10.865
Dayet El Ferd	89,66176	121.518

5.2. Exploring the association between heavy metals, physical-chemical interactions, and HPI

Statistical analyses were used to examine the existence of toxicants in water samples, and factors influencing the movement and distribution of metal pollutants. A source and pathway to particle media can be indicated by the coordination of metals (Proshad et *al*., 2021). The Pearson Coefficient (r) was used to evaluate the relationship between heavy metals and indicators of water quality as well as to identify possible contaminant sources (Sojobi, 2016; Tirkey et *al*., 2017). Analysis showed a strong positive correlation between Cu and Cd (r = 0.848), Cd and Zn (r = 0.736), and Cu and Zn (r = 0.456). This enhances our understanding of how contaminants are transported and distributed within aquatic systems. Also, these findings revealed that these factors have a great influence on the diffusion rate of poisonous metals as well as their environmental consequences. On top of that, there are strong associations depicted by physical and chemical interactions between EC and TDS(r=0.617), EC and salinity(r=1), TDS and salinity(r=0.617). Some variables have positive correlations but others lack enough interconnections among them at all levels of significance which are not statistically significant. The above relationship observed between concentration versus positive associations could be due to anthropogenic causes of pollution by humans whereas it is important to note that exist a robust association between the HPI and the Pb metal (r= 0,997), indicating that this metal exerts a significant impact on the HPI (Table III.9).

In addition to sewage discharge, runoff, and trash discharge from other sources, such as vehicle washing facilities and factories, go straight into the water system. This is probably the main reason for the significantly higher concentration of Pb in comparison. Liao et *al*. (2017), discovered that the concentrations of heavy metals were 120 times greater than the typical background values, mostly as a result of mining operations. However, in our particular

situation, various causes of water pollution have likely contributed to the very high concentrations of heavy metals, as seen in Table III.9. The absence of a substantive link between heavy metals and acidity may be attributed to the fact that the same degree of acidity can affect the chemical reactions of heavy metals in water. In addition, many complex and intersecting factors control the capture of heavy metals in water, including the interaction of heavy metals with organic matter in water, leading to the formation of soluble or non-soluble compounds. These interactions can significantly affect the mobility and availability of heavy metals. Several other negative correlations were observed, although their statistical significance was limited due to the weak strength of the link.

Table III-9. Correlation Analysis Among Heavy Metals and EC, TDS, pH, Salinity, and Temperature in the Water Body.

Variables	T(°C)	PH	EC s/cm)	TDS	Salinity (mg/L)	Pb	CU	Cd	Zn	HPI
T(°C)	**1**									
PH	0,126	**1**								
EC (s/cm)	0,028	-0,270	**1**							
TDS	0,042	0,024	0,617	**1**						
Salinity (mg/L)	0,028	-0,270	1,000	**0,617**	**1**					
Pb	-0,076	-0,284	-0,352	-0,372	-0,352	**1**				
CU	-0,250	0,047	-0,118	-0,143	-0,118	-0,253	**1**			
Cd	-0,097	0,031	-0,237	-0,119	-0,237	-0,279	**0,848**	**1**		
Zn	0,163	-0,012	0,054	0,082	0,054	-0,318	0,456	**0,736**	**1**	
HPI	-0,066	-0,279	-0,324	-0,353	-0,324	**0,997**	-0,314	-0,351	-0,368	**1**

5.3. Principal component analysis

The PCA is a statistical method used for data analysis and dimensionality reduction. It serves as a potent tool for understanding the distribution of heavy metals in polluted areas. When you use PCA with Varimax rotation, you get four factors above the elbow point where the value is greater than 1 (Table III.10). This shows that PCA works to reduce the size of the dataset being analyzed (Varol, 2020). The eigenvalue indicates that the first two components account for approximately 93.540% of the variance, while the remaining components contribute 6.459% or less to the overall variation. The results indicate that the primary components, PCA 1 and PCA 2, account for around 49.084% and 44.456% of the total

variation, respectively (Fig. III.24). On the other hand, PCA 3 and PCA 4 exhibit proportions below 5.015% and 1.444% of the variation, respectively.

Table III-10. The Eigenvalues of the Principal component matrix.

	Eigen value	Percentage of variance (%)	Cumulative
1	1,963	49,084 %	49,084 %
2	1,778	44,456 %	93,540 %
3	0,201	5,015 %	98,556 %
4	0,058	1,444 %	100 %

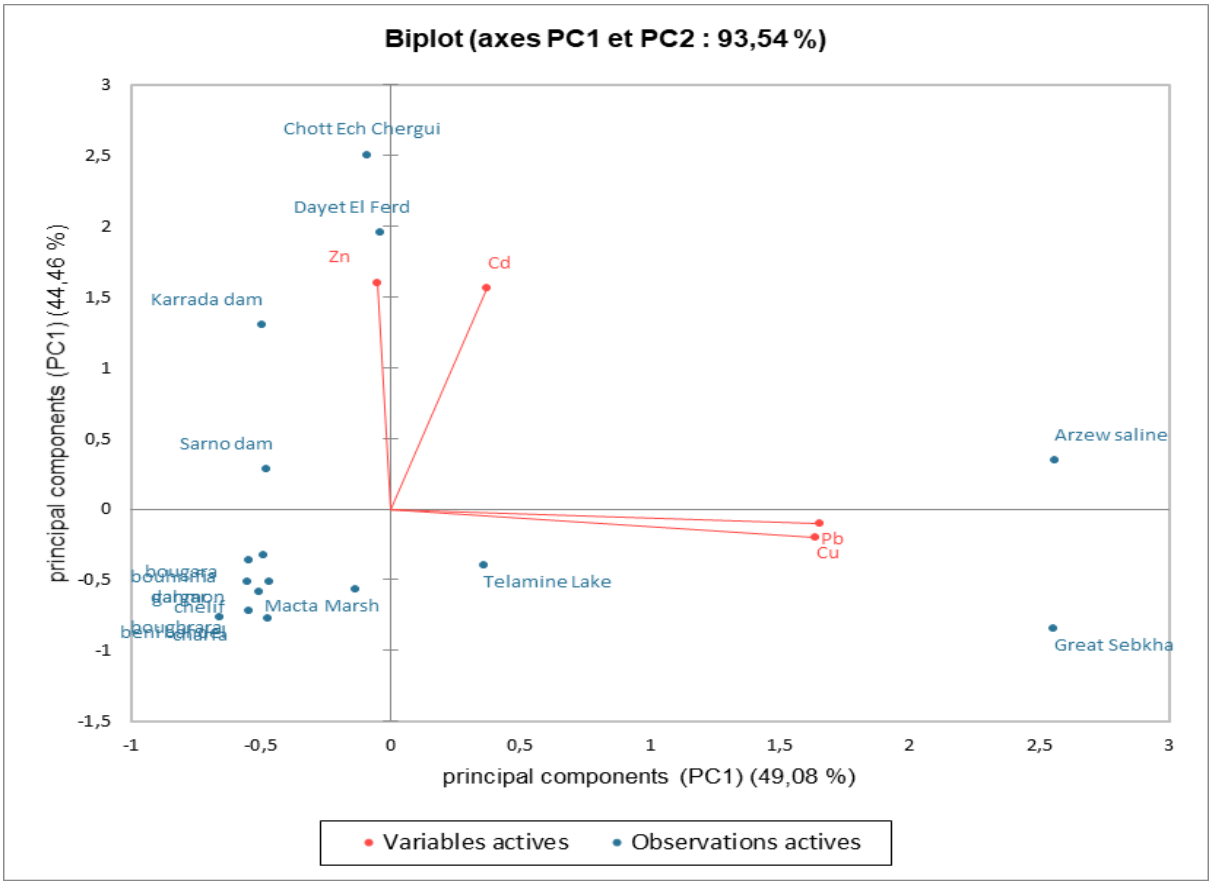

Figure III.24. Biplot Visualization of Principal Component Analysis of Heavy Metal Distribution Across Various Sampling Locations.

According to Liu et *al*. (2003), absolute scores have been used to classify trace elements. Any value above 0.75 is categorized as "strong," values between 0.75 and 0.5 are labeled as "medium," and values below 0.50 are classified as "weak." The bilateral analysis findings reveal that factor 1 exhibits weak positive loads of Cd, while factors 2 demonstrate low positive loads of Zn elements, and factor 3 shows low negative loads of elements Pb and Cu. Gyimah

et *al*. (2021)) assert that both natural and human activities, such as geological processes and the emission of pollutants from industrial units, have an impact on the indicators of positive ion load. PCA can be used to depict major determinants as sources of human and natural contamination at the analyzed sites. Li et *al*. (2018) and Varol (2020) found that wastewater discharge is the primary cause of water pollution. This highlights the need to understand the distribution and chemical interactions of heavy metals in aquatic environments. In this sense, the sampling areas located in the middle and downstream of the research area had the highest concentration of the parameters, possibly due to strong industrial and commercial activity in those areas.

The 16 sites were grouped into three significant categories using hierarchical cluster analysis, demonstrating spatial variability in Algeria (see Fig. III.25). The dendrogram illustrates these groupings, with Group 1 comprising two points, such as Great Sabkha and Arzew Saline, Group 2 comprising ten locations, such as Telamine Lake, Macta Marsh, Beni Bahdel Dam, Boughrara Dam, Bougara Dam, Chorfa Dam, the Gargar dam, the Dahmoni dam, the Bouhanifia dam, and the Cheliff dam) and finally Group 3 comprising four sites including the Karrada Dam, the Sarno Dam, Dayet El Ferd, and Chott Ech Chergui. These groupes show respectively low, medium, and high pollution levels, depending on similar characteristics and natural background sources used in the clustering method.

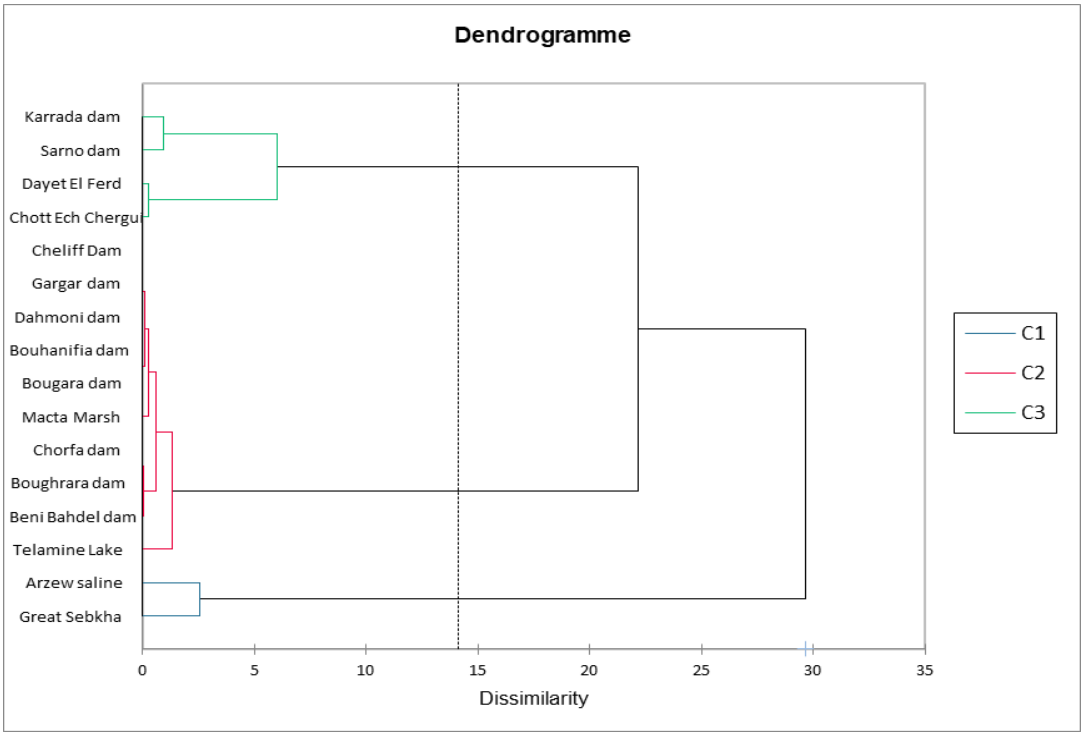

Figure III.25. Cluster Analysis of Sixteen Sampling Locations in Algeria Using Hierarchical Agglomerative Clustering (CAH).

5.4. Artificial Neural Network Modeling for Predicting Heavy Metal

To optimize the prediction of Cu, Cd, Zn, and Pb ion concentrations, the data underwent multiple training and test cycles using four distinct models. Lu et *al*. (2019) demonstrated that incorporating electrical conductivity (EC) values into the model for estimating certain metals could significantly impact its performance. Additionally, Lu et *al*. (2019) identified pH and temperature as crucial input variables for predicting mineral concentrations. The models with the highest specialty coefficient and the lowest mean square error were selected for each biological material considered during the training experiments.

Using MATLAB R2023b, a linear analysis was conducted on the input slopes and their corresponding outputs. Fig. III.26 illustrates the results for Pb, Cd, Cu, and Zn, while Fig. III.27 depicts the mean square root values used for assessing network performance. The tests and validation evaluations confirmed excellent performance, with the network architecture demonstrating an exceptional ability to reproduce experimental data.

Table III.11. indicates the average RMS values obtained when developing, checking and testing suggested artificial neural networks as regards Pb, Cu, Cd, and Zn. All the models recorded R2 values higher than 0.5 during testing which means low error values. Although this varies with model type, heavy metal content can be predicted relatively well based on such variables as temperature, pH EC, TDS, and Salinity. By doing so these ANN models together with easily measurable parameters allow quick detection of toxic heavy metals in water bodies. Based on test evaluation results for different types of heavy metals, the ranking of models follows from best to worst. River pollution control requires efficient identification with regard to growing importance of ANN applications in environmental fields like water resources management; water quality; hydrological analysis (Sarkar & Pandey, 2015).

Table III-11. Performance's multilayer of the artificial neural network models.

Inputs	Number of hidden layer nodes	Transfer function (hidden)	output	Transfer function Output	RMS errors		
					Training	Validation	Testing
Temp, pH, EC, TDS, Salinity	3	Logsig	Pb	Tansig	0.7111	0.7596	0.0843
Temp, pH, EC, TDS, Salinity	3	Logsig	Cd	Tansig	0.0701	0.0741	0.0721
Temp, pH, EC, TDS, Salinity	3	Logsig	Cu	Tansig	0.0036	0.0017	0.0216
Temp, pH, EC, TDS, Salinity	3	Logsig	Zn	Tansig	0.0655	0.0656	0.0721

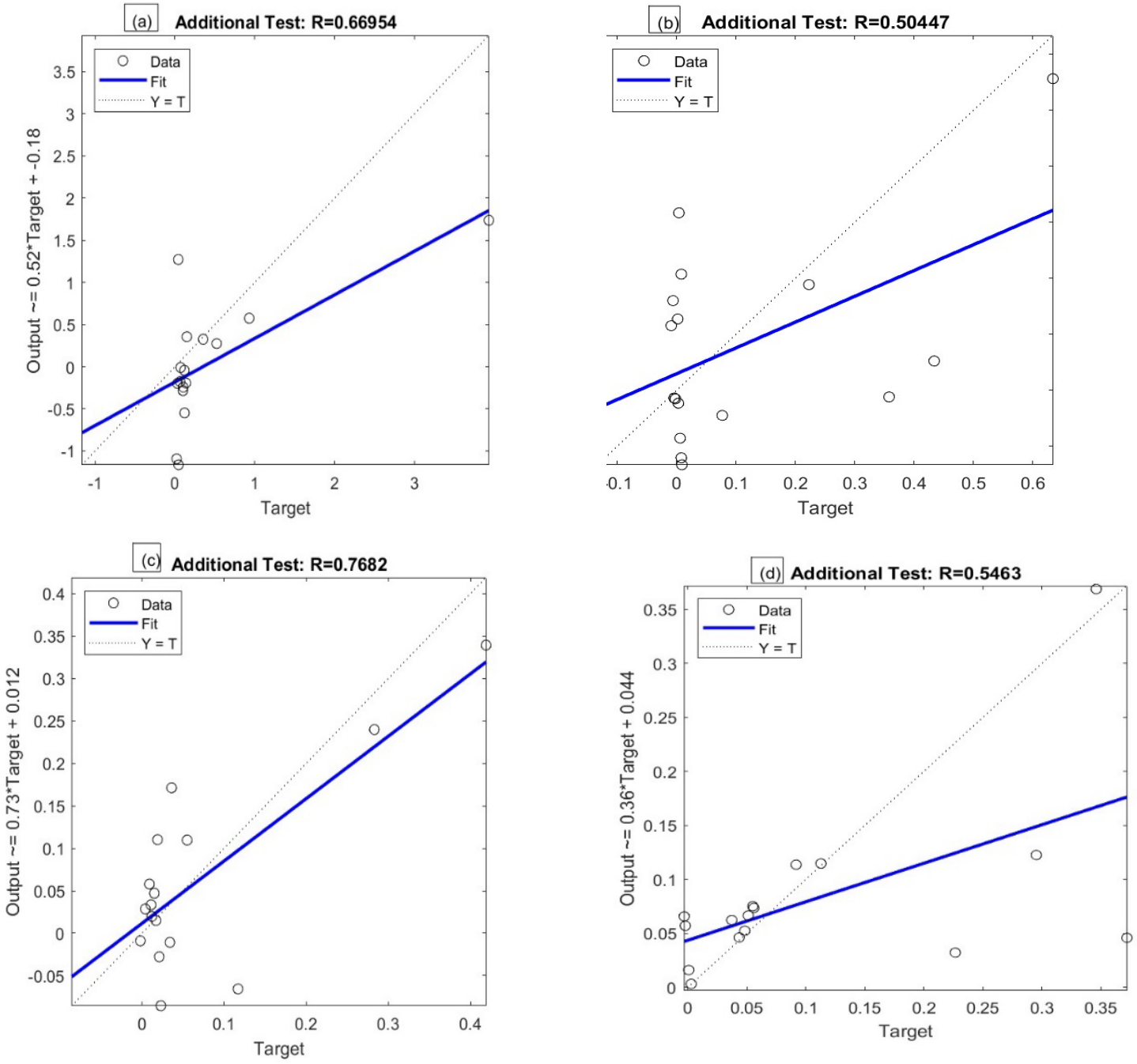

Figure III.26. Network regression for a (Pb), b(Cd), c (Cu) and d (Zn).

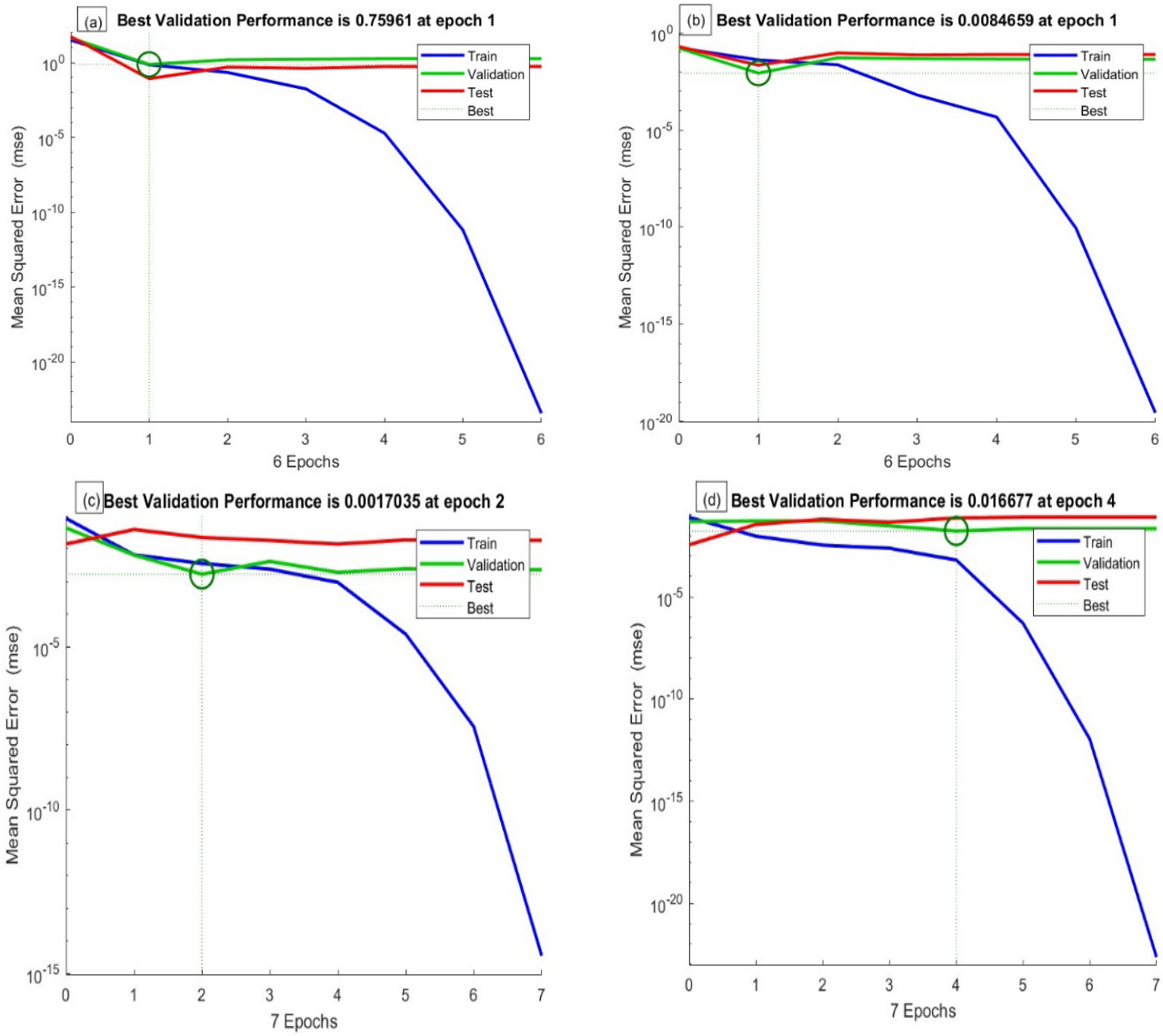

Figure III.27. RMS for a (Pb), b(Cd), c (Cu) and d (Zn).

Conclusion

Conclusion

Examining the time lag in understanding climatic changes, the dynamics of vegetation index, and the susceptibility of ecosystems to climate change is crucial. The research of 25 watershed districts determined that there has been a notable increase in aridity due to changing climatic conditions over the past decade. Vegetation exhibited a decreasing pattern. Decreased precipitation and rising temperatures negatively impacted vegetation growth from 1981 to 2021. For further comprehension, the study employed a partial correlation technique to examine the relationship between NDVI and meteorological conditions, revealing the level of vegetation degradation and dryness across all regions. The basins have seen a reduction in water levels. These changes will result in the extinction of numerous species, particularly in the Dayet El-Ferd and Great Sebkha basins, which are now facing an exceptional drought. The findings show that the warmer environment has gradually reduced its beneficial impact on plant growth. The vegetation index responded more to rainfall than to temperature.

A large dataset from the years 2000 to 2020 also showed the results of the study. The average mean NDVI values were between 0 and 0.7, and the mean percentage was between 0.098% and 0.34%. During the multi-year cycle, the research found that there was a discernible decrease in the values of the NDVI. Additionally, a severe decline in vegetation was observed in several locations, with values that did not reach 0.2. According to the findings of the research, the NDVI exhibited a more robust spatial and temporal response in comparison to the EVI, NDWI, and NDMI. The significant link that existed between NDVI and EVI was another factor that contributed to the conclusions as a whole. The fact that the normalized difference vegetation index (NDVI) has a negative correlation with the land surface temperature (LST) highlights the influence that drought and plant stress have on the vegetation in the regions under investigation (R2 = 0.109 - R2 = 0.5701). There is a considerable negative link between the values of NDVI and LST, which indicates that higher temperatures are related to a decrease in the density and health of vegetation. The readings of the NDMI, which accurately represent the amount of water stress in bodies of water, revealed a considerable downward trend. This demonstrates the impact that shifting levels of moisture availability have on the dynamics of plants contained inside bodies of water. Because of the data that was produced from the Mk trend analysis, the significance of NDVI was brought to light, and its significant relationship with EVI, NDWI, and NDMI was also highlighted.

Research is being conducted in the Reghaia basin to investigate the factors that lead to the deterioration of vegetation and how it reacts to droughts. As a consequence of these findings,

the quantity of greenery in the area has decreased over time, and the severity of the drought has increased, particularly in light of the climatic changes that have taken place. Furthermore, the trend of these alterations has shifted in recent years. In the autumn and summer, the NDVI found a negative relationship between reduced vegetation and increased drought. In the spring, the pattern was positive but reduced from 2018 to 2022, suggesting that the spectrum of changes in the abdomen took a direction toward drought. This was one of the seasonal variations that were observed in the association between the NDVI and the SPEI. During rare seasonal times, it was shown that there were negative relationships between climatic parameters and NDVI. The results of these investigations also demonstrated that there are distinct seasonal changes in plant development, as well as a record of temporal delays of one to two months as a result of delayed rainfall. The region's drought situation worsened as a result of the Reghaia watershed's decreased water level, which was a result of the change in rainfall patterns and the rise in temperature. In conclusion, this research demonstrates the detrimental impacts that severe climatic conditions have on vegetation, the elements that are responsible for the escalation of droughts, and the numerous factors that led to a decrease in the water level and a lack of vegetation.

This research had several key objectives, one of the most important of which was to assess the condition of surface water in sixteen basins in Algeria from the perspective of the availability of water, with a particular focus on the pollution of heavy metals. The research provided a substantial amount of new information on this pollutant. The results of the analyses performed on the samples that were obtained from these surface waters revealed that the mineral levels were raised, which suggests that these areas have very high quantities. Following the completion of the study, it was determined that Pb and Cd are the principal metals that pose the greatest threat to the quality of the water. As a result of the pollution detection indices, it was determined that the majority of the surface water samples were above the significant pollution criteria, which required special attention. The results of the analysis showed that more than ninety-nine percent of the samples had significant pollution levels according to the HPI index, and sixty percent of the samples had high pollution levels according to the HEI. This indicates that there is a large risk of contamination in these bodies of water.

A considerable number of causes of pollution have been found via the use of statistical analysis, Pearson correlation, and principal component analysis. According to the findings of many pieces of research, the mining industry is primarily responsible for the production of metals like Pb, Zn, Cu, and Cd. However, these metals did not show a strong link with any of

the other natural sources that were investigated. According to the results, the existence of lead and cadmium minerals may be attributed to chemical plants and the emissions that they produce. On the other hand, the sources of zinc and copper minerals may include fertilizers, rocks, and the effects of human activities.

To forecast heavy metal concentrations, neural networks were highlighted as a strategy that is both accurate and cost-effective. This approach has resulted in time and resource savings in the monitoring of water pollution. It was determined throughout the research that the most effective model for controlling pollution standards should be used; nonetheless, it is recommended that similar research be carried out for other types of water resources to monitor and simulate contamination.

It is possible to relate the extent of the modifications and deterioration that have been found in these locations to variables such as drought and other environmental factors that generate stress on vegetation. The results of this research, taken as a whole, highlight the intensity of these modifications and deterioration. In addition to stressing the need for good conservation and management actions in the places that were researched, these results provide vital data that can be used to comprehend the patterns of both water and vegetation stress.

Reference

References

Abulhawa. T., 2017. Inventaires culturels rapides des zones humides dans six États arabes dont des Sites Ramsar et des Biens du Patrimoine mondial. Rapport Secrétariat Ramsar et le Programme Tabe'a de l'UICN sur l'élaboration des inventaires culturels rapides, 120p.

Ahmim, M., 2019. Les mammiferes sauvages d'Algérie répartition et Biologie de la Conservation. Les Éditions du Net, 978-2312068961. Ffhal-02375326f., 295 pp.

Ajadi, O., Meyer, F., Webley. P., 2016. Change detection in synthetic aperture radar images using a multiscale-driven approach. Remote Sens 8 :482. https://doi.org/10.3390/rs8060482.

Ablat, X., Liu, G.H., Liu, Q.S., Huang, C., 2019. Application of Landsat derived indices and hydrological alteration matrices to quantify the response of floodplain wetland to river hydrology in arid regions based on different dam operation strategies. Sci. Total Environ. 688, 1389–1404.

Amani, M., Mahdavi, S., Afshar, M., Brisco, B., Huang, W., Mohammad Javad Mirzadeh, S., White, L., Banks. S., Montgomery, J., Hopkinson, C., 2019. Canadian Wetland Inventory using Google Earth Engine: The First Map and Preliminary Results. Remote Sensing. 11(7):842. https://doi.org/10.3390/rs11070842.

Amani, M., Ghorbanian, A., Ahmadi, S.A., Kakooei, M., Moghimi, A., MirmazloumiS, M., Moghaddam, S.H.A., Mahdavi, S., Ghahremanloo, M., Parsian, S., 2020. GoogleEarth Engine Cloud Computing Platform for Remote Sensing Big Data Applications: A Comprehensive Review. IEEE J. Sel. Top. Appl. Earth Obs. Remote Sens., 13, pp. 5326-5350.

Amarnath., G., Babar, S., Sri., M., Murthy, R., 2017. Evaluating MODIS vegetation continuous field products to assess tree cover change and forest fragmentation in India – a multi-scale satellite remote sensing approach. Egypt J Remote Sensing Space Sci 20:157–168. http://dx.doi.org/10.1016/j.ejrs.2017.05.004.

Babali, B., 2014. Contribution à une étude phytoécologique des monts de Moutas (Tlemcen, Algérie occidentale) : Aspects syntaxonomique, biogéographique et dynamique. Doctoral thesis, univ., Aboubakr Belkaid, Tlemcen, Algérie,174pp.

Bachouche, S., Houma, F., Gomiero, A. et al., 2017. Distribution and

Environmental Risk Assessment of Heavy Metal in Surface Sediments and Red Mullet (Mullus barbatus) from Algiers and BouIsmail Bay (Algeria). Environ Model Assess., 22, 473–490. doi.org/10.1007/s10666-017-9550-x.

Baeten, J., Langston, N., Lafreniere, D., 2018. A spatial evaluation of historic iron mining impacts on current impaired waters in Lake Superior's Mesabi Range. Ambio., 47, 231–244.

Bai, Y., Guo, C., Degen, A.A., Ahmad, A.A., Wang, W., Zhang, T., Li, W., Ma, L., Huang, M., Zeng, H., Qi, L., Long, R., Shang, Z., 2020. Climate warming benefits alpine vegetation growth in Three-River Headwater Region. China. Science of The Total Environment. 742, 140574.https://doi.org/10.1016/j.scitotenv.2020.140 574.

Bakalem, A., Dauvin, J.C., Grimes, S., 2014. New marine amphipod records on the Algerian coast. Journal of the Marine Biological Association of the United Kingdom, 94, 753-762. https://doi.org/10.1017/S0025315414000125.

Ban, C., Xu, Z., Zuo, D., Liu, X., Zhang, R., Wang, J., 2020. Vertical influence of temperature and precipitation on snow cover variability in the Yarlung Zangbo River basin, China. Int. J. Climatol, 41 (2), pp. 1148-1161.https://doi.org/10.1002/joc.v41.210.1002/joc.6776;5.

Barnaud, E., Fustec, E., 2007. Conserver les zones humides : pourquoi ? comment ? Éditions Quae, Versailles, 298 p.

Betbeder, J., Rapinel, S., Corpetti, T., Pottier, E., Corgne, S., et Hubert-Moy, L., 2014. Multitemporal classification of Terra SAR-X data for wetland vegetation mapping. Journal of Applied Remote Sensing, 8(1) :083648–083648.

Bhuiyan, M.A.H., Islam, M.A., Dampare, S.B., Parvez, L., Suzuki, S., 2010. Evaluation of hazardous metal pollution in irrigation and drinking water systems in the vicinity of a coal mine area of northwestern Bangladesh. J. Hazard Mater. 179, 1065–1077. doi.org/10.1016/j.jhazmat.2010.03.114.

Bhuyan, U., Zang, C., Vicente-Serrano, S., Menzel, A., 2017. Exploring relationships among tree-ring growth, climate variability, and seasonal leaf activity on varying timescales and spatial resolutions. Remote Sensing. 9, 526. https://doi.org/10.3390/rs9060526.

Burritt, R., Christ, K., 2018. Water risk in mining: Analysis of the Samarco dam failure. J. Clean. Prod., 178, 196–205.

Butler, L., Lall, U., Bonnafous, L., 2018. Cumulative Heavy Metals Contamination in Mining Areas of the **Rimac, Peru Basin. Columbia Water Cent. 1–27.**

Chang, S.Z., et al., 2011. Monitoring Cropland Phenology in Sanjiang Plain bansed on NDVI Data. Remote Sens. Technol. Appl. 26 (1), 82–88.

Chen, A., He, B., Wang, H., Huang, L., Zhu, Y., Lv, A., 2015. Notable shifting in the responses of vegetation activity to climate change in China. Physics and Chemistry of the Earth, 87–88, 60–66. https://doi.org/10.1016/j.pce.2015.08.008.

Chen, T., De Jeu, R., Liu, Y., Van Der Werf, G., Dolman, A., 2014. Using satellite-based soil moisture to quantify the water driven variability in NDVI: A case study over mainland Australia. Remote Sensing of Environment. 140, 330–338. https://doi.org/10.1016/. j.rse.2013.08.022.

Chen, X., Zhao, H., Li, P. & Yin, Z., 2006. Remote sensing image-based analysis of the relationship between urban heat island and land use/cover changes. Remote Sensing of Environment, 104, 133-146. https://doi.org/10.1016/j.rse.2005.11.016.

Chi, M., Plaza, A., Benediktsson, J.A., Sun, Z., Shen, J., Zhu, Y., 2016. Big data for remote sensing: Challenges and opportunities. Proceedings of the IEEE, 104, 2207 2219. https://doi.org/10.1109/JPROC.2016.2598228.

Claverie, M., Vermote, E.F., Franch, B., Masek, J.G., 2015. Evaluation of the Landsat-5 TM and Landsat-7 ETM+ surface reflectance products. Remote Sensing of Environment. 169, 390–403. https://doi.org/10.1016/j.rse.2015.08.030.

Congalton, R.G., 2010. Remote Sensing: An Overview. GIS cience & Remote Sensing 47, 443– 459. https://doi.org/10.2747/1548-1603.47.4.443.

Chu, H., Venevsky, S., Wu, C., Wang, M., 2019. NDVI-based vegetation dynamics and its response to climate changes at Amur-Heilongjiang River Basin from 1982 to 2015. Science of The Total Environment. 650, 2051–2062. https://doi.org/ 10.1016/j. scitotenv.2018.09.115.

Corbane, C., Lang, S., Pipkins, K., Alleaume, S., Deshayes, M., García Millán, V. E., et al., 2015, Remote sensing for mapping natural habitats and their conservation status – New opportunities and challenges, International Journal of Applied Earth Observation and Geoinformation, v.37, 7-16.

Cowardin, L.M., 1979. Classification of wetlands and deepwater habitats of the

United States, Fish and Wildlife Service, US Dept. of the Interior, Washington, 79 p.

Cowardin, L.M., SHAFFER, T.L. ET ARNOLD, P.M., 1995. Evaluations of duck habitat and estimation of duck population sizes with a remote-sensing-based system, National Biological Service, Biological Science Report 2, 26 p.

Didan, K., Munoz, A.B., Solano, R., Huete, A., 2015. MODIS Vegetation Index User'sGuide (MOD13 Series); Vegetation Index and Phenology Lab, University of Arizona: Tucson, AZ, USA.

Dobignard, A., Chatelain, C., 2010-2013. Index synonymique et bibliographique de la flore d'Afrique du Nord. Conservatoire et jardin botaniques, Genève, 1-5, 457pp.

Ducrot, D., 2005. Méthodes d'analyse et d'interprétation d'images de télédétection multi-sources, extraction de caractéristiques du paysage. Mémoire d'HDR, INP Toulouse, 240 p.

Donohue, R. J., Roderick, M. L., & McVicar, T. R., 2012. Roots, storms and soil pores: Incorporating key ecohydrological processes into Budyko's hydrological model. Journal of Hydrology, 436, 35–50. dx.doi.org/10.1016/j.jhydrol.2012.02.033.

Dubovyk, O., Landmann, T., Erasmus, B.F.N., Tewes ,A., Schellberg, J., 2015. Monitoring Vegetation Dynamics with Medium Resolution MODIS-EVI TimeSeries at Sub-Regional Scale in Southern Africa. Int. J. Appl. Earth Obs. Geoinf.,38, pp. 175-183. https://doi.org/10.1016/j.jag.2015.01.002;11.

Dybiec, J.M., Albert, D.A., Danz, N.P., Wilcox, D.A., Uzarski, D.G., 2020. Development of a preliminary vegetation-based indicator of ecosystem health for coastal wetlands of the Laurentian Great Lakes. Ecol. Ind. 119, 106768.

Eckert, S., Hüsler, F., Liniger, H., Hodel, E., 2015. Trend Analysis of MODIS NDVI Time Series for Detecting Land Degradation and Regeneration in Mongolia. J. AridEnviron., 113, pp. 16-28. https://doi.org/10.1016/j.jaridenv.2014.09.001.

Feng, H., Tao, H., Fan, Y., Liu, Y., Li, Z., Yang, G., Zhao, C., 2022. Comparison of winter wheat yield estimation based on near-surface hyperspectral and UAV hyperspectral remote sensing data. Remote Sens. 14, 4158. https://doi.org/10.1016/j.compag.2022.107433.

Fernandez-Vallejo, M., Lopez-Amo, M., 2012. Optical Fiber Networks for Remote Fiber Optic Sensors. Sensors. 12, 3929-3951. https://doi.org/10.3390/s120403929.

Filippa, G., Cremonese, E., Galvagno, M., Isabellon, M., Bayle, A., Choler, P., Carlson, B.Z., Gabellani, S., di Cella, U.M., Migliavacca, M., 2019. Climatic drivers of greening trends in the Alps. Remote Sensing. 11, 2527. https://doi.org/10.3390/rs11212527.

Fuldauer, L.I., Thacker, S., Haggis, R.A., Fuso-Nerini, F., Nicholls, R.J., Hall, J.W., 2022. Targeting climate adaptation to safeguard and advance the Sustainable Development Goals. Nat. Commun. 13, 3579.

Fytsilis, A.L., Prokos, A., Koutroumbas, K.D., Michail, D., Kontoes, C.C., 2016. A methodology for near real time changes detection between unmanned aerial vehicle and wide area satellite images. ISPRS J Photogramm Remote Sens 119 :165–186. https://doi.org/10.1016/j.isprsjprs.2016.06.001.

Gajbhiye, S., Meshram, C., Singh, S.K., Srivastava, P.K., Islam, T., 2016.Precipitation trend analysis of Sindh River basin, India, from 102-year record (1901-2002). Atmos Sci Lett 17 :71–77. doi:org/10.1002/asl.602.

Gandhi, M., Parthiban, S., Thummalu, N., Christy, A., 2015. Ndvi: vegetation change detection using remote sensing and GIS – a case study of Vellore District. 3rd Int Conf Recent Trends Comput 57 :1199–1210. https://doi.org/10.1016/j.procs.2015.07.415.

Gaussen, H.,1954. Théorie et classification des climats et microclimats, C.R. VIII° Congre. Int. Bot., Paris, Sect. 27: 125- 130.

Gao, F., et al., 2017. Toward mapping crop progress at field scales through fusion of Landsat and MODIS imagery. Remote Sens. Environ. 188, 9–25. https://doi.org/ 10.1016/j.rse.2016.11.004.

Guo, M., Li, J., He, H., Xu, J., & Jin, Y., 2018. Detecting Global Vegetation Changes Using Mann-Kendal (MK) Trend Test for 1982–2015 Time Period. Chinese Geographical Science, 28(6), 907-919. doi: 10.1007/s11769-018-1002-2.

Gao, W., Zheng C., Liu, X., Lu, Y., Chen, Y., Wei, Y., Ma, Y., 2022. NDVI-based vegetation dynamics and their responses to climate change and human activities from 1982 to 2020: A case study in the Mu Us Sandy Land, China, Ecological Indicators, 137:108745.

https://doi.org/10.1016/j.ecolind.2022.108745.

Garcia-jimenez, S., Jurio, A., Pagola, M., De Miguel, L., Barrenechea, E., Bustince, H., 2016. Forest fire detection: a fuzzy system approach based on overlap indices. Appl Soft Comput :1–9.

Gorelick, N., Hancher, M., Dixon, M., Ilyushchenko, S., Thau, D., Moore, R., 2017. Google Earth Engine: planetary-scale geospatial analysis for everyone. Remote Sensing of Environment. 202, 18–27. https://doi.org/10.1016/j.rse.2017.06.031.

Grimes, S., 2003. Biodiversité marine et littorale Algérienne, Laboratoire Réseau de surveillance environnemental. Université d'Es Senia, Oran, 314 p.

Hagag, A., Fan, X., El-samie, F.E.A., 2017. HyperCast: hyperspectral satellite image broadcasting with band ordering optimization. J. Vis Commun Image Represent 42 :14–27. http://dx.doi.org/10.1016/j.jvcir.2016.11.006.

Hao, M., Shi, W., Deng, K., Feng, Q., 2016. Superpixel -based active contour model for unsupervised change detection from satellite images. Int J Remote Sens 37 :4276–4295. https://doi.org/10.1080/01431161. 2016.1210838.

Haque, I., Basak, R., 2017. Land cover change detection using GIS and remote sensing techniques: a spatio-temporal study on Tanguar Haor, Sunamganj, Bangladesh. Egypt J Remote Sensing Space Sci 20 :251–263. http://dx.doi.org/10.1016/j.ejrs.2016.12.003.

He, K.Q., Zhang, Y., Li, W.H., Sun, G., McNulty, S., 2022. Detecting Coastal Wetland Degradation by Combining Remote Sensing and Hydrologic Modeling. Forests 13 (3), 411.

Hong, S. H., Wdowinski, S., 2014. Multitemporal Multitrack Monitoring of Wetland Water Levels in the Florida Everglades Using ALOS PALSAR Data with Interferometric Processing. IEEE Geoscience and Remote Sensing Letters, 11(8) :1355–1359. doi: 10.1109/LGRS.2013.2293492.

Hu, Y., Dao, R., Hu, Y., 2019. Vegetation change and driving factors: contribution analysis in the Loess Plateau of China during 2000–2015. Sustainability 11, 1320. https://doi.org/10.3390/su11051320.

Hua, J. W., S. Y. Zhu, and G. X. Zhang, 2018. Downscaling land surface temperature based on random forest algorithm. Remote Sens. Land Resour., 30, 78–86. https://doi:10.6046/gtzyyg.2018.01.11.

Huang, F., Chen, L., Yin., K., Huang, J., Gui, L., 2018. Object-oriented change detection and damage assessment using high-resolution remote sensing images, Tangjiao landslide, three gorges reservoir, China. Environ Earth Sci 77:1–19. https://doi.org/10.1007/s12665-018-7334-5.

Huang, W.H., Yang, X.G., Qu, H.H., Feng, L.P., Huang, B.X., Wang, J., Shi S.J., et al, 2009. Analysis of Spatio-Temporal Characteristic on Seasonal Drought of Spring Maize Based on Crop Water Deficit Index." Transactions of the Chinese Society of Agricultural Engineering, 25: pp. 28–34. https://doi：10.3969/j.issn.1002-6819.2009.08.006.

Hubert-Moy, L., 2003. Approches spatiales des zones humides dans le PNRZH", PhotoInterprétation. European Journal of Applied Remote Sensing, v.39, n.1, 12-15.

Huete, A., Justice, C., & Liu, H., 1994. Development of vegetation and soil indices for MODIS-EOS. Remote Sensing of Environment, 49, 224– 234. doi.org/10.1016/0034-4257(94)90018-3.

Huete, A., Liu, H. Q., Batchily, K., & van Leeuwen, W., 1997. A comparison of vegetation indices over a global set of TM images for EOS-MODIS. Remote Sensing of Environment, 59(3), 440–451. doi.org/10.1016/S0034-4257(96)00112-5.

Iino, S., Ito, R., Doi, K., Imaizumi, T., Hikosaka, S., 2018. CNN-based generation of high-accuracy urban distribution maps utilizing SAR satellite imagery for short-term change monitoring. Int J Image Data Fusion 9832 :1–17. https://doi.org/10.1080/19479832.2018.1491897.

Irons, J.R., Dwyer, J.L., Barsi, J.A., 2012.The next Landsat satellite: The Landsat data continuity mission. Remote Sensing of Environment. 122, 11–21. https://doi.org/10.1016/j.rse.2011.08.026.

Janssen, R., Goosen, H., Verhoeven, M. L., Verhoeven, J. T. A., Omtzigt, A. Q. A., Maltby, E., 2005. Decision support for integrated wetland management, Environmental Modelling & Software, V.20, n.2, 215-229.

Johnson, B, A., Iizuka, K., Bragais, M.A., Endo. I., Magcale-macandog, D, B., 2017. Employing crowdsourced geographic data and multitemporal / multi-sensor satellite imagery to monitor land cover change: a case study in an urbanizing region of the Philippines. Comput Environ Urban Syst 64 :184–193. https://doi:10.1016/J.COMPENVURBSYS.2017.02.002.

Joshi, D. M., Bhandari, N. S., Kumar, A., & Agrawal, N., 2009. Statistical analysis of physicochemical parameters of water of River Ganga in

Haridwar district. Rasayan Journal of Chemistry, 2(3), 579-587.

Justice, C.O., Townshend J.R.G., Vermote E.F., Masuoka E., Wolfe R.E., SaleousN., Roy D.P., Morisette J.T., 2002, An Overview of MODIS Land Data Processingand Product Status. Remote Sens. Environ., 83, pp. 3-15. https://doi.org/10.1016/S0034-4257(02)00084-6.

Kara, H.M., 2012. Freshwater fish diversity in Algeria with emphasis on alien species. Eur J Wildl Res 58, 243–253. https://doi.org/10.1007/s10344-011-0570-6.

Ke, L., Lin, Y., Zeng, Z., Zhang, L., Meng, L., 2018. Adaptive change detection with significance test. IEEE Access 6 :27442–27450. https://doi.org/10.1109/ACCESS.2018.2807380.

Kendall, M.G., 1975. Rank Correlation Methods. Griffin, London, UK.

Kennedy, R.E., Yang, Z., Cohen, W.B., 2010. Detecting trends in forest disturbance and recovery using yearly Landsat time series: 1. LandTrendr-temporal segmentation algorithms. Remote Sensing of Environme. 114, 2897–2910. https://doi.org/10.1016 /j.rse.2010.07.008.

Kennedy, R.E., Yang, Z., Gorelick, N., Braaten, J., Cavalcante, L., Cohen, W., Healey, S., 2018 Implementation of the LandTrendr algorithm on Google Earth Engine. Remote Sensing. 10, 691. https://doi.org/10.3390/rs10050691.

Kim, J. W., Lu, Z., Jones, J. W., Shum, C. K., Lee, H., Jia, Y., 2014. Monitoring Everglades freshwater marsh water level using L-band synthetic aperture radar backscatter. Remote Sensing of Environment, 150 :66–81.

Kumar, A., Kumar, V., Kumar, A., Kumar, G., 2014. Cuckoo search algorithm and wind driven optimization-based study of satellite image segmentation for multilevel thresholding using Kapur's entropy. Expert Syst Appl 41 :3538–3560. https://doi.org/10.1016/S2095-3119(17)61859-8.

Kumar, S., Machiwal, D., Dayal, D., 2017. Spatial modelling of rainfall trends using satellite datasets and geographic information system. Hydrol Sci J 62 :1636–1653. doi:org/10.1080/02626667.2017.1304643.

Lazo, P., Lazo, A., Hansen, H.K., Ortiz-Soto, R., Hansen, M.E., Arévalo, F., 2023. Gutiérrez, C. Removal of Heavy Metals from Mine Tailings in Central Chile Using Solidago chilensis Meyen, Haplopappus foliosus DC, and Lycium chilense Miers ex Bertero. Int. J. Environ. Res. Public Health,

20, 2749.

Lefsky, M. A., Cohen, W.B., Harding, D.J., Parker, G.G., Acker, S.A., Gower. S.T., 2002. Lidar Remote Sensing of Above-ground Biomass in Three Biomes." Global Ecology and Biogeography 11 (5): 393–399. doi:10.1046/j.1466-822x.2002.00303. x.

Leal, F.W., Wall, T., Barbir, J., Alverio, G.N., Dinis, M.A.P., Ramirez, J., 2022. Relevance of international partnerships in the implementation of the UN Sustainable Development Goals. Nat. Commun. 13, 613.

Li, H., Gong, M., Wang, Q., Liu, J., Su, L., 2015. A multi objective fuzzy clustering method for change detection in SAR images. Appl Soft Comput:1–11. http://dx.doi.org/10.1016/j.asoc.2015.10.044.

Li, Y., Li, C. k., Tao, J.-j., Wang, L. d., 2011. Study on Spatial Distribution of Soil Heavy Metals in Huizhou City Based on BP--ANN Modeling and GIS. Proced. Environ. Sci. 10, 1953–1960. doi: 10.1016/j.proenv.2011.09.306.

Liggins II, M., Hall, D., Llinas, J., 2009. Handbook of Multisensor Data Fusion: Theory and Practice, Second Edition (2nd ed.). CRC Press. 870 pp. https://doi.org/10.1201/9781420053098.

Liu, C. W., Lin, K. H., Kuo, Y. M., 2003. Application of factor analysis in the assessment of groundwater quality in a blackfoot disease area in Taiwan. Science of the Total Environment, 313(1–3), 77–89. doi.org/10.1016/ S0048-9697(02)00683-6.

Liao, J., Chen, J., Ru, X., Chen, J., Wu, H., Wei, C., 2017. Heavy Metals in River Surface Sediments Affected with Multiple Pollution Sources, South China: Distribution, Enrichment and Source Apportionment. J. Geochemical Exploration 176, 9–19. doi: 10.1016/j.gexplo.2016.08.013.

Liao, Z., Wang, X., Zhang, H., Qing, H., Li, C., Liu, Q., Cai, J., Wei, C., 2024. An integrated simulation framework for NDVI pattern variations with dual society-nature drives: A case study in Baiyangdian Wetland, North China. Ecological Indicators, V.158, 111-584. https://doi.org/10.1016/j.ecolind.2024.111584.

Lin, Y., Wang, D., Farooq, T.H., Luo, K., Wang, W., Qin, M., Chen, S., 2022. Effects of restoration strategies on wetland: A case-study of Xinqiang River National Wetland Park. Land Degrad. Dev. 33, 1114–1127. https://doi.org/10.1002/ldr.4242.

Liu., J., Gong, M., Qin, K., Zhang, P., 2018. A deep convolutional coupling network for change detection based on heterogeneous optical and radar

images. IEEE Trans Neural Networks Learn Syst 29 :545–559. https://doi.org/10.1109/TNNLS.2016.2636227.

Liu, P., 2015. A survey of remote-sensing big data. Front. Environ. Sci. 3,45. https://doi : 10.3389/fenvs.2015.00045.

Lu, D., Weng, Q., 2007. A survey of image classification methods and techniques for improving classification performance. International Journal of Remote Sensing 28, 823–870. https://doi.org/10.1080/01431160600746456.

Lu, H., Li, H., Liu, T., Fan, Y., Yuan, Y., Xie, M., Qian, X., 2019. Simulating heavy metal concentrations in an aquatic environment using artificial intelligence models and physicochemical indexes. Sci Total Environ 694 :133-591. doi.org/10.1016/j.scitotenv.2019.133591.

Lu, L., Kuenzer, C., Wang, C., Guo, H., Li, Q., 2015. Evaluation of Three MODIS-Derived Vegetation Index Time Series for Dryland Vegetation Dynamics Monitoring. Remote Sens. 7, 7597–7614. doi.org/10.3390/rs70607597.

Luo, X., Zhang, Z., Wu, X., 2016. A novel algorithm of remote sensing image fusion based on shift-invariant Shearlet transform and regional selection. Int J Electron Commun (AEÜ). 70 :186–197. http://dx.doi.org/10.1016/j.aeue.2015.11.004.

Luo, X., Ao, X., Zhang, Z., Wan, Q., Liu, X., 2020. Spatiotemporal variations of cultivated land use efficiency in the Yangtze River economic belt based on carbon emission constraints. Journal of Geographical Sciences. 30, 535–552. https://doi.org/10.1007/ s11442- 020-1741-8.

Luo, Z., Wu, W., Yu, X., Song, Q., Yang, J., Wu, J., Zhang, H., 2018.Variation of net primary production and its correlation with climate change and anthropogenic activities over the Tibetan Plateau. Remote Sensing. 10, 1352. https://doi.org/ 10.3390/rs10091352.

Ma, Q., Chai, L., Hou, F., Chang, S., Ma, Y., Tsunekawa, A., Cheng, Y., 2019.Quantifying grazing intensity using remote sensing in alpine meadows on Qinghai-Tibetan Plateau. Sustainability.11, 417. https://doi.org/10.3390/su11020417.

Ma, Q., Su, Y., Luo, L., Li, L., Kelly, M., Guo. Q., 2018. Evaluating the uncertainty of Landsat-derived vegetation indices in quantifying forest fuel treatments using bi-temporal LiDAR data. Ecol Indic 95 :298–310. https://doi.org/10.1016/j.ecolind.2018.07.050.

Maes, W.H., Steppe, K., 2019. Perspectives for Remote Sensing with Unmanned Aerial Vehicles in Precision Agriculture. Trends Plant Sci 24, 152–164. https://doi.org/10.1016/j.tplants.2018.11.007.

Mahdavi, S., Salehi, B., Granger, J., Amani, M., Brisco B., Huang, W., 2017. Remote sensing for wetland classification: a comprehensive review, GIS science & Remote Sensing, Vol.55, No.5, 623-658.

Mahmon, N.A., Ya'acob, N., 2014. A review on classification of satellite image using Artificial Neural Network (ANN), in: 2014 IEEE 5th Control and System Graduate Research Colloquium. Presented at the 2014 IEEE 5th Control and System Graduate Research Colloquium, 153–157. https://doi.org/10.1109/ICSGRC.2014.6908713.

Mann, H.B., 1945. Nonparametric tests against trend. Econometrica 13: 245–259. doi.org/10.2307/1907187.

Mao, D.H., Yang, H., Wang, Z.M., Song, K.S., Thompson, J.R., Flower, R.J., 2022. Reverse the hidden loss of China's wetlands. Science 376 (6597), 1061.

Marinelli, D., Bovolo, F., Bruzzone, L., 2017. A novel method for unsupervised multiple change detection in hyperspectral images based on binary spectral change vectors. 2017 9th Int work anal multitemporal.

Mateo, J.A., Geniez, P., Pether, J., 2013. Diversity and conservation of Algerian amphibian assemblages. In mphibian Biology. Status of Conservation and Decline of Amphibians: Eastern Hemisphere Part 2., 51-84.

Maurya, S.P., Yadav A.K., 2016. Evaluation of course change detection of Ramganga river using remote sensing and GIS, India. Weather Clim Extrem. 13:68–72. https://doi.org/10.1016/j.wace.2016.08.001.

Meng, X., et al., 2022. Spatio–Temporal–Spectral Collaborative Learning for SpatioTemporal Fusion with Land Cover Changes. IEEE Trans. Geosci. Remote Sens. 60, 1–16. https://doi.org/10.1109/TGRS.2022.3185459.

McKee T.B., Doesken N.J., Kleist J., 1993. The relationship of drought frequency and duration to time scales. Proceedings of the 8th Conference on Applied Climatology. Boston, MA. Am. Meteorol. Soc., 17 (22), pp. 179-183.

MEER., 2016. Stratégie et plan d'action nationaux pour la biodiversité, 2016-2030. La biodiversité pour le développement économique et social durable et l'adaptation au changement climatique. MEER « Ministère de

l'Environnement et des Energies Renouvelables », PNUD et gef. Sarl Studiocom. Production Audiovisuelle et Communication 16, Rue Rabah Noel (Alger).132 p.

Medjerab, A., Henia, L., 2005. Régionalisation des pluies annuelles dans l'Algérie nord occidentale, Revue Géographique de l'Est, 45(2). https://doi.org/10.4000/rge.501.

Meng, W., He, M., Hu, B., Mo, X., Li, H., Liu, B., Wang, Z., 2017. Status of wetlands in China: A review of extent, degradation, issues and recommendations for improvement. Ocean Coast. Manag. 146, 50–59. https://doi.org/10.1016/j.ocecoaman.2017.06.003.

McFeeters, S.K., 1996. The use of the Normalized Difference Water Index (NDWI) in the delineation of open water features. Int. J. Rem. Sens. 17 (7), 1425–1432. doi.org/10.1080/01431169608948714.

Mudgal, K. D., Kumari, M., Sharma, D. K., dev Mudgal, K., & Kumari, M., 2009. Hydromical analysis of drinking water quality of Alwar district, Rajasthan. Nat Sci, 7(2), 30-9

Myneni, R. B., Keeling, C. D., Tucker, C. J., Asrar, G., & Nemani, R. R.,1997. Increased plant growth in the northern high latitudes from 1981 to 1991. Nature, 386, 698–702. doi.org/10.1038/386698a0.

Narayan, B., Bovolo, F., Ghosh, A., Bruzzone, L., 2014. Spatio-contextual fuzzy clustering with Markov random fi eld model for change detection in remotely sensed images. Opt Laser Technol 57:284–292. http://dx.doi.org/10.1016/j.optlastec.2013.10.003**.**

Nedkov, S., Zhiyanski, M., Borisova, B., Nikolova, M., Bratanova, S., Semerdzhieva, L., Ihtimanski, I., Nikolov, P., Aidarova, Z., 2018. A geospatial approach to mapping and assessment of urban ecosystem services in Bulgaria, European Journal of Geography 9 4: 34–50.

Nemani, R.R, Keeling, C.D, Hashimoto, H, Jolly, W.M, Piper, S.C, Tucker, C.J, Myneni, R.B, Running, W., 2003. Climate-driven increases in global terrestrial net primary production from 1982 to 1999. Science 300, 1560–1563. doi: 10.1126/science.1082750.

Nink, S., Hill, J., Stoffels, J., Buddenbaum, H., Frantz, D., & Langshausen, J., 2019. Using Landsat and Sentinel-2 Data for the Generation of Continuously Updated Forest Type Information Layers in a Cross-Border Region. Remote Sensing, 11(20). https://doi.org/10.3390/rs11202337.

Pan, Z.H., Yang, S.T., Ren, X.Y., Lou, H.Z., Zhou, B.C., Wang, H.X., Zhang,

Y.J., Li, H., Li, J.K., Dai, Y.M., 2023. GEE can prominently reduce uncertainties from input data and parameters of the remote sensing-driven distributed hydrological model. Sci. Total Environ. 870, 161852.

Pandey, B.K., Khare, D., 2017. Analyzing and modeling of a large river basin dynamics applying integrated cellular automata and Markov model. Environ Earth Sci 76:1–12. https://doi.org/10.1007/s12665-017-7133-4.

Peng, H., Xia, H., Shi, Q., Chen, H., Chu, N., Liang, J., Gao, Z., 2022. Monitoring spatial and temporal dynamics of wetland vegetation and their response to hydrological conditions in a large seasonal lake with time series Landsat data. Ecol. Ind. 142, 109283 https://doi.org/10.1016/j.ecolind.2022.109283.

Peng, J., Wu, C., Zhang, X., Wang, X., Gonsamo, A., 2019. Satellite detection of cumulative and lagged effects of drought on autumn leaf senescence over the Northern Hemisphere. Glob. Change Biol. 25, 2174–2188. https://doi.org/10.1111/gcb.14627.

Peng, K., Jiang, W., Wang, X., Hou, P., Wu, Z., Cui, T., 2023. Evaluation of future wetland changes under optimal scenarios and land degradation neutrality analysis in the Guangdong-Hong Kong-Macao Greater Bay Area. Sci. Total Environ. 879, 163111 https://doi.org/10.1016/j.scitotenv.2023.163111.

Piao, S., Mohammat, A., Fang, J., Cai, Q., Feng, J., 2006. NDVI-based increase in growth of temperate grasslands and its responses to climate changes in China. Global Environmental Change. 16, 340–348. https://doi.org/10.1016/j. gloenvcha .2006. 02.002.

Piao, S. L., Wang, X. H., Ciais, P., Zhu, B., Wang, T., & Liu, J., 2011. Changes in satellite-derived vegetation growth trend in temperate and boreal Eurasia from 1982 to 2006. Global Change Biology, 17, 3228–3239. doi.org/10.1111/j.1365-2486.2011.02419. x.

Pingale, S.M., Khare, D., Jat, M.K., Adamowski, J., 2016 Trend analysis of climatic variables in an arid and semi-arid region of the Ajmer District, Rajasthan, India. J Water L Dev 28:3–18. doi:org/10.1515/jwld-2016-0001.

Potopová V., Štěpánek P., Možný M., Türkott L., Soukup J., 2015. Performance of the standardised precipitation evapotranspiration index at various lags for agricultural drought risk assessment in the Czech Republic. Agric. For. Meteorol.,202, pp. 26-38. https://doi.org/10.1016/j.agrformet.2014.11.022;35.

Pradhan, R., Aygun, R.S., Maskey, M., Ramachandran, R., Cecil, D.J., 2018. Tropical cyclone intensity estimation using a deep convolutional neural network. IEEE Trans Image Process 27 :692–702. https://doi.org/10.1109/TIP.2017.2766358.

Prasanna, M.V., Praveena, S.M., Chidambaram, S., Nagarajan, R., Elayaraja, A., 2012. Evaluation of water quality pollution indices for heavy metal contamination monitoring: a case study from Curtin Lake, Miri City, East Malaysia. Environ Earth Sci 67 :1987–2001. doi.org/10.1007/s12665-012-1639-6.

Proshad, R., Kormoker, T., Islam, S., 2021. Distribution, source identification, ecological and health risks of heavy metals in surface sediments of the Rupsa River, Bangladesh. Taylor & Francis 40(1) :77–101. doi. 10.1080/15569543.2018.1564143.

Qiu, B., Chen, G., Tang, Z., Lu, D., Wang, Z., Chen, C., 2017. Assessing the three-north shelter Forest program in China by a novel framework for characterizing vegetation changes. ISPRS J Photogramm Remote Sens 133:75–88.

Ojdaniˇc, N., Holcar, M., Golob, A., Gaberˇsˇcik, A., 2023. Environmental extremes affect productivity and habitus of common reed in intermittent wetland. Ecol. Eng. 189, 106911 https://doi.org/10.1016/j.ecoleng.2023.106911.

Ramade, F., 2009. Eléments d"écologie: Ecologie fondamentale. (4e Edition). DUNOD, Paris. 689p.

Rapinel, S., 2012. Contribution de la télédétection à l'évaluation des fonctions des zones humides : de l'observation à la modélisation prospective. Thèse, Université Rennes 2. 161pp.

Rapinel, S., Clément, B., et Hubert-Moy, L., 2019. Cartographie des zones humides par télédétection: approche multi-scalaire pour une planification environnementale, Cybergeo : European Journal of Geography. 1-20. Dio. 10.4000/cybergeo.31606.

Rapinel, S., Hubert-Moy, L., Clément, B., Maltby, E., 2016. Mapping wetland functions using Earth observation data and multi-criteria analysis, Environmental Monitoring and Assessment, Vol.188, No.11, 64.

Rawat, J.S., Kumar, M., 2015. Monitoring land use / cover change using remote sensing and GIS techniques: a case study of Hawalbagh block, district Almora, Uttarakhand, India. Egypt J Remote Sensing Space Sci 18 :77–84.

https://doi.org/10.1016/j.ejrs.2015.02.002.

Richards, J. A., Jia, X., 2006. Remote Sensing Digital Image Analysis: An Introduction, 4th Edition, Springer, 445pp.

Rodier, J., Legube, B. Merlet, N., 2009. L'analyse de l'eau. Dunod, 9 éme édition, 1526.

Roerink, G.J., Menenti, M., Soepboer, W., Su, Z., 2003. Assessment of climate impact on vegetation dynamics by using remote sensing. Physics and Chemistry of the Earth. 28, 103–109. https://doi.org/10.1016/S1474-7065(03)00011-1.

Sadeghi, V., Farnood Ahmadi, F., Ebadi, H., 2016 Design and implementation of an expert system for updating thematic maps using satellite imagery (case study: changes of Lake Urmia). Arab J Geosci 9 :1–17. https://doi.org/10.1007/s12517-015-2301-x.

Sagan, V., Maimaitijiang, M., Sidike, P., Eblimit, K., Peterson, K.T., Hartling, S., et al., 2019. Uav-based high resolution thermal imaging for vegetation monitoring, and plant phenotyping using ici 8640 p, flir vue pro r 640, and thermomap cameras. Remote Sens. 11, 330. https://doi.org/10.3390/rs11030330.

Sahoo, M.M., Swain, J.B., 2020. Modified heavy metal Pollution index (m-HPI) for surface water Quality in river basins, India. Environ. Sci. Pollut. Res. 27 :15350–15364. doi.org/10.1007/ s11356-020-08071-1.

Santana, C., Montalván, D., Silva, V., Luzardo, F., Velasco, F., de Jesus, R., 2020. Assessment of water resources pollution associated with mining activity in a semi-arid region. J. Environ. Manag., 273, 111-148.

Sarkar, A., Pandey, P., 2015. River water quality modelling using artificial neural network technique. Aquatic Procedia 4 :1070–1077. doi: 10.1016/j.aqpro.2015.02.135.

Sen, P.K., 1968. Estimates of the Regression Coefficient Based on Kendall's Tau, Journal of the American Statistical Association, 63 :324, 1379-1389. doi: 10.1080/01621459.1968.10480934.

Schmid, J. N.,2017. Using Google Earth Engine for Landsat NDVI time series analysis to indicate the present status of forest stands. https:// doi.org/10.13140/RG.2.2.34134.14402/6.

Sharma, A., Ganguly, R., Kumar, A., 2020. Impact Assessment of Leachate Pollution Potential on Groundwater: An Indexing Method. J. Environ. Eng.

146, 0501- 9007. https:// doi.org/10.1007/s10661-017-6417-1.

Sica, Y.V., Quintana, R.D., Radeloff, V.C., Gavier-Pizarro, G.I., 2016. Wetland loss due to land use change in the Lower Paran´ a River Delta, Argentina. Sci. Total Environ. 568, 967–978.

Singh, K.K., Singh, A., 2016, Identification of flooded area from satellite images using Hybrid Kohonen Fuzzy C-Means sigma classifier, Egypt. J. Remote Sensing Space Sci. i 20:147–155. http://dx.doi.org/10.1016/j.ejrs.2016.04.003.

Siegel, F.R., 2002. Environmental geochemistry of potentially toxic metals. Springer, Berlin; New York. https:// doi.10.1007/978-3-662-04739-2.

Sojobi, A.O., 2016. Evaluation of groundwater quality in a rural community in North Central of Nigeria. Environ Monitor Assessment., 188(3):1–17. https:// doi.org/10.1007/s10661-016-5149-y.

Song, J., Liu, Q., Sheng, Y., 2019. Distribution and risk assessment of trace metals in riverine surface sediments in gold mining area. Environ. Monit. Assess., 191, 191.

Su, L., Gong, M., Zhang, P., Zhang, M., Liu, J., Yang, H., 2017. Deep learning and mapping based ternary change detection for information unbalanced images. Pattern Recogn :2–42. http://dx.doi.org/10.1016/j.patcog.2017.01.002.

Suresh, S., Lal, S., 2017. Modified differential evolution algorithm for contrast and brightness enhancement of satellite images. Appl Soft Comput J 61:622–641. https://doi.org/10.1016/j.asoc.2017.08.019.

Suryavanshi, S., Pandey, A., Chaube, U.C., Joshi, N., 2014. Long-term historic changes in climatic variables of Betwa Basin, India. Theor Appl Climatol. 117:403–418. doi:org/10.1007/s00704-013-1013-y.

Tabari, H., Somee, B.S., Zadeh, M.R., 2011.Testing for long-term trends in climatic variables in Iran. Atmos Res 100 :132–140. doi.org/10.1016/j.atmosres.2011.01.005.

Tan Z.Q., Tao H., Jiang J.H., Zhang Q., 2015. Influence of climate extremes on NDVI (Normalized Difference Vegetation Index) in the poyang lake basin, China. Wetlands. 35, pp.1033–1042. https://https://doi.org/10.1007/s13157-015-0692-9.

Thornthwaite C., 1948. An approach toward a rational classification of climate. Geogr. Rev., 38, pp. 55-94. https://doi.org/10.2307/210739;39.

Tian, D., Gong, M., 2018. A novel edge-weight based fuzzy clustering method for change detection in SAR images. Inf Sci (Ny) 467: 415–430. https://doi.org/10.1016/j.ins.2018.08.015.

Tokatlı, C., Mutlu, E., Arslan, N., 2021. Assessment of the potentially toxic element contamination in water of Şehriban Stream (Black Sea Region, Turkey) by using statistical and ecological indicators. Water Environ Res 00:1–12. doi.org/10.1002/wer.1576.

Tucker, C. J., Fung, I. Y., Keeling, C. D., & Gammon, R. H.,1986. Relationship between atmospheric CO2 variations and a satellite-derived vegetation index. Nature, 319,195–199. doi.org/10.1038/319195a0.

Vermote, E., Justice, C., Claverie, M., Franch, B., 2016. Preliminary analysis of the performance of the Landsat 8/OLI land surface reflectance product. Remote Sens. Environ. 185, 46–56. doi: 10.1016/j.rse.2016.04.008.

Varol, M., 2020. Spatio-temporal changes in surface water quality and sediment phosphorus content of a large reservoir in Turkey. Environmental Pollution, 259, 113860. doi.org/10.1016/j.envpol.2019.113860.

Vicente-Serrano S., Gouveia C., Camarero J., Beguería S., Trigo R., López-MorenoJ., Azorín-Molina C., Pasho E., Lorenzo-Lacruz J., Revuelto J., 2013. Response of vegetation to drought time-scales across global land biomes. Proc. Natl. Acad. Sci. USA., 110, pp. 52-57. https://doi.org/10.1073/pnas.1207068110;40.

Wallace, L., Lucieer, A., Watson, C., Turner, D., 2012. Development of a UAV-LiDAR System with Application to Forest Inventory. Remote Sens. 4, 1519–1543. https:// doi.org/10.3390/rs4061519.

Wang, L., et al., 2012. NDVI Analysis and Yield Estimation in Winter Wheat Based on GreenSeeker. Act Agronomica Sinica. 38 (4), 747–753. https://doi.org/10.3724/SP. J.1006.2012.00747.

Wang, L., Shu Z., Wang G., Sun Z., Yan H., Bao Z., 2022. Analysis of Future Meteorological Drought Changes in the Yellow River Basin under Climate Change. Water, 14, pp. 1896. https://doi.org/10.3390/w14121896;43.

Wang, M.R., Janssen, A.B.G., Bazin, J., Strokal, M., Ma, L., Kroeze, C., 2022. Accounting for interactions between Sustainable Development Goals is essential for water pollution control in China. Nat. Commun. 13, 730.

Wang, Q., Shi, W., Atkinson, P.M., Li, Z., 2014. Land cover change detection at subpixel resolution with a Hopfield neural network. IEEE J Sel Top Appl Earth Obs Remote Sens 8 :1339–1352.

https://doi.org/10.1109/JSTARS.2014.2355832.

Wang, Q., Zhang, X., Chen, G., Dai, F., Gong, Y., Zhu, K., 2018. Change detection based on faster R-CNN for high-resolution remote sensing images. Remote Sens Lett 9 :923–932. https://doi.org/10.1080/2150704X.2018.1492172

Wang, S., et al., 2022. Research on vegetation cover and land use change in Guangdong Province based on MODIS-NDVI. Acta Ecol. Sin. 42 (06), 2149–2163. https://doi. org/10.5846/stxb202104261100.

Wang, Y., Zhao, F., Chen, P., 2017. A framework of spatiotemporal fuzzy clustering for land-cover change detection using SAR time series. Int J Remote Sens 38:450–466. https://doi.org/10.1080/01431161.2016.1268736.

Wang, Y. T., D. H. Xie, and Y. H. Li, 2014. Downscaling remotely sensed land surface temperature over urban areas using trend surface of spectral index. J. Remote Sens., 18, 1169–1181. doi :10.11834/jrs.20144115.

Weiss, M., Jacob, F., & Duveiller, G., 2020. Remote sensing for agricultural applications: A meta-review. 236, 111402. https://doi.org/10.1016/j.rse.2019.111402.

Woodcock, C.E., Allen, R., Anderson, M., Belward, A., Bindschadler, R., Cohen, W., Gao, F., Goward, S. N., Helder, D., Helmer, E., Nemani, R., Oreopoulos, L., Schott, J., Thenkabail, P. S., Vermote, E. F., Vogelmann, J., Wulder, M. A., and Wynne, R., 2008. Free access to landsat imagery, Science, vol. 320, no. 5879, pp. 1011–1011. doi.org/10.1126/science.320.5879.1011a.

Wu, D., Zhao, X., Liang, S., Zhou, T., Huang, K., Tang, B., Zhao, W., 2015. Time-lag effects of global vegetation responses to climate change. Glob. Change Biol. 21, 3520–3531. doi :10.1111/gcb.12945.

Wu, X.T., Fu, B.J., Wang, S., Song, S., Li, Y.J., Xu, Z.C., Wei, Y.P., Liu, J.G., 2022. Decoupling of SDGs followed by re-coupling as sustainable development progresses. Nat. Sustainability 5, 452–459.

Wu, Z., Sun, J., Zhang, Y., Wei, Z., Chanussot, J., 2021 Recent developments in parallel and distributed computing for remotely sensed big data processing. Proc. IEEE 109, 1282–1305. https://doi.org/10.1109/JPROC.2021.3087029.

Xu, D., Chen, R., Xing, X., Lin, W., 2017. Detection of decreasing vegetation cover based on empirical orthogonal function and temporal unmixing

analysis. Math Probl Eng 2017:1–10. https://doi.org/10.1155/2017/5032091.

Xu, H., Wang, X., Zhang, X., 2016. Alpine grasslands response to climatic factors and anthropogenic activities on the Tibetan Plateau from 2000 to 2012. Ecological Engineering. 92, 251–259. https://doi.org/10.1016/j.ecoleng.2016.04.005.

Xu H., Wang X., Zhao C., Yang X., 2018. Diverse responses of vegetation growth to meteorological drought across climate zones and land biomes in northern China from 1981 to 2014. Agric. For. Meteorol., 262, pp. 1-13. https://doi.org/10.1016/j.agrformet.2018.06.027.

Xu, N., F. Deng, B. Q. Liu, et al., 2021. Changes in the urban surface thermal environment of a Chinese coastal city revealed by downscaling MODIS LST with random forest algorithm. J. Meteor. Res., 35(5),59–774. doi: 10.1007/s13351-021-0023-4.

Xu, Z.C., Chau, S.N., Chen, X.Z., Zhang, J., Li, Y.J., Dietz, T., Wang, J.Y., Winkler, J.A., Fan, F., Huang, B.R., Li, S.X., Wu, S.H., Herzberger, A., Tang, Y., Hong, D.Q., Li, Y.K., Liu, J.G., 2020. Assessing progress towards sustainable development over space and time. Nature 577, 74–78.

Ye, S., Rogan, J., Sangermano, F., 2018. Monitoring rubber plantation expansion using Landsat data time series and a Shapelet-based approach. ISPRS J Photogramm Remote Sens 136 :134–143. https://doi.org/10.1016/j.isprsjprs.2018.01.002.

Yuan, H., Wu, C., Lu, L., Wang, X., 2018. A new algorithm predicting the end of growth at five evergreen conifer forests based on nighttime temperature and the enhanced vegetation index. ISPRS J Photogramm Remote Sens 144 :390–399. https://doi.org/10.1016/j.isprsjprs.2018.08.013.

Zanchetta, A., Bitelli, G., Karnieli, A., 2016. Monitoring desertification by remote sensing using the Tasselled cap transform for long-term change detection. Nat Hazards 83 :223–237. https://doi.org/10.1007/s11069-016-2342-9.

Zeng, W.Z., et al., 2018. Comparison of partial least square regression support vector machine and deep-learning techniques for estimating soil salinity from hyperspectral data. J. Appl. Remote Sens. 12 (2), 022204 https://doi.org/10.1117/1. JRS.12.022204.

Zhang, B., Niu, Z.G., Zhang, D.Q., Huo, X.L., 2022. Dynamic Changes and Driving Forces of Alpine Wetlands on the Qinghai-Tibetan Plateau Based

on Long-Term Time Series Satellite Data: A Case Study in the Gansu Maqu Wetlands. Remote Sens. (Basel) 14 (17), 4147.

Zhang, Y., Ye A., 2020. Spatial and Temporal Variations in Vegetation CoverageObserved Using AVHRR GIMMS and Terra MODIS Data in the Mainland ofChina. Int. J. Remote Sens., 41, pp. 4238-4268.https://doi.org/10.1080/01431161.2020.1714781;53.

Zhao, A., Zhang A., Cao S., Liu X., Liu J., Cheng D., 2018. Responses of vegetation productivity to multi-scale drought in Loess Plateau, China. Catena, 163, pp. 165-171. https://doi.org/10.1016/j.catena.2017.12.016.

Zhou, X., Yamaguchi, Y., Arjasakusuma, S., 2018. Distinguishing the vegetation dynamics induced by anthropogenic factors using vegetation optical depth and AVHRR NDVI: A cross-border study on the Mongolian Plateau. Science of The Total Environment. 616–617, 730–743. https://doi.org/10.1016/j.scitotenv.2017.10.253.

Zhe, M., Zhang, X., 2021. Time-lag effects of NDVI responses to climate change in the Yamzhog Yumco Basin, South Tibet. Ecol. Indic. 124, 107431. doi.org/10.1016/j.ecolind.2021.107431.

Zhou, J., et al., 2021. Sensitivity of six typical spatiotemporal fusion methods to different influential factors: A comparative study for a normalized difference vegetation index time series reconstruction. Remote Sens. Environ. 252, 112130 https://doi.org/ 10.1016/j.rse.2020.112130.

Zhu, L., Suomalainen, J., Liu, J., Hyyppä, J., Kaartinen, H., Haggren, H., 2018. A review: Remote sensing sensors. Multi Purp. Appl. Geospat. 19–42. https://doi: 10.5772/intechopen.71049.

Zhu, L.J., Ke, Y.H., Hong, J.M., Zhang, Y.H., Pan, Y., 2022. Assessing degradation of lake wetlands in Bashang Plateau, China based on long-term time series Landsat images using wetland degradation index. Ecol. Ind. 139, 108903.

Zhu, Z., Wang, S., Woodcock, C.E., 2015. Improvement and expansion of the Fmask algorithm: cloud, cloud shadow, and snow detection for Landsat 4–7, 8, and Sentinel 2 images. Remote Sensing of Environment. 159, 269–277. https://doi.org/10.1016/j. rse.2014.12.014.

Zolfaghari, F., Azarnivand, H., Khosravi, H., Zehtabian, G., Sigaroudi, S.K., 2022. Monitoring the severity of degradation and desertification by remote sensing (case study: Hamoun International Wetland). Front. Environ. Sci. 10, 902687.

APPENDIX

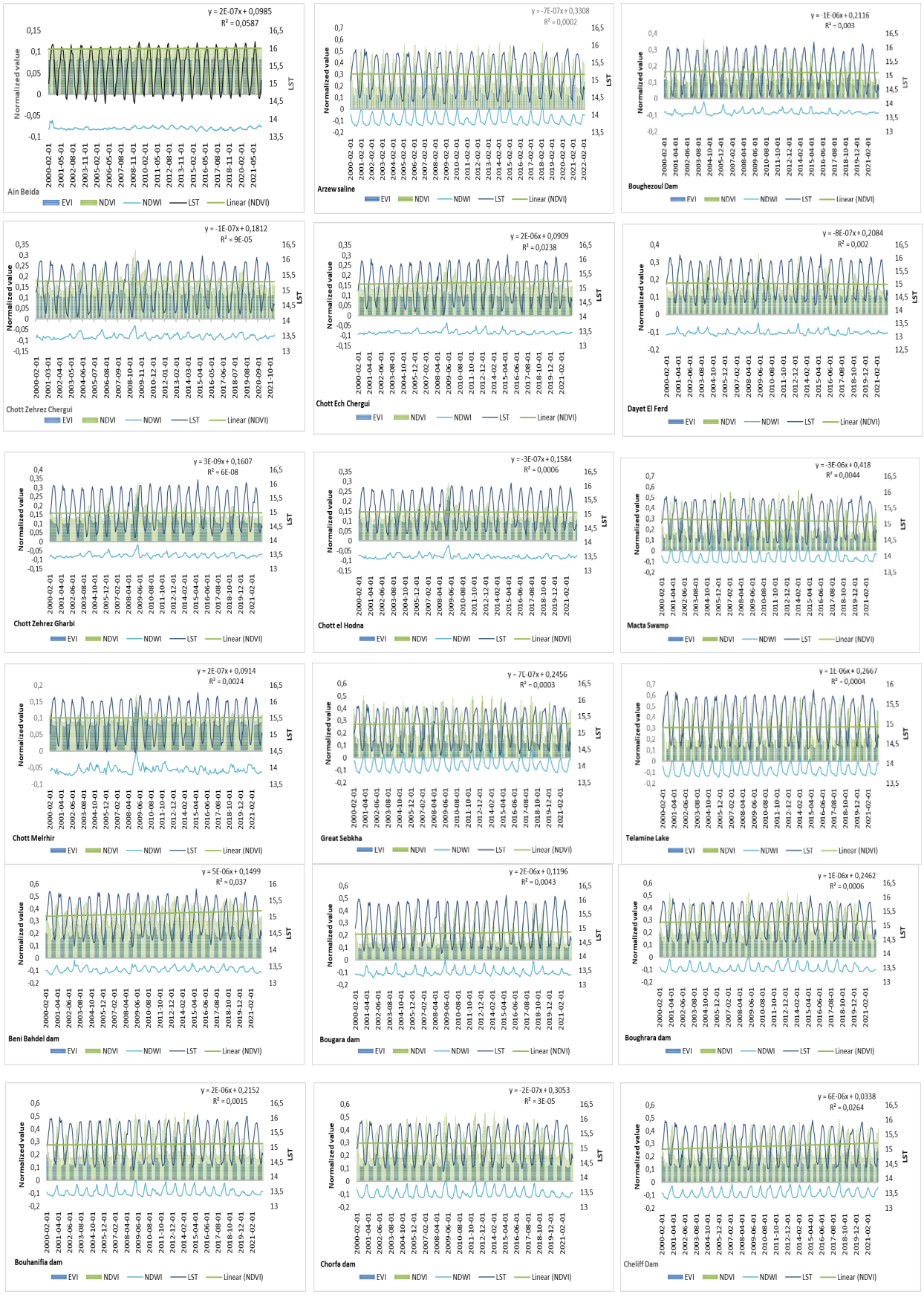

Figure. 1. Year-wise change in the values of the spectral indices from 2000 to 20222.

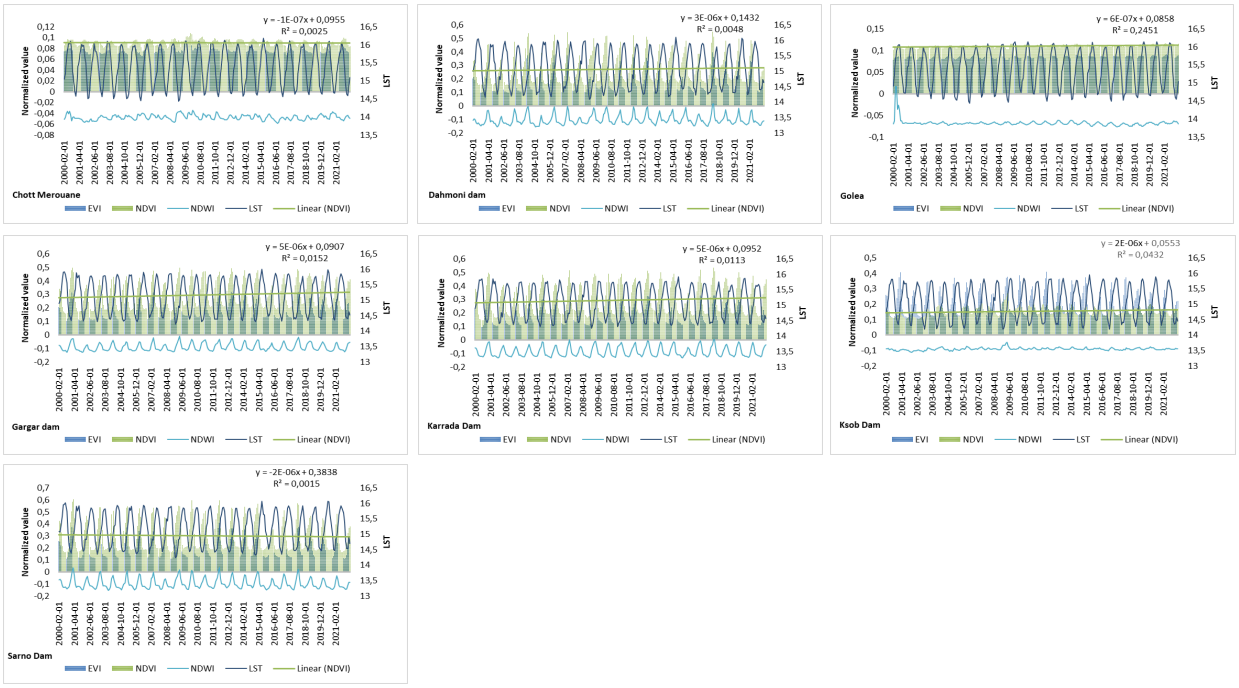

Figure. 1. (continued).

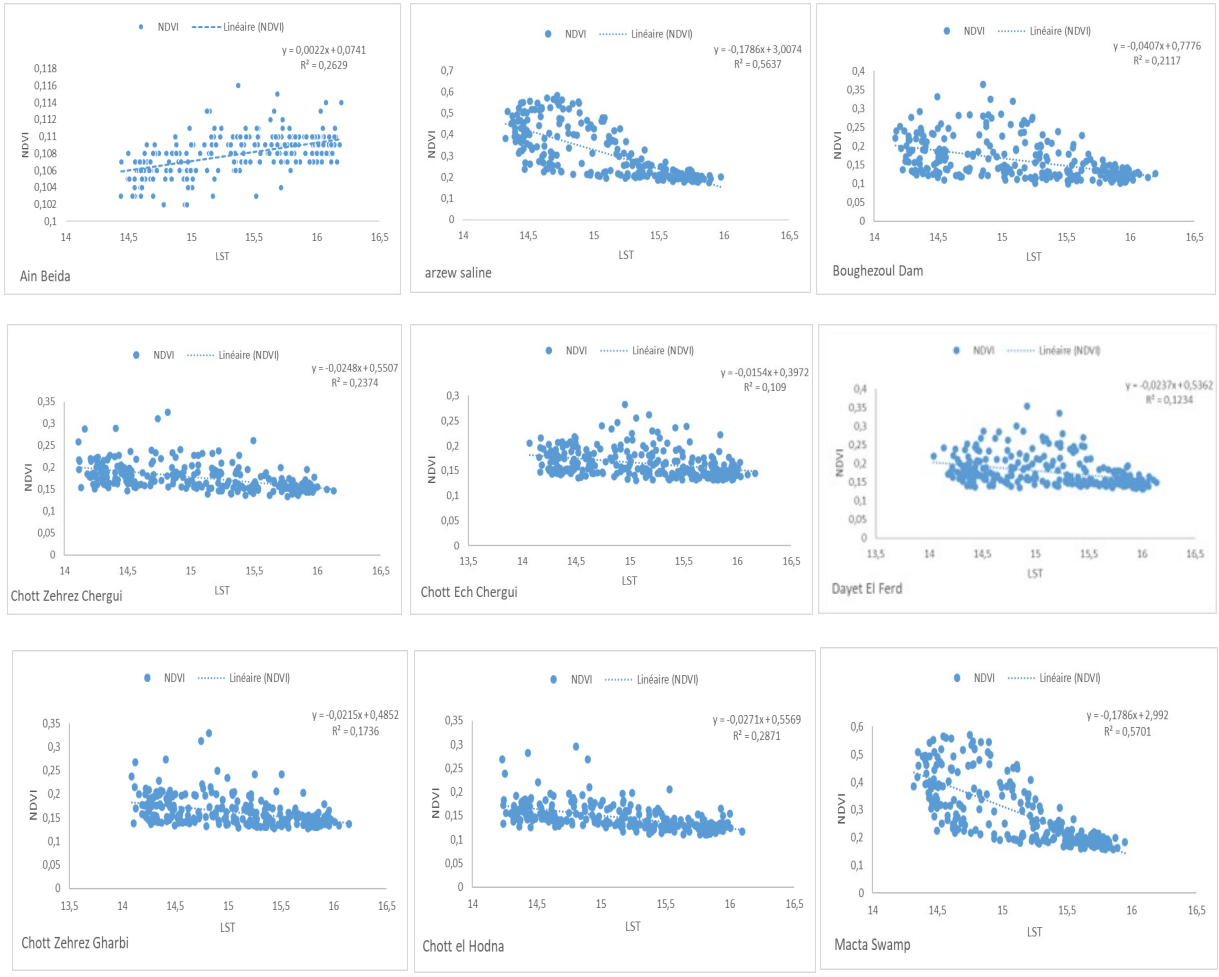

Figure. 2. Annual assessment on NDVI and LST indices relationship during 2000-2022.

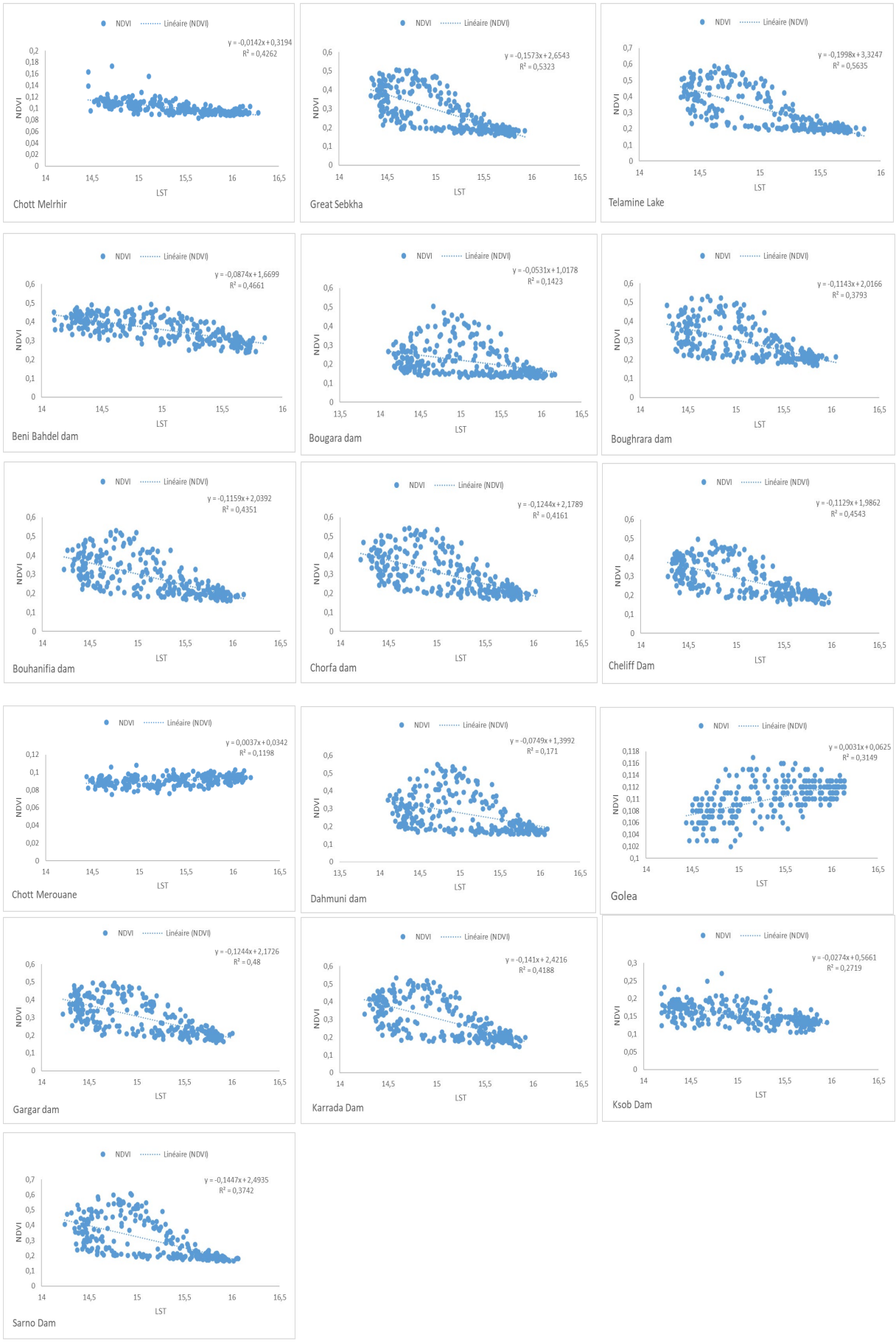

Figure. 2. (continued).

Table1: Calculation of Heavy pollution index for Great Sebkha

Si	Li	Mi	Wi	Mi-Li	Si-Li	Qi= Mi-Li/Si-Li*100	Wi*Qi	Wi	HPI mean
10	0	3	0,1	3	10	30	3	0,300	109,650
1500	50	1	0,0006	-49	1450	3,379	0,0022	0,300	
5	3	0,003	0,2	-2,997	2	149,85	29,97	0,300	
15000	5000	0,0704	6,66667E-05	-4999,9	10000	49,9993	0,0033	0,300	

Table2: Calculation of Heavy pollution index for Macta Marsh

Si	Li	Mi	Wi	Mi-Li	Si-Li	Qi= Mi-Li/Si-Li*100	Wi*Qi	Wi	HPI mean
10	0	2,2	0,1	2,2	10	22	2,2	0,300	106,79
1500	50	6,3	0,0006	-43,7	1450	3,013	0,0020	0,300	
5	3	0,009	0,2	-2,991	2	149,55	29,91	0,300	
15000	5000	0,0641	6,66667E-05	-4999,9	10000	49,9994	0,0033	0,3007	

Table3: Calculation of Heavy pollution index for Arzew saline

Si	Li	Mi	Wi	Mi-Li	Si-Li	Qi= Mi-Li/Si-Li*100	Wi*Qi	Wi	HPI mean
10	0	3,93	0,1	3,93	10	39,3	3,93	0,300	100,93
1500	50	1	0,0006	-49	1450	3,3793	0,0022	0,300	
5	3	0,358	0,2	-2,642	2	132,1	26,42	0,300	
15000	5000	0,358	6,66667E-05	-4999,6	10000	49,9964	0,0033	0,3007	

Table 4: Calculation of Heavy pollution index for Sarno dam

Si	Li	Mi	Wi	Mi-Li	Si-Li	Qi= Mi-Li/Si-Li*100	Wi*Qi	Wi	HPI mean
10	0	8,2	0,1	8,2	10	82	8,2	0,300	126,77
1500	50	0,0027	0,0006	-49,9	1450	3,44	0,0022	0,300	
5	3	0,008	0,2	-2,992	2	149,6	29,92	0,300	

15000	5000	0,337	6,66667E-05	-4999,6	10000	49,9966	0,0033	0,300	

Table 5: Calculation of Heavy pollution index for Beni Bahdel dam

Si	Li	Mi	Wi	Mi-Li	Si-Li	Qi= Mi-Li/Si-Li*100	Wi*Qi	Wi	HPI mean
10	0	29,3	0,1	29,3	10	293	29,3	0,300	197,30
1500	50	-0,002	0,0006	-50,002	1450	3,44	0,002	0,300	
5	3	-0,003	0,2	-3,003	2	150,15	30,03	0,300	
15000	5000	-0,003	6,67E-05	-5000	10000	50	0,003333	0,300	

Table 6: Calculation of Heavy pollution index for Boughrara dam

Si	Li	Mi	Wi	Mi-Li	Si-Li	Qi= Mi-Li/Si-Li*100	Wi*Qi	Wi	HPI mean
10	0	50,1	0,1	50,1	10	501	50,1	0,300	266,23
1500	50	0,0013	0,000	-49,99	1450	3,4481	0,0022	0,300	
5	3	0,004	0,2	-2,996	2	149,8	29,96	0,300	
15000	5000	0,004	6,66667E-05	-4999,9	10000	50	0,0033	0,300	

Table 7: Calculation of Heavy pollution index for Bougara dam

Si	Li	Mi	Wi	Mi-Li	Si-Li	Qi= Mi-Li/Si-Li*100	Wi*Qi	Wi	HPI mean
10	0	9,9	0,1	9,9	10	99	9,9	0,300	132,49
1500	50	0,017	0,0006	-49,983	1450	3,447	0,0022	0,300	
5	3	0,006	0,2	-2,994	2	149,7	29,94	0,300	
15000	5000	0,135	6,66667E-05	-4999,8	10000	49,99	0,0033	0,300	

Table 8: Calculation of Heavy pollution index for Chorfa dam

Si	Li	Mi	Wi	Mi-Li	Si-Li	Qi= Mi-Li/Si-Li*100	Wi*Qi	Wi	HPI mean
10	0	14,9	0,1	14,9	10	149	14,9	0,300	149,370

1500	50	0,023	0,0006	-49,977	1450	3,446	0,002	0,300
5	3	-0,0015	0,2	-3,0015	2	150,075	30,015	0,300
15000	5000	0,0531	6,66667E-05	-4999,9	10000	49,9995	0,003	0,300

Table 9: Calculation of Heavy pollution index for Karrada dam

Si	Li	Mi	Wi	Mi-Li	Si-Li	Qi= Mi-Li/Si-Li*100	Wi*Qi	Wi	HPI mean
10	0	17,5	0,1	17,5	10	175	17,5	0,300	150,55
1500	50	0,004	0,0006	49,976	1450	3,446	0,0022	0,300	
5	3	0,223	0,2	2,777	2	138,85	27,77	0,300	
15000	5000	0,3462	6,66667E-05	4999,6	10000	49,99	0,003	0,300	

Table 10: Calculation of Heavy pollution index for Telamine lake

Si	Li	Mi	Wi	Mi-Li	Si-Li	Qi= Mi-Li/Si-Li*100	Wi*Qi	Wi	HPI mean
10	0	1,4	0,1	1,4	10	14	1,4	0,300	101,86
1500	50	2	0,0006	-48	1450	3,3103	0,0022	0,300	
5	3	0,077	0,2	-2,923	2	146,15	29,23	0,300	
15000	5000	0,08	6,66667E-05	-4999,9	10000	49,9992	0,003	0,300	

Table 11: Calculation of Heavy pollution index for Dahmoni dam

Si	Li	Mi	Wi	Mi-Li	Si-Li	Qi= Mi-Li/Si-Li*100	Wi*Qi	Wi	HPI mean
10	0	8,1	0,1	8,1	10	81	8,1	0,300	126,84
1500	50	0,019	0,0006	-49,981	1450	3,446	0,002	0,300	
5	3	-0,004	0,2	-3,004	2	150,2	30,04	0,300	
15000	5000	0,082	6,66667E-05	-4999,9	10000	49,9992	0,003	0,300	

Table 12: Calculation of Heavy pollution index for Gargar dam

Si	Li	Mi	Wi	Mi-Li	Si-Li	Qi= Mi-Li/Si-Li*100	Wi*Qi	Wi	HPI
10	0	95	0,1	95	10	950	95	0,300	415,60
1500	50	0,012	0,0006	-49,98	1450	3,447	0,002298	0,300	
5	3	0,002	0,2	-2,998	2	149,9	29,98	0,300	
15000	5000	0,0745	6,67E-05	-4999,9	10000	49,99	0,003333	0,300	

Table 13: Calculation of Heavy pollution index for Chott Ech Chergui

Si	Li	Mi	Wi	Mi-Li	Si-Li	Qi= Mi-Li/Si-Li*100	Wi*Qi	Wi	HPI mean
10	0	10,6	0,1	10,6	10	106	10,6	0,300	120,58
1500	50	19,4	0,0006	-30,6	1450	2,1103	0,0014	0,300	
5	3	0,434	0,2	-2,566	2	128,3	25,66	0,300	
15000	5000	0,3722	6,66667E-05	-4999,6	10000	49,9992	0,0033	0,300	

Table 14: Calculation of Heavy pollution index for Bouhanifia dam

Si	Li	Mi	Wi	Mi-Li	Si-Li	Qi= Mi-Li/Si-Li*100	Wi*Qi	Wi	HPI mean
10	0	29,4	0,1	29,4	10	294	29,4	0,300	197,26
1500	50	0,011	0,0006	-49,98	1450	3,447	0,0022	0,300	
5	3	0,008	0,2	-2,992	2	149,6	29,92	0,300	
15000	5000	0,118	6,66667E-05	-4999,8	10000	49,99	0,00333	0,300	

Table 15: Calculation of Heavy pollution index for Cheliff Dam

Si	Li	Mi	Wi	Mi-Li	Si-Li	Qi= Mi-Li/Si-Li*100	Wi*Qi	Wi	HPI mean
10	0	10,6	0,1	10,6	10	106	10,6	0,300	135,08
1500	50	0,015	0,00066	-49,985	1450	3,447	0,0022	0,300	

5	3	-0,002	0,2	-3,002	2	150,1	30,02	0,300
15000	5000	0,0546	6,66667E-05	-4999,9	10000	49,9995	0,003	0,300

Table 16: Calculation of Heavy pollution index for Dayet El Ferd

Si	**Li**	**Mi**	**Wi**	**Mi-Li**	**Si-Li**	**Qi= Mi-Li/Si-Li*100**	**Wi*Qi**	**Wi**	**HPI mean**
10	0	3,3	0,1	3,3	10	33	3,3	0,300	89,66
1500	50	29,1	0,00066	-20,9	1450	1,4206	0,0009	0,300	
5	3	0,634	0,2	-2,366	2	118,3	23,66	0,300	
15000	5000	0,2954	6,66667E-05	-4999,70	10000	49,997	0,0033	0,300	

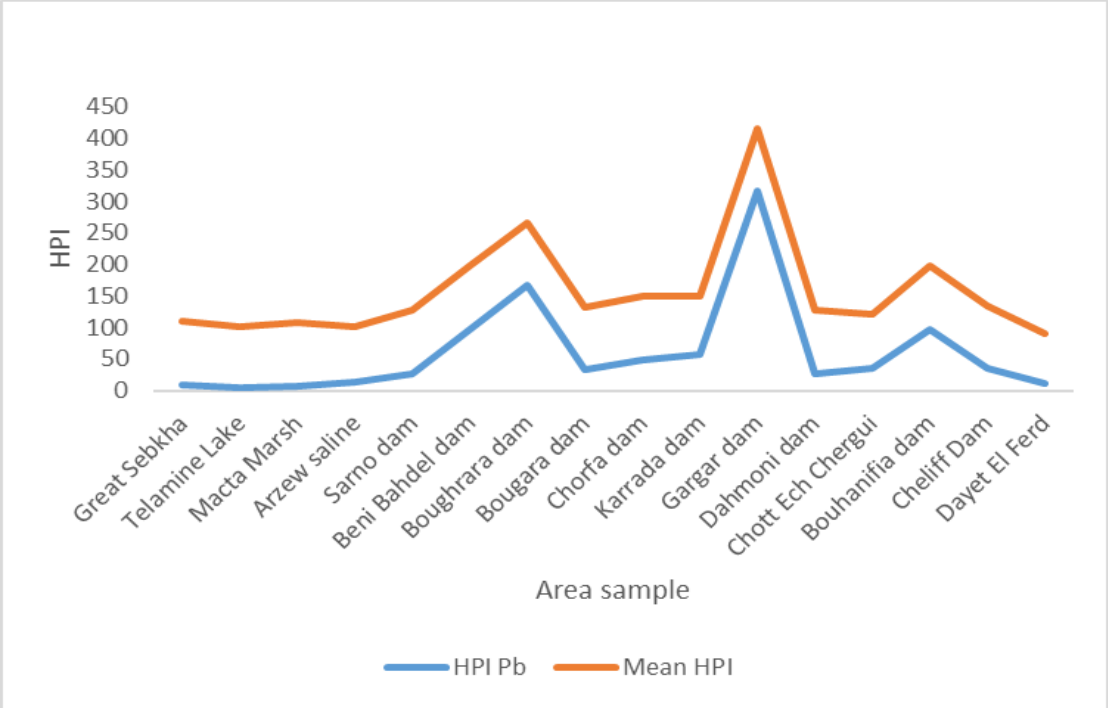

Figure. 3. HPI values of Pb Metal relation to the mean value.

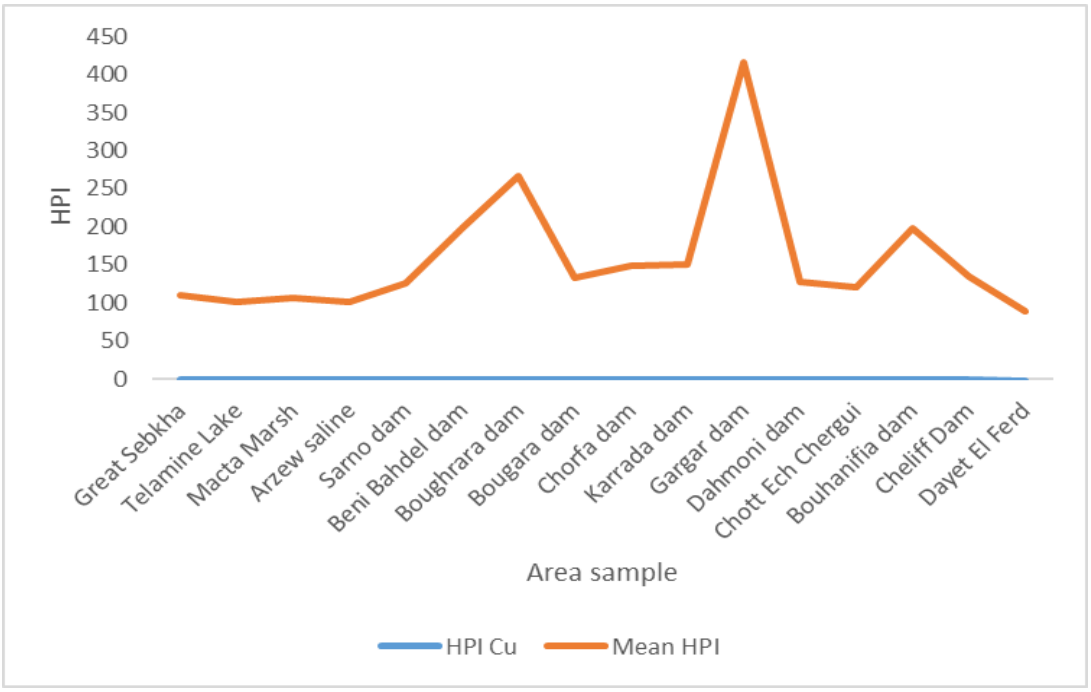

Figure. 4. HPI values of Cu Metal relation to the mean value.

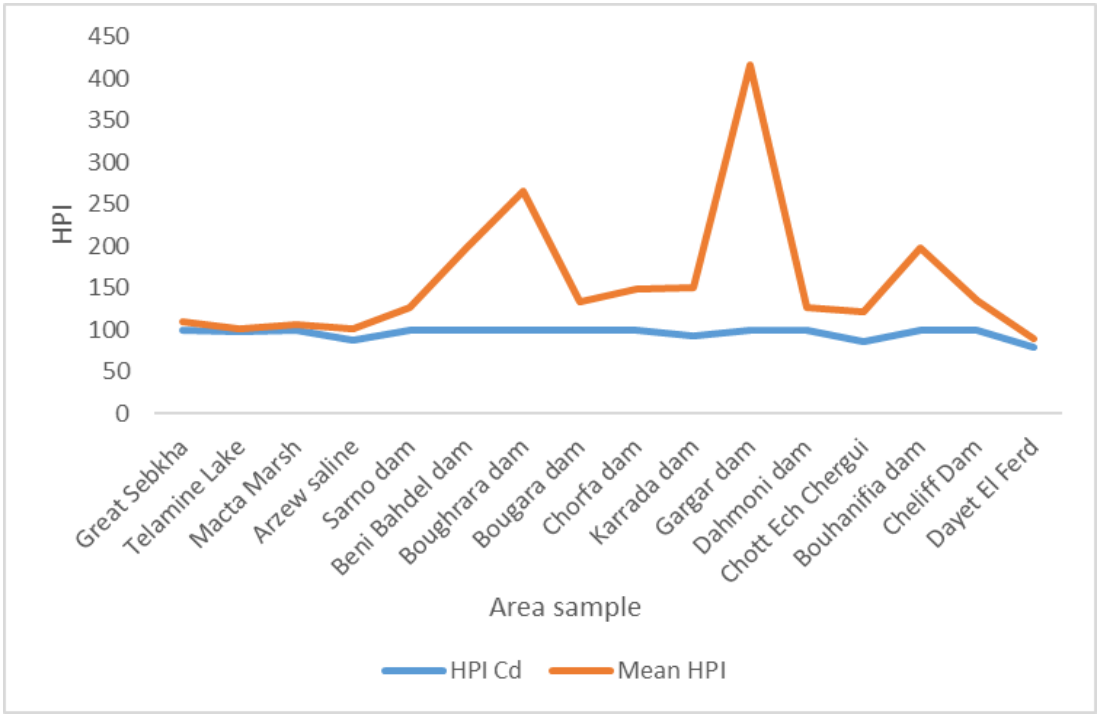

Figure. 5. HPI values of Cd Metal relation to the mean value.

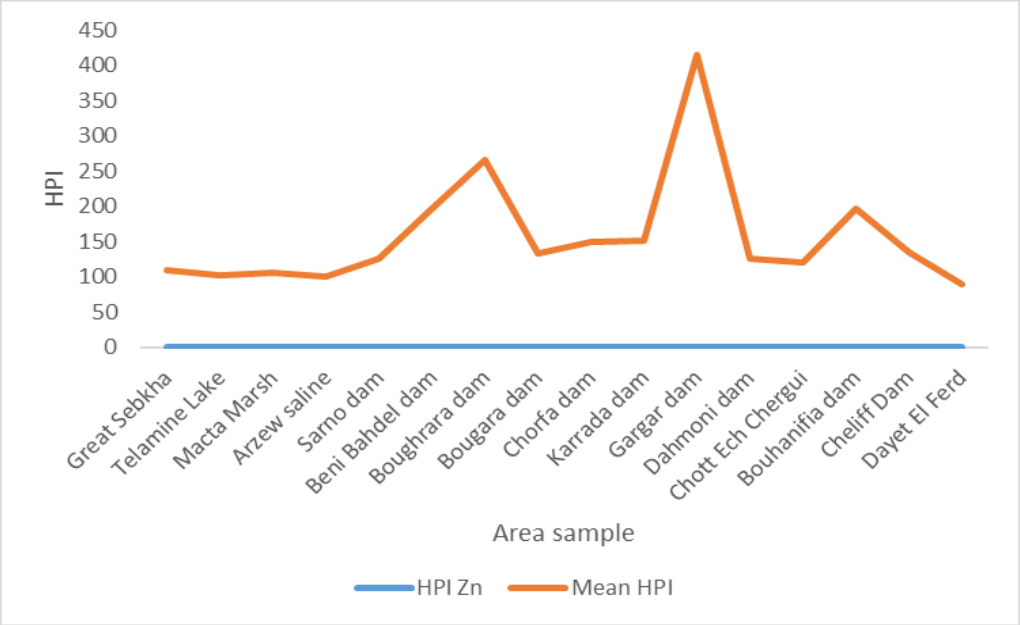

Figure. 6. HPI values of Zn Metal relationto the mean value.

Natural Hazards
https://doi.org/10.1007/s11069-024-06532-1

ORIGINAL PAPER

Assessment of the long-term effects of climate on vegetation in 25 watersheds in dry and semi-dry areas, Algeria

Hadjer Keria[1] · **Ettayib Bensaci**[2] · **Asma Zoubiri**[2]

Received: 27 February 2023 / Accepted: 28 February 2024

Abstract
It is necessary to understand vegetation evolution and its sensitivity to the global climate, particularly with regard to ecosystems and environmental balance. 25 watersheds were selected in Algeria for this study. Here, the vegetation index (NDVI) and climatic variables (precipitation and temperature) were used to verify the temporal-spatial patterns and impact of the time difference from 1981 to 2021 by applying the correlation coefficient and time delay analysis. The NDVI showed a significant decline, especially in recent years, and spatial differences in NDVI in all areas of study were narrow (slope values from 0.0005 to 0.04), decrease in surface water area from year to year was observed in all regions. The vegetation index was negatively associated with low rainfall and high temperatures. The vegetation's reaction to temperature has been greater than that too rainfall. In general, a time lag in the vegetation response was found over a time period of at least 1 month. This study provided new insights into variations in vegetation change and the importance of vegetation recovery.

Keywords Climatic factors · NDVI · Vegetation dynamic · Correlation · Algeria

1 Introduction

Climate change stands as a pivotal force shaping vegetation transformation, a critical component in environmental equilibrium. Consequently, investigating these impacts has emerged as a paramount global challenge (Zhang et al. 2013; Liu et al. 2019). Conversely, anthropogenic environmental activities play a significant role in altering vegetation dynamics (Wang et al. 2015). Moreover, shifts in long-term environmental conditions are poised to yield profound ramifications for extant plant diversity patterns, particularly amidst escalating global warming (Wang et al. 2020a). Broadly, the effects

✉ Hadjer Keria
hadjer.keria@univ-msila.dz

[1] Laboratory of Biodiversity and Biotechnological Techniques for the Valorisation of Plant Resources (BBT_VPR), Department of Natural and Life Sciences, University of Mohamed Boudiaf, M'sila 28000, Algeria

[2] Department of Natural and Life Sciences, University of Mohamed Boudiaf, M'sila 28000, Algeria

Published online: 14 March 2024

of temperature and rainfall are already discernible in natural systems, with the magnitude of these impacts varying across different regions (Wang et al. 2020b).

In the forthcoming decades, climate change is poised to induce notable alterations in wind patterns, temperature, and ecological conditions, consequently precipitating a significant shift in the dynamics of sandy desert environments. Such changes could potentially foster the expansion of vast sandy desert areas across the Earth's surface. Understanding the behavior of vegetation and its impact on ecosystems in the context of global warming is imperative for accurately forecasting ecosystem dynamics and devising effective strategies to mitigate wind-induced soil erosion (Parteli 2022). Vegetation plays a pivotal role in preserving and assessing ecosystems (Zhou et al. 2014; Eisavi et al. 2015), with numerous studies focusing on diverse aspects such as assessing CO_2 levels and their influence on vegetation greenness (Liu et al. 2022), evaluating drought severity in watershed regions (Zhan et al. 2022), and analyzing the effects of temporal lag (Ding et al. 2020; Qin et al. 2023). These ongoing changes exhibit a long-term, irreversible trend that has been unfolding over time, necessitating comprehensive studies on temporal and spatial variations to monitor natural transformations (Seddon et al. 2016; Liu et al. 2017; Zhao et al. 2020). Furthermore, the Normalized Difference Vegetation Index (NDVI) serves as a reliable benchmark for studying these changes (Myneni et al. 2002).

Within the climate system, precipitation and temperature stand as pivotal determinants of plant growth across various regions (Martiny et al. 2006). However, this system's perturbations disrupt the natural balance of ecosystems and hasten environmental degradation through processes such as desertification and other ecological challenges (Islam et al. 2021). Numerous studies have highlighted temporal disparities between vegetation and climate indicators, as well as the diverse impacts of time lags resulting from extreme weather events on vegetation growth in different locales (Xu et al. 2014; Liu and Lei 2015; Li et al. 2018; Luo et al. 2020). Examining this relationship on a monthly scale, in contrast to long-term investigations, can enhance understanding of the factors constraining vegetation development (Luo et al. 2020). While investigating concurrent associations can aid in mitigating the impacts of climate variability, it may not fully capture the processes through which plants respond to environmental stimuli (Vicente-Serrano et al. 2013; Pan et al. 2018; Zhang et al. 2020).

Comprehending the response of vegetation to climate conditions over time stands as a significant and pressing challenge, particularly amidst the conditions and alterations brought about by the increasingly extreme global climate (Jong et al. 2013). Temporal gaps further complicate this task (Wu et al. 2015). This reveals a complex spatial response of these landscapes to climate factors, which vary depending on the type of vegetation present (Ding et al. 2020).

In this context, our primary objective is to assess the impact of climate on the long-term dynamics of vegetation, spanning the period from 1981 to 2021. Leveraging remote sensing data and meteorological data, we focused on 25 distinct regions across Algeria. The specific aims of this research are as follows: (1) To delineate spatial alterations in vegetation indices over 40 years across the 25 different regions of Algeria; (2) To investigate the temporal relationship between the NDVI index and climate parameters; (3) To utilize the Normalized Difference Vegetation Index (NDVI) to analyze the effects of climatic variations on vegetation growth, identifying both widespread independent effects and common impacts of such changes; and (4) To ascertain the enduring effects of temporal delays on vegetation dynamics.

2 Materials and methods

2.1 Study area

The study area is situated in northern Africa, covering a total expanse of 2,381,741 km^2. It stretches 1200 km from east to west along the Mediterranean Sea and nearly 2000 km from north to south. Algeria's northern region is characterized by a Mediterranean climate featuring hot summers and relatively mild, rainy winters. In contrast, the southern regions endure a climate of hot summers and cold winters, with scant rainfall on the high plains south of the Atlas Mountains. With the Sahara Desert enveloping 80% of the nation, summer temperatures can soar to extreme levels, while winter temperatures typically remain warm during the day and cold at night, occasionally dropping as low as 5 °C. The study encompasses a diverse array of wetlands, each with unique hydrological characteristics. Table 1 presents details of the physical attributes of these basins, including average rainfall and annual temperatures. Prominent sites include Makta Marsh, Greater Sabha, Lake Tilamine, Arzew Salt, Boughezoul Dam, Chott Zehrez Chergui, Chot Ech Chergue, Dayet El Ferd, Chutt Zehres Gharbi, and Chott El Hodna, all classified as semi-arid. However, distinct hydrological disparities distinguish areas such as Shut Chott Melghir, Beni Bahdel Dam, Bougara Dam, Bouhanifia Dam, Chorfa Dam, Cheliff Dam, Dahmoni Dam, Gargar Dam, Karrada Dam, Ksob Dam, and Sarno Dam. Despite their semi-arid classification, these sloping basins present specific challenges in water management. Furthermore, the study area encompasses arid environments such as Chott Marouane and Chott Ain El Beida, characterized by irregular hydrology. Notably, Chott Marouane is acknowledged as a crucial habitat for birds and biodiversity, contributing to the region's hydrological complexity. Additionally, permanent sites like El Golea and Chott Ain El Beida are situated within a semi-arid context (Fig. 1). The selection of wetlands in Algeria for study purposes was based on their environmental and economic significance, particularly considering their designation by Ramsar, an international organization committed to the conservation and sustainable utilization of wetlands.

2.2 Dataset

2.2.1 NDVI dataset

The Landsat archives provide globally consistent and temporally accurate data with a resolution of 30 m and a 16-day revisit cycle (Irons et al. 2012; Claverie et al. 2015). In this study, we accessed and analyzed all Landsat data using the Google Earth Engine (GEE) platform, which offers cloud-based accessibility (Gorelick et al. 2017). From 1981 to 2021, we compiled a time series consisting of cloud-free images spanning January to December. Landsat datasets 5, 7, and 8 were utilized, with surface reflectance adjusted using "USGS Landsat Surface Reflectance Tier 1" data. Additionally, atmospheric correction and masking for clouds, water, shadows, and snow were performed using CFMASK (Zhu et al. 2015; Kennedy et al. 2018).

We employed LandTrendr, a chronological classification method available in GEE, for detecting and analyzing vegetation changes. LandTrendr identifies short-term events and elucidates long-term patterns by separating spectral trajectories based on satellite observations or spectral indices (Kennedy et al. 2010). Utilizing Landsat data, we tracked

Table 1 The physical characteristics and climate of the basins

Watershed	Watershed area (ha)	Water quality	Hydrological cadency	Latitude (N)	Longitude (E), (W)	Annual precipitation (mm)	Annual temperature (°C)	Climate
Macta Marsh	44.500	Salty	Permanent	35° 38′ 52″	00° 06′ 16″ W	300–400	20	Semi-arid
Great Sebkha	56.870	Salty	Permanent	35° 31′ 29″	00° 47′ 12″ W	300–370	18.7	Semi-arid
Telamine Lake	2.399	Salty	Permanent	35° 44′ 09″	00° 22′ 57″ W	300–390	18.5	Semi-arid
Arzew saline	5.778	Salty	Permanent	35° 41′ 25″	00° 19′ 22″ W	300–400	18.2	Semi-arid
Boughezoul Dam	9.058	Salty	Permanent	35° 41′ 55″	02° 47′ 34″ E	500–550	14.7	Semi-arid
Chott Zehrez Chergui	50.985	Salty	Permanent	35° 12′ 59″	03° 31′ 58″ E	320–335	14.9	Semi-arid
Chott Ech Chergui	855.500	Salty	Permanent	34° 16′ 09″	00° 33′ 25″ E	410–420	15.3	Semi-arid
Dayet El Ferd	3.323	Salty	Permanent	34° 29′ 55″	01° 14′ 23″ W	400–500	15.4	Semi-arid
Chott Zehrez Gharbi	52.200	Salty	Permanent	34° 56″	02° 48′ 06″ E	320–350	14.9	Semi-arid
Chott El Hodna	362.000	Salty	Permanent	35° 26′ 04″	04° 41′ 54″ E	250–270	18.9	Semi-arid
Chott Melghir	551.500	Salty	Irregular	34° 10.631″	06° 17.322″ E	65–100	21.2	Arid
Beni Bahdel Dam	54.630	Salty	Irregular	34° 42′ 42.70″	1° 30′ 13.24″ W	400–500	15	Semi-arid
Bougara Dam	11.320	Salty	Irregular	36° 32′ 26″	3° 5′ 7″ E	340–360	16.2	Semi-arid
Boughrara Dam	175.450	Salty	Irregular	34° 88′ 3854″	01° 67′ 6169′ W	400–500	15.2	Semi-arid
Bouhanifia dam	34.52	Salty	Irregular	35° 16′ 39″	0° 3′ 36″ W	400–450	17.4	Semi-arid
Chorfa Dam	70.210	Salty	Irregular	35° 25′ 55″	0° 14′ 43″ W	400–500	17	Semi-arid
Cheliff Dam	50.000	Salty	Irregular	35° 59′ 00″	0° 24′ 47″ W	380–400	18.3	Semi-arid
Chott Marouane	337.700	Salty	Irregular	34° 02′ 433″	5° 58′ 748″ E	60–100	21.6	Arid
Dahmoni dam	39.520	Salty	Irregular	35° 41′ 67″	14° 76′ 29″ E	450–470	15.5	Semi-arid
Gargar Dam	358.280	Salty	Irregular	35° 55′ 52″	0° 59′ 15″ E	400–420	18.4	Semi-arid
Karrada Dam	65.000	Salty	Irregular	36° 05′ 1162″	00° 38′ 5519″ E	440–440	18	Semi-arid
Ksob Dam	22.72	Salty	Irregular	35° 58′ 05″	04° 42′ 33″	250–270	18.7	Arid
Sarno Dam	21.250	Salty	Irregular	35° 29′ 94′ 99″	00° 59′ 0768″ W	420–430	17.3	Semi-arid
El Golea	18.947	Salty	Permanent	20° 25′ 00″	02° 95′	35–70	22.9	Arid

Table 1 (continued)

Watershed	Watershed area (ha)	Water quality	Hydrological cadency	Latitude (N)	Longitude (E), (W)	Annual precipitation (mm)	Annual temperature (°C)	Climate
Chott Ain El Beida	6.853	Salty	Irregular	31° 57′ 30″	31° 59′ 2″	30–80	22.2	Arid

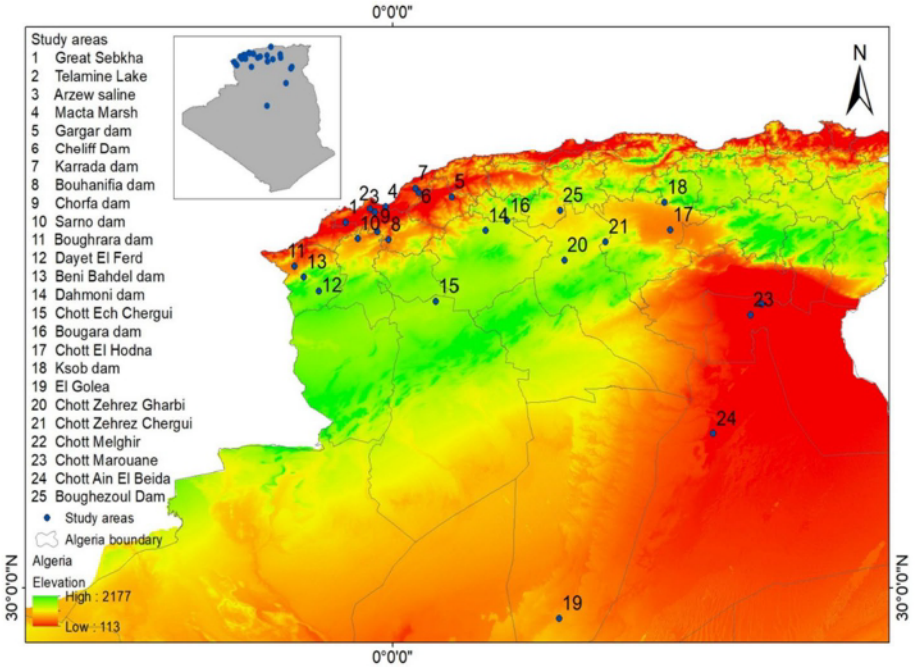

Fig. 1 Distribution of the 25 watersheds in Algeria

vegetation changes over 40 years using Normalized Difference Vegetation Index (NDVI) values, which were available throughout the year at a spatial resolution of 30 m.

While the 30-m resolution of Landsat data enabled comprehensive analysis over the study duration, it's essential to acknowledge the potential benefits of using higher-resolution datasets. Fine-grained data could reveal additional insights and nuances in vegetation dynamics, particularly in areas with complex land cover patterns or at smaller scales. However, during our study timeframe, access to such datasets was limited, necessitating the use of Landsat data to fulfill our research objectives. Incorporating higher-resolution datasets in future research endeavors holds promise for further enhancing our understanding of vegetation dynamics and ecosystem processes.

2.2.2 Climate dataset

We utilized temperature records with a precision of 0.05° sourced from the Climate Forecast System Reanalysis (CFSR) and precipitation datasets from the Climate Hazards Group InfraRed Precipitation with Station (CHIRPS) project, both available on a daily basis. These datasets were accessed through the Climate Engine platform (http://climateengine.org). CHIRPS data proved valuable for calculating multi-annual and growing season total rainfall averages, aiding in time series trend analysis and drought monitoring. Additionally, we obtained multi-annual and seasonal mean temperatures, with resolutions of 1/5° and 3/10° respectively, from the National Center for Environmental Prediction's CFSR datasets. These temperature records were then integrated and reprocessed alongside Normalized Difference Vegetation Index (NDVI) data spanning from 1981 to 2021.

2.3 Methods

2.3.1 Regression analysis of long-term vegetation index

The linear regression model utilized to evaluate NDVI and climate (precipitation and temperature) variation trends at each pixel's scale can be defined as follows (Hu et al. 2019):

$$\text{Slope} = \frac{\text{n} \times \sum_{\text{i}=1}^{\text{n}} \text{i} \times \text{NDVI}_{\text{i}} - \sum_{\text{i}=1}^{\text{n}} \text{i} \sum_{\text{i}=1}^{\text{n}} \text{NDVI}_{\text{i}}}{\text{n} \times \sum_{\text{i}=1}^{\text{n}} \text{i}^2 - \left(\sum_{\text{i}=1}^{\text{n}} \text{i}\right)^2} \tag{1}$$

where *NDVIi* represents either the yearly average or the highest NDVI value, *n* indicates the length of the NDVI time series, and *i* denotes the ranking of years within the study period from 1 to 30. The slope indication and its value illustrate the trend and magnitude of increase for the NDVI data sequence. The incline value signifies the mean annual NDVI over the study years. When the incline is greater than 0, NDVI reflects an escalating trend, indicating an increase or improvement in vegetation cover. Conversely, when the incline is less than 0, the NDVI time series tends to decline, suggesting a deterioration in vegetation health, with vegetation color turning brown or soil degradation occurring. The significance test for the orientation of the NDVI parameter was conducted using a t-test, where a statistically significant trend was defined as $P<0.05$ (Gao et al. 2022).

2.3.2 Normalization data

To evaluate the spatial and temporal disparities of NDVI, precipitation, and temperature, we employed min–max normalization, which scales the values between 0 and 1. The formulas for min–max normalization are as follows (Luo et al. 2020):

$$x' = \frac{x - x_{min}}{x_{max} - x_{min}} \tag{2}$$

here, x represents the true value, x_{min} and x_{max} denote the lowest and highest values of the dataset, and $x\prime$ represents the normalized value after min–max normalization.

2.3.3 Correlation analyses among the vegetation index and climatic change

We computed the relationship between temperature, rainfall, and NDVI to assess vegetation responses to climate variables, following the methodology outlined below (Bhuyan et al. 2017):

$$r_k(x,y) = \frac{\sum_{i=1}^{n-k} \left[\left(x_i - \overline{x}\right) \times \left(y_i - \overline{y}\right)\right]}{\sqrt{\sum_{i=1}^{n-k} \left(x_i - \overline{x}\right) \times \sum_{i=1}^{n-k} \left(y_i - \overline{y}\right)}} \tag{3}$$

with $r_k(x,y)$, which represents the sequence of correlation analyses between NDVI and climatic factors, n indicating the span of the chain, x_i representing the NDVI time series, k denoting the time lapse, y_{i+1} representing the temperature or rainfall time series with a k time lag.

Previous research has indicated that the period of climate and plant changes usually falls within a monthly range; the relationship between vegetation and climate changes in season periods can be used to determine time differences or time lag. Climate variables like temperatures and precipitation have a direct impact on vegetation, which affects the timing of plants' growth and changes throughout the year (Peng et al. 2019; Zhe and Zhang 2021). Thus, delays or presentations of certain seasons can be monitored for normal conditions. In addition, significant changes in typical climatic conditions can delay the growing season by three months, having a drastic impact on the ecosystem. Using available data on vegetation and climate change, this relationship can be analyzed, and the temporal effects of climate change on the plant environment determined (Chen et al. 2014; Wu et al. 2015).

3 Results

3.1 The temporal-spatial distributions for NDVI during the past 40 years

The NDVI results exhibit notable spatial variations throughout the period from 1981 to 2021 (Fig. 2). Approximately 59.6% of the total greenery area exhibits an NDVI level lower than 0.45, with particularly low values identified in regions such as Chott Ech Chergui, Arzew Saline, Chott Melghir, and Chott Merouane. Conversely, NDVI values exceeding 0.45 are distributed across numerous regions, accounting for a total of 40.4%, although the increase is relatively modest. Notably, the highest NDVI values are observed in areas including Macta Swamp, Great Sebkha, Sarno Dam, Chott Zehrez Chergui, and Karrada Dam. Additionally, negative NDVI values predominantly characterize water bodies, as depicted in Fig. 2. These water sources have also experienced reductions in their aerial extent, with some disappearing over time. Remarkably, the volume of surface water bodies has declined annually across all regions, likely attributed to various factors such as agricultural expansion, indiscriminate use of chemical substances, grazing activities, infrastructure development (e.g., dams, hydroelectric projects), and urbanization, all contributing to a significant reduction in vegetation. Consequently, the ratio of NDVI vegetation has undergone marked changes over the past four decades. The observed distribution pattern of NDVI trends in each location highlights a strong correlation among vegetation indices, elevation, and water availability. Spatial disparities in NDVI across all study regions remained consistent (slope values ranging from 0.0005 to 0.04) throughout the study period (1981–2022).

3.2 The association between the vegetation index and climatic changes

In arid and semiarid regions, changes in vegetation and climatic variables are intricately intertwined. According to Fig. 3, partial correlation analysis between Normalized Difference Vegetation Index (NDVI) values and rainfall (NDVI-P) exhibited negative associations across all watersheds, while the relationship varied for temperature (NDVI-T), with positive correlations observed in certain areas (such as Chott Zehrez Chergui, Chott Ech Chergui, Dayet El Ferd, Chott Zehrez Gharbi, Chott El Hodna, Beni Bahdel Dam, Chott Merouane, Dahmoni Dam, Golea, Gargar Dam, and Ksob Dam) during the period 1981–2021. Furthermore, NDVI-T displayed a declining trend over this period, indicating that higher temperatures do not necessarily promote plant growth, and the beneficial effects of climate change on natural vegetation diminish over time.

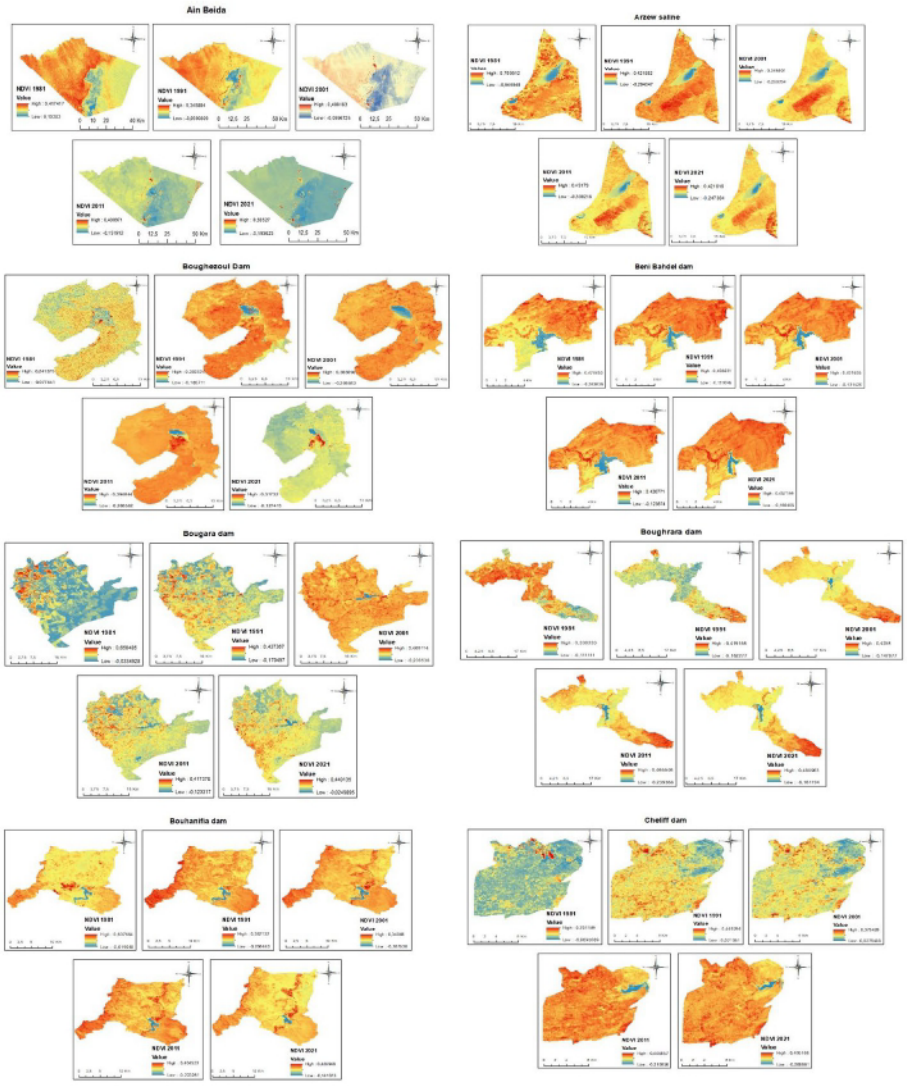

Fig. 2 Patterns of NDVI change trends in 25 basins in Algeria from 1981 to 2021, with yearly average NDVI change

In general, NDVI exhibited a stronger correlation with temperature than with precipitation. This could be attributed to the dry and semiarid climatic conditions, where the influence of temperature on vegetation was more significant than that of rainfall on vegetative cover. Additionally, analysis of specific seasonal relationships revealed that NDVI in spring exhibited the highest positive association with temperature and rainfall. This suggests that NDVI decreases with increased rainfall and temperature in spring, especially in recent years. Conversely, NDVI showed a significant positive correlation with rainfall and temperature in all wetlands during autumn, except for Chott Melghir, Chott Merouan, Golea, Chott Houdna, Chott Zehrez Chergui, and Chott Zehrez Gharbi.

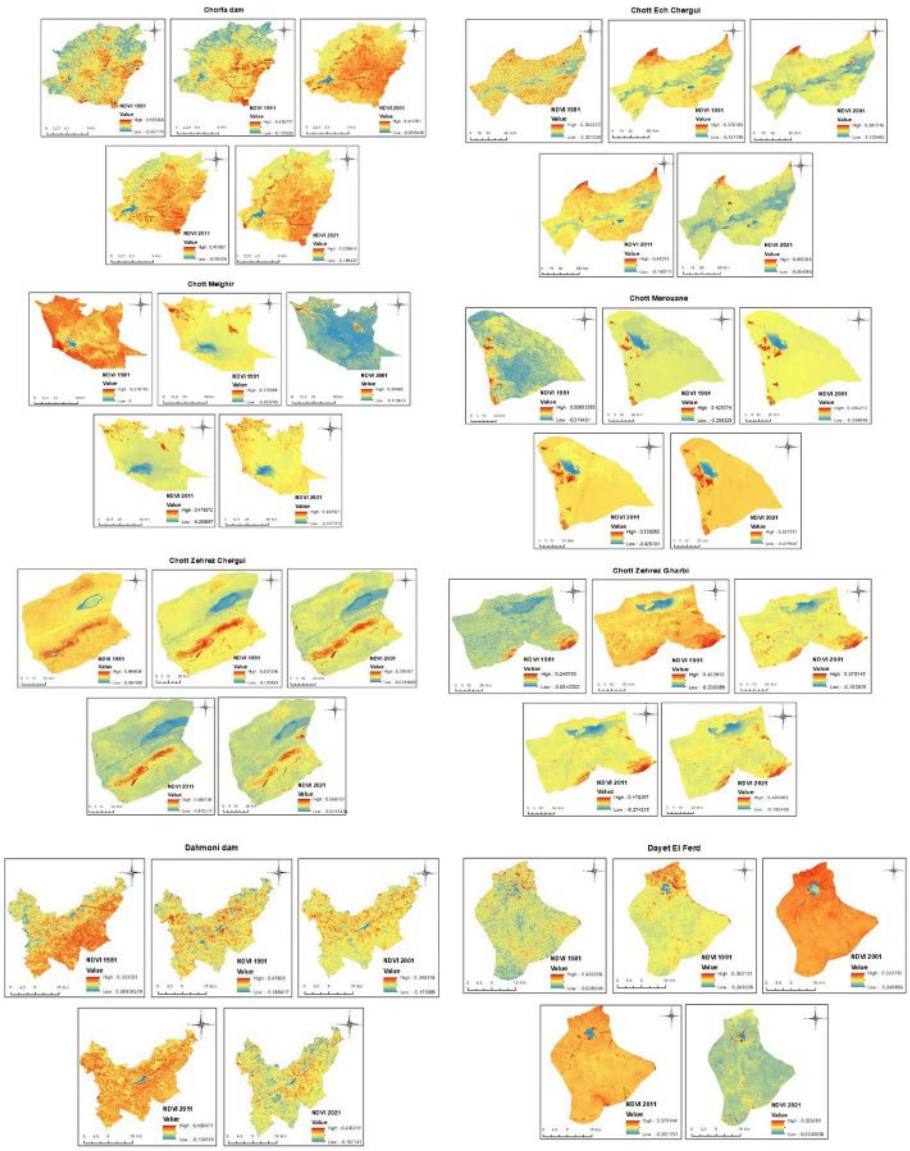

Fig. 2 (continued)

However, the link between NDVI and rainfall and temperature were weaker in summer, particularly with temperature.

The intricate interplay between NDVI and climatic variability was elucidated through month-level NDVI data and the normalization of rainfall and temperatures across 25 water bodies from 1981 to 2021 (Fig. 4). While temperatures exhibited smooth cyclical changes across the basins, cyclical precipitation changes were more widely dispersed. Maximum NDVI readings did not consistently align with climate data trends, suggesting significant

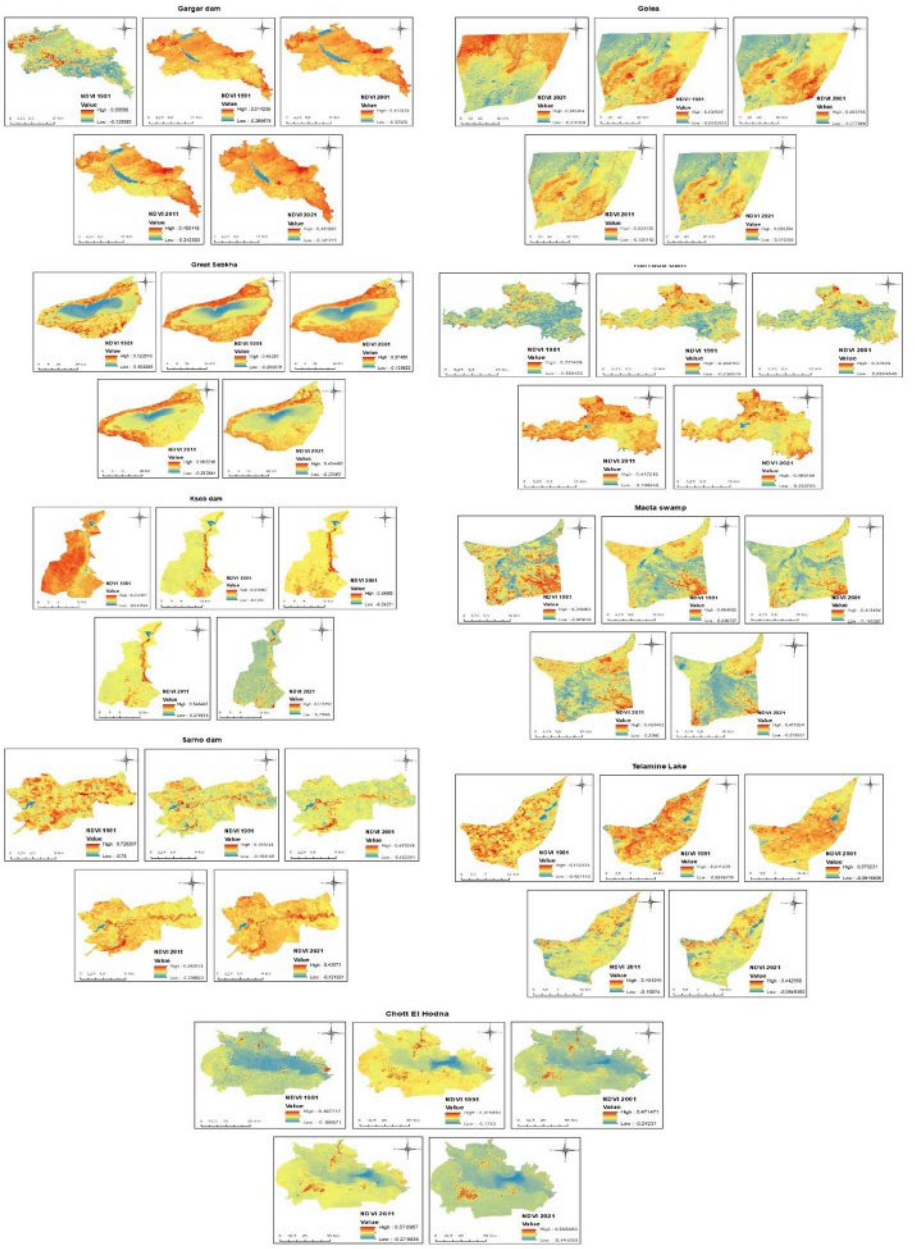

Fig. 2 (continued)

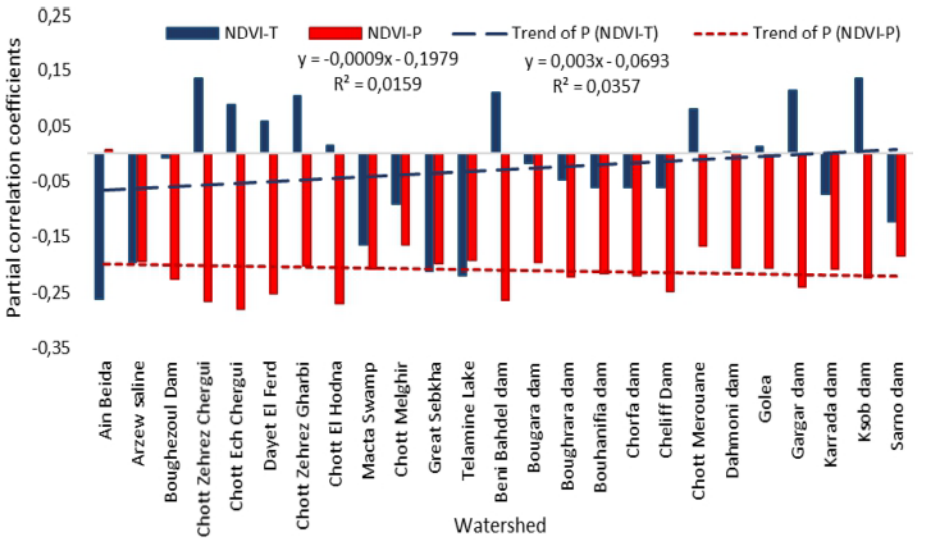

Fig. 3 The factor of partial correlation of growth season between NDVI, rainfall, and temperature in the 25 watersheds during 1981–2021

delays over the study period. These findings indicate that the influences of rainfall and temperature on NDVI in these basins exhibit temporal delays.

3.3 Long-time impact response for NDVI with rainfall/temperature variations

The effects of the delay period are being examined by considering annual and seasonal coherence factors between NDVI and climate indicators in basins, as depicted in Tables 2 and 3. Annual correlations between NDVI and rainfall across all basins showed negative associations, with similar negative correlations observed across all seasons. There appears to be an uneven distribution, with this correlation's impact being more pronounced in autumn. From September to December, rainfall appears to correlate somewhat with the climatic drought experienced in spring, attributed to a lack of rainfall from mid-March to June. Conversely, temperature exhibited positive correlations in many basins throughout the seasons; however, plant density decreased due to higher temperatures and reduced rainfall in spring and autumn.

Furthermore, these analyses revealed significant seasonal variations in plant growth within the basins, with delays in plant growth attributed to delayed rainfall. At times, this delay resulted in a 1–3 months lag in recording due to the delayed NDVI response to climate changes. Vegetation also displays periodic fluctuations, corresponding to variations in temperature and precipitation. While the overall functions of these two components, along with temperature and precipitation, govern periodic vegetation adjustments, the maximum value of NDVI during a given period does not precisely align with precipitation and temperature, indicating a slight delay (Fig. 5). Additionally, periods of abundant rainfall were not necessarily linked to low NDVI values.

Moreover, significant annual changes were observed, with the Normalized Difference Vegetation Index (NDVI) declining in 1989–1998 across all regions and rising

Fig. 4 Standardized long-term fluctuations in NDVI and climatic variables (rainfall and temperature) across the 25 watersheds in Algeria during 1981–2021

in 1994–1996 compared to the preceding period. These changes highlight the impact of delays in vegetation response to changes in temperature and precipitation.

3.4 Spatial distribution and influence of climatic factors on vegetation cover

Figure 6 depicts the spatial correlation between vegetation growth and climatic factors over 40 years, illustrating that NDVI values are strongly correlated with temperature and rainfall across more than 95% of the greenery area ($p < 0.05$). The correlation between NDVI and temperature is less than 0.4 over approximately 85% of the vegetation area. During these periods (Fig. 6a), which exhibit negative effects on vegetation

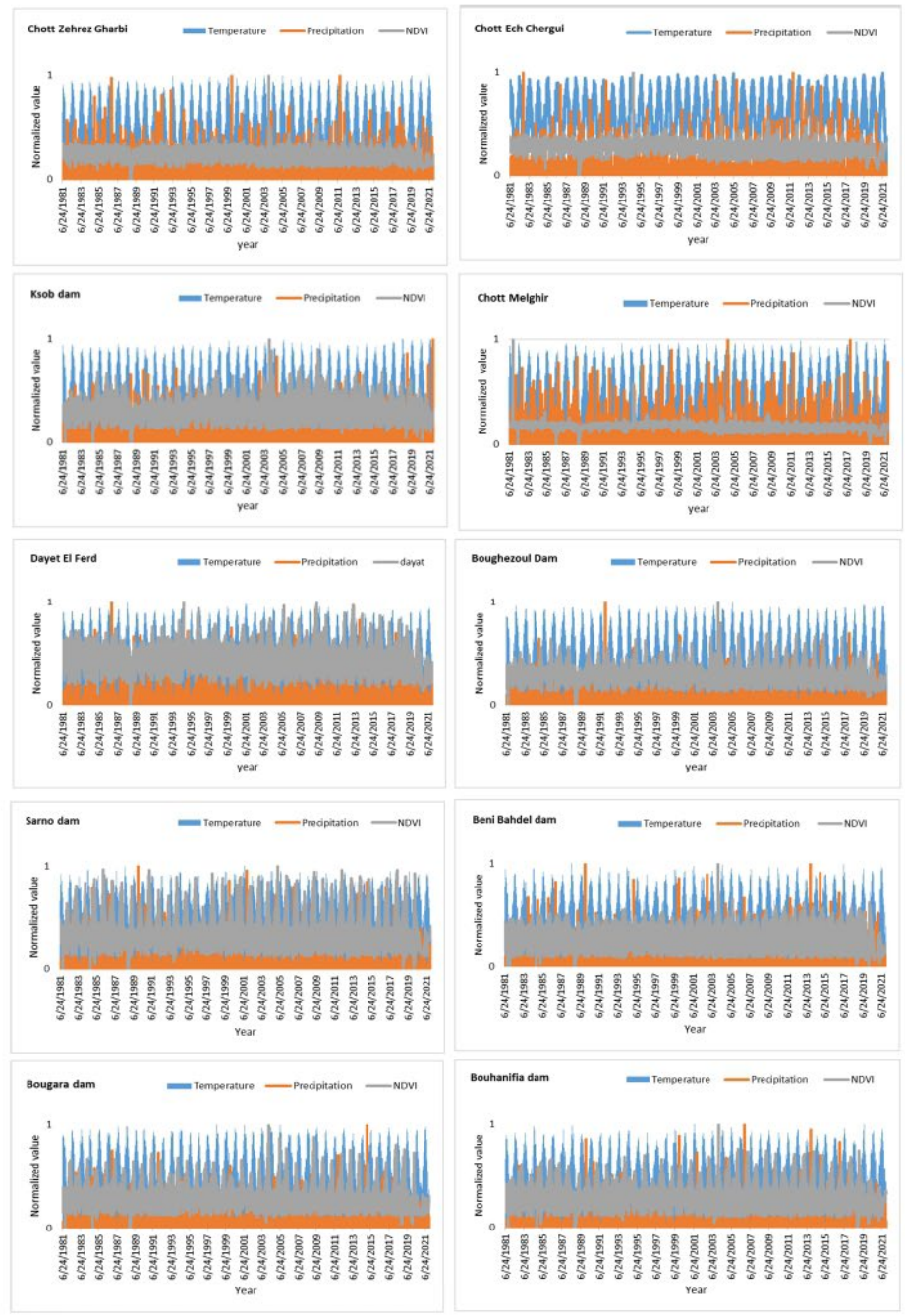

Fig. 4 (continued)

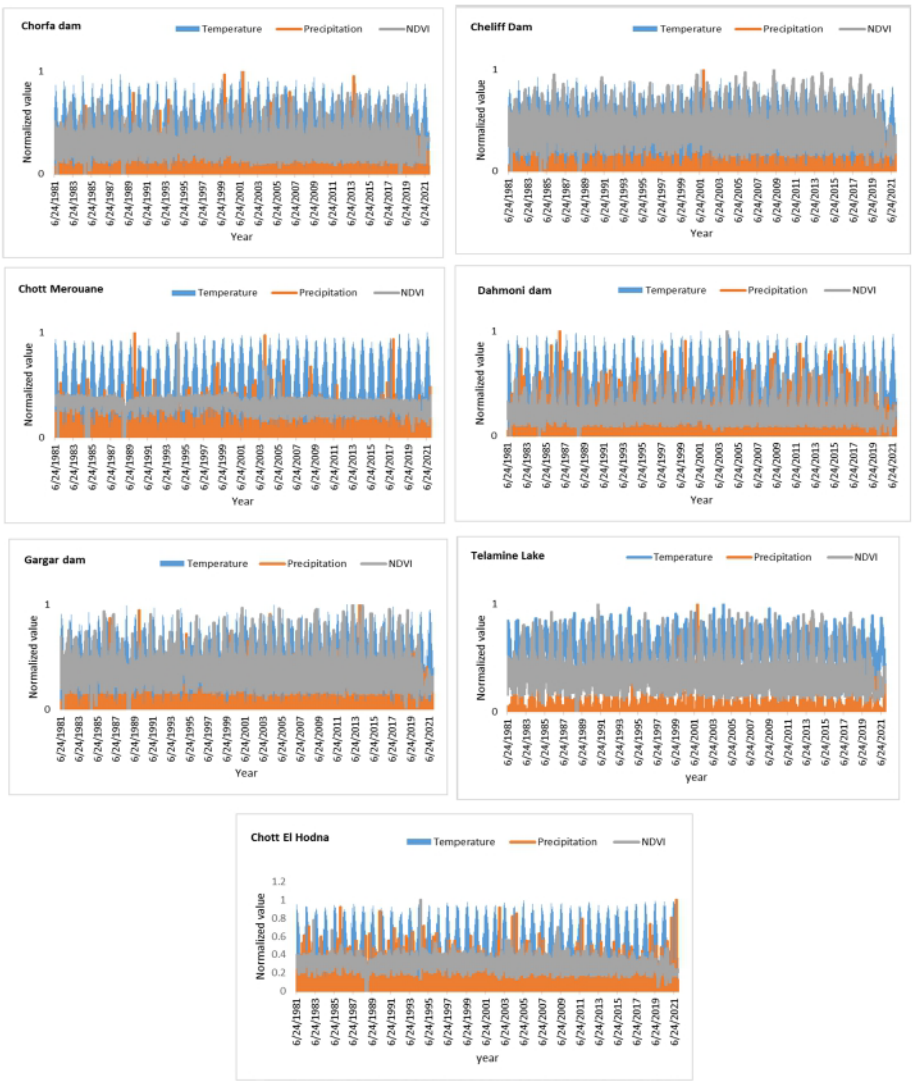

Fig. 4 (continued)

across all regions, the corresponding NDVI-P relationship displays a similar pattern (Fig. 6b), suggesting an increasing negative response to vegetation cover and the beneficial impact of rainfall. Specifically, NDVI-P exhibits more than 70% negative or transitioning from positive to negative changes, particularly in recent years, indicating that precipitation is the primary driver of vegetation density in these regions. However, it should be noted that 45% of the NDVI-T changes from improvement to deterioration, indicating a significant shift in vegetation productivity due to climate warming in these areas.

Table 2 The correlation coefficient among climatic indicators and the vegetation indices

Basins	Correlation coefficient		
	NDVI-T	NDVI-P	R^2
Ain Beida	−0.26187	0.007151	0.0106
Arzew Saline	−0.19597	−0.1938	0.0096
Boughezoul Dam	−0.00785	−0.22668	0.0237
Chott Zehrez Chergui	0.135913	−0.26638	0.0518
Chott Ech Chergui	0.088362	−0.27977	0.0439
Dayet El Ferd	0.058209	−0.25218	0.0191
Chott Zehrez Gharbi	0.104216	−0.20293	0.0339
Chott El Hodna	0.014254	−0.26994	0.04
Macta Swamp	−0.16343	−0.20898	0.0073
Chott Melghir	−0.09173	−0.16453	0.0005
Great Sebkha	−0.21125	−0.19904	0.0047
Telamine Lake	−0.21915	−0.19317	0.0155
Beni Bahdel Dam	0.109324	−0.2635	0.0013
Bougara Dam	−0.01723	−0.19687	0.0175
Boughrara Dam	−0.04696	−0.22146	0.0034
Bouhanifia Dam	−0.061	−0.21703	0.0016
Chorfa Dam	−0.06196	−0.22078	0.005
Cheliff dam	−0.06187	−0.24869	0.0098
Chott Merouane	0.079735	−0.16671	0.0917
Dahmoni Dam	0.000705	−0.20711	0.0072
Golea	0.011864	−0.20599	0.0442
Gargar Dam	0.114363	−0.23949	0.0034
Karrada Dam	−0.07234	−0.20797	0.002
Ksob Dam	0.135599	−0.2246	0.0049
Sarno Dam	−0.12339	−0.18363	0.0047

4 Discussion

The NDVI in all areas where the study was conducted showed a marked decrease from 1981 to 2021. The relationship and effects of the time difference between climate variables and vegetation coverage have been studied in 25 areas of Algerian water bodies, which hold significant importance and are crucial for comprehending environmental processes in these regions (Zhou et al. 2018; Bai et al. 2020). Vegetation in these areas is strongly linked to climate change (Roerink et al. 2003; Piao et al. 2006; Chu et al. 2019).

According to the research outcomes, the positive relationship between temperature and NDVI turned negative during the study period, indicating that the positive effect of rising temperatures on greenery cover has diminished over time. This negative impact is likely the main cause of the drought experienced in the watersheds over the last few decades. While temperature may indirectly affect vegetation water, it remains an important factor influencing poor vegetation growth. The negative correlation of NDVI-P covered 70% of the study area, with its negative effect evident in all regions, consistent with NDVI-T. This persistent and increasing negative effect, particularly in recent years, highlights the drought affecting these basins. It underscores the importance of

Table 3 Seasonal correlations between climatic conditions and NDVI (NDVI-P, NDVI-T) in the Basins

Basins	NDVI- T			NDVI-P		
	Autumn	Spring	Summer	Autumn	Spring	Summer
Ain Beida	−0.01	0.11	0.15	0.03	−0.012	−0.010
Arzew Saline	−0.01	0.001	−0.23	−0.20	−0.023	−0.023
Boughezoul Dam	0.03	0.001	0.13	−0.20	−0.027	−0.022
Chott Zehrez Chergui	0.10	0.04	0.10	−0.22	−0.033	−0.02
Chott Ech Chergui	0.13	0.04	0.07	−0.21	−0.029	−0.029
Dayet El Ferd	0.04	0.10	0.20	−0.23	−0.029	−0.022
Chott Zehrez Gharbi	0.11	0.02	0.05	−0.017	−0.023	−0.022
Chott El Hodna	0.05	0.07	0.03	−0.022	−0.031	−0.024
Macta Swamp	0.03	0.15	0.08	−0.021	−0.025	−0.023
Chott Melghir	−0.08	0.08	0.08	−0.013	−0.029	−0.014
Great Sebkha	0.06	0.19	0.07	−0.021	−0.026	−0.021
Telamine Lake	0.001	−0.21	0.03	−0.020	−0.026	−0.020
Beni Bahdel Dam	0.10	0.13	0.19	−0.025	−0.029	−0.022
Bougara Dam	0.06	−0.12	0.06	−0.025	−0.025	−0.019
Boughrara Dam	0.12	0.03	0.17	−0.022	−0.026	−0.019
Bouhanifia Dam	0.05	−0.07	0.12	−0.022	−0.025	−0.024
Chorfa Dam	0.04	−0.07	0.08	−0.020	−0.027	−0.023
Cheliff dam	0.04	−0.09	0.10	−0.023	−0.027	−0.024
Chott Merouane	0.01	0.09	0.001	−0.013	−0.026	−0.019
Dahmoni Dam	0.11	0.12	0.26	−0.022	−0.027	−0.023
Golea	−0.03	0.02	−0.06	−0.018	−0.026	−0.023
Gargar Dam	0.26	0.17	−0.09	−0.023	−0.029	−0.023
Karrada Dam	0.12	−0.05	−0.22	−0.020	−0.025	−0.018
Ksob Dam	0.08	0.16	−0.05	−0.018	−0.025	−0.020
Sarno Dam	0.06	−0.18	−0.09	−0.021	−0.024	−0.20

precipitation, especially in vegetation growth, as a crucial driver. Hence, it can be emphasized that rainfall and temperature play pivotal roles in determining vegetation dynamics and interpreting them effectively, particularly in dry and semi-dry areas (Gao et al. 2022).

Additionally, it's important to note the decrease in water levels in these basins. These changes may lead to the disappearance of many water bodies, as evidenced in the Dayet El Ferd and Great Sebkha basins, which are currently experiencing unprecedented drought. These results also indicate that the warming climate has diminished its positive effect on vegetation growth over time.

Vegetation response to climate change varies greatly, influenced by environmental patterns and climate conditions (Filippa et al. 2019). However, it's crucial to acknowledge that climatic factors alone are insufficient in the presence of human factors, such as agricultural and urban land expansion and overgrazing, which also impact vegetation growth (Xu et al. 2016; Luo et al. 2018; Ma et al. 2019). These aspects will be the focus of future studies, along with examining the overall relationship between vegetation and other impacts, such as relative humidity, evaporation, topographic, and demographic factors.

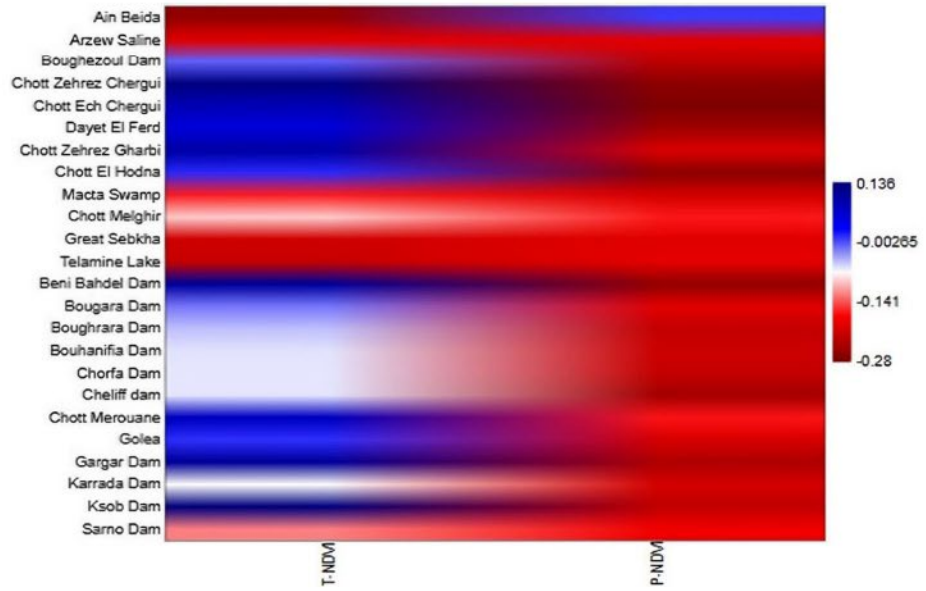

Fig. 5 Time-lag transfer matrix among NDVI and climate factors in 25 Algerian watersheds from 1981 to 2021

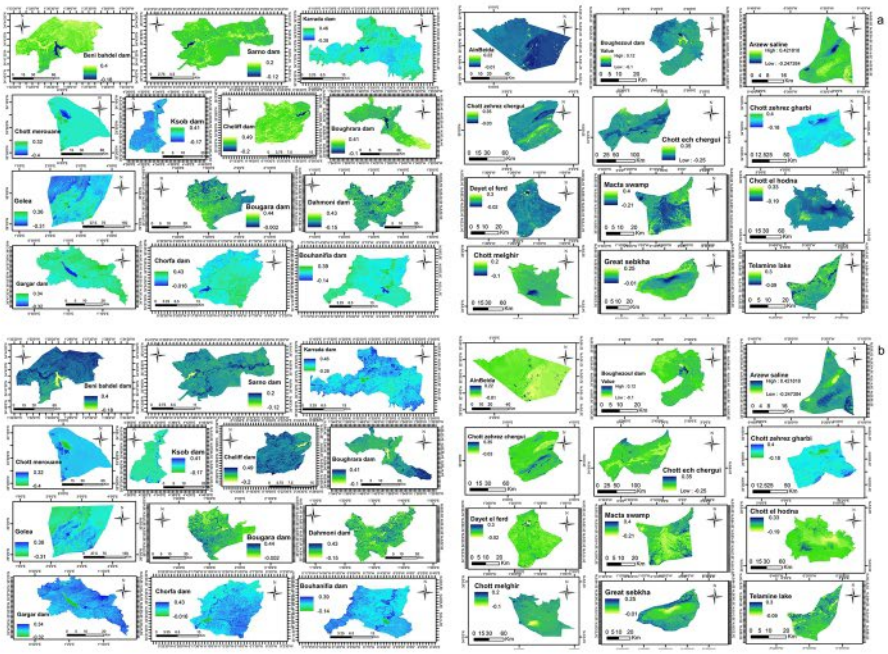

Fig. 6 The Pearson correlation distribution pattern between both the multi-year average vegetation indices (NDVI) and the climatic factors temperature (**a**), and rainfall (**b**) in 25 basins from 1981 to 2021

5 Conclusions

Studying climate changes and their time lag to comprehension, vegetation index dynamism, and the vulnerability of ecological systems to climate change is of great importance. This study, encompassing 25 regions of watersheds, concluded that climatic conditions have exhibited a significantly drier trend that has intensified in recent years. Consequently, vegetation has shown a downward trend, attributed to reduced rainfall and increased temperatures observed from 1981 to 2021. To delve deeper into this phenomenon and investigate the association between NDVI and climatic conditions, a partial correlation approach was employed. This analysis revealed the extent of degradation of vegetation and the prevalence of drought across all areas.

It's noteworthy that these basins have experienced a decline in water levels, raising concerns about the potential disappearance of many of them. This concern is particularly evident in the Dayet El-Ferd and Great Sebkha basins, which are currently grappling with an unprecedented drought. Additionally, the findings of this study suggest that the warming climate has gradually diminished its positive effect on vegetation growth over time. Notably, the vegetation index's response to temperature was found to be less pronounced compared to rainfall.

Given these findings, it becomes imperative to determine the ecological absorptive capacity through further study in these areas. These results underscore the importance of implementing policies aimed at restoring vegetation and managing vegetation recovery, especially considering the changing landscape of these regions. By prioritizing such initiatives, we can better address the challenges posed by climate change and safeguard the ecological integrity of these vital ecosystems.

Author contributions HK: designed the research, methodology, and software, implemented the data computation, formal analysis, and cartography. EB: review and editing and supervision. AZ: validation. All authors participated significantly in the content development and authorized this manuscript's publishing.

Funding Not applicable.

Declarations

Competing interests The authors proclaim that they have no conflicts of interest that might impact or prejudice the content of this article.

References

Bai Y, Guo C, Degen AA, Ahmad AA, Wang W, Zhang T, Li W, Ma L, Huang M, Zeng H, Qi L, Long R, Shang Z (2020) Climate warming benefits alpine vegetation growth in Three-River Headwater Region, China. Sci Total Environ 742:140574. https://doi.org/10.1016/j.scitotenv.2020.140574

Bhuyan U, Zang C, Vicente-Serrano S, Menzel A (2017) Exploring relationships among tree-ring growth, climate variability, and seasonal leaf activity on varying timescales and spatial resolutions. Remote Sens 9:526. https://doi.org/10.3390/rs9060526

Chen T, De Jeu R, Liu Y, Van Der Werf G, Dolman A (2014) Using satellite-based soil moisture to quantify the water driven variability in NDVI: a case study over mainland Australia. Remote Sens Environ 140:330–338. https://doi.org/10.1016/.j.rse.2013.08.022

Chu H, Venevsky S, Wu C, Wang M (2019) NDVI-based vegetation dynamics and its response to climate changes at Amur-Heilongjiang River Basin from 1982 to 2015. Sci Total Environ 650:2051–2062. https://doi.org/10.1016/j.scitotenv.2018.09.115

Claverie M, Vermote EF, Franch B, Masek JG (2015) Evaluation of the landsat-5 TM and landsat-7 ETM+ surface reflectance products. Remote Sens Environ 169:390–403. https://doi.org/10.1016/j.rse.2015.08.030

Ding Y, Li Z, Peng S (2020) Global analysis of time-lag and accumulation effects of climate on vegetation growth. Int J Appl Earth Obs Geoinf 92:102179. https://doi.org/10.1016/j.jag.2020.102179

Eisavi V, Homayouni S, Yazdi AM, Alimohammadi A (2015) Land cover mapping based on random forest classification of multitemporal spectral and thermal images. Environ Monit Assess 187:291. https://doi.org/10.1007/s10661-015-4489-3

Filippa G, Cremonese E, Galvagno M, Isabellon M, Bayle A, Choler P, Carlson BZ, Gabellani S, di Cella UM, Migliavacca M (2019) Climatic drivers of greening trends in the Alps. Remote Sens 11:2527. https://doi.org/10.3390/rs11212527

Gao W, Zheng C, Liu X, Lu Y, Chen Y, Wei Y, Ma Y (2022) NDVI-based vegetation dynamics and their responses to climate change and human activities from 1982 to 2020: a case study in the Mu Us Sandy Land, China. Ecol Ind 137:108745. https://doi.org/10.1016/j.ecolind.2022.108745

Gorelick N, Hancher M, Dixon M, Ilyushchenko S, Thau D, Moore R (2017) Google earth engine: planetary-scale geospatial analysis for everyone. Remote Sens Environ 202:18–27. https://doi.org/10.1016/j.rse.2017.06.031

Hu Y, Dao R, Hu Y (2019) Vegetation change and driving factors: contribution analysis in the Loess Plateau of China during 2000–2015. Sustainability 11:1320. https://doi.org/10.3390/su11051320

Irons JR, Dwyer JL, Barsi JA (2012) The next Landsat satellite: the LANDSAT data continuity mission. Remote Sens Environ 122:11–21. https://doi.org/10.1016/j.rse.2011.08.026

Islam A, Islam HMT, Shahid S, Khatun MK, Ali MM, Rahman MS, Ibrahim SM, Almoajel AM (2021) Spatiotemporal nexus between vegetation change and extreme climatic indices and their possible causes of change. J Environ Manag 289:112505. https://doi.org/10.1016/j.jenvman.2021.112505

Jong R, Schaepman ME, Furrer R, Bruin S, Verburg PH (2013) Spatial relationship between climatologies and changes in global vegetation activity. Glob Change Biol 19:1953–1964. https://doi.org/10.1111/gcb.12193

Kennedy RE, Yang Z, Cohen WB (2010) Detecting trends in forest disturbance and recovery using yearly Landsat time series, 1: LandTrendr—temporal segmentation algorithms. Remote Sens Environ 114:2897–2910. https://doi.org/10.1016/j.rse.2010.07.008

Kennedy RE, Yang Z, Gorelick N, Braaten J, Cavalcante L, Cohen W, Healey S (2018) Implementation of the LandTrendr algorithm on Google Earth Engine. Remote Sens 10:691. https://doi.org/10.3390/rs10050691

Li C, Leal Filho W, Yin J, Hu R, Wang J, Yang C, Yin S, Bao Y, Ayal DY (2018) Assessing vegetation response to multi-time-scale drought across inner Mongolia plateau. J Clean Prod 179:210–216

Liu C, Liu J, Zhang Q, Ci H, Gu X, Gulakhmadov A (2022) Attribution of NDVI dynamics over the globe from 1982 to 2015. Remote Sens 14:2706. https://doi.org/10.3390/rs14112706

Liu S, Cheng F, Dong S, Zhao H, Hou X, Wu X (2017) Spatiotemporal dynamics of grassland aboveground biomass on the Qinghai-Tibet Plateau based on validated MODIS NDVI. Sci Rep 7(1):1–10. https://doi.org/10.1038/s41598-017-04038-4

Liu YL, Lei HM (2015) Responses of natural vegetation dynamics to climate drivers in China from 1982 to 2011. Remote Sens 7:10243–10268. https://doi.org/10.3390/rs70810243

Liu Q, Zhao DS, Wu SH, Dai EF, Gao JB (2019) Using the NDVI to analyze trends and stability of grassland vegetation cover in Inner Mongolia. Theor Appl Climatol 135(3–4):1629–1640. https://doi.org/10.1007/s00704-018-2614-2

Luo X, Ao X, Zhang Z, Wan Q, Liu X (2020) Spatiotemporal variations of cultivated land use efficiency in the Yangtze River economic belt based on carbon emission constraints. J Geogr Sci 30:535–552. https://doi.org/10.1007/s11442-020-1741-8

Luo Z, Wu W, Yu X, Song Q, Yang J, Wu J, Zhang H (2018) Variation of net primary production and its correlation with climate change and anthropogenic activities over the Tibetan Plateau. Remote Sens 10:1352. https://doi.org/10.3390/rs10091352

Ma Q, Chai L, Hou F, Chang S, Ma Y, Tsunekawa A, Cheng Y (2019) Quantifying grazing intensity using remote sensing in alpine meadows on Qinghai-Tibetan Plateau. Sustainability 11:417. https://doi.org/10.3390/su11020417

Martiny N, Camberlin P, Richard Y, Philippon N (2006) Compared regimes of NDVI and rainfall in semi-arid regions of Africa. Int J Remote Sens 27(23):5201–5223. https://doi.org/10.1080/01431160600567787

Myneni RB, Hoffman S, Knyazikhin Y et al (2002) Global products of vegetation leaf area and fraction absorbed PAR from year one of MODIS data. Remote Sens Environ 83:214–231. https://doi.org/10.1016/S0034-4257(02)00074-3

Pan N, Feng X, Fu B, Wang S, Ji F, Pan S (2018) Increasing global vegetation browning hidden in overall vegetation greening: insights from time-varying trends. Remote Sens Environ 214:59–72. https://doi.org/10.1016/j.rse.2018.05.018

Parteli EJR (2022) Predicted expansion of sand deserts. Nat Clim Chang 12:967–968. https://doi.org/10.1038/s41558-022-01506-2

Peng J, Wu C, Zhang X, Wang X, Gonsamo A (2019) Satellite detection of cumulative and lagged effects of drought on autumn leaf senescence over the Northern Hemisphere. Glob Change Biol 25:2174–2188. https://doi.org/10.1111/gcb.14627

Piao S, Mohammat A, Fang J, Cai Q, Feng J (2006) NDVI-based increase in growth of temperate grasslands and its responses to climate changes in China. Glob Environ Chang 16:340–348. https://doi.org/10.1016/j.gloenvcha.2006.02.002

Qin J, Ma M, Shi J, Ma S, Wu B, Su X (2023) The time-lag effect of climate factors on the forest enhanced vegetation index for subtropical humid areas in China. Int J Environ Res Public Health 20:799. https://doi.org/10.3390/ijerph20010799

Roerink GJ, Menenti M, Soepboer W, Su Z (2003) Assessment of climate impact on vegetation dynamics by using remote sensing. Phys Chem Earth 28:103–109. https://doi.org/10.1016/S1474-7065(03)00011-1

Seddon AWR, Macias-Fauria M, Long PR, Benz D, Willis KJ (2016) Sensitivity of global terrestrial ecosystems to climate variability. Nature 531(7593):229–243. https://doi.org/10.1038/nature16986

Vicente-Serrano SM, Gouveia C, Camarero JJ, Beguería S, Trigo R, López moreno JI, Azorínmolina C, Pasho E, Lorenzolacruz J, Revuelto J (2013) Response of vegetation to drought time-scales across global land biomes. Proc Natl Acad Sci USA 110:52–57. https://doi.org/10.1073/pnas.1207068110

Wang M, Fu J, Wu Z, Pang Z (2020a) Spatiotemporal variation of NDVI in the vegetation growing season in the source region of the Yellow River China. ISPRS Int J Geo-Inf 282:1. https://doi.org/10.3390/ijgi9040282

Wang H, Kang C, Tian Z, Zhang A, Cao Y (2020b) Vegetation periodic changes and relationships with climate in Inner Mongolia Based on the VMD method. Ecol Indic 34:107964. https://doi.org/10.1016/j.gecco.2022.e02034

Wang H, Liu D, Lin H, Montenegro A, Zhu X (2015) NDVI and vegetation phenology dynamics under the influence of sunshine duration on the Tibetan plateau. Int J Climatol 35:687–698. https://doi.org/10.1002/joc.4013

Wu D, Zhao X, Liang S, Zhou T, Huang K, Tang B, Zhao W (2015) Time-lag effects of global vegetation responses to climate change. Glob Chang Biol 21(9):3520–3531. https://doi.org/10.1111/gcb.12945

Xu H, Wang X, Zhang X (2016) Alpine grasslands response to climatic factors and anthropogenic activities on the Tibetan Plateau from 2000 to 2012. Ecol Eng 92:251–259. https://doi.org/10.1016/j.ecoleng.2016.04.005

Xu G, Zhang H, Chen B, Zhang H, Innes JL, Wang G, Yan J, Zheng Y, Zhu Z, Myneni RB (2014) Changes in vegetation growth dynamics and relations with climate over China landmass from 1982 to 2011. Remote Sens 6:3263–3283. https://doi.org/10.3390/rs6043263

Zhan C, Liang C, Zhao L, Jiang S, Niu K, Zhang Y, Cheng L (2022) Vegetation dynamics and its response to climate change in the Yellow River Basin, China. Front Environ Sci 450:1

Zhang Q, Buyantuev A, Fang X, Han P, Li A, Li FY, Liang C, Liu Q, Ma Q, Niu J et al (2020) Ecology and sustainability of the Inner Mongolian Grassland: looking back and moving forward. Landsc Ecol 35:2413–2432. https://doi.org/10.1007/s10980-020-01083-9

Zhang YL, Gao JG, Liu LS, Wang ZF, Ding MJ, Yang XC (2013) NDVI-based vegetation changes and their responses to climate change from 1982 to 2011: a case study in the Koshi river basin in the middle Himalayas. Global Planet Change 108:139–148. https://doi.org/10.1016/J.GLOPLACHA.2013.06.012

Zhao J, Huang S, Huang Q, Wang H, Leng G, Fang W (2020) Time-lagged response of vegetation dynamics to climatic and teleconnection factors. CATENA 189:104474. https://doi.org/10.1016/j.catena.2020.104474

Zhe M, Zhang X (2021) Time-lag effects of NDVI responses to climate change in the Yamzhog Yumco Basin, South Tibet. Ecol Indic 124:107431. https://doi.org/10.1016/j.ecolind.2021.107431

Zhou L, Tian Y, Myneni RB et al (2014) Widespread decline of Congo rainforest greenness in the past decade. Nature 509:86–90

Zhou X, Yamaguchi Y, Arjasakusuma S (2018) Distinguishing the vegetation dynamics induced by anthropogenic factors using vegetation optical depth and AVHRR NDVI: a cross-border study on the Mongolian Plateau. Sci Total Environ 616–617:730–743. https://doi.org/10.1016/j.scitotenv.2017.10.253

Zhu Z, Wang S, Woodcock CE (2015) Improvement and expansion of the Fmask algorithm: cloud, cloud shadow, and snow detection for Landsat 4–7, 8, and Sentinel 2 images. Remote Sens Environ 159:269–277. https://doi.org/10.1016/j.rse.2014.12.014

Abbes Laghrour University, KHENCHELA
Faculty of Natural and Life Sciences
Department of Ecology and Environment
The 1st International virtual conference on Climate Change, Georesources and Sustainable Development "1st I2CGSD 2022"
Khenchela May 23 th, 2022

1st I2CGSD 2022

CERTIFICATE of participation

The dean of the faculty of natural and life sciences of Abbes Laghrour, Khenchela University, and the president of The 1st International hybrid conference on Climate Change, Georesources and Sustainable Development "1st I2CGSD 2022", certifies that :

Mr(s). KERIA Hadjer

Participated with an (Oral) communication entitled: Climate variability and its effect on normalized difference vegetation index (NDVI) using remote sensing in semi-arid area (Djelfa).
Co-authors : BENSACI Ettayib, ZOUBIRI Asma

Conference president

رئيس الملتقى
د. بولعبايز محرز

Dean of the Faculty

BARTIN UNIVERSITY
FACULTY OF FORESTRY

CERTIFICATE
OF PARTICIPATION

THIS IS TO CERTIFY THAT

HADJER KERIA

HAS CONTRIBUTED WITH A ORAL PRESENTATION TITLED:
ASSESSING VEGETATION RESPONSE TO CLIMATIC CHANGES AND DROUGHT IN THE REGHAIA BASIN: INSIGHTS FROM MODIS DATA AND CORRELATION ANALYSIS
IN THE 5TH INTERNATIONAL NON-WOOD FOREST PRODUCTS SYMPOSIUM HELD ONLINE ON SEPTEMBER 27-28, 2023.

B. Durkaya

PROF. DR. BİRSEN DURKAYA
BARTIN UNIVERSITY
DEAN OF THE FACULTY OF FORESTRY

People's Democratic Republic of Algeria
Ministry of Higher Education and Scientific Research
University Abbes Laghrour-Khenchela
Faculty of Nature and Life Sciences
Laboratory of Biotechnology, Water, Environment and Health

Biotechnologie, Eau, Environnement et Santé

CERTIFICATE OF PARTICIPATION

The president of the First International Webinar on:
Promotion and Exploitation of Plants of Ecological and Economic Interest
held between 15 and 16March 2023, certifies that:

KERIA HADJER

Participated with an oral Communication

***Entitled:* Changes in vegetation dynamics and relations with extreme climate in Algeria**

Co-authors:

Webinar chair	Laboratory manager	Dean of the Faculty
Dr. Djamel Bensizerara	*Pr. Kenza Kadi*	*Pr. Sofiane Hemmam Mounine*

Ministry of High Education and Scientific Research
M'hamed Bougara University, Boumerdes, Algeria
High National School of Agronomy, Algiers, Algeria

ENSA

Certificate of participation

Awarded to

KERIA Hadjer

For participating in the International seminar "Sustainable Agriculture under Climate Change: Challenges and Perspectives."

By communication entitled: " Étude des relations entre la couverture végétale et la température de surface calculées à partir des données Landsat ETM+ à l'échelle du bassin versant de Chott Zohra Gharbi"

Co-authors: E. BENSACI, A. ZOUBIRI

VICE PRESIDENT
Dr. Bilal RAHMOUNE

Université M'hamed Bougara-Boumerdes
Agriculture Durable Face aux Changements Climatiques Enjeux et Perspectives
Faculté des Sciences

PRESIDENT
Dr. Ghilès KACI

République Algérienne Démocratique et Populaire.
Ministère de l'enseignement supérieur et de la recherche scientifique.
Université Badji Mokhtar-Annaba.
Faculté des sciences de la Terre.

GIS day ALGERIA 2022

Le Laboratoire de Recherche
« Analyses Urbaines et Environnementales »

Attestation de participation

Le Président du Comité d'organisation du **Webinaire International**, intitulé : « **GIS DAY ALGERIA 2022** ».
Organisé par le Laboratoire de Recherche « **Analyses Urbaines et Environnementales** »,
le 16 novembre 2022 à Annaba /Algérie, atteste que :
Mme. Hadjer KERIA, Mr. Ettayib BENSACI, Mme Asma ZOUBIRI
A présenté une communication intitulée :

Ndvi: Vegetation change detection using remote sensing and GIS–A case study of Djelfa

Fait à Annaba le : 16 Novembre 2022

Le Président du Webinaire
Dr Rabah ZENNIR
Dr. ZENNIR Rabah
Maître de Conférences, Classe A
La Géographie & Aménagement du Territoire

Le Directeur du Laboratoire
Dr HDR Djamel TELAIDJIA
الدكتور: تلايجية جمال

République Algérienne Démocratique et Populaire
Ministère de l'Enseignement Supérieur et de la Recherche Scientifique
L'Université Mohamed Chérif Messaadia. Souk-Ahras
Institut des Sciences Agronomiques et Vétérinaires
Laboratoire des Sciences et Techniques du Vivant
1ère Séminaire National Sur L'agriculture et le Développement Durable en Zones Semi-Arides le 15 et 16 Novembre 2022 (Online)

Attestation de Participation

Le Comité d'organisation du « *1ER Séminaire National Sur L'agriculture et le Développement Durable en Zones Semi-Arides* », Atteste que :
M^me^, M^elle^, M^r^ : KERIA Hadjer
A participé au Séminaire avec une Communication « ORALE » Intitulée *«Comparative study of NDVI végétation indices in Chott Zohra Gharbi watershed district Semi-arid areas»*

Coauteurs : BEN SACI Ettayib & ZOUBIRI Asma

Directeur de l'Institut
مدير معهد العلوم الفلاحية و البيطرية
إمضاء: د. نور الدين قسم الله

Directeur de Laboratoire LSTV
et Président du Séminaire

International Journal of Natural Resources and Environment

Algerian Journal of Biosciences
AJB

Université Ferhat Abbas Sétif-1

Faculté des Sciences de la Nature et de la Vie
Laboratoire de Valorisation des Ressources Biologiques Naturelles

1er Séminaire National sur :
« La Valorisation des Ressources Naturelles et de l'Environnement »
(VRNE 2022)
30 Mars 2022

L.V.R.B.N
VRNE 2022

Attestation de participation

N° **T1A93**

Le comité d'organisation du séminaire atteste par la présente que : Melle/Mme/Mr. : **KERIA Hadjer** a participé à cette manifestation par une communication **affichée**, intitulée **: «Contributions du SIG et de la Télédétection à la Corrélation Entre le NDVI et LST Pour L'étude de la Variabilité Climatique Dans le Bassin de Chott Zohra Gharbi.».**

Co-auteurs(s): **BEN SACI Ettayin , ZOUBIRI Asma**

Le président du séminaire

جامعة فرحات عباس - سطيف1
كلية علوم الطبيعة والحياة
مخبر تقييم الموارد الطبيعية البيولوجية
الملتقى العلمي الوطني
(تثمين الموارد الطبيعية والبيئة)

REPUBLIQUE ALGERIENNE DEMOCRATIQUE ET POPULAIRE
MINISTERE DE L'ENSEIGNEMENT SUPERIEUR ET DE LA RECHERCHE SCIENTIFIQUE

جامعة باجي مختار–عنابة
Badji Mokhtar Annaba University
Laboratoire d'Analyses Urbaines et Environnementales
L.A.U.E

LAUE UBMA

Attestation de participation

Le Président du Comité d'organisation du Webinaire national, intitulé : « **GIS DAY ALGERIA 2023** »,
Organisé par le Laboratoire de Recherche « **Analyses Urbaines et Environnementales** »,
le 15 novembre 2023 à Annaba /Algérie, atteste que :

Mme KERIA Hadjer, Pr. Bensaci Ettayib, Mme Ben si said Zineb, M. PULAT Esra et Pr. Ateşoğlu Ayhan

A présenté une communication intitulée :

«Comprendre la Dynamique de la Réponse de la Végétation au Changement Climatique et Élucider les Causes de la Sécheresse dans le Bassin de Reghaia : Une Étude Complète Utilisant les Données MODIS»

GIS DAY ALG 2023/LAUE

Fait à Annaba le : 15 Novembre 2023

Le Directeur du Laboratoire
Dr HDR Djamel TELAIDJIA

Le Président du Webinaire
Dr Rabah ZENNIR
Dr. ZENNIR Rabah
Maitre de Conférences, Classe A
En Géographie & Aménagement du Territoire

GIS day ALGERIA 2023

Université Badji Mokhtar ANNABA – le Directeur – Laboratoire d'Analyses Urbaines et Environnementales

laue@univ-annaba.dz
Laboratoire d'analyses urbaines et environnementales
http://laue.univ-annaba.dz/

Abstract

Wetlands are regarded locally and globally as vital environments of great biological and economic importance and play an important role in the conservation of biodiversity and the preservation of ecosystems. However, wetlands face many challenges and major crises that threaten their long-term sustainability. Long-term monitoring to determine the volatility of these water systems is crucial while examining climate change and the causes of the droughts they face. In this research, we presented a long-term variation of remote sensing indicators in 26 areas of Algeria's wetlands by integrating various sources of Modis and Landsat satellites. A time series has been developed for 22 years and 40 years, respectively, combined with climate changes. Research to study pollution in these environmental systems and to determine its source has been extended through various indicators to comprehensively assess the scale of mineral pollution in Algeria's surface waters and its potential public health effects. and study predictions using synthetic neural networks (ANN). The results indicated that 70% of this land experienced a significant reduction in vegetation in the seasonal and annual periods. A decrease in surface water area from year to year was observed in all regions, and the negative relationship between the vegetation index and climate changes showed the impact of drought and its rise in varying proportions, especially in summer and autumn, with a time delay of at least one month. NDMI results also indicate water stress in water bodies and a low water level. On the other hand, high levels of heavy metals were recorded in water bodies, as more than 99% of samples showed significant pollution levels according to HPI, while 60% showed high pollution levels according to HEI. The study revealed that RMS values for all heavy metal models have minimal error values throughout the test phase, and the developed models showed R2 values that exceeded 0.5 during the test.

Keywords: Remote sensing, Wetlands, Ecology index, Heavy Metals, ANN, Algeria.

Résumé

Les zones humides sont considérées localement et globalement comme des environnements vitaux d'une grande importance biologique et économique et jouent un rôle important dans la conservation de la biodiversité et la préservation des écosystèmes. Cependant, les zones humides sont confrontées à de nombreux défis et à des crises majeures qui menacent leur durabilité à long terme. La surveillance à long terme afin de déterminer la volatilité de ces systèmes d'approvisionnement en eau est cruciale tout en examinant les changements climatiques et les causes des sécheresses auxquelles ils sont confrontés. Dans cette recherche, nous avons présenté une variation à long terme des indicateurs de télédétection dans 26 zones humides algériennes en intégrant diverses sources de satellites Modis et Landsat. Une série chronologique a été développée pendant 22 ans et 40 ans, respectivement, combinée avec les changements climatiques. La recherche visant à étudier la pollution dans ces systèmes environnementaux et à en déterminer la source a été étendue grâce à divers indicateurs afin d'évaluer globalement l'ampleur de la pollution minérale dans les eaux de surface algériennes et ses effets potentiels sur la santé publique. Et étudier les prédictions à l'aide de réseaux de neurones synthétiques (ANN). Les résultats indiquent que 70 % de ces terres ont connu une réduction significative de la végétation au cours des périodes saisonnières et annuelles. Une diminution de la superficie des eaux de surface d'une année à l'autre a été observée dans toutes les régions, et la relation négative entre l'indice de végétation et les changements climatiques a montré l'impact de la sécheresse et son augmentation dans des proportions variables, en particulier en été et en automne, avec un délai d'au moins un mois. Les résultats de NDMI indiquent également un stress hydrique dans les plans d'eau et un faible niveau d'eau. D'autre part, des niveaux élevés de métaux lourds ont été enregistrés dans les plans d'eau, car plus de 99 % des échantillons présentaient des niveaux de pollution significatifs selon l'HPI, tandis que 60 % présentaient des niveaux de pollution élevés selon HEI. L'étude a révélé que les valeurs RMS pour tous les modèles de métaux lourds ont des valeurs d'erreur minimales tout au long de la phase d'essai et les modèles développés ont montré des valeurs R2 supérieures à 0,5 pendant le test.

Mots-clés : Télédétection, Zones humides, Indices écologique, Métaux lourds, ANN, Algérie.

الملخص:

تعتبر الأراضي الرطبة على المستوى المحلى والعالمي ببيئات حيوية ذات أهمية بيولوجية واقتصادية كبيرة كما تلعب دورا مهما في الحفاظ على التنوع البيولوجي والحفاظ على النظم البيئة ومع ذلك تواجه الأراضي الرطبة العديد من التحديات وأزمات كبيرة التي تهدد استدامتها على المدى البعيد. إن الرصد طويل الأمد لتحديد التقلبات التي تواجهها هذه النظم المائية أمر بالغ الأهمية، مع دراسة التغيرات المناخية وأسباب حالات الجفاف التي تواجهها. في هذا البحث قمنا بتقديم تباين طويل الأمد لمؤشرات الاستشعار عن بعد في 26 منطقة من الأراضي الرطبة في الجزائر من خلال دمج مصادر مختلفة من الأقمار الصناعية موديس ولاندسات. تم تطوير مجموعة بيانات زمنية متسلسلة تمتد ل 22 سنة و 40 سنة على التوالي. مع دمجها بالتغيرات المناخية. وامتد مجال البحث لدراسة التلوث في هذه النظم البيئة وتحديد مصدرها من خلال مؤشرات متنوعة لتقييم شامل لحجم تلوث المعادن في المياه السطحية للجزائر وآثاره المحتملة على الصحة العامة. ودراسة التنبؤات باستخدام الشبكات العصبية الاصطناعية (ANN). أشارت النتائج إلى أن 70 % من هذا الأرضي شهدت انخفاضا كبيرا في الغطاء النباتي في الفترات الموسمية والسنوية. ولوحظ انخفاض في مساحة المياه السطحية من عام إلى آخر في جميع المناطق، وأظهرت العلاقة السلبية بين مؤشر الغطاء النباتي والتغيرات المناخية تأثير الجفاف وارتفاعه بنسب متفاوتة خاصة في فصل الصيف والخريف مع تسجيل تأخير زمني لا يقل عن شهر واحد. كما إشارات نتائج NDMI إلى الإجهاد المائي في المسطحات المائية وانخفاض منسوب المياه. من جهة أخرى سجلت مستويات مرتفعة من المعادن الثقيلة في المسطحات المائية حيث إن أكثر من 99٪ من العينات أظهرت مستويات تلوث كبيرة وفقا ل HPI، في حين أظهر 60٪ مستويات تلوث مرتفعة وفقا ل HEI. كشفت الدراسة أن قيم RMS لجميع نماذج المعادن الثقيلة لديها الحد الأدنى من قيم الخطأ طوال مرحلة الاختبار، وأظهرت النماذج المطورة قيم R2 التي تتجاوز 0.5 أثناء الاختبار.

الكلمات المفتاحية: الاستشعار عن بعد، الأراضي الرطبة، مؤشر البيئة، المعادن الثقيلة، ANN، الجزائر.